Transmitter and receiver design for inherent interference cancellation in MIMO filter-bank based multicarrier systems

Rostom Zakaria

CONSERVATOIRE NATIONAL DES ARTS ET MÉTIERS

le cnam

École Doctorale Technologique et Professionnelle
CEDRIC/LAETITIA

THÈSE DE DOCTORAT

Présentée pour obtenir le Grade de Docteur
du Conservatoire National des Arts et Métiers

Discipline: Lasers, Métrologie, Communications
Spécialité: Communications et Electronique

Rostom Zakaria

Conception d'émetteur et récepteur pour l'élimination des interférences intrinsèques dans les systèmes multiporteuses à base de bancs de filtres et à antennes multiples.

Soutenue le 7 Novembre 2012 devant le jury composé de:

Rapporteurs
Prof. Jérôme Louveaux, Université Catholique de Louvain, Belgique
Prof. Antoine Berthet, Supélec, Gif-sur-Yvette, France

Examinateurs
Prof. Jean-François Hélard, INSA Rennes, France
Prof. Inbar Fijalkow, ENSEA/ Université de Cergy-Pontoise, France
M. Philippe Mège, CASSIDIAN, Élancourt, France

Directeurs :
Prof. Didier Le Ruyet, CNAM Paris, France

Abstract

Multicarrier (MC) Modulation attracts a lot of attention for high speed wireless transmissions because of its capability to cope with frequency selective fading channels turning the wideband transmission link into several narrowband subchannels whose equalization, in some situations, can be performed independently and in a simple manner. Nowadays, orthogonal frequency division multiplexing (OFDM) with the cyclic prefix (CP) insertion is the most widespread modulation among all MC modulations, and this thanks to its simplicity and its robustness against multipath fading using the cyclic prefix. Systems or standards such as ADSL or IEEE802.11a have already implemented the CP-OFDM modulation. Other standards like IEEE802.11n combine CP-OFDM and multiple-input multiple-output (MIMO) in order to increase the bit rate and to provide a better use of the channel spatial diversity. Nevertheless, CP-OFDM technique causes a loss of spectral efficiency due to the CP as it contains redundant information. Moreover, the rectangular prototype filter used in CP-OFDM has a poor frequency localization. This poor frequency localization makes it difficult for CP-OFDM systems to respect stringent specifications of spectrum masks.

To overcome these drawbacks, filter-bank multicarrier (FBMC) was proposed as an alternative approach to CP-OFDM. Indeed, FBMC does not need any CP, and it furthermore offers the possibility to use different time-frequency well-localized prototype filters which allow much better control of the out-of-band emission. In the literature we find several FBMC systems based on different structures. In this thesis, we focus on the Saltzberg's scheme called OFDM/OQAM (or FBMC/OQAM). The orthogonality constraint for FBMC/OQAM is relaxed being limited only to the real field while for OFDM it has to be satisfied in the complex field. Consequently, one of the characteristics of FBMC/OQAM is that the demodulated transmitted symbols are accompanied by interference terms caused by the neighboring transmitted data in time-frequency domain. The presence of this interference is an issue for some MIMO schemes and until today their combination with FBMC remains an open problem.

The aim of this thesis is to study the combination between FBMC and MIMO techniques, namely spatial multiplexing with ML detection. In the first part, we propose to analyze different intersymbol interference (ISI) cancellation techniques that we adapt to the FBMC/OQAM with MIMO context. We show that, in some cases, we can cope with the presence of the inherent FBMC interference and overcome the difficulties of performing ML detection in spatial multiplexing with FBMC/OQAM. After that, we propose a modification in the conventional FBMC/OQAM modulation by transmitting complex QAM symbols instead of OQAM ones. This proposal allows to reduce considerably the inherent interference but at the expense of the orthogonality condition. Indeed, in the proposed FBMC/QAM,

the data symbol and the inherent interference term are both complex. Finally, we introduce a novel FBMC scheme and a transmission strategy in order to avoid the inherent interference terms. This proposed scheme (that we call FFT-FBMC) transforms the FBMC system into an equivalent system formulated as OFDM regardless of some residual interference. Thus, any OFDM transmission technique can be performed straightforwardly to the proposed FBMC scheme with a corresponding complexity growth. We develop the FFT-FBMC in the case of single-input single-output (SISO) configuration. Then, we extend its application to SM-MIMO configuration with ML detection and Alamouti coding scheme.

Keywords: OFDM, FBMC, Filter Bank, Multicarrier, MIMO, Maximum Likelihood detection, ML, Interference Cancellation, Alamouti.

Résumé

Grâce à leur capacité de faire face à la sélectivité fréquentielle des canaux de transmission, les modulations multi-porteuses (MC) attirent de plus en plus d'attention. De nos jours, la modulation OFDM avec le préfixe cyclique (CP) est la plus utilisée, et cela grâce à sa simplicité et à sa robustesse. Cependant, la technique CP-OFDM présente une perte dans l'efficacité spectrale à cause de l'introduction du CP puisqu'il contient des informations redondantes. De plus, la réponse rectangulaire du filtre de mise en forme utilisé en OFDM a une mauvaise localisation fréquentielle.

Afin de surmonter ces inconvénients, la modulation multi-porteuse à base des bancs de filtres (FBMC) a été proposée en tant qu'une approche alternative à la modulation OFDM. En effet, on n'a pas besoin d'insérer un intervalle de garde, tel que le CP, dans la modulation FBMC. D'autre part, la bonne localisation fréquentielle de la réponse du filtre de mise en forme permet un meilleur contrôle de la radiation hors-bande du système. Dans la littérature, on trouve plusieurs types de la modulations FBMC basés sur différentes structures. Dans cette thèse, nous ne nous intéressons que sur le schéma de Saltzberg appelé OFDM/OQAM ou FBMC/OQAM. Dans ce schéma, les symboles envoyés sur chaque sous-porteuse sont tirés d'une constellation PAM réelle, et les symboles réels sont envoyés à une cadence de $2/T$. La condition d'orthogonalité est réduite sur l'ensemble des réels uniquement. En conséquence, le symbole démodulé et égalisé est infecté par un terme d'interférence purement imaginaire. Ce terme d'interférence est une combinaison linaire des symboles transmis dans le voisinage du symbole concerné. La présence de cette interférence inhérente cause des difficultés de détection dans certains schéma multi-antennes (MIMO).

L'objectif de cette thèse est d'étudier l'association de la modulation FBMC aux techniques MIMO, à savoir le multiplexage spatiale avec détection de maximum de vraisemblance (ML). Dans un premier temps, nous proposons d'analyser différentes techniques d'annulation d'interférence que nous adaptons au contexte de MIMO-FBMC. Nous montrons que, dans certains cas, nous pouvons bien retirer l'interférence et appliquer la détection ML. Ensuite, nous proposons d'apporter une légère modification dans la modulation FBMC en transmettant des symbole QAM complexes. Evidement, cela brise la condition d'orthogonalité mais nous montrons qu'ainsi la puissance d'interférence sera considérablement réduite. Enfin, nous introduisons un nouveau schéma basé sur la modulation FBMC. Ce schéma, que nous avons baptisé FFT-FBMC, transforme le modèle du système à un modèle équivalent à celui de l'OFDM. Ainsi, n'importe quelle technique multi-antennes pourra être appliquée sans aucune difficulté. D'abord, nous développons le système FFT-FBMC dans un contexte SISO, et puis nous évaluons ces performances dans le contexte MIMO.

Mots clès: OFDM, FBMC, Banc de filtres, Multi-porteuses, MIMO, Détection de Maximum de Vraisemblance, ML, Annulation d'Interférence, Alamouti.

Résumé des travaux de thèse

Introduction

De nos jours, dans un monde de très grande mobilité, la vitesse et la capacité des systèmes de transmissions sont des éléments essentiels afin de pouvoir maintenir les gens du monde entier en communication. Les premiers systèmes de communications numériques était basés sur la modulation mono-porteuse. En général, lorsque l'on veut augmenter le débit d'une transmission, on doit déminuer la durée de symbole. Cependant, la présence d'un canal multi-trajet a comme effet d'introduire de l'interférence inter-symboles (ISI), ce qui nécissite à la réception une égalization complexe. Ainsi, les modulations multi-porteuses [1, 2] ont été proposées en tant que des solutions alternatives afin de contrer les effets des canaux multi-trajets. En effet, les données dans les modulations multi-porteuses sont transmises sur plusieurs fréquences porteuses en divisant ainsi le canal large-bande sélectif en fréquence en plusieurs sous-canaux non-sélectifs en fréquence.

La technique OFDM est la modulation multi-porteuse la plus répandue et elle est utilisée dans nombreux systèmes de communications sans fil tel que WiFi IEEE 802.11, WiMax IEEE 802.16 [2–4], LTE [2, 5], ... ect. La grande popularité de la modulation OFDM vient principalement de:

- Sa grande efficacité spectrale dûe à l'espacement étroit entre ses sous-porteuses orthogonales.
- Sa robustesse aux effets du multi-trajet et sa capacité d'éviter les interférences inter-symboles et inter-porteuses grâce à l'ajout de préfix cyclique (CP).
- Son implémentaient numérique facile et efficace en utilisant l'algorithme de la tranformée de Fourier rapide (FFT).

Néanmoins, malgré ces avantages, la modulation OFDM a quelques inconvénients. Tout d'abord, l'ajout du préfixe cyclique cause une perte en efficacité spectrale car le préfixe cyclique n'est qu'une copie de quelques symboles déjà transmis, ce qui réduit le débit effectif. D'autre part, l'utilisation d'un filtre rectangulaire génère des lobes secondaires importantes, cela veut dire que les signaux transmis sur les bords de la bande sont nuisibles aux autres systèmes occupant les bandes adjacentes [6].

Ces inconvénients ont motivé les chercheurs à développer d'autres solutions alternatives tels que les modulations multi-porteuses à base des bancs de filtres (FBMC) [7, 8]. Dans ce mémoire, nous ne nous intéresserons qu'au schéma de Saltzberg [9] appelé FBMC/OQAM (aussi OFDM/OQAM ou SMT). En fait, la modulation FBMC/OQAM peut faire face à la selectivité en fréquence du canal sans introduire aucun intervalle de garde. En outre,

FBMC utilise un filtre de mise en forme bien localisé en fréquence, ce qui réduit considérablement l'effet de débordement du spectre hors bande. Ainsi, un nombre plus important de sous-porteuses peuvent être utilisées d'une bande allouée. En FBMC/OQAM, chaque sous-porteuse est modulée avec la modulation OQAM, et la condition d'orthogonalité est maintenue dans le domaine réel [10]. En effet, les données transmis sont portées par la partie réelle des symboles reçus, et leurs partie imaginaire représente l'interférence intrinsèque de la modulation FBMC/OQAM.

Ces dernières années, la modulation FBMC a attiré l'attention des chercheurs, et plusieurs algorithmes d'égalisation et détection ont été développés. Il a été démontré dans [11] que le multiplexage spatial peut être directement appliqué à la modulation FBMC lorsque l'on utilise un égaliseur linéaire tel que MMSE ou ZF. Par contre, l'utilisation d'un détecteur de maximum de vraisemblance (ML), ou bien l'application d'un codage spatio-temporel d'Alamouti (STBC), avec la modulation FBMC reste encore un sujet ouvert [12]. En effet, la présence de l'interférence intrinsèque de la modulation FBMC empêche l'application de ces deux techniques MIMO aux systèmes à base du bancs de filtres.

Le principal objectif de cette dissertation est d'analyser et d'étudier l'association de la modulation FBMC avec un système de multiplexage spatial basé sur la détection ML. Nous analysons la possibilité d'annuler l'interférence avant l'application du ML. Ainsi, le plan de la thèse est le suivant:

- Chapitre 2 est dédié à rappeler les notion de bases et donner l'état de l'art des diffèrents concepts nécessaires pour la thèse. Nous commençons par introduire les bases des systèmes multi-antennes. En suite, nous entamons les modulations multi-porteuses OFDM et FBMC. Enfin, nous regarderons en détail le problème de l'association de la modulation FBMC aux quelques systèmes MIMO.

- Dans le chapitre 3, nous proposons quelques schémas de récepteurs basés sur l'estimation et l'annulation de l'interférence intrinsèque. Premièrement, nous proposons un schèma appelé MMSE-ML où l'interférence est estimée via l'égaliseur MMSE. En suite, nous proposons des solutions itératives où l'interférence est réestimée à chaque itération afin d'affiner l'estimation. D'autres schémas seront également proposés qui sont basés sur l'annulation partielle de l'interférence et sur l'utilisation d'un algorithme de Viterbi.

- Dans le chapitre 4, nous proposons d'apporter une modification à la modulation FBMC/OQAM afin de réduire la puissance d'interférence. La modification consiste à transmettre un symbole QAM complexe à chaque période T au lieu de transmettre un symbole PAM réel à chaque demi période $T/2$. Premièrement, nous décrirons en détail notre schéma proposé. En suite, nous adapterons les récepteurs étudiés dans le chapitre précèdent à cette nouvelle approche.

- Dans le 5ième chapitre, nous introduisons un nouveau schéma pour la modulation FBMC. Ce schéma , appelé FFT-FBMC, transforme le modèle de canal à un modèle équivalent à celui de la modulation OFDM. Ainsi, n'importe quelle technique utilisée en OFDM pourra être facilement appliquée au système FFT-FBMC. Dans un premier temps, nous développons le schéma FFT-FBMC dans un contexte SISO; Puis, nous étendrons son application aux système MIMO.

Chapitre 2- Etat de l'art

L'idée principale des modulations multi-porteuses est de deviser le flux des données à transmettre en plusieurs flux d'une cadence $1/T$ inférieure, et transmettre chacun des flux sur un sous-canal diffèrent. Ainsi, chaque signal transmis occupera une bande relativement étroite et subira un évanouissement moins important.

OFDM

La technique OFDM est une modulations multi-porteuse dont les sous-porteuses sont orthogonales malgré que les réponses fréquentielles des sous-canaux se chevauchent entre eux. Supposons qu'un symbole $s_{k,n}$ est à envoyer sur la sous-porteuse k et à l'instant nT. Alors, le signal transmis s'écrit en bande de base comme [13]:

$$s[m] = \frac{1}{\sqrt{M}} \sum_{k=0}^{M-1} \sum_{n} s_{k,n} g[m - nM] e^{j2\pi \frac{km}{M}}, \tag{0.1}$$

où M est le nombre de sous-porteuses et la fonction $g[m]$ est donnée par:

$$g[m] = \begin{cases} 1 & 0 \leq m < M \\ 0 & \text{otherwise} \end{cases} \tag{0.2}$$

Dans un canal parfait, la reconstruction des symboles transmis est assurée grâce à la condition d'orthogonalité:

$$\sum_{m} g[m - nM] g[m - n'M] e^{j2\pi \frac{km}{M}} e^{j2\pi \frac{k'm}{M}} = \delta_{k,k'} \delta_{n,n'} \tag{0.3}$$

L'expression de l'équation (0.1) peut être facilement et efficacement obtenue en utilisant la transformée inverse rapide de Fourier (IFFT). Ainsi, l'algorithme IFFT est appliqué sur chaque vecteur $\mathbf{s}_n = [s_{0,n} \quad s_{1,n} \quad ... \quad s_{M-1,n}]^T$ que l'on appelle un symbole OFDM.

Lorsque le signal est transmis à travers un canal sélectif en fréquence, on observera une interférence entre les symboles du même bloc (symbole OFDM), mais aussi entre les symboles issus de deux symboles OFDM (bloc) successifs. Afin d'éviter cette dernière interférence, un intervalle de garde entre chaque deux symboles OFDM est nécessaire. Cet intervalle de garde doit avoir une longueur supérieure à l'étalement du canal. De plus, il a été démontré [13] qu'en mettant dans cet intervalle de garde une copie des derniers symboles d'un bloc, on parvient à supprimer également l'interférence entre les symboles du même bloc. Ainsi, cet intervalle de garde est baptisé "préfixe cyclique" (CP) [14, 15]. A la réception, le préfixe cyclique est d'abord écarté, et puis l'opération FFT est appliquée sur les symboles restants. En conséquence, le symbole reçu à la sortie du bloc FFT à l'instant n et à la sous-porteuse k est exprimé:

$$r_{k,n} = h_k s_{k,n} + \gamma_{k,n}, \tag{0.4}$$

où $\gamma_{k,n}$ est le terme du bruit et h_k est le $k$ième coefficient de la DFT de la réponse impulsionnelle du canal.

Dans un système de multiplexage spatial avec N_t antennes d'émission et N_r antennes de réception, chaque antenne transmet un symbole diffèrent $s_{k,n}^{(j)}$. A la réception, chaque

antenne reçoit un mélange des tous les signaux transmis par les antennes d'émission, et après la démodulation à la $i$ième antenne de réception, nous obtenons:

$$r_{k,n}^{(i)} = \sum_{j=1}^{N_t} h_k^{(ij)} s_{k,n}^{(j)} + \gamma_{k,n}^{(i)}, \tag{0.5}$$

où $h_k^{(ij)}$ est le coefficient du canal entre l'antenne j d'émission et l'antenne i de réception. Sous forme matricielle, nous pouvons écrire:

$$\begin{bmatrix} r_{k,n}^{(1)} \\ \vdots \\ r_{k,n}^{(N_r)} \end{bmatrix} = \underbrace{\begin{bmatrix} h_{k,n}^{(11)} & \cdots & h_{k,n}^{(1N_t)} \\ \vdots & \ddots & \vdots \\ h_{k,n}^{(N_r1)} & \cdots & h_{k,n}^{(N_rN_t)} \end{bmatrix}}_{\mathbf{H}_{k,n}} \begin{bmatrix} s_{k,n}^{(1)} \\ \vdots \\ s_{k,n}^{(N_t)} \end{bmatrix} + \begin{bmatrix} \gamma_{k,n}^{(1)} \\ \vdots \\ \gamma_{k,n}^{(N_r)} \end{bmatrix}. \tag{0.6}$$

Il y a différentes façons d'égalisation permettant de récupérer les symboles transmis $\{s_{k,n}^{(j)} \setminus j = 1, ..., N_t\}$ à partir des symboles reçus $\{r_{k,n}^{(i)} \setminus i = 1, ..., N_r\}$ en supposant la connaissance des coefficients des canaux données par la matrice $\mathbf{H}_{k,n}$. La plus basique d'entre elles est l'inversion du canal connue sous l'appellation "Forçage à zéro" (ZF). La matrice d'égalisation en ZF est donné par la matrice pseudo-inverse de Moore-Penrose [16]:

$$\mathbf{W}^H = (\mathbf{H}^H\mathbf{H})^{-1}\mathbf{H}^H. \tag{0.7}$$

Donc, les symboles égalisés sont obtenue par:

$$\hat{\mathbf{s}} = \mathbf{W}^H\mathbf{r}. \tag{0.8}$$

L'inconvénient majeur de cette égalisation est que le bruit peut être amplifié lors de la multiplication matricielle par $\mathbf{W}^H$. Afin d'éviter cette amplification, une autre matrice d'égalisation est utilisée:

$$\mathbf{W} = \left(\mathbf{H}\mathbf{H}^H + \frac{\sigma^2}{\sigma_s^2}\mathbf{I}_{N_r}\right)^{-1}\mathbf{H}, \tag{0.9}$$

où σ^2 et σ_s^2 sont respectivement la puissance du bruit et du signal transmis. Cette matrice d'égalisation est obtenue en minimisant l'erreur moyenne quadratique:

$$J(\mathbf{W}) = \mathbb{E}\{\|\mathbf{s} - \mathbf{W}^H\mathbf{r}\|^2\}. \tag{0.10}$$

D'où son appellation "erreur moyenne quadratique minimale" (MMSE). La figure 0.1 présente les performances en BER des deux égaliseurs ZF et MMSE pour différente configurations du SM.

Les deux égaliseurs ci-dessus sont dits linéaire et sont sous-optimales. Le détecteur de maximum de vraisemblance (ML) est un détecteur optimale étant donné qu'il minimise la probabilité d'erreur. Le détecteur ML effectue une recherche exhaustive sur toutes les valeurs possibles que le vecteur $\mathbf{s}_{k,n}$ des symboles émis peut prendre. Ensuite, il choisira le vecteur qui maximise la probabilité de recevoir le vecteur reçu $r_{k,n}$. Lorsque le bruit dans les antennes de réception est Gaussien et indépendant d'une antenne à l'autre, ça revient au même pour le détecteur ML de choisir le vecteur $\hat{\mathbf{s}}_{k,n}$ minimisant la distance Euclidienne:

$$\hat{\mathbf{s}}_{k,n} = \arg\min_{\mathbf{s}_{k,n}}\{\|\mathbf{r}_{k,n} - \mathbf{H}_{k,n}\mathbf{s}_{k,n}\|^2\}. \tag{0.11}$$

Figure 0.2 montre les performance en BER du détecteur ML pour différentes configurations.

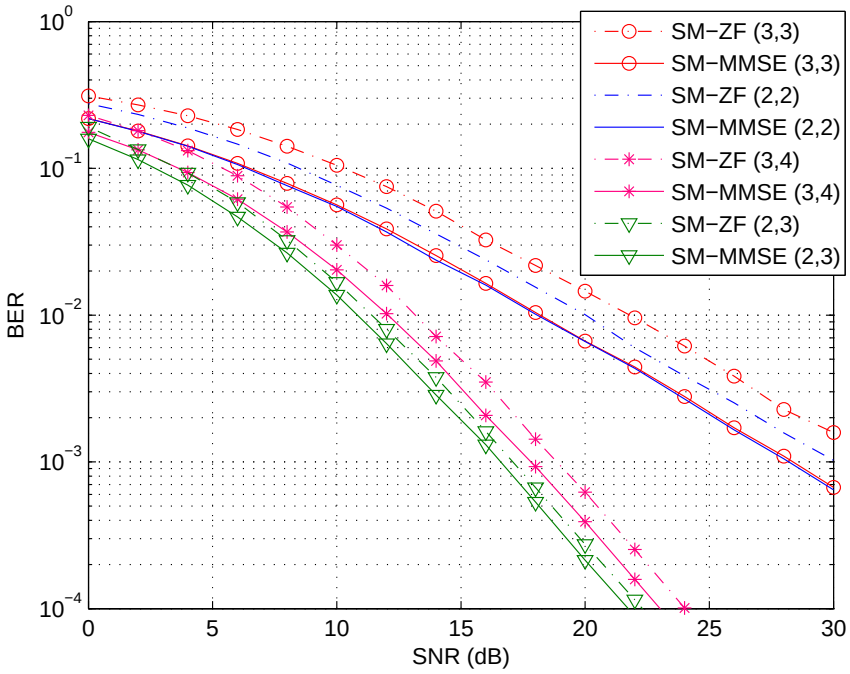

Figure 0.1: Les performances en BER des égaliseurs ZF et MMSE pour différentes configuration du SM en utilisant la constellation QPSK.

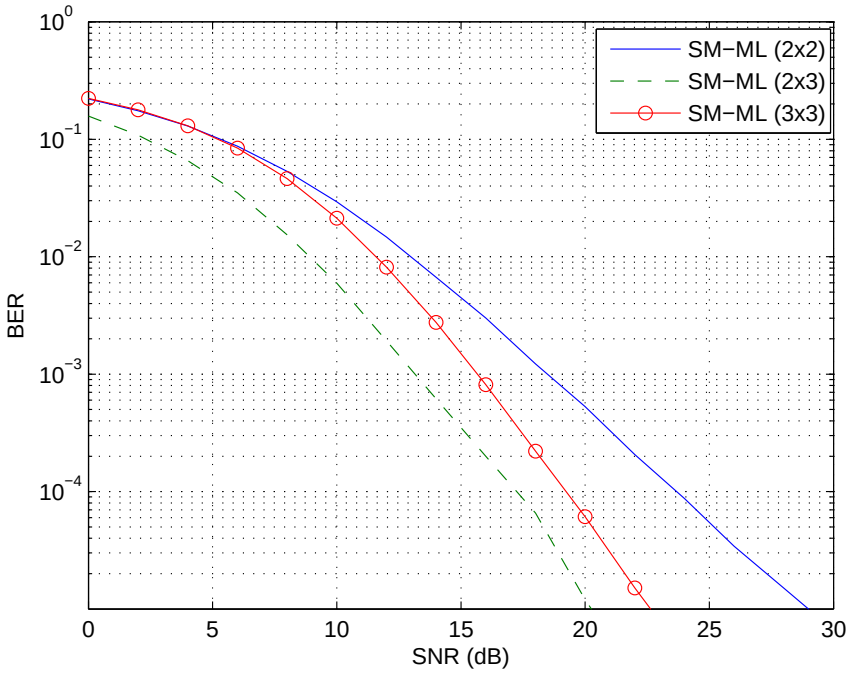

Figure 0.2: Les performances en BER du détecteur ML pour différentes configurations du SM en utilisant la constellation QPSK.

FBMC

L'idée principale de la FBMC/OQAM est de transmettre des symboles offset-QAM (OQAM) au lieu des symboles QAM (Quadrature Amplitude Modulation) conventionnels où un décalage d'une demi-période symbole $T/2$ est introduit entre la partie réelle et la partie imaginaire d'un symbole QAM donné. La seconde spécificité est que le filtre d'émmission utilisé est diffèrent de la fonction porte et s'étale sur plusieurs symboles multi-porteuse. Le signal FBMC numérique en bande de base peut être écrit sous la forme suivante [10]:

$$s[m] = \sum_{k=0}^{M-1} \sum_{n=-\infty}^{+\infty} a_{k,n} g[m - nM/2] e^{j\frac{2\pi k}{M}(m-D/2)} e^{j\phi_{k,n}}, \tag{0.12}$$

où $D/2$ est le terme de retard qui dépend de L_g la longueur du filtre prototype. Le terme de phase $\phi_{k,n}$ garantie le respect de la condition d'orthogonalité réelle [17]. Les symboles $a_{k,n}$ sont tirés d'une constellation PAM réelle. $g[m]$ est la réponse impulsionnelle du filtre prototype. Dans un canal parfait, le signal à la sortie du récepteur s'écrit comme suit:

$$r_{k,n} = \sum_{k'=0}^{M-1} \sum_{n'=-\infty}^{+\infty} a_{k',n'} \sum_{m=-\infty}^{+\infty} g_{k',n'}[m] g^*_{k,n}[m]. \tag{0.13}$$

où

$$g_{k,n}[m] = g[m - nM/2] e^{j\frac{2\pi k}{M}(m-D/2)} e^{j\phi_{k,n}}. \tag{0.14}$$

Ainsi, la condition d'orthogonalité dans un système FBMC/OQAM est donnée par:

$$\Re\left\{ \sum_{m=-\infty}^{+\infty} g_{k',n'}[m] g^*_{k,n}[m] \right\} = \delta_{k,k'} \delta_{n,n'}. \tag{0.15}$$

En présence du canal multi-trajets, le signal reçu s'écrit alors:

$$\begin{aligned} r[m] &= \sum_{l=0}^{L_h-1} h[l] s[m-l] \\ &= \sum_{n=-\infty}^{+\infty} \sum_{k=0}^{M-1} a_{k,n} e^{j\frac{2\pi k}{M}(m-D/2)} e^{j\phi_{k,n}} \underbrace{\sum_{l=0}^{L_h-1} h[l] g\left[m - l - nM/2\right] e^{-j2\pi\frac{kl}{M}}}_{\Theta}, \end{aligned} \tag{0.16}$$

où $h[l]$ est la réponse impulsionnelle du canal. En général, l'étalement du canal L_h est très petit devant la longueur du filtre L_g qui est un multiple M ($L_h \ll L_g = KM$). Cela nous permet de poser l'hypothèse que $g[m - l - nM/2] \approx g[m - nM/2]$ pour $l \in \{0, ..., L_h - 1\}$. Alors, Θ peut être approximé par:

$$\Theta \approx g[m - nM/2] \sum_{l=0}^{L_h-1} h[l] e^{-j2\pi\frac{kl}{M}}. \tag{0.17}$$

Donc nous pouvons écrire:

$$r[m] \approx \sum_{n=-\infty}^{+\infty} \sum_{k=0}^{M-1} h_{k,n} a_{k,n} g_{k,n}[m] + \gamma[m], \tag{0.18}$$

où $h_{k,n} = \sum_{l=0}^{L_h-1} h[l]e^{-j2\pi\frac{kl}{M}}$ et $\gamma[m]$ est le terme du bruit à l'entrée du démodulateur. A la sortie du démodulateur FBMC/OQAM, nous obtenons:

$$\begin{aligned} r_{k,n} &= \sum_{m=-\infty}^{+\infty} r[m]g_{k,n}^*[m] \\ &= \sum_{n'=-\infty}^{+\infty}\sum_{k'=0}^{M-1} h_{k',n'}a_{k',n'} \underbrace{\sum_{m=-\infty}^{+\infty} g_{k',n'}[m]g_{k,n}^*[m]}_{\langle g_{k',n'},g_{k,n}\rangle} + \underbrace{\sum_{m=-\infty}^{+\infty}\gamma[m]g_{k,n}^*[m]}_{\gamma_{k,n}}. \end{aligned} \tag{0.19}$$

Donc, à partir de la condition d'orthogonalité (0.15), nous avons:

$$r_{k,n} = h_{k,n}a_{k,n} + \underbrace{\sum_{(k',n')\neq(k,n)} h_{k',n'}a_{k',n'}\langle g_{k',n'},g_{k,n}\rangle}_{\bar{I}_{k,n}} + \gamma_{k,n}. \tag{0.20}$$

Le filtre prototype est censé être bien localisé dans le domaine temps-fréquence. Alors, il existe un ensemble $\Omega_{k,n}$ tel que $\Omega_{k,n} = \{(k',n')/(k',n') \notin \Omega_{k,n} \Rightarrow \langle g_{k',n'},g_{k,n}\rangle = 0\}$. En supposons que le coefficient du canal est constant sur $\Omega_{k,n}$, nous avons alors:

$$\begin{aligned} \bar{I}_{k,n} &\approx h_{k,n}\sum_{(k',n')\in\Omega_{k,n}^*} a_{k',n'}\langle g_{k',n'},g_{k,n}\rangle \\ &\approx jh_{k,n}u_{k,n}, \end{aligned}$$

où $\Omega_{k,n}^* = \Omega_{k,n} - (k,n)$, et la dernière égalité est obtenue en tenant compte de (0.15); ce qui implique que le terme d'interférence $u_{k,n}$ est purement réel. Enfin, nous pouvons donc écrire:

$$r_{k,n} \approx h_{k,n}(a_{k,n} + ju_{k,n}) + \gamma_{k,n}. \tag{0.21}$$

Si nous considérons un système de multiplexage spatial avec la modulation FBMC/OQAM, les symboles démodulés sont écrits sous forme matricielle:

$$\underbrace{\begin{bmatrix} r_{k,n}^{(1)} \\ \vdots \\ r_{k,n}^{(N_r)} \end{bmatrix}}_{\mathbf{r}_{k,n}} = \underbrace{\begin{bmatrix} h_{k,n}^{(11)} & \cdots & h_{k,n}^{(1N_t)} \\ \vdots & \ddots & \vdots \\ h_{k,n}^{(N_r1)} & \cdots & h_{k,n}^{(N_rN_t)} \end{bmatrix}}_{\mathbf{H}_{k,n}} \underbrace{\begin{bmatrix} a_{k,n}^{(1)} + ju_{k,n}^{(1)} \\ \vdots \\ a_{k,n}^{(N_t)} + ju_{k,n}^{(N_t)} \end{bmatrix}}_{\mathbf{a}_{k,n}+j\mathbf{u}_{k,n}} + \underbrace{\begin{bmatrix} \gamma_{k,n}^{(1)} \\ \vdots \\ \gamma_{k,n}^{(N_r)} \end{bmatrix}}_{\gamma_{k,n}}. \tag{0.22}$$

Donc pour appliquer un égaliseur ZF ou MMSE, nous multiplions d'abord le vecteur reçu par la matrice d'égalisation correspondante, puis nous prenons sa partie réelle [11].

Par contre, à cause de la présence des termes d'interférence, l'application d'un détecteur ML directement sur le vecteur reçu est impossible, car ces termes d'interférence dépendent des symboles transmis dans le voisinage et leurs valeurs est aléatoires. Dans la suite de la thèse, nous étudions la possibilité d'estimer et d'annuler cette interférence intrinsèque d'une façon itérative.

Chapitre 3 - Annulation d'interférence et détection ML dans un système de multiplexage spatial basé sur la modulation FBMC

Avant d'entamer les différentes techniques d'annulation d'interférence, nous essayons d'abord d'étudier les performances que nous pouvons avoir si l'interférence instrinsèque est complète-

ment retirée. Dans ce cas, le signal reçu après que l'interférence soit retirée peut s'écrire en forme matricielle:

$$\mathbf{y} = \mathbf{Ha} + \mathbf{n}, \tag{0.23}$$

où le vecteur $\mathbf{a}$ est à valeurs réels bien évidement. Le vecteur $\mathbf{a}$ prend ses valeurs d'une constellation PAM de taille $\sqrt{q}$. L'énergie de chaque symbole de $\mathbf{a}$ est de $E_s/2$. Pour le calcul du BER en fonction de SNR, nous pouvons utiliser la méthode décrite dans [18] où nous aurons à calculer le paramètre α' pour ce modèle. Nous avons:

$$\alpha' = q^{-\frac{N_t}{2}} \sum_m \sum_j \sum_i a_{s_m,ij}^{-N_r}. \tag{0.24}$$

Pour un système de multiplexage spatial en OFDM, nous obtenons:

$$\alpha = q^{-N_t} \sum_m \sum_j \sum_i a_{s_m,ij}^{-N_r}. \tag{0.25}$$

Ainsi, pour une même valeur de BER en FBMC et OFDM, nous aurons le rapport des SNR (respectivement γ_{c_2} et γ_{c_1}) suivant:

$$\frac{\gamma_{c_2}}{\gamma_{c_1}} = \frac{1}{2} \sqrt[N_r]{\frac{\alpha}{2\alpha'}}. \tag{0.26}$$

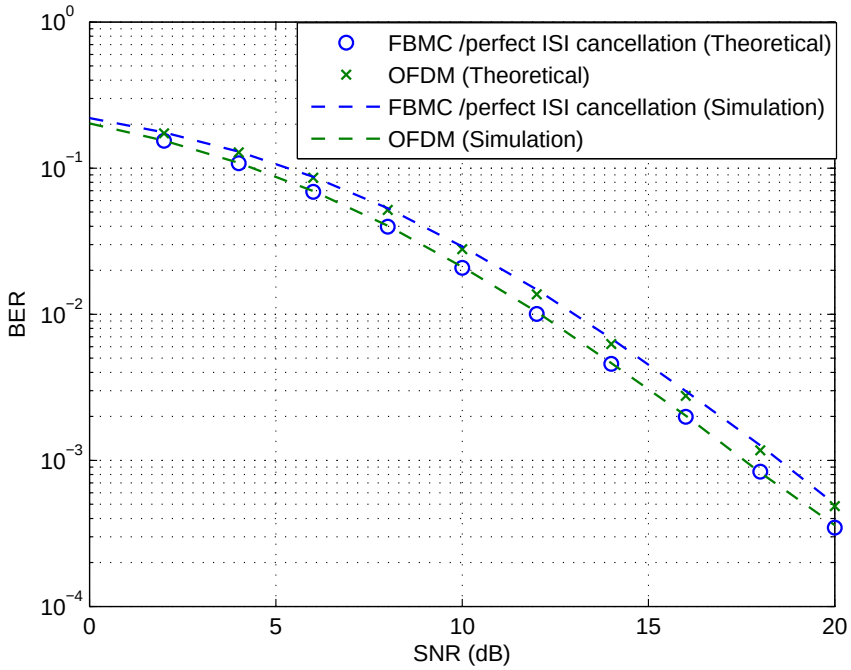

Figure 0.3: Illustation du gain potential en SNR d'un système FBMC sur l'OFDM dans un schéma SM de 2×2

Pour une modulation QPSK et un système MIMO 2×2, nous avons $\alpha = \frac{541}{144}$ et $\alpha' = \frac{5}{16}$, donc $G = 10 \log_{10}(\frac{\gamma_{c_2}}{\gamma_{c_1}}) \approx 0.88\ dB$. Dans la figure 0.3, nous illustrons le gain en SNR que peut avoir un système FBMC par rapport au l'OFDM.

Détecteur MMSE-ML

Le premier détecteur proposé dans cette thèse est le MMSE-ML. L'idée de base de ce schéma est d'estimer l'interférence est de soustraire sa contribution du signal reçu, et puis d'appliquer le détecteur ML en supposant que le nouveau vecteur des symboles reçu est sans interférence. Vu que l'égaliseur MMSE peut être adapté à la modulation FBMC/OQAM sans dégrader les performances, nous avons opté à l'utiliser pour l'estimation d'interférence. En effet, puisque le terme d'interférence est la partie imaginaire qui accompagne le symbole égalisé, l'estimation se fait alors par l'extraction de la partie imaginaire des symboles à la sortie de l'égaliseur MMSE. Une fois cette interférence est estimée, sa contribution est retirée des signaux reçus. Nous obtenons alors le vecteur suivant:

$$\begin{aligned}\mathbf{y}_{k,n} &= \mathbf{r}_{k,n} - j\mathbf{H}_{k,n}\tilde{\mathbf{u}}_{k,n}, \\ &= \mathbf{H}_{k,n}(\mathbf{a}_{k,n} + j(\mathbf{u}_{k,n} - \tilde{\mathbf{u}}_{k,n})) + \mathbf{n}_{k,n}, \\ &= \mathbf{H}_{k,n}(\mathbf{a}_{k,n} + j\epsilon_{k,n}) + \mathbf{n}_{k,n}, \end{aligned} \tag{0.27}$$

où $\tilde{\mathbf{u}}_{k,n}$ est le vecteur des termes d'interférence estimé. En supposant que le vecteur d'erreur d'estimation $\epsilon_{k,n}$ a une faible valeur, nous considérons que le vecteur $\mathbf{y}_{k,n}$ est sans interférence, et nous appliquons le détecteur ML. Evidement, cette hypothèse n'est pas tout à fait exacte, car il y a toujours une probabilité d'erreur non nulle lors de l'égalisation MMSE. Ainsi, nous noue attendons que les performances de ce récepteur MMSE-ML ne soient optimales. La figure 0.4 montre les performances du récepteur MMSE-ML, MMSE et celui du Genie-Aided (Supposant que l'interférence est parfaitement annulée) avec deux configuration MIMO: 2×2 et 4×4.

Comme nous l'avons signaler auparavant, la solution MMSE-ML est sous optimale car ces performances en BER sont encore loin de celles du Genie-Aided. Par contre, nous remarquons qu'il y a une amélioration en performance par rapport à l'égaliseur MMSE. Nous tenons à souligner que l'avantage de ce récepteur est qu'il n'introduise pas du retard dans le traitement puisque l'interférence est immédiatement estimée à la sortie de l'égaliseur MMSE.

Détecteur Rec-ML

Le récepteur Rec-ML que nous proposons dans cette section est basé sur le MMSE-ML. En fait, nous avons vu que le MMSE-ML présente des performances sous optimales, mais il améliore la probabilité d'erreur par rapport à l'égaliseur MMSE. Donc, l'idée principale est de se servir des symboles décidés à la sortie de MMSE-ML afin de réestimer le terme d'interférence sur chaque antenne de réception. En effet, puisque nous connaissons la réponse impulsionnelle du transmultiplexeur du système FBMC/OQAM, nous pouvons alors estimer l'interférence si nous avons une estimation sur les symboles transmis dans le voisinage du point en considération. Le schéma en bloc du Rec-ML est donné dans la figure 0.5. Les performances en BER obtenues avec le récepteur Rec-ML sont présentées dans la figure 0.6 avec un système de multiplexage spatial 2×2.

Nous remarquons que là encore le récepteur est sous optimale et n'atteint pas les performances du Genie-Aided. Nous tenons à préciser que l'opération peut être refaite plusieurs fois afin d'améliorer les performances d'une façon itérative, mais les simulations montrent que

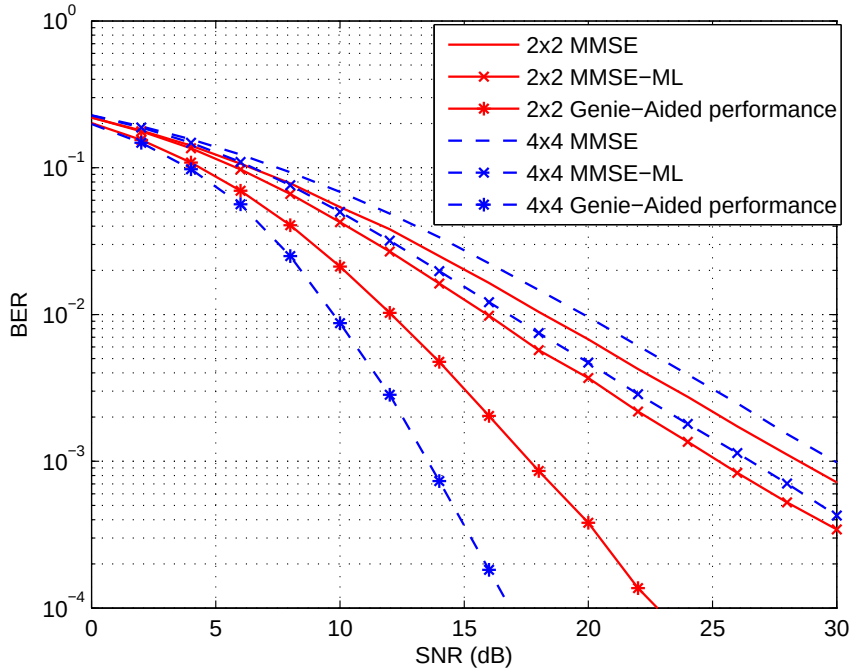

Figure 0.4: Performances en BER du récepteur MMSE-ML comparé à MMSE et au Genie-Aided dans un SM 2×2 et SM 4×4.

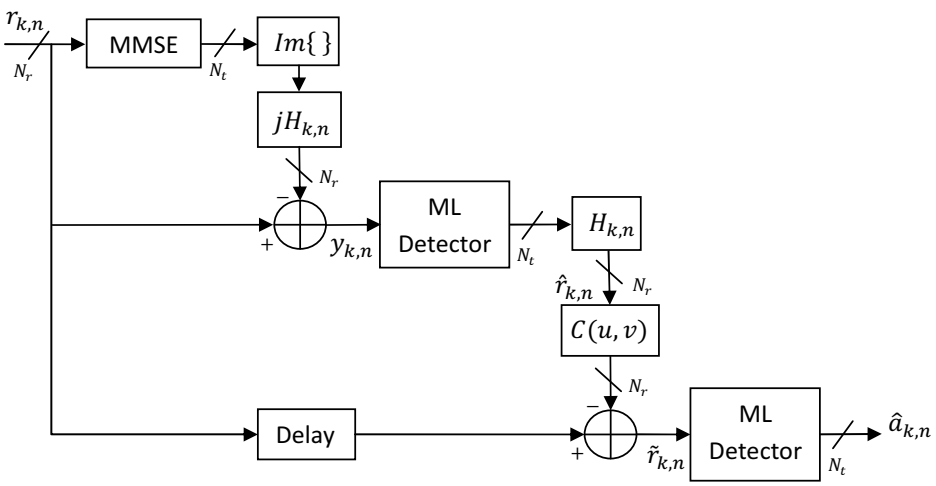

Figure 0.5: Schéma de base du récepteur Rec-ML

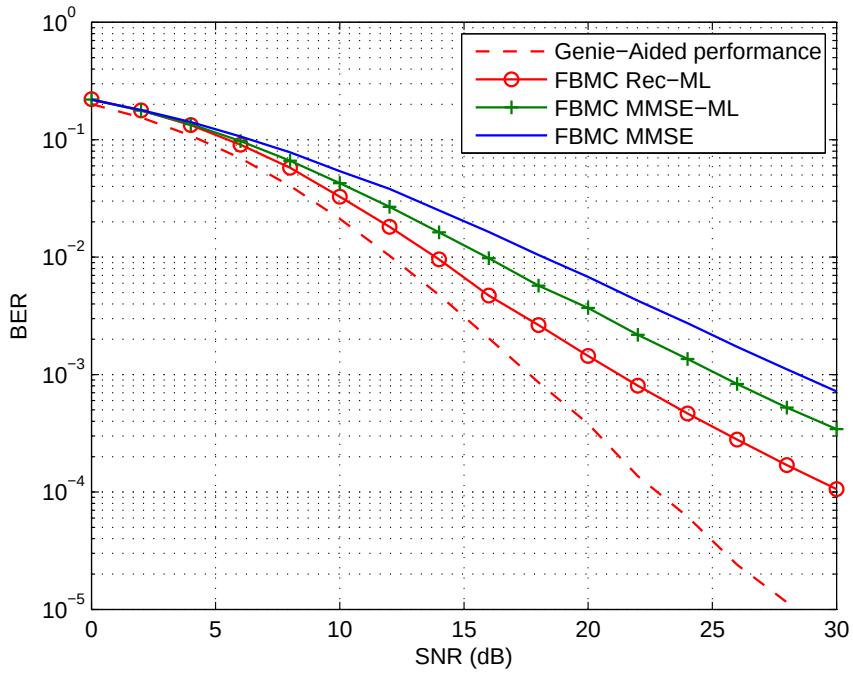

Figure 0.6: Performance en BER du Rec-ML comparé à MMSE, MMSE-ML et au Genie-Aided dans un SM 2×2.

le système souffre de la propagation d'erreur. Cet effet de la propagation d'erreur est causé essentiellement du fait que la variance d'interférence est importante comparée à la variance des données elles-mêmes; en FBMC/OQAM nous savons que la puissance d'interférence est égale à celle des données.

L'écart en performance qui est entre le Genie-Aided et le Rec-ML peut être réduit si nous considérons le codage des données. Dans la figure 0.7 et 0.8, nous présentons les performances de Rec-ML, MMSE-ML et OFDM avec le codage convolutif (171,133) respectivement dans un canal de modèle Ped-A et Veh-A.

Nous remarquons que lorsque nous utilisons le codage, le récepteur Rec-ML donne les mêmes performances que celles données par l'OFDM.

Détecteur PaIC-Viterbi

En se basant sur la conclusion de la section précédente, nous cherchons à éviter la propagation d'erreur. Pour cela, il faut que l'interférence concernée par l'estimation et l'annulation successive ait une puissance relativement petite par rapport à la puissance des données. Ainsi, nous proposons dans cette section un récepteur effectuant une suppression partielle de l'interférence et le reste d'interférence est traité par un algorithme de Viterbi. L'algorithme de Viterbi est connu d'être un algorithme optimal mais avec une complexité qui augmente exponentiellement avec le nombre de taps. Donc, nous sommes devant un dilemme: En réduisant la taille de Viterbi nous diminuons le coût d'implémentation, mais la variance d'interférence concernée par l'annulation ne sera pas suffisamment petite. D'autre part, si

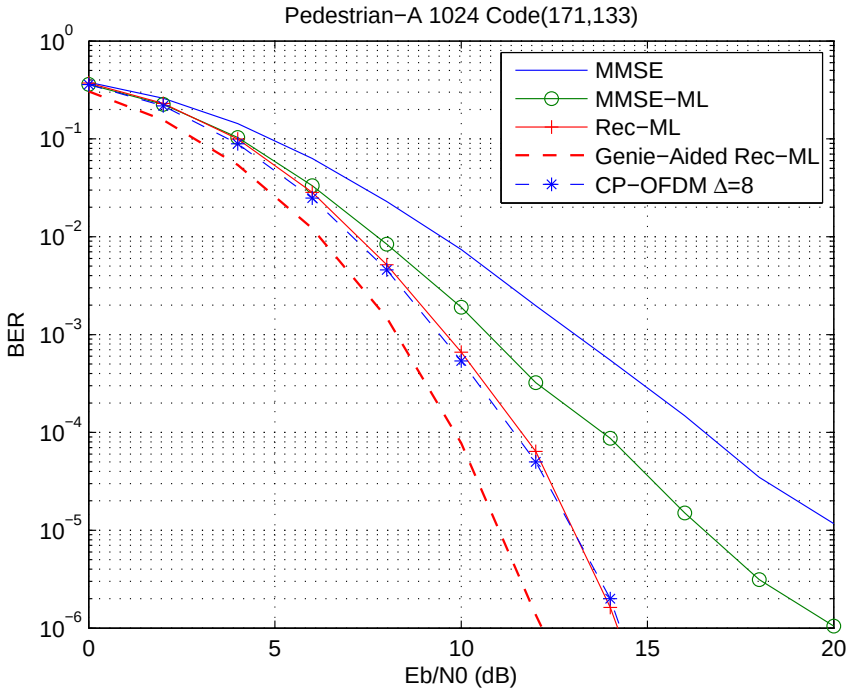

Figure 0.7: Comparaison des performances en BER entre le CP-OFDM et l'FBMC pour MIMO 2×2 avec Ped.-A

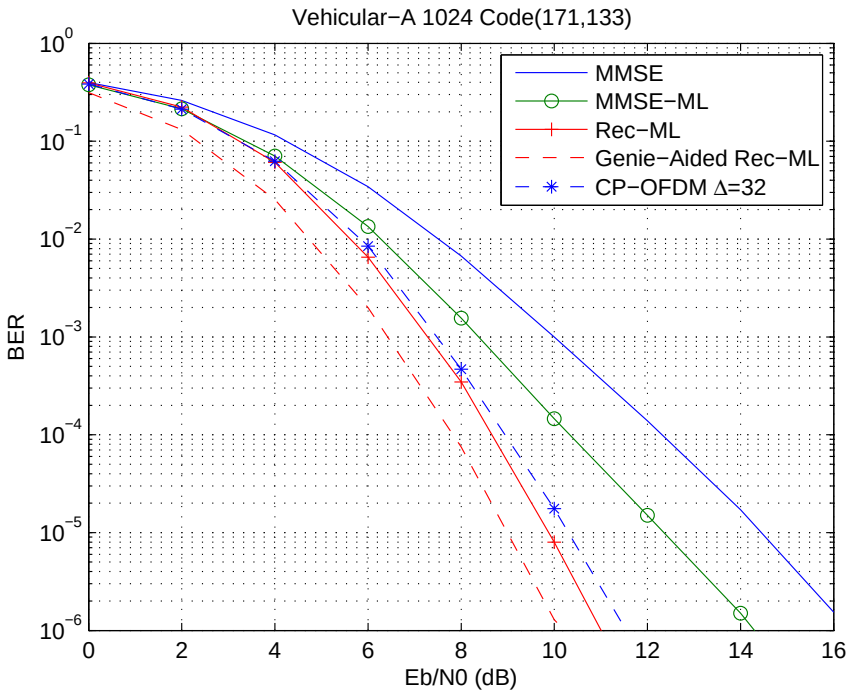

Figure 0.8: Comparaison des performances en BER entre le CP-OFDM et l'FBMC pour MIMO 2×2 avec le canal Veh.-A

nous augmentons la taille de Viterbi, le coût d'implémentation sera élevé. Pour cela, nous devons choisir un Viterbi qui engloberai les coefficients d'interférence les plus importants. Nous avons choisi alors 3 configuration selon le choix du Vterbi; les fonctions définissant l'algorithme de Viterbi sont :

$$f_0^{(1)}(a_{k,n}) = a_{k,n}, \tag{0.28}$$

$$f_0^{(2)}(a_{k,n}, a_{k,n-1}) = a_{k,n} + \Gamma_{0,-1} \times a_{k,n-1}, \tag{0.29}$$

et

$$f_0^{(3)}(a_{k,n+1}, a_{k,n}, a_{k,n-1}) = \Gamma_{0,1} a_{k,n+1} + a_{k,n} + \Gamma_{0,-1} a_{k,n-1}, \tag{0.30}$$

où $\Gamma_{k,n}$ sont les terme d'interférence. Les résultats de simulations sont présentés dans la figure 0.9. Nous comparons les performances des 3 configurations choisies dans un système de multiplexage spatial 2×2. Nous remarquons que la configuration qui donne des performances

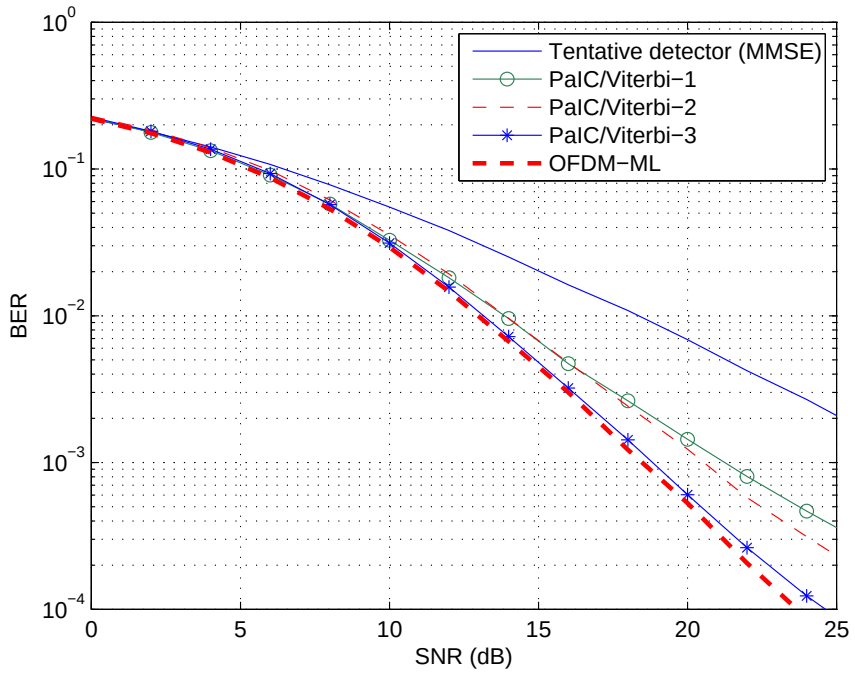

Figure 0.9: Performances de PaIC/Viterbi pour SM 2×2

satisfaisantes est le PaIC/Viterbi-3 dont le Viterbi a une taille de 3. La complexité de ce système peut être quand même réduite en optant à une variante du Viterbi tel que l'algorithme de M.

Chapitre 4 - Annulation d'interférence dans la modulation FBMC/QAM

Nous avons vu dans le chapitre précédant que lorsque la variance d'interférence n'est pas suffisamment petite, le récepteur itératif annulant l'interférence souffre de l'effet de la propagation d'erreur. D'autre part, nous avons vu aussi qu'en FBMC/OQAM la puissance d'interférence est la même que celle des données transmises. Donc, une annulation

d'interférence globale n'est pas possible. Dans ce chapitre, nous proposons une modification dans la modulation FBMC afin de réduire l'interférence intrinsèque et espérer que sa variance sera ainsi suffisamment petite pour qu'il n'y ait pas une propagation d'erreur. Ainsi, nous avons proposé d'abandonner la modulation OQAM qui nous garantissait l'orthogonalité réelle, et de transmettre des symboles tirés de la constellation QAM. Evidement, cela implique que nous perdrons la condition d'orthogonalité, mais de point de vu d'un détecteur ML, cette condition n'est pas importante puisqu'il effectue une recherche exhaustive sur toutes les possibilités.

Détecteur IIC-ML

L'utilisation des symboles QAM à la place des symboles OQAM dans un système FBMC implique que les échantillons aux instants multiples impairs de $T/2$ sont à zéros. Cela veut dire que les coefficients d'interférence dans les instants impairs sont annulés. Cela diminue considérablement la puissance d'interférence [19]. Evidement, la réduction d'interférence est selon le filtre prototype utilisé. Nous démontrons facilement que lorsque le filtre prototype IOTA est utilisé, nous baisserons la variance d'interférence jusqu'à 40%, tandis que nous allons jusqu'à 18% lorsque le filtre prototype de PHYDYAS est utilisé.

Le signal FBMC/QAM transmis sera donc:

$$s[m] = \sum_{k=0}^{M-1} \sum_{n \in \mathbf{Z}} s_{k,n} g[m - nM] e^{j\frac{2\pi k}{M}(m-\frac{D}{2})} e^{j\phi_{k,2n}}, \tag{0.31}$$

où les symboles $s_{k,n}$ sont QAM complexes. Le terme de phase $\phi_{k,2n}$ peut être abandonné puisque dans cette modulation nous n'aurons plus besoin de l'orthogonalité. A la sortie du démodulateur, le symbole complexe $s_{k,n}$ sera accompagné d'un terme d'interférence complexe lui aussi. Ainsi, même si nous égaliserons le canal, la détection sera tout de même erronée. Pour cela, il faut d'une manière itératif estimer l'interférence et l'annuler. Dans la figure 0.10 nous montrons les performances du récepteur IIC pour chaque itération utilisant le filtre prototype IOTA.

Nous observons que les performances sont mauvaises et qu'elles convergent vers une courbe sous-optimale. Finalement, pour le filtre IOTA la variance d'interférence n'est pas suffisamment réduite. Les performances relatives au filtre prototype PHYDYAS sont présentées dans la figure 0.11. Cette fois ci, nous remarquons que les performances convergent vers l'optimum. Nous déduisons de cela que la réduction de la variance d'interférence jusqu'à 18% est suffisante pour qu'il n'y ait plus de propagation d'erreurs.

Dans un système de multiplexage spatial, nous aurons à la réception après la démodulation, le vecteur suivant:

$$\underbrace{\begin{bmatrix} r_{k,n}^{(1)} \\ \vdots \\ r_{k,n}^{(N_r)} \end{bmatrix}}_{\mathbf{r}_{k,n}} = \underbrace{\begin{bmatrix} h_{k,n}^{(11)} & \cdots & h_{k,n}^{(1N_t)} \\ \vdots & \ddots & \vdots \\ h_{k,n}^{(N_r 1)} & \cdots & h_{k,n}^{(N_r N_t)} \end{bmatrix}}_{\mathbf{H}_{k,n}} \underbrace{\begin{bmatrix} s_{k,n}^{(1)} + I_{k,n}^{(1)} \\ \vdots \\ s_{k,n}^{(N_t)} + I_{k,n}^{(N_t)} \end{bmatrix}}_{\mathbf{s}_{k,n}+\mathbf{I}_{k,n}} + \underbrace{\begin{bmatrix} b_{k,n}^{(1)} \\ \vdots \\ b_{k,n}^{(N_r)} \end{bmatrix}}_{\mathbf{b}_{k,n}}, \tag{0.32}$$

où le terme d'interférence $\mathbf{I}_{k,n}$ est complexe comme ils le sont les symboles transmis. Cela implique que les égaliseurs linéaires tel que le ZF et MMSE ne pourront plus être appliqués

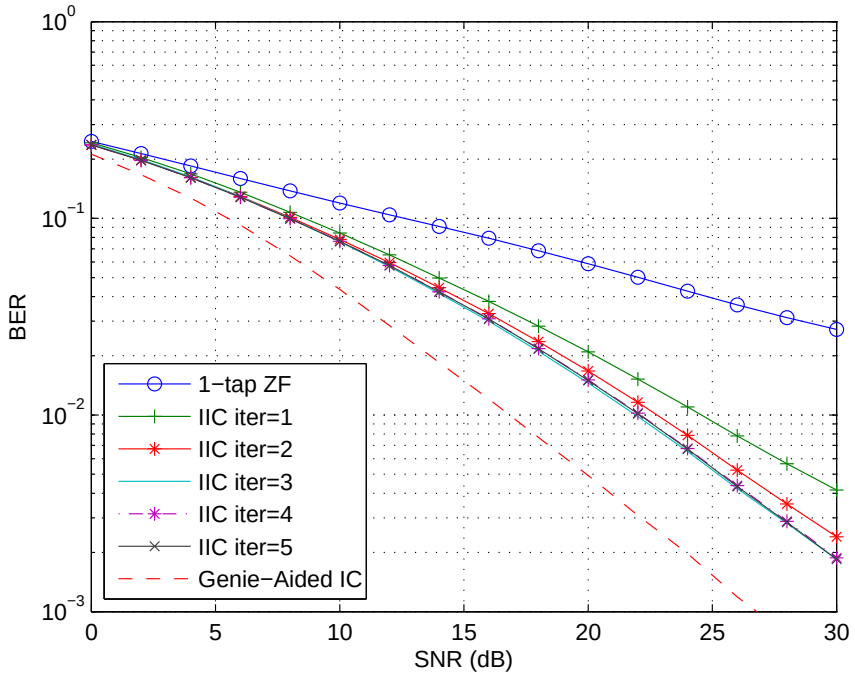

Figure 0.10: Performances de IIC de FBMC/QAM utilisant le filtre IOTA pour un système SISO

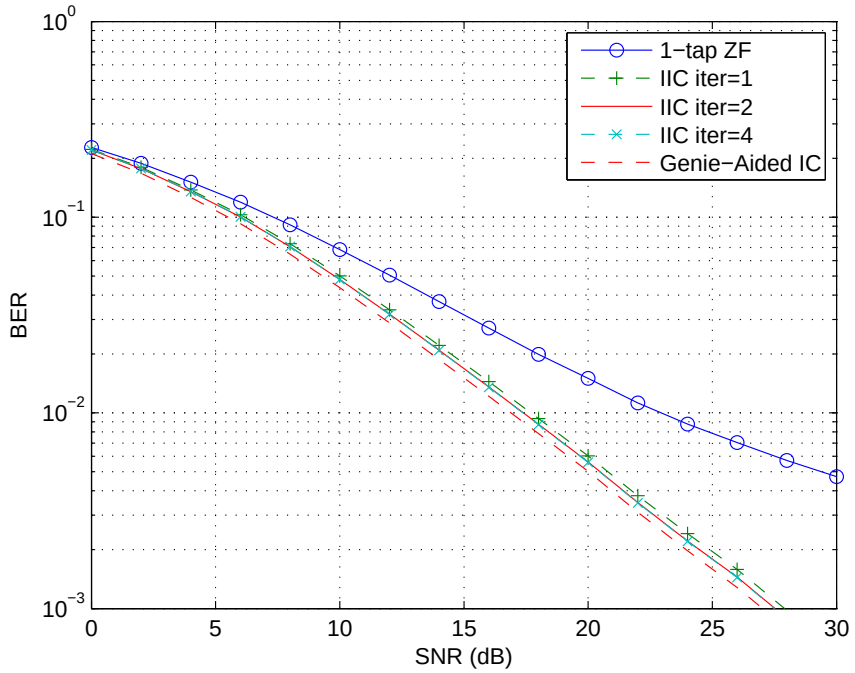

Figure 0.11: Performances de IIC de FBMC/QAM utilisant le filtre PHYDYAS pour un système SISO

directement. Donc, pour cette modulation FBMC/QAM nous proposons un récepteur IIC-ML qui utilise dès la première itération un détecteur ML pour tenter estimer les symboles envoyés. En se basant sue ces décisions, le récepteur estimera alors l'interférence et annule sa contribution du vecteur reçu juste après le démodulateur FBMC/QAM. Cette opération est refaite plusieurs fois jusqu'à la convergence. La figure 0.12 nous montre maintenant les performances du récepteur IIC-ML pour chaque itération et celles de Rec-ML (pour l'FBMC/OQAM) en utilisant le filtre PHYDYAS. Tous comme dans le cas SISO, les per-

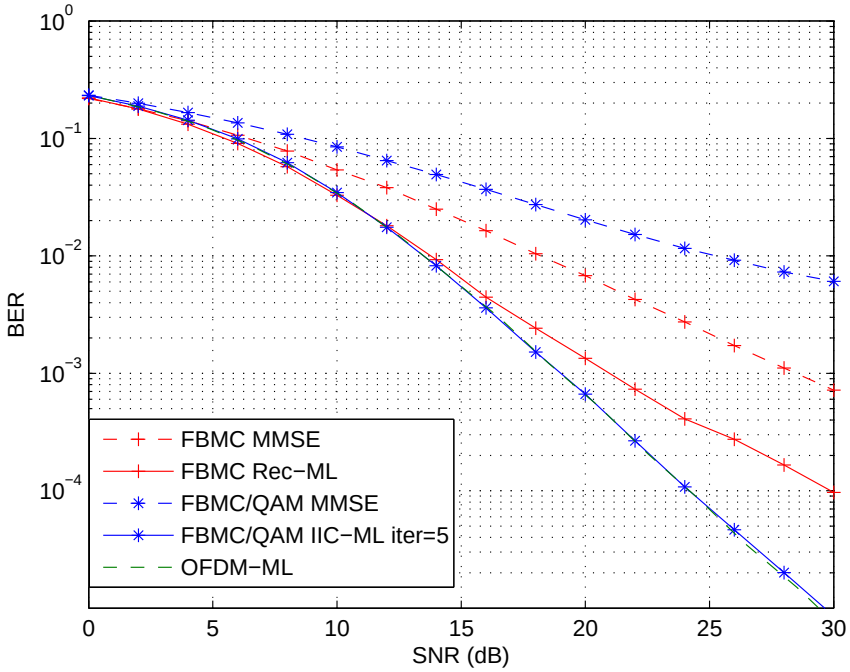

Figure 0.12: Comparaison de performances entre le Rec-ML de FBMC/OQAM et le IIC-ML de FBMC/QAM utilisant le filtre PHYDYAS pour SM 2×2

formances de IIC-ML convergents vers l'optimum. Nous pouvons voir aussi la différence en performance entre le récepteur Rec-ML pour le FBCM/OQAM et le IIC-ML. Pour le filtre IOTA, les performances sont présentées dans la figure 0.13. Pareil que le cas SISO, le récepteur IIC-ML souffre de la propagation d'erreurs.

Détecteur PaIC-Viterbi

Comme dans la modulation FBMC/OQAM, nous allons tester l'algorithme PaIC/Viterbi avec 3 différentes tailles de Viterbi. Donc, nous devons sélectionner les trois plus grands coefficients pour les inclure dans le détecteur de Viterbi. Evidement, puisque les symboles de données en FBMC/QAM sont envoyés chaque période T, la réponse impulsionnelle de transmultiplexeur sera différentes. Il se trouve que pour les deux filtres prototypes IOTA et PHYDYAS les trois plus grands coefficients sont allignés sur l'axe des fréquences contrairement au cas de la modulation FBMC/OQAM. Cela veut dire que l'algorithme de Viterbi sera appliqué sur chaque symbole multi-poreuse séparément. De point de vue de

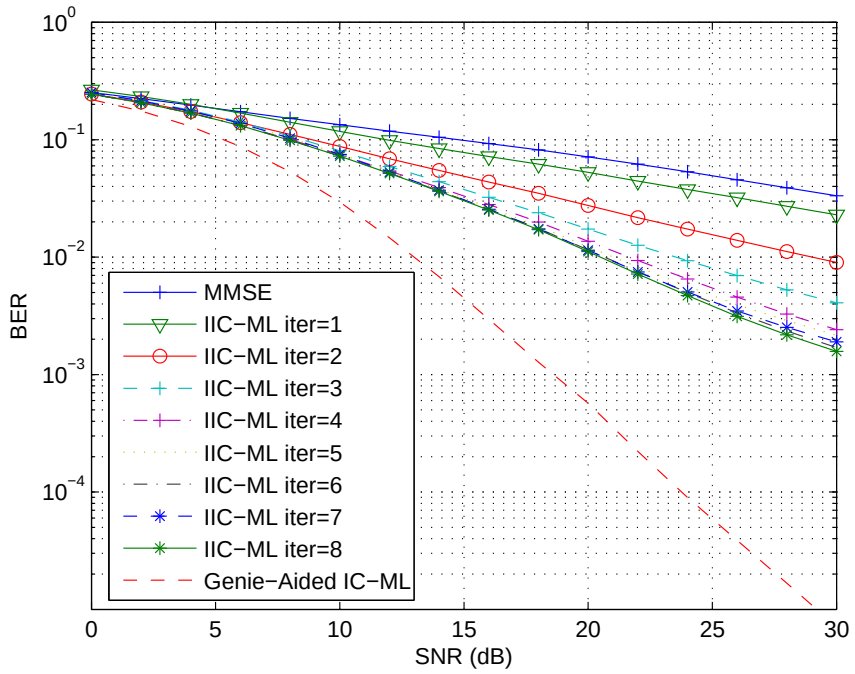

Figure 0.13: Performances de IIC-ML avec FBMC/QAM utilisant le filtre IOTA pour SM 2×2

la complexité d'implémentation, le PaIC/Viterbi est moins coûteux avec la modulation FBMC/QAM qu'avec la modulation FBMC/OQAM. Dans la figure 0.14 nous montrons les performances obtenues avec le PaIC/Viterbi-3 utilisant le filtre IOTA. Nous remarquons que les performances convergent vite vers une courbe sous-optimale. La puissance d'interférence résiduelles de ce schéma est de 0.0065, ce qui explique la rapidité de la convergence. Par contre, la sous-optimalité de ce récepteur réside dans le fait que la séquence d'erreur ayant la plus petite distance Euclidienne est celle qui contient 3 ou 4 erreurs. Nous notons une perte en SNR de 1.5 dB environ. Quant au filtre PHYDYAS, nous pouvons voir dans la figure 0.15 que les performances de PaIC/Viterbi-3 convergent rapidement vers l'optimum. La puissance d'interférence résiduelle est de 0.0626.

Quant au récepteur PaIC/Viterbi-2, Les performances sont présentées dans la figure 0.16 pour le filtre IOTA, et dans la figure 0.17 pour le filtre PHYDYAS. Nous remarquons encore que le récepteur PaIC/Viterbi-2 souffre de la propagation d'erreur lorsque le filtre IOTA est utilisé. Cela est dû au fait que la puissance d'interférence résiduelle n'est pas suffisamment petite (0.2 environ). Lorsque le filtre PHYDYAS est utilisé, la puissance d'interférence résiduelle est de 0.12 environ, ce qui a permis au récepteur PaIC/Viterbi-2 d'annuler presque complètement l'interférence au bout de trois itérations.

Donc comme nous venons le remarquer, les performances des récepteurs et schémas proposés sont fortement liées au choix du filtre prototype.

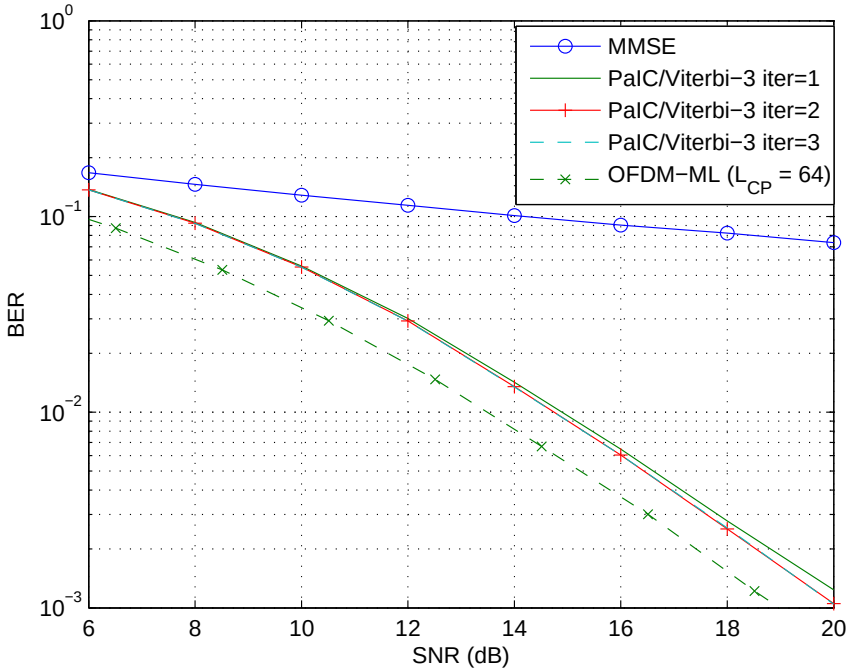

Figure 0.14: Performances en BER du récepteur PaIC/Viterbi-3 utilisant la modulation FBMC/QAM et le filtre IOTA.

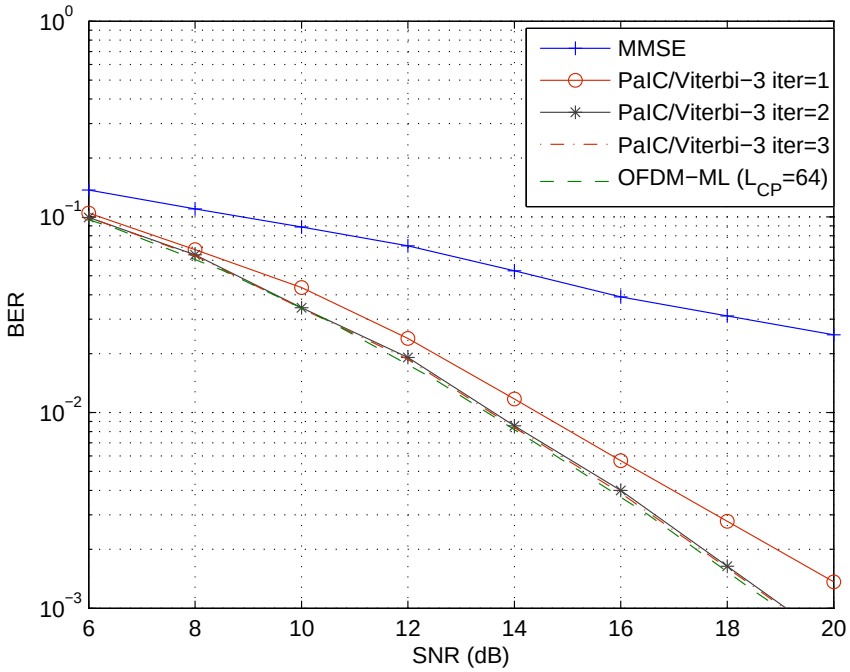

Figure 0.15: Performances en BER du récepteur PaIC/Viterbi-3 utilisant la modulation FBMC/QAM et le filtre PHYDYAS.

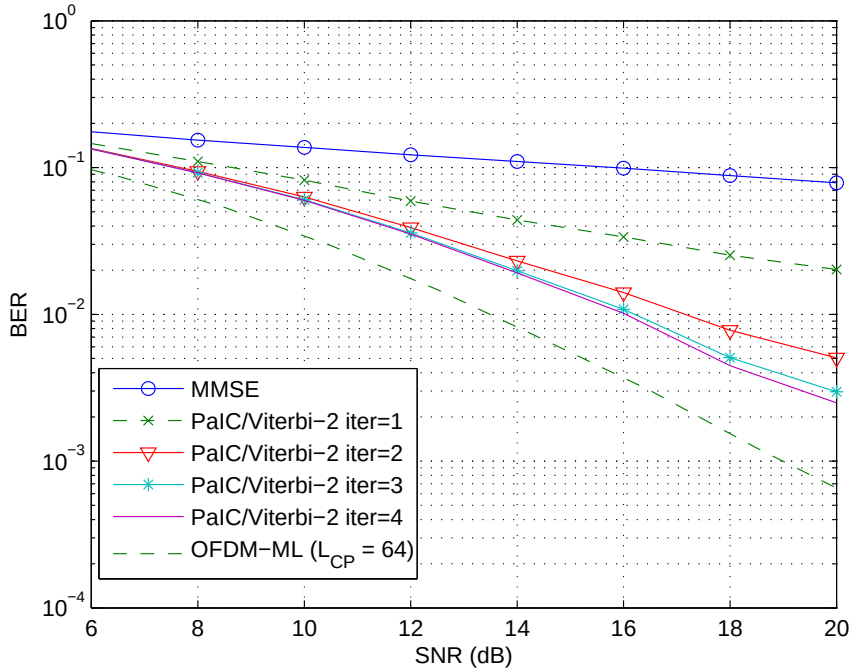

Figure 0.16: Performances en BER du récepteur PaIC/Viterbi-2 utilisant la modulation FBMC/QAM et le filtre IOTA.

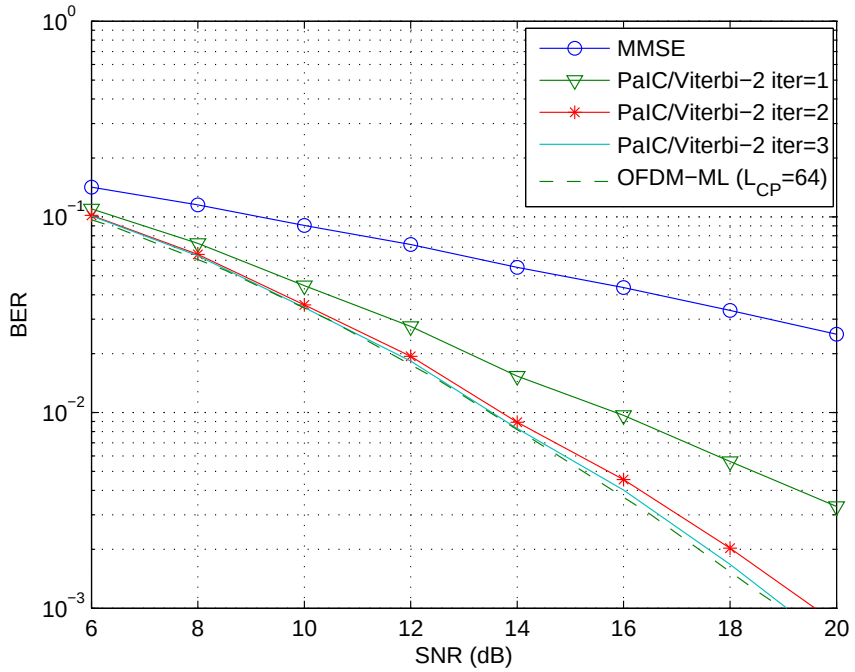

Figure 0.17: Performances en BER du récepteur PaIC/Viterbi-2 utilisant la modulation FBMC/QAM et le filtre PHYDYAS.

Chapitre 5 - Un nouvelle modulation basée sur les bancs de filtres

Dans ce chapitre, nous allons proposé une nouvelle modulation multi-porteuses basée sur les bancs de filtres. Ce schéma requiert une stratégie ou agencement spécial de transmission. Supposons d'abord que la réponse impulsionnelle du transmultiplexeur est limitée à une sous-porteuse de part et d'autre. Les symboles envoyés sur une même sous-porteuse sont convulés avec la réponse centrale du multiplexeur. Ainsi, on peut considérer que le signal reçu sur une sous-porteuse est la somme de trois signaux filtrés par 3 filtres diffèrents:

$$r_{k,n} \cong \underbrace{\sum_{i=-\Delta}^{\Delta} f_0^{(k)}(i) a_{k,n-i}}_{t_k} + \underbrace{\sum_{i=-\Delta}^{\Delta} f_1^{(k-1)}(i) a_{k-1,n-i}}_{t_{k-1}} + \underbrace{\sum_{i=-\Delta}^{\Delta} f_{-1}^{(k+1)}(i) a_{k+1,n-i}}_{t_{k+1}}, \tag{0.33}$$

Donc, comme en OFDM, nous pouvons éviter l'interférence inter-symboles en utilisant des IDFT/DFT de taille N et un préfixe cyclique. Si on suppose que le CP est suffisamment grand, on peut écrire:

$$Y_{k,n} \cong \underbrace{F_{0,n}^{(k)} d_{k,n}}_{T_k} + \underbrace{F_{1,n}^{(k-1)} d_{k-1,n}}_{T_{k-1}} + \underbrace{F_{-1,n}^{(k+1)} d_{k+1,n}}_{T_{k+1}}. \tag{0.34}$$

où

$$Y_{k,n} = \frac{1}{\sqrt{N}} \sum_{n'=0}^{N-1} r_{k,n'} e^{\frac{-j2\pi nn'}{N}},$$

$$d_{k,n} = \frac{1}{\sqrt{N}} \sum_{n'=0}^{N-1} a_{k,n'} e^{\frac{-j2\pi nn'}{N}},$$

et

$$F_{j,n}^{(k)} = \sum_{n'=-\frac{N}{2}}^{\frac{N}{2}-1} f_j^{(k)}(n') e^{\frac{-j2\pi nn'}{N}}.$$

La figure 0.18 montre le schéma de base du système proposé. Nous l'avons appelé FFT-FBMC. Donc, comme le montre l'équation (0.34), la seule interférence qui reste est l'interférence inter-porteuses. Les données $d_{k,n}$ sont multipliées alors par le coefficient $F_{0,n}^{(k)}$. La figure 0.19 montre l'évaluation du coefficient $F_{0,n}^{(k)}$ en fonction de n pour des valeurs de k paire et impaire.

Nous remarquons donc que dans une moitié de l'intervalle, les données sont amplifiées, et dans l'autre motié, elles sont amorties. Nous remarquons également que les intervalles ci-dessus sont intervertis lorsque nous incrémentons ou décrémentons l'indice de sous-porteuse k. D'où l'agencement que nous proposons: Sur une sous-porteuse donnée k, nous transmettons les données sur l'intervalle amplifié et nous mettons des zéros sur l'intervalle amorti. Donc sur la sous-porteuse $k+1$, nous faisons la même chose et les données sont alors transmis uniquement sur l'intervalle opposé par rapport à la sous-porteuse k. Afin de garantir

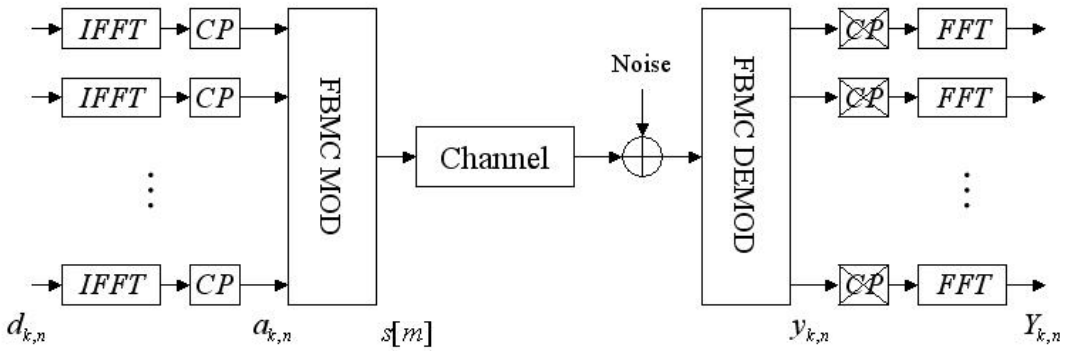

Figure 0.18: Le schéma de base du FFT-FBMC.

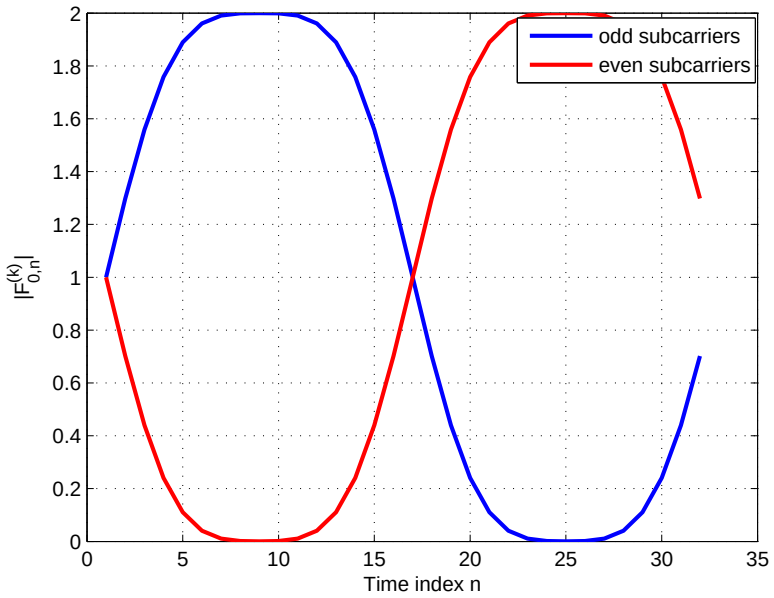

Figure 0.19: L'amplitude de $F_{0,n}^{(k)}$ en fonction de n dans un bloc de données.

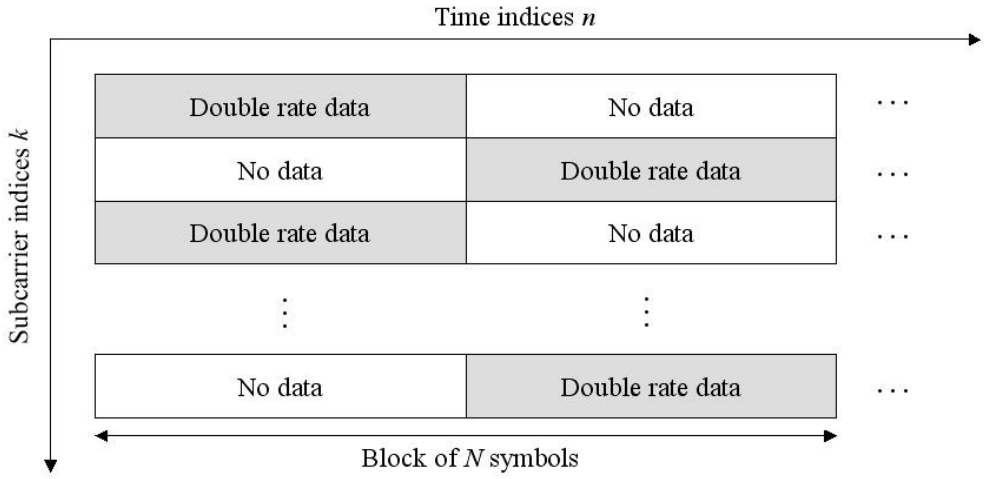

Figure 0.20: L'agencement de la transmission d'un bloc de données dans la FFT-FBMC.

le même débit, les données envoyées doivent être complexes au lieu d'être réelles. La figure 0.20 explique l'agencement proposé. Ainsi, les données reçues sur une sous-porteuse k n'aura pas d'interféreur, car à cet intervalle sur la sous-porteuse $k-1$ ou $k+1$, il n'y a que des zéros. Finalement, nous pouvons écrire:

$$Y_{k,n} \cong \begin{cases} F_{0,n}^{(k)} d_{k,n} & n \in \Omega^{(k)} \\ F_{1,n}^{(k_1)} d_{k-1,n} + F_{-1,n}^{(k+1)} d_{k+1,n} & n \notin \Omega^{(k)} \end{cases} \tag{0.35}$$

où $\Omega^{(k)}$ est l'intervalle d'amplification. Dans la présence du canal, nous pouvons montré que:

$$Y_{k,n} \cong h_{k,n} F_{0,n}^{(k)} d_{k,n} + \Gamma_{k,n} \tag{0.36}$$

Les analyses théorique menées dans cette thèse montrent que le rapport signal à bruit (SNR) à la sortie du démodulateur est presque le même que celui à l'entrée du modélateur. Donc, le démodulateur n'introduit pas du perte en SNR. Nous avons montré aussi que ce schéma offre un plus grand confinement spectral du signal transmis. Nous avons pu montré facilement que le le spectre du signal transmis en bande de base s'écrit comme suit:

$$A(\nu) = \frac{\sigma_d^2}{N(N+L)} \sum_{l=0}^{\frac{N}{2}-1} \frac{\sin\left(\frac{X_l(\nu)(N+L)}{2}\right)^2}{\sin\left(\frac{X_l(\nu)}{2}\right)^2}. \tag{0.37}$$

La figure 0.21 donne la comparaison entre les spectres des signaux de FFT-FBMC et celui de FBMC classique. Nous remarquons que le spectre du FFT-FBMC est plus confiné que celui de FBMC.

Evidement, un des plus grand inconvénient de système est l'introduction d'un CP sur chaque sous-porteuse. Nous avons montré que nous pouvons réduire cette intervalle de garde, voir le retirer. Mais, bien sûr au détriment de la présence d'interférence. Nous avons montré

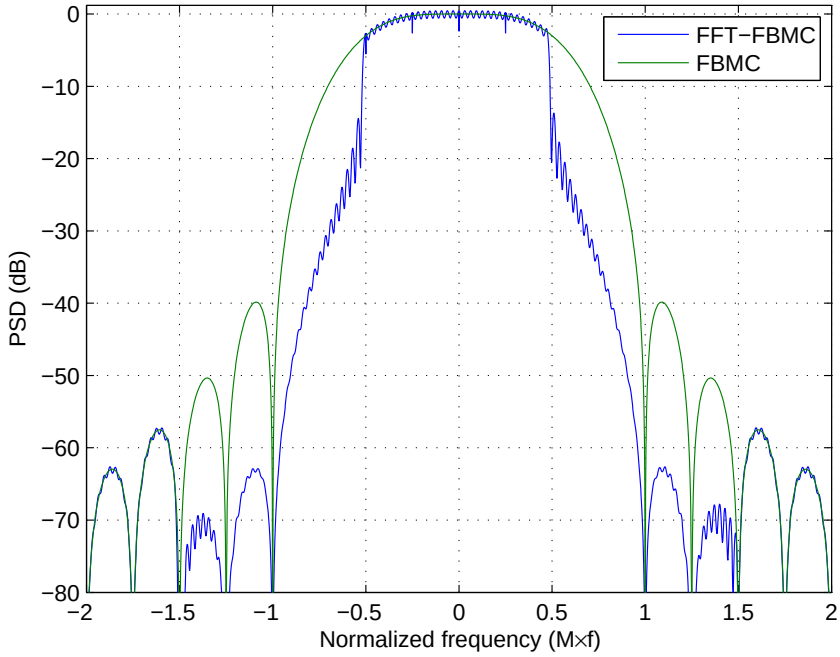

Figure 0.21: Comparaison entre la DSP des signaux de FBMC et FFT-FBMC ($N = 64$,$L = 4$) utilisant le filtre PHYDYAS.

que dans les pire des cas (lorsque il n'y a pas de CP), le rapport de signal à interférence (SIR) avoisine les 16 dB pour les deux filtres prototypes PHYDYAS et IOTA. Par contre, dans les meilleurs cas, le SIR de FFT-FBMC avec PHYDYAS tend vers l'infinie, alors que dans le cas du filtre IOTA, le SIR est saturé à 27 dB.

Finalement donc, nous avons pu rendre le système basé sur les bancs de filtres équivalent à un système OFDM avec un seul tap. Cela implique que toutes les technique utilisées dans OFDM peuvent être appliquées sans problème. Donc, pour un système de multiplexage spatial, nous avons l'équation suivante:

$$\mathbf{Y}_{k,n} = F_{0,n}^{(k)} \mathbf{H}_{k,n} \mathbf{d}_{k,n} + \mathbf{\Gamma}_{k,n},$$

où les élement en gras de cette équation sont des vecteurs et sauf $\mathbf{H}_{k,n}$ qui est la matrice du canal. Puisque le terme d'interférence ne parait plus dans cet équation, donc le détecteur ML pourra être appliqué facilement. Pareil pour le schéma de codage Alamouti.

Résultats de simulations

Dans cette section, nous allons voir les performances obtenues avec le système FFT-FBMC en terme de BER en fonction de SNR. Nous supposons que le récepteur a une parfaite connaissance du canal. Le nombre de sous-porteuses pour les simulations est de $M = 512$. La période d'échantillonnage est de $T_s = 100$ ns, et la fréquence porteuse est de $f_c = 2.5$ GHz.

Pour le shcéma FFT-FBMC, nous avons considéré plusieurs configurations correspon-

dantes à $(N, L) \in \{16, 32, 64\} \times \{0, 2\}$. Quant au OFDM, la taille du CP est adapté au modèle de canal. La perte en efficacité spectrale est définie par $\mu = \frac{L}{N+L}$ pour le FFT-FBMC et par $\mu = \frac{L_{CP}}{M+L_{CP}}$ pour l'OFDM.

Concernant le multiplexage spatial avec détection ML, nous testons la modulation FFT-FBMC dans la configuration de MIMO 2×2. Dans les figures 0.22 et 0.23 nous montrons les performances de FFT-FBMC avec un canal Ped-A et une constellation QPSK, respectivement, en utilisant le filtre de PHYDYAS et IOTA. nous remarquons que lorsque $L = 0$,

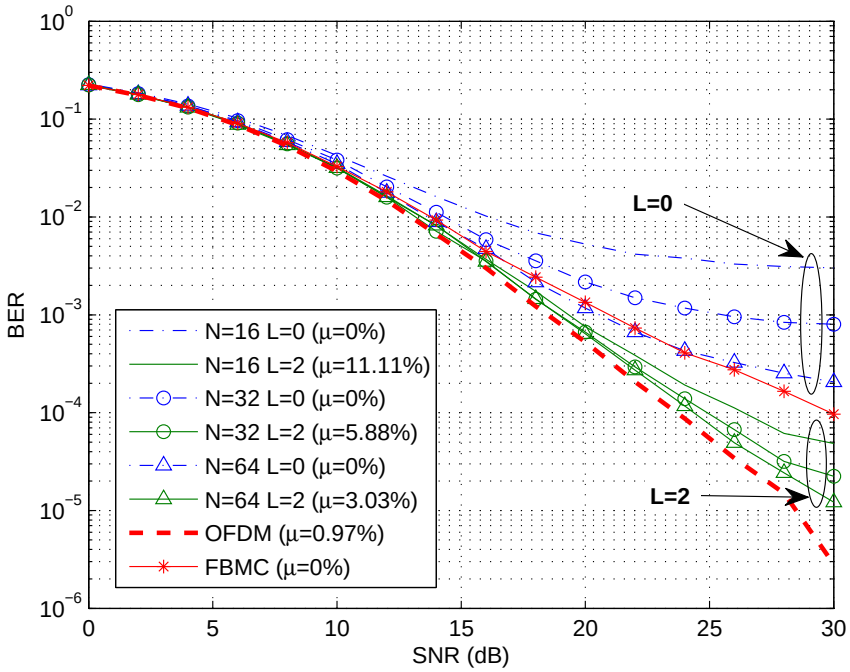

Figure 0.22: Performances de FFT-FBMC utilisant le filtre PHYDYAS avec spatial multiplexing (2×2) et QPSK dans le canal Ped-A.

les performances de FFT-FBMC sont mauvaises et souffrent de l'effet de palier de BER. Tandis qu'avec $L = 2$, les performances sont meilleurs. Evidement aussi, les performances s'améliorent avec l'augmentation de N. La différence qu'on peut constater entre le filtre IOTA et PHYDYAS est que les performances pour IOTA et $L = 2$ ne changement pas en fonction de N. Cela est expliqué par le fait que le SIR est saturé dans le cas de IOTA lorsque en augmente L.

Dans la figure 0.24, nous montrons les performance de FFT-FBMC avec le filtre IOTA dans le canal Veh-A, où nous trouvons que nous obtenue presque les performances que dans le canal Ped-A.

Nous avons également tester le FFT-FBMC/PHYDYAS avec la modulation 16QAM. Les performances obtenues dans le canal Ped-A et Veh-A sont présentées respectivement dans la figure 0.25 et 0.26. Nous remarquons que dans ce cas l'effet du palier de BER est plus accentué.

Concernant le codage Alamouti, nous présentons ses performances avec FFT-FBMC dans un canal Ped-A avec le filtre IOTA et PHYDYAS respectivement dans les figures 0.27

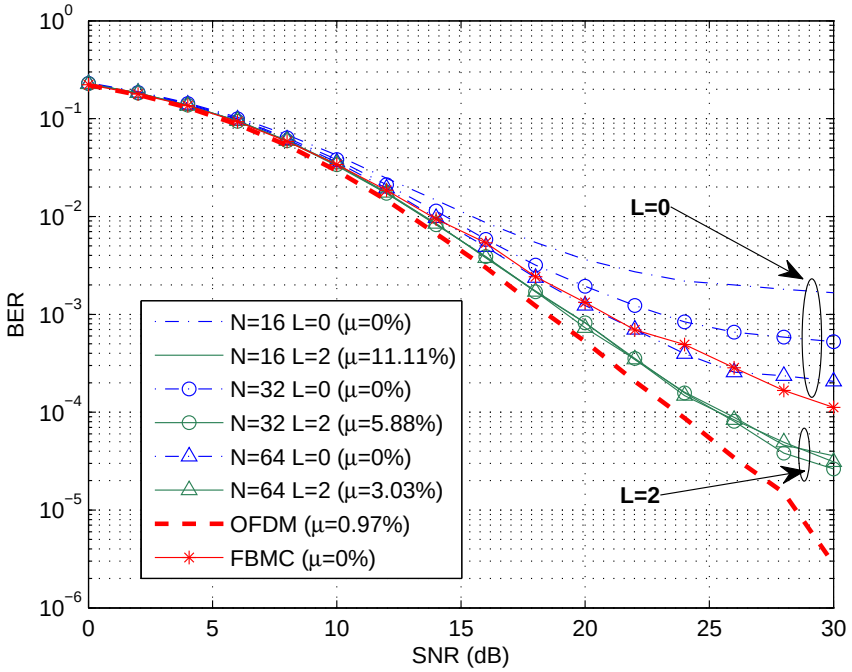

Figure 0.23: Performances de FFT-FBMC utilisant le filtre IOTA avec spatial multiplexing (2×2) et QPSK dans le canal Ped-A.

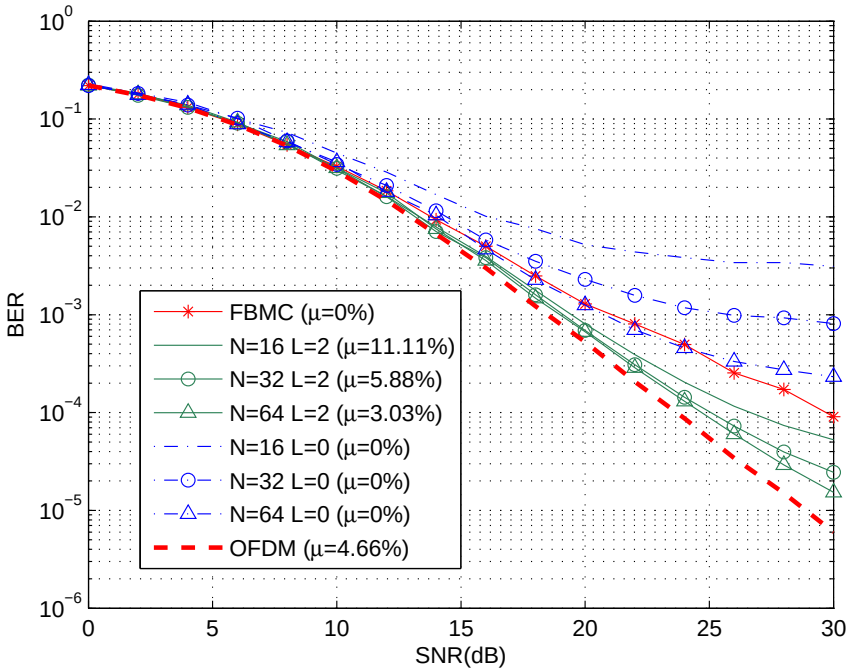

Figure 0.24: Performances de FFT-FBMC utilisant le filtre PHYDYAS avec le multiplexage spatial (2×2) et la modulation QPSK dans le canal Veh-A.

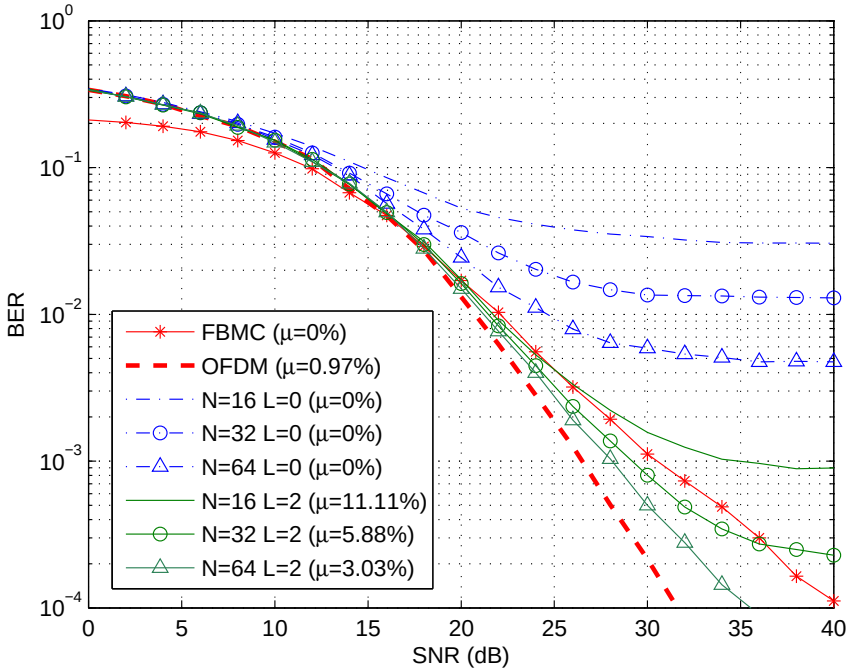

Figure 0.25: Performances de FFT-FBMC utilisant le filtre PHYDYAS avec le multiplexage spatial (2×2) et la modulation 16-QAM dans le canal Ped-A.

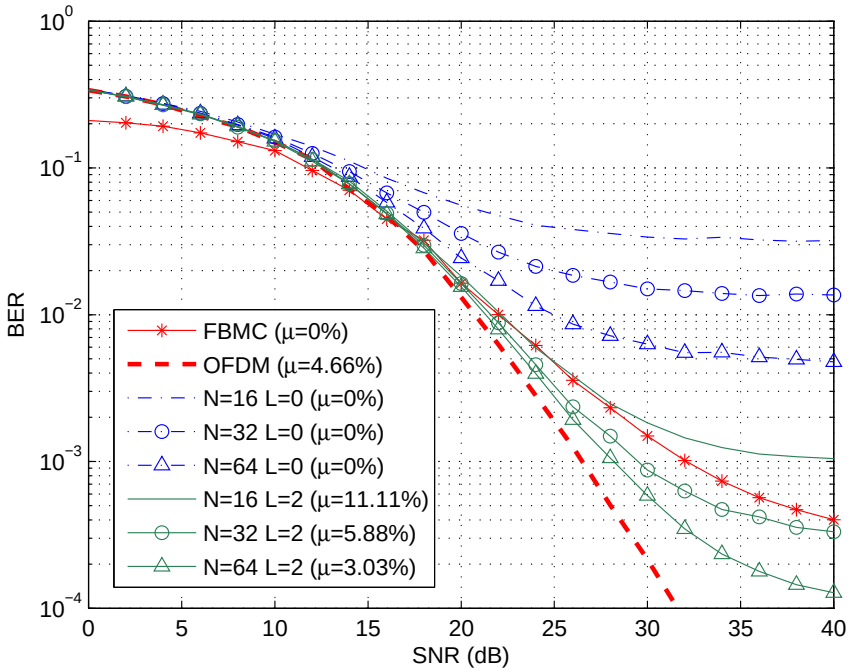

Figure 0.26: Performances de FFT-FBMC utilisant le filtre PHYDYAS avec le multiplexage spatial (2×2) et la modulation 16-QAM dans le canal Veh-A.

et 0.28. Nous constatons que presque dans tous les configurations, les performances sont presque identiques à celle de l'OFDM sauf dans le cas du filtre IOTA avec $(N, L) = (16, 0)$.

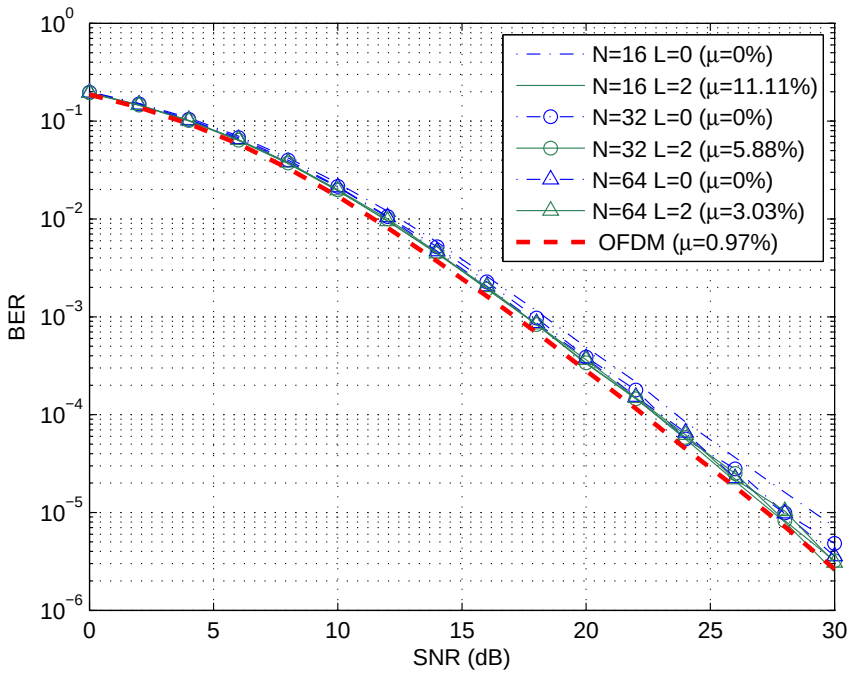

Figure 0.27: Performances de FFT-FBMC utilisant le filtre IOTA avec Alamouti (2×1) et la modulation QPSK dans le canal Ped-A.

Chapitre 6 - Conclusions

Nous avons abordé dans cette thèse le problème de l'association de la modulation FBMC avec quelques techniques MIMO telle que le multiplexage spatial avec détection ML et le codage spatio-temporelle de Alamouti. Nous avons vu que la modulation FBMC génère une interférence intrinsèque qui empêche l'application de ces deux techniques évoquées supra. Premièrement nous avons proposé d'estimer et d'annuler l'interférence, nous avons proposé plusieurs schémas pour cela. Les plus importants sont le MMSE-ML et le Rec-ML. Cependant, nous avons constaté que ces deux schémas sont sous-optimaux à cause de la propagation d'erreur qui survient surtout lorsque la variance de l'interférence à supprimer est relativement importante. Donc, nous avons cherché à trouvé une méthode pour la réduction de l'interférence. Ainsi, nous avons proposé de modifier la modulation FBMC/OQAM en transmettant des symboles QAM au lieu des symboles OQAM (ou deux fois PAM). Nous avons prouvé que cette modification permet de réduire l'interférence, et ainsi nous avons testé les schéma développés précédemment avec la nouvelle modulation FBMC/QAM. Nous avons vu que les schémas basés sur l'annulation itérative d'interférence offrent des meilleurs performances et ne souffrent pas de la propagation d'erreurs. Finalement, nous avons aussi proposé un tout autre schéma de modulation basé sur FBMC, à savoir le FFT-FBMC. Cette technique effectue des DFT et IDFT sur les symboles de chaque sous-porteuse avant

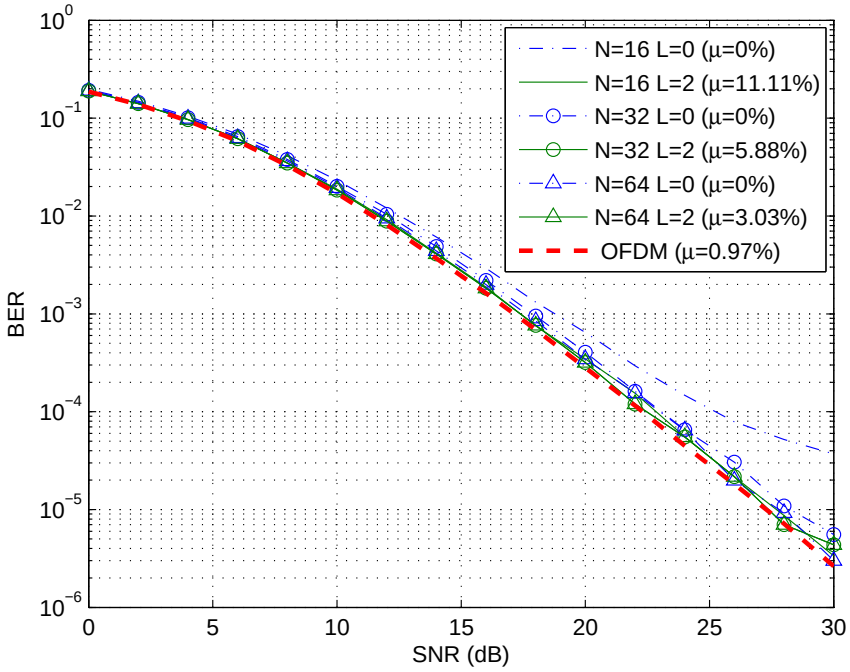

Figure 0.28: Performances de FFT-FBMC utilisant le filtre PHYDYAS avec Alamouti (2×1) et la modulation QPSK dans le canal Ped-A.

de les moduler avec le FBMC. Un agencement de transmission est aussi proposé pour éliminer complètement l'interférence intrinsèque. Ainsi, le modèle équivalent de ce schéma est celui de l'OFDM. Donc, n'importe quelle technique utilisée en OFDM pourra être appliquée d'une façon simple en FFT-FBMC. Ainsi, nous avons tester cette nouvelle modulation avec le multiplexage spatial avec la détection ML et avec le codage Alamouti. Nous avons vu que globalement cette technique offre les même performances que celle obtenues en OFDM.

Contents

List of Figures

List of Tables

Nomenclature

Abbreviations and Acronyms

ADSL	Asymmetric Digital Subscriber Line
APP	A Posteriori Probability
AWGN	Additive White Gaussian Noise
BER	Bit Error Rate
BPSK	Binary Phase Shift Keying.
CDMA	Code Division Multiple Access
CMT	Cosine modulated MultiTone
CP	Cyclic Prefix
CSI	Channel State Information
DFE	Decision Feedback Equalization
DVB	Digital Video Broadcasting
DFT	Discrete Fourier Transform
EGF	Extended Gaussian Function
FBMC	Filter Bank based MultiCarrier
FFT	Fast Fourier Transform
FIR	Finite Impulse Response
FMT	Filtered MultiTone
i.i.d.	independent and identically distributed
IC	Interference Cancellation
ICI	Inter-Carrier-Interference
IDFT	Inverse Discrete Fourier Transform
IEEE	Institute of Electrical and Electronics Engineers
IFFT	Inverse Fast Fourier Transform
IIC	Iterative Interference Cancellation
IOTA	Isotropic Orthogonal Transfer Algorithm
ISI	Inter-Symbol-Interference
LLR	Log Likelihood Ratio
LTE	Long Term Evolution
MC	Multicarrier
MIMO	Multiple-Input Multiple-Output
MISO	Multiple-Input Single-Output
ML	Maximum Likelihood

MLD	Maximum Likelihood Detection
MMSE	Minimum Mean Square Error
MRC	Maximum Ratio Combining.
MSE	Mean Square Error
OFDM	Orthogonal Frequency Division Multiplexing
OQAM	Offset Quadrature Amplitude Modulation
PaIC	Partial Interference Cancellation
PAM	Pulse Amplitude Modulation
PDF	Probability Density Function
Ped	Pedestrian
PHYDYAS	PHYsical layer for DYnamic spectrum AccesSand cognitive radio
PPN	PolyPhase Network
PSD	Power Spectral Density
QAM	Quadrature Amplitude Modulation
QPSK	Quadrature Phase Shift Keying
SIC	Successive Interference Cancellation
SINR	Signal-to-Interference-plus-Noise Ratio
SIR	Signal-to-Interference Ratio
SISO	Single-Input Single-Output
SIMO	Single-Input Multiple-Output
SM	Spatial Multiplexing
SMT	Staggered MultiTone
SNR	Signal-to-Noise Ratio
SRRC	Square Root Raised Cosine
STBC	Space Time Block Coding
Veh	Vehicular
UMTS	Universal Mobile Telecommunications System
WiMAX	Worldwide Interoperability for Microwave Access
ZF	Zero Forcing

Notations

Vectors and matrices are denoted by bold letters (e.g. $\mathbf{X}$). Other notational conventions are summarized as follows:

$\mathbb{C}^n$, $\mathbb{R}^n$	The sets of vectors of length n, with complex and real elements.
$\mathbb{C}^{p\times n}$, $\mathbb{R}^{p\times n}$	The set of matrices with p rows and n columns, with complex and real elements.
$\mathbb{N}$	The set of positive integer elements.
$\log(\cdot)$	The natural logarithm.
$\log_2(\cdot)$	The base 2 logarithm.
x^*	Complex conjugate of the complex value x.
$\lvert x\rvert$	The absolute value of a scalar.
$\lfloor x\rfloor$	The floor operator, i.e. the smallest integer less than x.
$\lceil x\rceil$	The ceil operator, i.e. the smallest integer greater than or equal to x.
$\lvert\Omega\rvert$	The cardinality of the set Ω, i.e. the number of elements in the finite set Ω.
$\cap$	The intersection operator.
$\cup$	The union operator.
$\mathbb{E}\{\cdot\}$	The expectation operator.
$[\cdot]^T$	The transpose operator.
$[\cdot]^H$	The complex conjugate (Hermitian) transpose operator.
$\mathbf{X}^{-1}$	The inverse of matrix $\mathbf{X}$.
$\mathbf{I}_n$	The identity matrix of size n.
$\mathbf{0}_n$	The square zero matrix of size n.
$\mathbf{0}_{n\times m}$	The zero matrix of size $n_r \times n_t$.
$\lVert\mathbf{v}\rVert$	Euclidean norm of vector $\mathbf{v}$.
$\mathfrak{Re}\{x\}$	Real part of the complex value x.
$\mathfrak{Im}\{x\}$	Imaginary part of the complex value x.
$*$	Convolution operator.

Thesis Specific Notations

The following list is not exhaustive, and consists of the most relevant notations used in the dissertation.

Notations applicable in all chapters:

M	Number of subcarriers in multicarrier modulations.
L_{CP}	Cyclic prefix length in OFDM.
T	Symbol duration.
T_s	Sampling period.
f_s	Sampling frequency.
L	Length of the channel impulse response.
K	Overlapping factor in FBMC.
k	Subcarrier index.
n	Time index of a multicarrier symbol.
m	Sample time index.
B	Total available bandwidth.
$g[m]$	Prototype filter function in FBMC.
$G(f)$	Spectrum of the prototype filter.
σ^2	Variance of the AGWN noise.
N_t	Number of transmit antennas.
N_r	Number of receive antennas.
$\mathbf{H}_{k,n}$	MIMO channel matrix at subcarrier k and time index n.

Notations specific to Chapters 3 and 4:

σ^2_{ISI}	Variance of the inherent interference in FBMC.
σ^2_{RISI}	Variance of Residual inherent interference in FBMC.
ϵ	Error event.
$w(\epsilon)$	Number of error positions in an error event ϵ.
$d_0(\epsilon)$	Spectrum distance of an error event.
$\mathbf{R}$	Normalized autocovariance matrix of the noise.
$\Gamma_{p,q}$	Coefficients of the transmultiplexer impulse response.

Notations specific to Chapters 5:

N	FFT-FBMC block length.
L	Cyclic prefix length in FFT-FBMC.
$\Omega^{(k)}$	Set of useful symbol positions in subcarrier k in FFT-FBMC.
μ	Spectral efficiency loss.
T_c	Coherence time.
N_c	Coherence number of multicarrier symbols.
Δ	One side maximum spread in time domain of the transmultiplexer impulse response.

$f_k^{(k_0)}(n)$	Coefficient of the transmultiplexer impulse response when the impulse is applied at subcarrier k_0.
$F_k^{(k_0)}(n')$	DFT of $f_k^{(k_0)}(n)$.

Chapter 1

Introduction

Nowadays, in a world of high mobility, transmission system speed and capacity are essential components to maintain communication among remote people all around the world. The early digital communication systems were based on single carrier modulation. Generally, if we want to increase the bit rate of a transmission system, we have to reduce the symbol duration. However, the presence of a multipath channel introduces intersymbol interference (ISI) which requires complex equalization. Multicarrier modulations [1, 2] have been then introduced as a good alternative in order to counteract the multipath fading effects. Indeed, in multicarrier communications the data is transmitted over many frequencies instead of a single carrier, dividing the wideband frequency selective communication channel into several subbands with mildly selective fading.

Orthogonal Frequency Division Multiplexing (OFDM) is the most widespread multicarrier modulation scheme and it has been considered as fundamental part in numerous wireless communication systems such as WiFi based on the IEEE 802.11 standard, WiMax (Worldwide Interoperability for Microwave Access) [2], [3], [4] based on the IEEE 802.16 standard, Long Term Evolution (LTE) [2], [5], LTE-advanced, ... etc. The large popularity of OFDM mainly comes from a number of attractive features such as:

- Its high spectral efficiency using closely spaced orthogonal subcarriers.
- Its robustness to multipath fading effects and its ability to avoid both intersymbol and intercarrier interference (ISI and ICI) by appending a cyclic prefix (CP) that significantly reduces the complexity of the equalization to a single complex coefficient per subcarrier equalizer. This holds as long as the CP covers the maximum delay spread of the channel.
- The digital implementation of both OFDM modulator and demodulator can be efficiently realized making use of fast Fourier transform (FFT).

Nevertheless, in spite of these advantages, OFDM has some shortcomings. First of all,

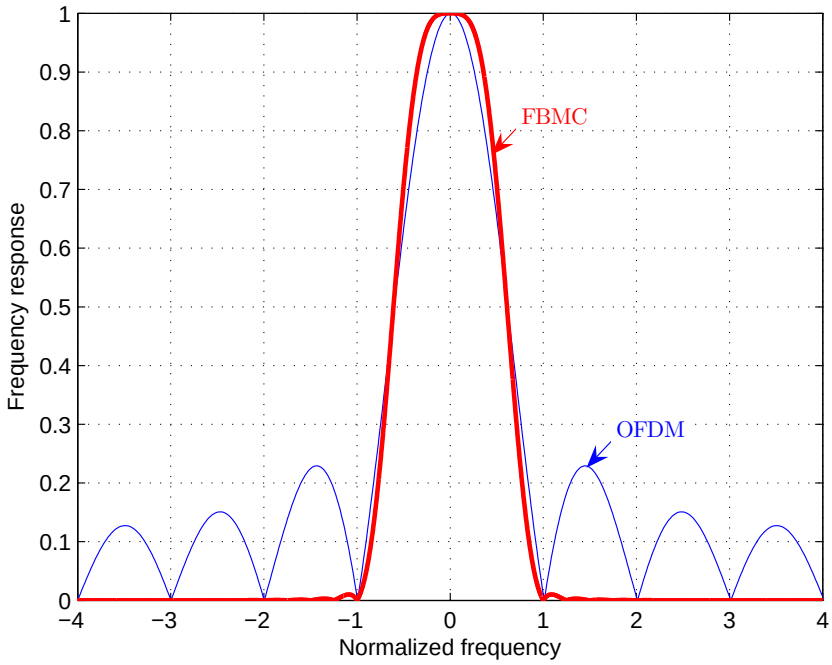

Figure 1.1: Frequency responses of OFDM and FBMC

there is a loss in spectral efficiency due to the cyclic prefix insertion. Indeed, the cyclic prefix is a copy of part of the transmitted OFDM symbol, and this redundancy reduces the effective throughput. Secondly, OFDM is very sensitive to residual frequency and timing offsets that can be generated by a defective synchronization as well as the Doppler effect [20, 21]. Moreover, the use of a rectangular impulse response in OFDM causes large sidelobes at each subcarrier. Hence, the subchannels at the edge of the transmission bandwidth could be a source of interference for other neighboring systems [6].

These drawbacks have motivated researchers to develop alternative solutions and propose enhanced physical layers based on filter bank processing [22]. There are mainly three filter bank multicarrier (FBMC) techniques that have been studied in the literature: Filtered MultiTone (FMT) [23–25], Offset Quadrature Amplitude Modulation (OQAM) [9] (also called Staggered MultiTone (SMT) [26]), and Cosine Modulated multiTone (CMT) [27, 28]. In this dissertation, we focus on the Saltzberg's scheme [9] called FBMC/OQAM (also called OFDM/OQAM or SMT). In fact, FBMC/OQAM technique can deal with the channel frequency selectivity without any guard interval requirement. Furthermore, FBMC uses a frequency well-localized pulse shaping which reduces significantly the out-of-band leakage, thus a higher number of subcarriers can be used within the allocated frequency band. Fig. 1.1 shows the frequency response comparison between OFDM and FBMC system[1]. Saltzberg showed, in [9], that by introducing a shift of half the symbol period between the in-phase and quadrature components of QAM symbols, it is possible to achieve a baud-rate spacing between adjacent subcarrier channels and still recover the information

[1]The prototype filter used for FBMC for comparison is the one designed by Bellanger in [29].

symbols free of intersymbol interference (ISI) and intercarrier interference (ICI). Thus, each subcarrier is modulated with an offset QAM (OQAM) and the orthogonality conditions are considered only in the real field [10]. Indeed, the data at the receiver side is carried only by the real (or imaginary) components of the signal, and the imaginary (or real) parts appear as interference terms. An efficient discrete Fourier transform (DFT) implementation of this modulation method has been proposed by Hirosaki [30].

In recent years, FBMC has attracted a lot of interest and many equalization and synchronization [31, 32] methods have been developed for this modulation technique. However, most of these works are related to single-input single-output (SISO) systems. To increase data rate or performance, multi-antennas techniques are now implemented [33]. Indeed, transmitting different data over different antennas (spatial multiplexing) can easily increase the throughput. Thus it seems relevant to look at the combination between FBMC and multiple-input multiple-output (MIMO) techniques. It has been shown in [11] that spatial multiplexing (SM) could be directly applied to FBMC with minimum mean square error (MMSE) equalizer. SM with maximum likelihood detection (SM-MLD) and the Alamouti space time block coding (STBC) [34] are some of the classical techniques which constitute a central ingredient in advanced wireless communication. Unfortunately, their combination with FBMC does not work well and has remained an open problem [12]. Indeed, the presence of the inherent FBMC interference in the received signal prevents the application of Alamouti scheme and SM-MLD in a straightforward manner. Regarding Alamouti coding, some works have been carried out such as [35] where the authors showed that Alamouti coding can be performed when it is combined with code division multiple access (CDMA). A pseudo-Alamouti scheme was introduced in [36] but at the expense of the spectral efficiency since it requires the appending of a CP to the FBMC signal. Another solution was proposed by Renfors *et al.* in [12] where the Alamouti coding is performed in a block-wise manner inserting gaps (zero-symbols and pilots) in order to isolate the blocks.

The main objective of this thesis is to analyze and study the combination of FBMC technique with spatial multiplexing system using maximum likelihood detection. We analyze the possibility to cancel the interference before applying ML detection. Indeed, the interference cancellation approaches generally offer the possibility of removing interference with low complexity increase and without enhancing the level of noise already present in the received signal. The next paragraph gives the outline of the thesis.

- **Chapter 2** is devoted to introduce the background and the state of the art related to the different concepts to be used throughout this thesis. First, we start by giving the basics of multi-antennas systems. Next, the OFDM system and its implementation are described and its straightforward combination with MIMO is emphasized. After that, we give the fundamental theory of FBMC technique, where the polyphase implementation of the filter bank transceiver and the prototype filter design are reviewed. We finally discuss some issues about the combination between FBMC and MIMO techniques in the last part of this chapter.

- **In chapter 3**, we propose some different receiver schemes based on inherent interference estimation and cancellation. First, we propose to estimate the interference by making use of the MMSE equalizer. After that, we give a brief overview on interference cancellation technique using tentative detection. Then, in light of this background, we

derive conditions for optimal interference cancellation scheme using tentative detection in the FBMC-MIMO context. We present the performance results obtained by simulation in both uncoded and coded cases. Next, we analyze another interference cancellation approach based on Viterbi algorithm and partial interference cancellation. Finally, we finish the chapter by a conclusion where the main results are summarized.

- **In chapter 4**, we propose a modification in the conventional FBMC/OQAM system in order to reduce the inherent interference. Indeed, the proposal consists to transmit QAM data symbols instead of OQAM ones. This allows to reduce the interference power but at the expense of the orthogonality. First, we start by describing the proposed system model and deriving some related equations and results. After that, we adapt and analyze, in this FBMC/QAM context, the receiver schemes studied in the chapter 3.

- **In chapter 5**, we introduce a novel FBMC scheme and transmission strategy in order to get rid of the inherent interference terms. This proposed scheme (that we call FFT-FBMC) transforms the FBMC system into an equivalent system formulated as OFDM regardless of some residual interference. Thus, any OFDM transmission technique can be performed straightforwardly to the proposed FBMC scheme with a corresponding complexity growth compared to the classical FBMC. First, we develop the FFT-FBMC in the case of single-input single-output (SISO) configuration. Then, we extend its application to SM-MIMO configuration with MLD and Alamouti coding scheme. An SNR evaluation at the output of the proposed demodulator is detailed, and a brief computational complexity evaluation is included.

- **Chapter 6** draws final conclusions of the thesis, briefly summarizes the main obtained results, and highlights perspectives and possible future research directions.

1.1 List of publications

Journal papers

1. R. Zakaria and D. Le Ruyet "A Novel Filter-Bank Multicarrier Scheme to Mitigate the Intrinsic Interference: Application to MIMO Systems", *IEEE Transactions on Wireless Communications*, vol. 11(3), pp. 1112-1123, 2012.

2. R. Zakaria and D. Le Ruyet "Filter-bank intrinsic interference cancellation in spatial multiplexing system." in preparation.

Conference papers

1. R. Zakaria, D. le Ruyet, Y. Medjahdi "On ISI cancellation in MIMO-ML detection using FBMC/QAM modulation", ISWCS, September 2012, pp.1-5, Paris, France.

2. Y. Medjahdi, D. le Ruyet, D. Roviras, H. Shaiek, R. Zakaria "On the Impact of the Prototype Filter on FBMC Sensitivity to Time Asynchronism", ISWCS, August 2012, pp.1-5, Paris, France.

3. R. Zakaria, D. le Ruyet "Partial ISI Cancellation with Viterbi Detection in MIMO Filter-Bank Multicarrier Modulation", ISWCS, November 2011, pp.322-326, Aachen, Germany.

4. R. Zakaria, D. le Ruyet "On Spatial Data Multiplexing over Coded Filter-Bank Multicarrier with ML Detection", PIMRC, November 2011, Toronto, Canada.

5. R. Zakaria, D. le Ruyet "On Maximum Likelihood MIMO Detection in QAM-FBMC Systems", PIMRC, December 2010, pp.183-187, Istanbul, Turkey.

6. R. Zakaria, D. le Ruyet "A novel FBMC scheme for Spatial Multiplexing with Maximum Likelihood detection", ISWCS, November 2010, pp.461 - 465 , York, England.

7. R. Zakaria, D. le Ruyet, M. Bellanger "Maximum Likelihood Detection in spatial multiplexing with FBMC", European Wireless, June 2010, pp.1038-1041, Lucca, Italy.

8. C. Lélé, D. le Ruyet, R. Zakaria "On the decoding of single delay STTC using filter bank based multicarrier modulation", ISWCS, October 2009, pp.86 - 90, Tuscany , Italy,

Project Technical Reports

1. D. le Ruyet, R. Zakaria "MIMO Techniques and Beamforming", *technical contribution report in the deliverable D4.2-* European ICT-211887 FP7 PHYDYAS project, Feb. 2010.

2. M. Bellanger, D. le Ruyet, R. Zakaria "MIMO transmit and receive processing" *technical contribution report in the deliverable D4.2-a-* European ICT-211887 FP7 PHYDYAS project, April 2010.

Chapter 2

State of the art

In this chapter, we give the background and the main state of the art that allow us to lead our research studies during this Ph.D thesis. The first section aims to give the basics of multi-antenna systems, then in the following section we describe CP-OFDM. In the third section, we present the FBMC modulation (we specially focus on OFDM/OQAM) that is an alternative to CP-OFDM, which permits to overcome some technical drawbacks of CP-OFDM modulation.

2.1 Multi-antennas channel

The aim of this section is to present the usefulness of having several antennas at the transmitter and/or at the receiver side. This concept, called Multiple-Input Multiple-Output (MIMO) allows to increase the system throughput and/or to exploit the spatial diversity leading the system to be more robust. The special case in which $N_t = N_r = 1$ is called a Single-Input Single-Output (SISO) channel. A second special case is one in which $N_t = 1$ and $N_r \geq 2$. The resulting system is called a Single-input Multiple-Output (SIMO) system. Finally, a third special case is one in which $N_t \geq 2$ and $N_r = 1$. The resulting system is called a Multiple-Input Single-Output (MISO) channel [37]. The initial excitement about MIMO was sparked by the pioneering work of Winters [38], Foschini [39], Gans [40], and Telatar [41] predicting remarkable spectral efficiencies for wireless systems with multiple transmit and receive antennas [13].

We consider the time-invariant MIMO channel model with N_t transmit antennas and N_r receive antennas, subject to Additive White Gaussian Noise (AWGN). We denote the equivalent lowpass channel impulse response between the jth transmit antenna and the ith receive antenna as $h_{ij}(\tau)$, where τ is the delay variable. Thus, the channel is characterized

by the $N_r \times N_t$ matrix $\mathbf{H}(\tau)$, defined as [37]:

$$\mathbf{H}(\tau) = \begin{bmatrix} h_{11}(\tau) & h_{12}(\tau) & \cdots & h_{1N_t}(\tau) \\ h_{21}(\tau) & h_{22}(\tau) & \cdots & h_{2N_t}(\tau) \\ \vdots & \vdots & & \vdots \\ h_{N_r1}(\tau) & h_{N_r2}(\tau) & \cdots & h_{N_rN_t}(\tau) \end{bmatrix} \tag{2.1}$$

When the jth antenna transmits the complex signal $s_j(t)$, $j = 1, 2, ..., N_t$. Then the received signal at the ith antenna in the presence of noise can be expressed as:

$$\begin{aligned} r_i(t) &= \sum_{j=1}^{N_t} \int_{-\infty}^{\infty} h_{ij}(\tau) s_j(t-\tau) d\tau + n_i(t) \\ &= \sum_{j=1}^{N_t} (h_{ij} * s_j)(t) + n_i(t), \quad i = 1, 2, ..., N_r \end{aligned} \tag{2.2}$$

where the asterisk $(*)$ denotes the convolution operator, and $n_i(t)$ denotes the AWGN with variance σ^2 at the ith antenna. In the matrix form, Equation (2.2) becomes:

$$\mathbf{r}(t) = \mathbf{H}(t) * \mathbf{s}(t) + \mathbf{n}(t), \tag{2.3}$$

where $\mathbf{s}(t) \in \mathbb{C}^{N_t \times 1}$ is the transmitted vector of complex symbols, the received vector $\mathbf{r}(t) \in \mathbb{C}^{N_r \times 1}$, and the noise vector $\mathbf{n}(t) \in \mathbb{C}^{N_r \times 1}$.

For a frequency-nonselective channel, the channel matrix is simplified as:

$$\mathbf{H} = \begin{bmatrix} h_{11} & h_{12} & ... & h_{1N_t} \\ h_{21} & h_{22} & ... & h_{2N_t} \\ & & ... & \\ h_{N_r1} & h_{N_r2} & ... & h_{N_rN_t} \end{bmatrix}$$

In this case, the received signal vector after match filtering is simply

$$\mathbf{r} = \mathbf{H}\mathbf{s} + \mathbf{n}. \tag{2.4}$$

In the general formulation of a MIMO system as described above, we observe that the transmitted symbols on the N_t transmitting antennas completely overlap in both time and frequency. As a consequence, there is interchannel interference between signals $(r_i, 1 \leq i \leq N_r)$ received from the spatial channel.

The time-invariant frequency-nonselective channel model embodied in (2.4) is the simplest model for signal transmission in a MIMO channel. Furthermore, if we assume that each signal from a transmitting antenna to a receiving antenna undergoes frequency-nonselective Rayleigh fading, then the entries of $\mathbf{H}$ are zero-mean and independent, identically distributed (*i.i.d.*) complex Gaussian, each with independent real and imaginary parts with variance $\frac{1}{2}$. In the following subsections, we employ this model and consider coherent detection by assuming perfect knowledge of the channel coefficients at the receiver side. We will also denote by p_{eb} the Bit Error Probability (BEP). The BEP will be computed for uncoded bits and mainly for QPSK modulation with Gray mapping. The choice of these parameters are done to illustrate the performance characteristics of MIMO systems. Let us look at some features obtained with MIMO transmission. One of the first major benefit of having multiple antennas is the spatial diversity gain.

2.1.1 Spatial diversity

In presence of AWGN channel and for a SISO system, *i.e.* when $r = s + n$, the bit error probability for QPSK modulation is given by $p_{eb} = Q(\sqrt{SNR_t})$, where $SNR_t = \sigma_s^2/\sigma^2$ is the signal to noise ratio at the transmitter side, and Q represents the so-called Q-function defined by [37]:

$$Q(x) = \frac{1}{\sqrt{2\pi}} \int_x^{+\infty} e^{-t^2/2} dt. \tag{2.5}$$

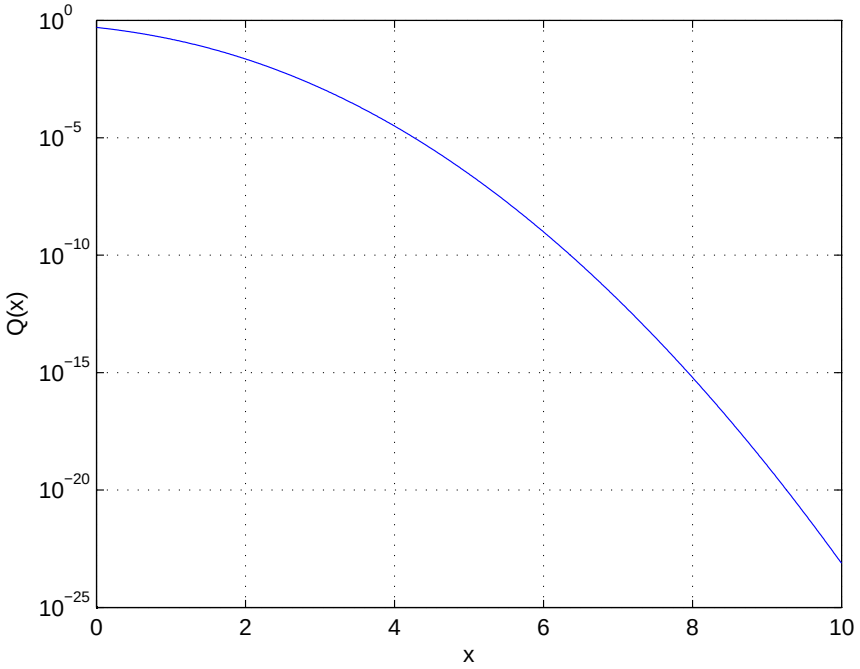

Figure 2.1: $Q(x)$ as a function of x.

The Rayleigh frequency-nonselective channel model, *i.e.* $r = hs + n$, can be virtually seen as the transmission of hs in presence of an AWGN channel, and therefore its p_{eb} is given by:

$$p_{eb} = Q(\sqrt{|h|^2 SNR_t}). \tag{2.6}$$

The product $|h|^2 SNR_t$ is defined as the signal to noise ratio at the receiver side SNR_r. As $Q(x)$ rapidly tends to zero when x increases, see Fig. 2.1, the p_{eb} decreases when either the SNR_t or $|h|$ increases. The SNR_t can not be increased as much as we want since the regulation imposes limit to the transmitted power for healthy reasons and system coexistence. h is random and mainly depends on the channel conditions. When $|h|$ is close to zero the p_{eb} is bad, this is generally referred to as deep fade. When the channel path is in a deep fade, any communication scheme will likely suffer from errors. A natural solution

to improve the performance is to ensure that the data symbols pass through multiple paths, each of which fades independently, making sure that reliable communication is possible as long as one of the path is strong enough. This technique is called diversity, and can dramatically improve the performance over fading channels [42].

There are many ways to obtain diversity. Diversity over time can be obtained via coding and interleaving: information is coded and the coded symbols are dispersed over time in different coherence periods so that different parts of the codewords experience independent fades. Analogously, one can also exploit diversity over frequency if the channel is frequency-selective. In a channel with multiple transmit and/or receive antennas, diversity can be obtained over space as well. Since diversity is such an important resource, a wireless system typically uses several types of diversity.

Antenna diversity, or spatial diversity, can be obtained by placing multiple antennas, sufficiently far apart, at the transmitter and/or the receiver. The channel gains between different antenna pairs fade more or less independently, and independent paths are thus created. The required antenna separation depends on the local scattering environment as well as on the carrier frequency. Basically, in line of sight, *i.e.* when there is no dispersive environment between the transmitter and the receiver, the separation is of 10's of carrier wavelengths. In presence of a multi-path channel, a separation of half to one wavelength is sufficient. More explanations are given in [42].

We notice that p_{eb} given in (2.6) is random since the channel coefficient h is a random variable. Hence, we define the average error probability as:

$$\bar{p}_{eb} = \int_0^{+\infty} p_{eb} P_{|h|^2}(\gamma) d\gamma, \tag{2.7}$$

where $P_{|h|^2}(\gamma)$ is the probability density function (PDF) of the random variable $|h|^2$. For Rayleigh flat fading channel, we can easily show that $P_{|h|^2}(\gamma)$ is an exponential distribution given by:

$$P_{|h|^2}(\gamma) = e^{-\gamma}. \tag{2.8}$$

Integrating (2.6) over the distribution (2.8) yields the following average bit error probability [13]:

$$\bar{p}_{eb} \approx \int_0^{\infty} Q(\sqrt{\gamma SNR_t}) e^{-\gamma} d\gamma = \frac{1}{2}\left[1 - \sqrt{\frac{SNR_t}{2 + SNR_t}}\right] \approx \frac{1}{2SNR_t}, \tag{2.9}$$

where the last approximation is valid only in high SNR.

An analytical expression, given in [13], to calculate the diversity order is

$$d = -\lim_{SNR_t \to +\infty} \frac{\log(\bar{p}_{eb})}{\log(SNR_t)}, \tag{2.10}$$

where the log can be in any base. Therefore, according to these two last expressions, we conclude that the diversity order for a SISO Rayleigh channel is one.

Single-input Multiple-Output (SIMO) system

Let us assume that we have at the receiver side N_r antennas and a single transmit antenna. This communication format is often described as Single-input Multiple-Output (SIMO). Fig.

2.2 gives its representation. If we regroup the received samples from the different receive antennas in a column vector, Equation (2.4) becomes:

$$\mathbf{r} = \mathbf{h}s + \mathbf{n}, \tag{2.11}$$

where $\mathbf{h} = [h_{11}\ h_{21}\ ...\ h_{N_r1}]^T$ is an $N_r \times 1$ vector.

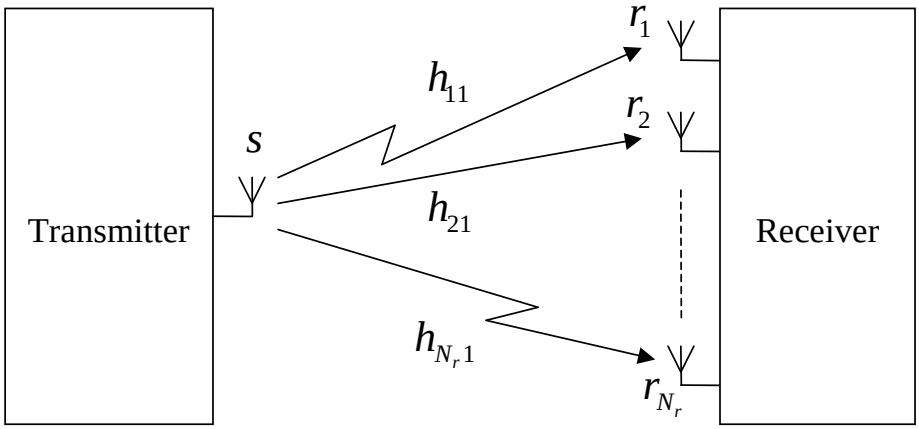

Figure 2.2: SIMO representation model.

As we are concerned about p_{eb}, which depends on SNR_r, maximizing SNR_r after detection, leads to minimize the p_{eb}. It is well known that the maximum SNR_r value after detection is achieved thanks to the matched filter [37]:

$$\hat{s} = \frac{\mathbf{h}^H}{\|\mathbf{h}\|^2}\mathbf{r} = s + \frac{\mathbf{h}^H}{\|\mathbf{h}\|^2}\mathbf{n}. \tag{2.12}$$

Then p_{eb} is given by:

$$p_{eb} = Q(\sqrt{\|\mathbf{h}\|^2 SNR_t}), \tag{2.13}$$

where $\|\mathbf{h}\|^2 = \sum_{i=1}^{N_r} |h_{i1}|^2$. Assuming that $|h_{i1}|$ are zero-mean *i.i.d.* Rayleigh random variables with variances equal to one, the distribution of $\|\mathbf{h}\|^2$ is chi-squared with $2N_r$ degrees of freedom, expected value of N_r, and variance equals to $2N_r$:

$$P_{\|\mathbf{h}\|^2}(\gamma) = \frac{\gamma^{N_r-1}}{(N_r-1)!}e^{-\gamma}; \quad \gamma \geq 0. \tag{2.14}$$

We can obtain a simple upper bound on the average error probability by applying the Chernoff bound [13] $Q(x) \leq e^{-x^2/2}$ to the Q-function. Integrating (2.13) over the chi-squared distribution for $\|\mathbf{h}\|^2$ yields [13]:

$$\bar{p}_{eb} \leq \left(1 + \frac{1}{2}SNR_t\right)^{-N_r}. \tag{2.15}$$

Thus, the more the number of receive antennas increases, the more $\bar{p}_{eb}$ decreases. Then, when the channel coefficients are uncorrelated with each other, the probability to be in deep fade decreases as N_r increases. Indeed, it is less likely that all the channel coefficients are

in deep fade at the same time. This corresponds to the diversity order of the system which is equal to N_r as we can show using (2.10):

$$d = -\lim_{SNR_t \to +\infty} \frac{-N_r \log(1 + \frac{SNR_t}{2})}{\log(SNR_t)} = N_r. \tag{2.16}$$

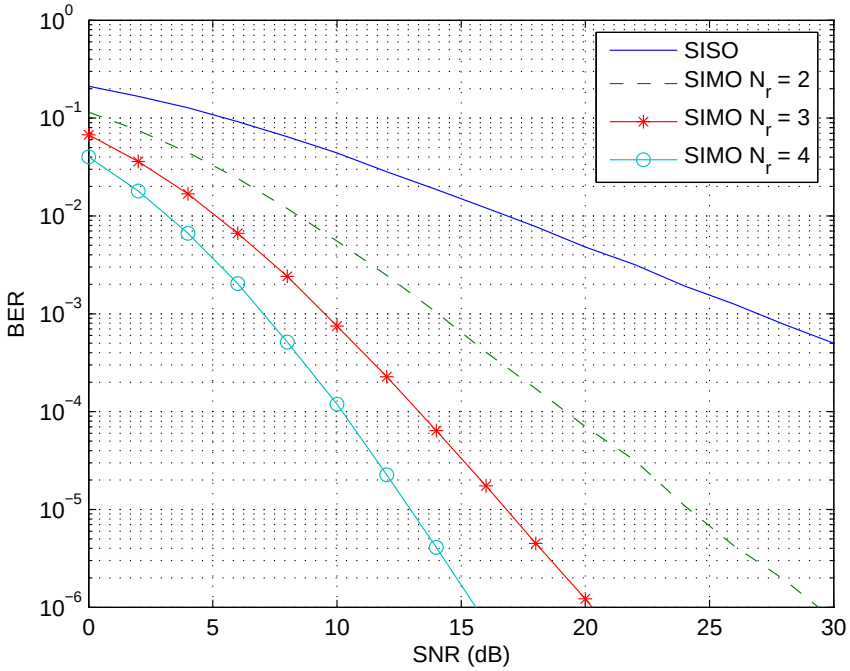

Figure 2.3: BER performance as a function of the SNR for SIMO model with QPSK modulation and different values of the receive antennas N_r.

In Fig. 2.3, we plot the Bit Error Rate (BER) as a function of the SNR_t for different SIMO configurations. The symbols are QPSK modulated, and the channel coefficients are totally uncorrelated. As we can see, when N_r increases, the performance in terms of the BER decreases more rapidly. The slopes of the curves illustrate the gain in diversity order. The performance at $SNR_t = 0\ dB$ is linked to the averaging of the noise over the receive antennas [17].

Multiple-input Single-output (MISO) system

Let us consider N_t transmit antennas and a single receive antenna. This communication format is often described as Multiple-Input Single-Output (MISO). Fig. 2.4 gives the corresponding representation. The received signal can be given by:

$$r = \mathbf{hs} + n, \tag{2.17}$$

where $\mathbf{h} = [h_{11}\ h_{11}\ ...\ h_{1N_t}]$ is a $1 \times N_t$ row vector.

In the SIMO channel, the sufficient statistic is the projection of the $N_r \times 1$ received signal vector on $\mathbf{h}$ (Matched filter). A natural reciprocal transmission strategy for the

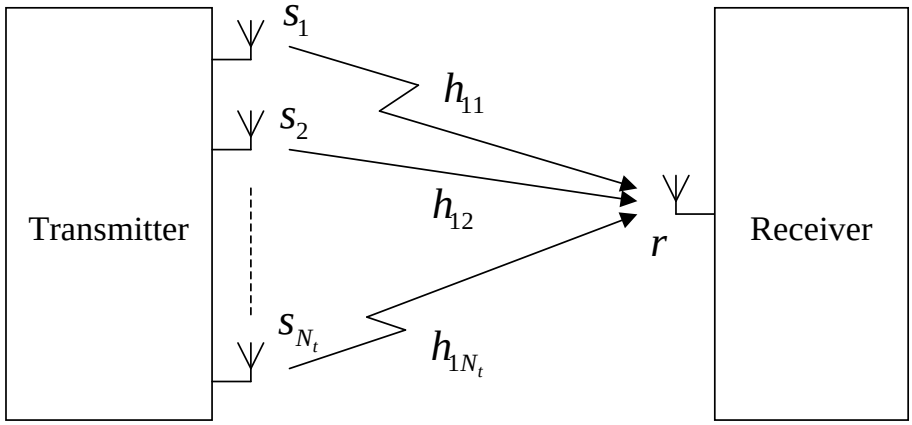

Figure 2.4: MISO representation model.

MISO channel would send information only in the direction of the channel vector $\mathbf{h}$ [42]; information sent in any orthogonal direction will be nulled out by the channel anyway. Thus, the channel coefficients h_{1i} must be known at the transmitter side. Therefore, the transmitted vector $\mathbf{s}$ is obtained as:

$$\mathbf{s} = \frac{\mathbf{h}^H}{\|\mathbf{h}^T\|} s. \tag{2.18}$$

Thus, the average transmit power is equal to $\mathbb{E}\left\{\sum_{i=1}^{N_t} |s_i|^2\right\} = \sigma_s^2$. The received signal r is the sum of all the contributions coming from the different transmit antennas and affected by the corresponding attenuation coefficients. Hence, the MISO channel is reduced to:

$$r = \sum_{i=1}^{N_t} \frac{|h_{1i}|^2}{\|\mathbf{h}^T\|} + n = \|\mathbf{h}^T\| s + n. \tag{2.19}$$

Hence, the estimate of the transmitted symbol s is obtained by:

$$\hat{s} = \frac{r}{\|\mathbf{h}^T\|} = s + \frac{n}{\|\mathbf{h}^T\|}. \tag{2.20}$$

Then the p_{eb} value is given by:

$$p_{eb} = Q\left(\sqrt{\|\mathbf{h}^T\|^2 SNR_t}\right). \tag{2.21}$$

We notice that we obtain the same expression of p_{eb} as (2.13) for the SIMO channel. In Fig. 2.5, we plot the BER as a function of the SNR_t in dB with QPSK modulation. As with the SIMO configuration, when N_t increases, the performance increases as well as the slope of the curve. The slopes of the curves illustrate the gain in diversity which is equal to N_t.

Intuitively, the transmission strategy maximizes the received SNR as the received signals from the various transmit antennas add up in-phase (coherently) and the transmit antenna with the better gain has more allocated power. This strategy, "aligning the transmit signal in the direction of the transmit antenna array pattern", is called transmit beamforming [42].

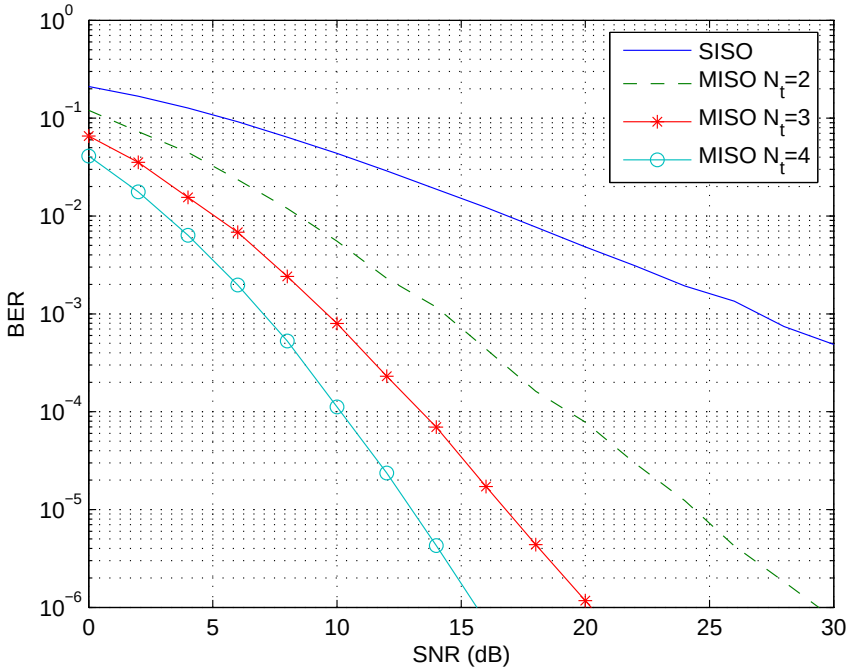

Figure 2.5: BER performance as a function of the SNR for MISO model with QPSK modulation and different values of the transmit antennas N_t.

Space Time Block Coding (STBC)

Let us now consider the MIMO system illustrated in Fig. 2.6. A space-time block code (STBC) is defined by a generator matrix $\mathbf{G}$, having L rows and N_t columns, of the form [37]:

$$\mathbf{G} = \begin{bmatrix} g_{11} & g_{12} & \cdots & g_{1N_t} \\ g_{21} & g_{22} & \cdots & g_{2N_t} \\ & & \cdots & \\ g_{L1} & g_{L2} & \cdots & g_{LN_t} \end{bmatrix} \tag{2.22}$$

in which the elements $\{g_{ij}\}$ are signal symbols. By employing N_t transmit antennas, each row of $\mathbf{G}$ consisting of N_t symbols is transmitted on the N_t antennas in a time slot. Thus, the first row of N_t symbols is transmitted on the N_t antennas in the first time slot, the second row of N_t symbols is transmitted on the N_t antennas in the second time slot, and so on. Therefore, L time slots are used to transmit the symbols in the L rows of the generator matrix $\mathbf{G}$.

In the design of the generating matrix of an STBC, it is desirable to focus on two principal objectives: (1) achieving the optimal tradeoff between diversity order and spatial rate, and (2) minimizing the complexity of the decoder.

Alamouti [34], in 1998, devised a STBC for $N_t = 2$ transmit antennas and $Nr = 1$ receive antennas. The Alamouti code is widely used and proposed for practical systems

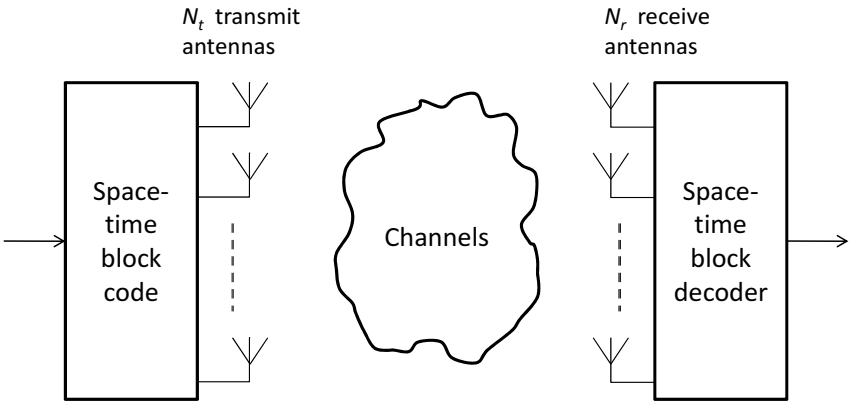

Figure 2.6: Space-time block coded MIMO system.

such as DVB-T2 [43]. The generator matrix for the Alamouti code is given as:

$$\mathbf{G} = \frac{1}{\sqrt{2}} \begin{bmatrix} s_1 & s_2 \\ -s_2^* & s_1^* \end{bmatrix} \tag{2.23}$$

where s_1 and s_2 are two data symbols. In the first time slot, $\frac{s_1}{\sqrt{2}}$ is transmitted on the first antenna whereas the second one transmits $\frac{s_2}{\sqrt{2}}$. Then at the second time slot, the first antenna transmits $\frac{-s_2^*}{\sqrt{2}}$, and the second one transmits $\frac{s_1^*}{\sqrt{2}}$. The factor $\frac{1}{\sqrt{2}}$ is used to ensure that the total transmitted power from both antennas is equal to σ_s^2. Thus, two symbols, $\frac{s_1}{\sqrt{2}}$ and $\frac{s_2}{\sqrt{2}}$, are transmitted in two time slots. Consequently, the spatial code rate $R_s = 1$ for the Alamouti code. This is the highest possible rate for an orthogonal STBC [37]. We observe that the column vectors $\mathbf{v}_1 = [s_1, -s_2^*]^T$ and $\mathbf{v}_2 = [s_2, s_1^*]^T$ are orthogonal; *i.e.* $\mathbf{v}_1^H \mathbf{v}_2 = 0$ and

$$\mathbf{G}^H \mathbf{G} = \frac{(|s_1|^2 + |s_2|^2)}{2} \mathbf{I}_2, \tag{2.24}$$

where $\mathbf{I}_2$ is a 2×2 identity matrix.

The MISO channel matrix for the $N_t = 2$, $N_r = 1$ channel, based on a frequency-nonselective model, is:

$$\mathbf{H} = \begin{bmatrix} h_{11} & h_{12} \end{bmatrix}. \tag{2.25}$$

In the decoding of the STBC, we assume that $\mathbf{H}$ is constant over the two time slots. Consequently, the signal at the receiver in the two time slots is:

$$\begin{cases} r_1 = \frac{1}{\sqrt{2}}(h_{11}s_1 + h_{12}s_2) + n_1 \\ r_2 = \frac{1}{\sqrt{2}}(-h_{11}s_2^* + h_{12}s_1^*) + n2 \end{cases} \tag{2.26}$$

where n_1 and n_2 are zero-mean, circularly symmetric complex-valued uncorrelated Gaussian noise with variance σ^2. This leads to the matrix equation:

$$\begin{bmatrix} r_1 \\ r_2^* \end{bmatrix} = \frac{1}{\sqrt{2}} \underbrace{\begin{bmatrix} h_{11} & h_{12} \\ h_{12}^* & -h_{11}^* \end{bmatrix}}_{\underline{\mathbf{H}}} \begin{bmatrix} s_1 \\ s_2 \end{bmatrix} + \begin{bmatrix} n_1 \\ n_2^* \end{bmatrix} \tag{2.27}$$

where $\underline{\mathbf{H}}$ in an orthogonal matrix with $\underline{\mathbf{H}}^H\underline{\mathbf{H}} = (|h_{11}|^2+|h_{12}|^2)\mathbf{I}_2$. Thus, using the Maximum Ratio Combining (MRC), the estimates $\hat{s}_1$ and $\hat{s}_2$ are obtained by:

$$\begin{aligned}\begin{bmatrix}\hat{s}_1\\ \hat{s}_2\end{bmatrix} &= \frac{\sqrt{2}}{|h_{11}|^2+|h_{12}|^2}\begin{bmatrix}h_{11}^* & h_{12}\\ h_{12}^* & -h_{11}\end{bmatrix}\begin{bmatrix}r_1\\ r_2^*\end{bmatrix}\\ &= \begin{bmatrix}s_1\\ s_2\end{bmatrix} + \begin{bmatrix}\acute{n}_1\\ \acute{n}_2\end{bmatrix}\end{aligned} \tag{2.28}$$

with

$$\begin{bmatrix}\acute{n}_1\\ \acute{n}_2\end{bmatrix} = \frac{\sqrt{2}}{|h_{11}|^2+|h_{12}|^2}\begin{bmatrix}h_{11}^* & h_{12}\\ h_{12}^* & -h_{11}\end{bmatrix}\begin{bmatrix}n_1\\ n_2^*\end{bmatrix}. \tag{2.29}$$

As the noise components n_1 and n_2 are uncorrelated, we have $\mathbb{E}\{|\acute{n}_1|^2\} = \mathbb{E}\{|\acute{n}_1|^2\} = \frac{2\sigma^2}{|h_{11}|^2+|h_{12}|^2}$. Thus according to (2.28), the p_{eb} value is given by:

$$p_{eb} = Q\left(\sqrt{\frac{|h_{11}|^2+|h_{12}|^2}{2}SNR_t}\right). \tag{2.30}$$

Therefore, if the two channel coefficients are sufficiently uncorrelated, we have a diversity gain of two. Indeed, the sum $|h_{11}|^2 + |h_{12}|^2$ follows the chi-squared distribution with 4 degrees of freedom, expected value of 2, and variance equals to 4. Hence, using the Chernoff bound, the average probability of error for the Alamouti scheme can be given by:

$$\bar{p}_{eb} \leq \left(1+\frac{1}{4}SNR_t\right)^{-2}. \tag{2.31}$$

Thus, the Alamouti scheme achieves full diversity and maximum spatial code rate ($R_s = 1$) with low decoding complexity. Fig. 2.7 depicts the BER as a function of the SNR_t in dB for the Alamouti ($N_t = 2$, $N_r = 1$) scheme with channel coefficients totally uncorrelated, and the symbols are QPSK modulated. When comparing with the SISO model, we see that both curves start at approximatively the same point ($SNR_t = 0\ dB$), however the slope of Alamouti is steeper than the SISO one.

The Alamouti scheme described above can be extended to the case with multiple receive antennas ($N_r \geq 2$). In this case, the $N_r \times 2$ channel matrix is:

$$\mathbf{H} = \begin{bmatrix}\mathbf{h}_1 & \mathbf{h}_2\end{bmatrix} = \begin{bmatrix}h_{11} & h_{12}\\ h_{21} & h_{22}\\ \vdots & \vdots\\ h_{N_r1} & h_{N_r2}\end{bmatrix} \tag{2.32}$$

Using the same generator matrix $\mathbf{G}$, the received signal, in the first time slot, is:

$$\mathbf{r}_1 = \frac{1}{\sqrt{2}}\mathbf{H}\begin{bmatrix}s_1\\ s_2\end{bmatrix} + \mathbf{n}_1, \tag{2.33}$$

and in the second time slot, the received signal is

$$\mathbf{r}_2 = \frac{1}{\sqrt{2}}\mathbf{H}\begin{bmatrix}-s_2^*\\ s_1^*\end{bmatrix} + \mathbf{n}_2, \tag{2.34}$$

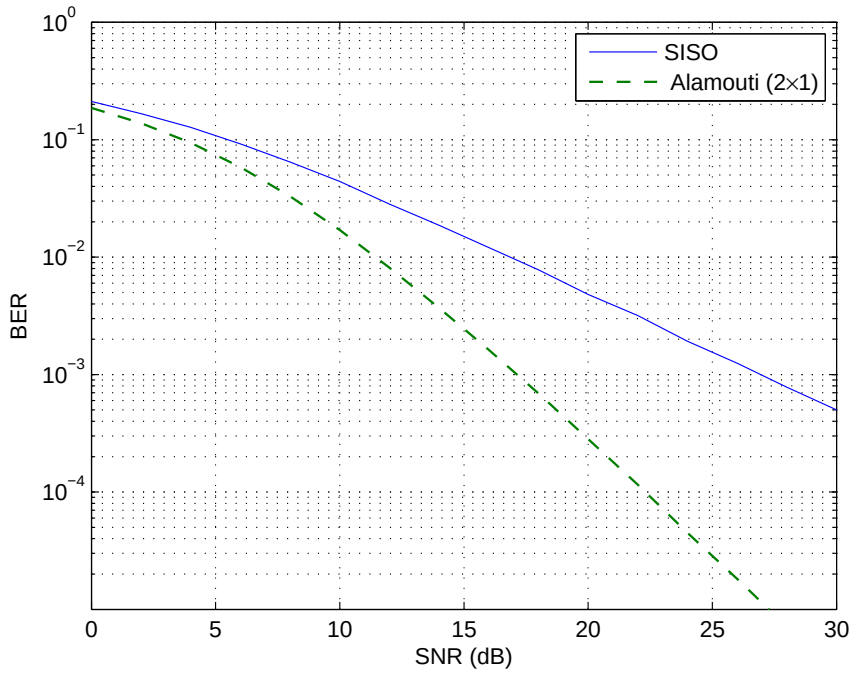

Figure 2.7: BER performance comparison between the Alamouti (2×1) and SISO schemes with QPSK modulation.

where $\mathbf{n}_1$ and $\mathbf{n}_2$ are the noise $N_r \times 1$ vectors, respectively, at the first and second time slot. Using the time invariance of the channels and combining these equations, as in the case of the MISO Alamouti, we obtain:

$$\begin{bmatrix} \mathbf{r}_1 \\ \mathbf{r}_2^* \end{bmatrix} = \frac{1}{\sqrt{2}} \underbrace{\begin{bmatrix} \mathbf{h}_1 & \mathbf{h}_2 \\ \mathbf{h}_2^* & -\mathbf{h}_1^* \end{bmatrix}}_{\underline{\mathbf{H}}} \begin{bmatrix} s_1 \\ s_2 \end{bmatrix} + \begin{bmatrix} \mathbf{n}_1 \\ \mathbf{n}_2^* \end{bmatrix} \tag{2.35}$$

where $\mathbf{h}_1$ and $\mathbf{h}_2$ are the column vectors of the channel matrix given in (2.32). We note that the matrix $\underline{\mathbf{H}}$ is orthogonal and we have $\underline{\mathbf{H}}^H \underline{\mathbf{H}} = (\|\mathbf{h}_1\|^2 + \|\mathbf{h}_2\|^2)\mathbf{I}_2$. Thus, using the MRC equalization, the estimates $\hat{\mathbf{s}}_1$ and $\hat{\mathbf{s}}_2$ are obtained by:

$$\begin{bmatrix} \hat{s}_1 \\ \hat{s}_2 \end{bmatrix} = \frac{\sqrt{2}}{\|\mathbf{h}_1\|^2 + \|\mathbf{h}_2\|^2} \underbrace{\begin{bmatrix} \mathbf{h}_1^H & \mathbf{h}_2^T \\ \mathbf{h}_2^H & -\mathbf{h}_1^T \end{bmatrix}}_{\underline{\mathbf{H}}^H} \begin{bmatrix} \mathbf{r}_1 \\ \mathbf{r}_2^* \end{bmatrix} = \begin{bmatrix} s_1 \\ s_2 \end{bmatrix} + \begin{bmatrix} \acute{n}_1 \\ \acute{n}_2 \end{bmatrix} \tag{2.36}$$

with

$$\begin{bmatrix} \acute{n}_1 \\ \acute{n}_2 \end{bmatrix} = \frac{\sqrt{2}}{\|\mathbf{h}_1\|^2 + \|\mathbf{h}_2\|^2} \underline{\mathbf{H}}^H \begin{bmatrix} \mathbf{n}_1 \\ \mathbf{n}_2^* \end{bmatrix}. \tag{2.37}$$

Thus, since the noise components of $\mathbf{n}_1$ and $\mathbf{n}_2$ are uncorrelated, we have $\mathbb{E}\{|\acute{n}_1|^2\} =$

$\mathbb{E}\{|\acute{n}_2|^2\} = \frac{2\sigma^2}{\|\mathbf{h}_1\|^2+\|\mathbf{h}_2\|^2}$. Therefore, the p_{eb} is given by:

$$p_{eb} = Q\left(\sqrt{\frac{\|\mathbf{h}_1\|^2 + \|\mathbf{h}_2\|^2}{2} SNR_t}\right) = Q\left(\sqrt{\frac{1}{2}\sum_{j=1}^{2}\sum_{i=1}^{N_r}|h_{ij}|^2 SNR_t}\right). \tag{2.38}$$

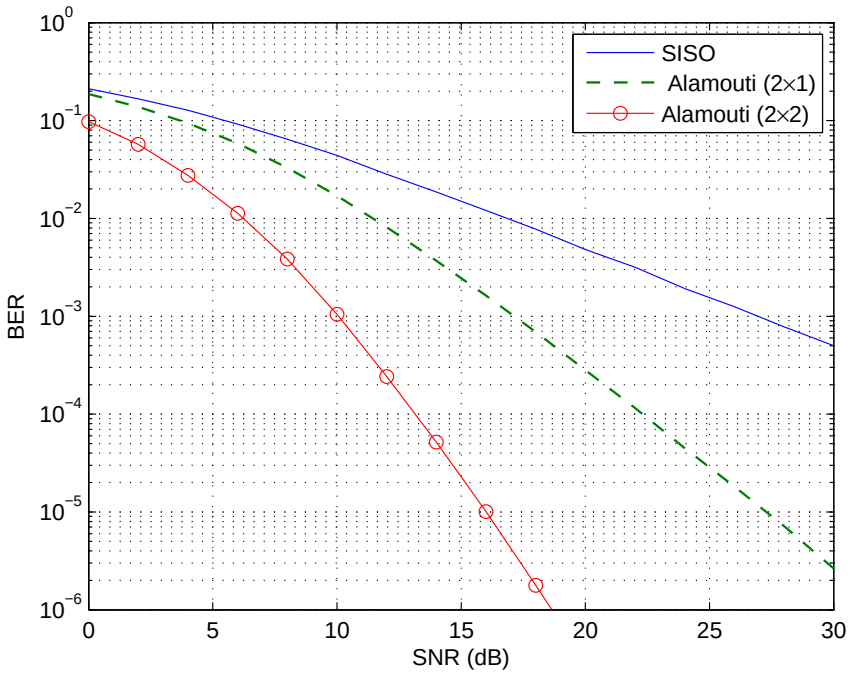

Figure 2.8: BER performance of Alamouti (2×1) and (2×2) schemes with QPSK modulation.

We conclude that the Alamouti code achieves the full diversity of $2N_r$ available in the MIMO system with $N_t = 2$ transmit and N_r receive antennas. Fig. 2.8 shows the Alamouti ($N_t = 2$, $N_r = 2$) and ($N_t = 2$, $N_r = 1$) BER performance with QPSK modulation. We see that by adding an additional antenna at the receiver side we improve the performance.

Tarokh *et al.* [44] constructed orthogonal space-time block codes for real and complex alphabets for arbitrary number of antennas. In particular, Tarokh *et al.* constructed real orthogonal space-time block codes with rate-one for any number of transmit antennas and complex orthogonal space-time block codes with rate 3/4 for three and four antennas, and with rate 1/2 for more than four antennas. Orthogonal space-time codes for three and four transmit antennas [45] are given by:

$$\mathbf{G} = \begin{bmatrix} s_1 & 0 & -s_2^* \\ 0 & s_1 & -s_3 \\ s_2 & s_3^* & s_1^* \\ -s_3 & s_2^* & 0 \end{bmatrix}, \text{ and } \mathbf{G} = \begin{bmatrix} s_1 & 0 & -s_2^* & s_3^* \\ 0 & s_1 & -s_3 & -s_2 \\ s_2 & s_3^* & s_1^* & 0 \\ -s_3 & s_2^* & 0 & s_1^* \end{bmatrix}. \tag{2.39}$$

The construction of maximal rate complex orthogonal space-time block codes was studied by Liang in [46]. The maximal rate of a complex orthogonal space-time block code with M

transmit antennas is given by [46]:

$$R_s = \frac{\lceil M/2 \rceil + 1}{2 \lceil M/2 \rceil}. \tag{2.40}$$

As can be seen from this formula, the code rate tend to 1/2 as the number of antennas increases. This drawback is one of the reasons that provided the motivation to construct other STBC schemes such as diagonal algebraic space-time (DAST) block codes. DAST block codes are a family of linear space-time codes constructed by the use of rotated constellations [47, 48]. The word algebraic in the description of DAST codes comes from the fact that rotation matrices used in DAST codes were constructed using algebraic number field theory [49]. The word diagonal refers to the structure of the code matrix, wherein the rotated information symbols are spread over the diagonal of the square code matrix. The DAST block codes not only achieve full diversity order for arbitrary number of transmit antennas, but they also achieve a transmission rate of one symbol per channel use.

Several other nonorthogonal STBC schemes can be found in the literature, we cite, for example, Quasiorthogonal Space-Time Block Codes [50–54], and Semi-Orthogonal Space-Time (SAST) Block Codes [55].

2.1.2 Spatial multiplexing

The implementation of multi-antenna system at the transmitter and receiver side can be used to increase the data rate (throughput). This scenario is called Spatial Multiplexing (SM). The symbols to be transmitted are grouped by block of N_t different symbols to form the vector

$$\mathbf{s} = \begin{bmatrix} s_1 & s_2 & \cdots & s_{N_t} \end{bmatrix}^T. \tag{2.41}$$

Then the N_t symbols are simultaneously transmitted, each by a single transmit antenna. Therefore, we have the following equation:

$$\mathbf{r} = \begin{bmatrix} r_1 \\ r_2 \\ \vdots \\ r_{N_r} \end{bmatrix} = \begin{bmatrix} h_{11} & h_{12} & ... & h_{1N_t} \\ h_{21} & h_{22} & ... & h_{2N_t} \\ & & ... & \\ h_{N_r1} & h_{N_r2} & ... & h_{N_rN_t} \end{bmatrix} \begin{bmatrix} s_1 \\ s_2 \\ \vdots \\ s_{N_t} \end{bmatrix} + \begin{bmatrix} n_1 \\ n_2 \\ \vdots \\ n_{N_r} \end{bmatrix} \tag{2.42}$$

To recover the vector $\mathbf{s}$ without ambiguity from the received vector $\mathbf{r}$, we need at least N_t independent observations since $\mathbf{s}$ has N_t unknown symbols. This implies that $N_r \geq N_t$. Many techniques have been proposed to derive an estimate vector $\hat{\mathbf{s}}$ of $\mathbf{s}$. We consider only three different detectors for recovering the transmitted data symbols and evaluate their performance. Throughout this development, we assume that the detector perfectly knows the elements of the channel matrix $\mathbf{H}$. In practice, the elements of $\mathbf{H}$ are estimated by using channel probe signals [37].

Zero Forcing (ZF) detector

The Zero Forcing (ZF) detector combines linearly the received signals $\{r_i, 1 \leq i \leq N_r\}$ to form an estimate of the transmitted symbols $\{s_j, 1 \leq j \leq N_t\}$. The linear combining is

represented in matrix form as:

$$\hat{\mathbf{s}} = \mathbf{W}^H \mathbf{r}, \tag{2.43}$$

where $\mathbf{W}$ is an $N_r \times N_t$ weighting matrix. ZF performs the detection by using the Moore-Penrose pseudo-inverse matrix of $\mathbf{H}$ [16]:

$$\mathbf{W}^H = (\mathbf{H}^H \mathbf{H})^{-1} \mathbf{H}^H. \tag{2.44}$$

The weighting matrix $\mathbf{W}$ verifies the condition: $\mathbf{W}^H \mathbf{H} = \mathbf{I}_{N_t}$, where $\mathbf{I}_{N_t}$ is the identity matrix of size $N_t \times N_t$. Then, $\hat{\mathbf{s}}$ is obtained by computing:

$$\begin{aligned} \hat{\mathbf{s}} &= \mathbf{W}^H \mathbf{r} \\ &= \mathbf{s} + \mathbf{W}^H \mathbf{n}. \end{aligned} \tag{2.45}$$

Each element of the estimate $\hat{\mathbf{s}}$ is then quantized to the closest transmitted symbol value. We note that the ZF detector estimate $\hat{\mathbf{s}}$ is not corrupted by interchannel interference. However, the major problem with this technique is that the noise term can be enhanced while multiplying by $\mathbf{W}^H$. To avoid this noise enhancement, the MMSE method is often used.

Minimum Mean-Square-Error (MMSE) detector

The MMSE detector also forms an estimate of $\mathbf{s}$ by linearly combining the received signals $\{r_i, 1 \leq i \leq N_r\}$. In this case, the weighting matrix $\mathbf{W}$ is selected to minimize the mean square error:

$$J(\mathbf{W}) = \mathbb{E}\{\|\mathbf{s} - \mathbf{W}^H \mathbf{r}\|^2\}. \tag{2.46}$$

Minimization of $J(\mathbf{W})$ leads to the solution for the optimum weight vectors $\mathbf{w}_1$, $\mathbf{w}_2$, ..., $\mathbf{w}_{N_t}$ as [37]

$$\mathbf{w}_i = \mathbf{R}_{rr}^{-1} \mathbb{E}\{s_i^* \mathbf{r}\}, \quad i = 1, 2, ..., N_t \tag{2.47}$$

where $\mathbf{R}_{rr}$ is the $N_r \times N_r$ autocorrelation matrix of the received signal vector and given by:

$$\begin{aligned} \mathbf{R}_{rr} &= \mathbb{E}\{\mathbf{r}\mathbf{r}^H\} \\ &= \mathbf{H}\mathbf{R}_{ss}\mathbf{H}^H + \sigma^2 \mathbf{I}_{N_r}, \end{aligned} \tag{2.48}$$

where $R_{ss} = \mathbb{E}\{\mathbf{s}\mathbf{s}^H\}$, and $\mathbb{E}\{\mathbf{n}\mathbf{n}^H\} = \sigma^2 \mathbf{I}_{N_r}$. Since the signal vector $\mathbf{s}$ has uncorrelated zero-mean components, $\mathbf{R}_{ss}$ is a diagonal matrix $R_{ss} = \sigma_s^2 \mathbf{I}_{N_t}$ where σ_s^2 is the signal variance on each transmit antenna. Furthermore, we have:

$$\begin{aligned} \mathbb{E}\{\mathbf{s}_i^* \mathbf{r}\} &= \mathbb{E}\{\mathbf{s}_i^* \mathbf{H}\mathbf{s}\} + \mathbb{E}\{\mathbf{s}_i^* \mathbf{n}\} \\ &= \mathbb{E}\{\mathbf{s}_i^* \sum_{j=1}^{N_t} \mathbf{h}_j s_j\} \\ &= \sigma_s^2 \mathbf{h}_i, \end{aligned} \tag{2.49}$$

where $\mathbf{h}_i$ is the ith vector (or column) of the channel matrix $\mathbf{H}$. Then, according to (2.48) and (2.49), Equation (2.47) becomes

$$\mathbf{w}_i = \sigma_s^2(\sigma_s^2\mathbf{H}\mathbf{H}^H + \sigma^2\mathbf{I}_{N_r})^{-1}\mathbf{h}_i, \quad i = 1, 2, ..., N_t \tag{2.50}$$

Therefore, the weighting matrix $\mathbf{W}$ for the MMSE detector is given by

$$\mathbf{W} = \left(\mathbf{H}\mathbf{H}^H + \frac{\sigma^2}{\sigma_s^2}\mathbf{I}_{N_r}\right)^{-1}\mathbf{H}. \tag{2.51}$$

Finally, the estimated vector of $\mathbf{s}$ is obtained by $\hat{\mathbf{s}} = \mathbf{W}^H\mathbf{r}$. Then, each component of the estimate $\hat{\mathbf{s}}$ is quantized to the closest transmitted value.

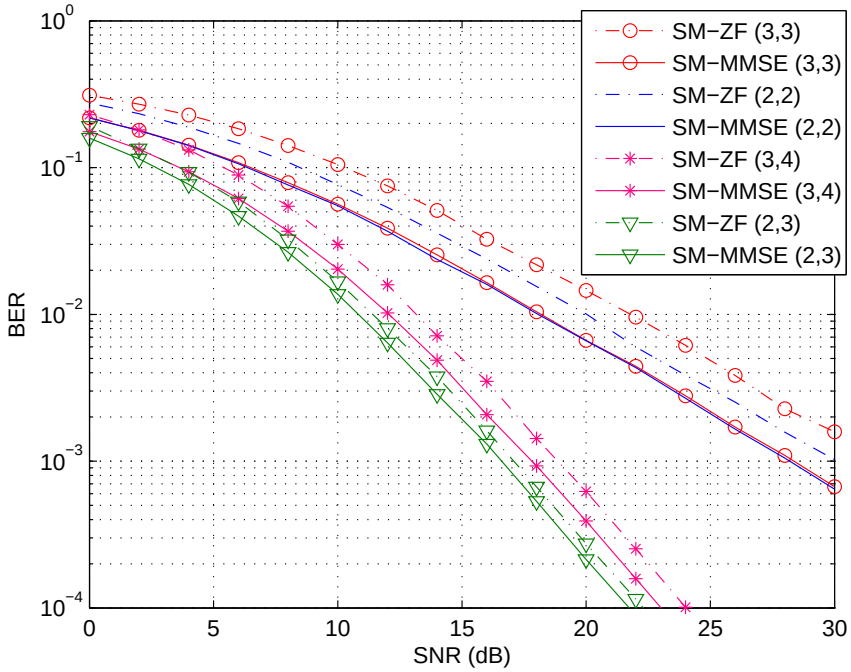

Figure 2.9: BER performance as a function of the SNR for different SM schemes with QPSK modulation and both ZF and MMSE equalizers.

In general, with spatial multiplexing, the linear detectors such as ZF and MMSE achieve a diversity order of $N_r - N_t + 1$, for any $N_r \geq N_t$. Indeed, with N_t antennas transmitting independent data streams and N_r receiving antennas, a linear detector has N_r degrees of freedom. In detecting any one data stream, in the presence of $N_t - 1$ interfering signals from the other transmitting antennas, the linear detectors utilize $N_t - 1$ degrees of freedom to cancel out the $N_t - 1$ interfering signals [37]. Therefore, the effective order of diversity for the linear detectors is $N_r - (N_t - 1) = N_r - N_t + 1$. A thorough performance study of the ZF and MMSE detectors can be found in [56]. Fig. 2.9 gives a comparison between ZF and MMSE performance, for different configurations, in terms of BER as a function of SNR, with QPSK modulation. We note that MMSE detector outperforms the ZF one, although both achieve the same diversity order.

Maximum Likelihood (ML) detection

The Maximum Likelihood (ML) detector is the optimum one in the sense that it minimizes the probability of error [57]. In ML decoding, the estimate $\hat{\mathbf{s}}$ is the vector among all possible transmitted vector $\mathbf{s}$, which minimizes the error probability subject to the N_r observations. Since the additive noise at the N_r receiving antennas are statically independent and identically distributed zero-mean Gaussian, the joint conditional PDF $p(\mathbf{r}/\mathbf{s})$ is also Gaussian. Therefore, the ML detector selects the symbol vector $\hat{\mathbf{s}}$ that minimizes the Euclidean distance metric:

$$d(\mathbf{s}) = \sum_{i=1}^{N_r} \left| r_i - \sum_{j=1}^{N_t} h_{ij} s_j \right|^2 \tag{2.52}$$

Therefore, the estimate $\hat{\mathbf{s}}$ in ML detection is obtained by:

$$\begin{aligned} \hat{\mathbf{s}} &= \arg\max_{\mathbf{s}} \{p(\mathbf{r}/\mathbf{s})\} \\ &= \arg\min_{\mathbf{s}} \{d(\mathbf{s})\} \\ &= \arg\min_{\mathbf{s}} \{\|\mathbf{r} - \mathbf{H}\mathbf{s}\|^2\}. \end{aligned} \tag{2.53}$$

The ML decoder leads to the best performance in term of error probability per symbol but its complexity increases exponentially with N_t and polynomially with N_r. To reduce this complexity, Sphere Decoding algorithms have been proposed in [58, 59].

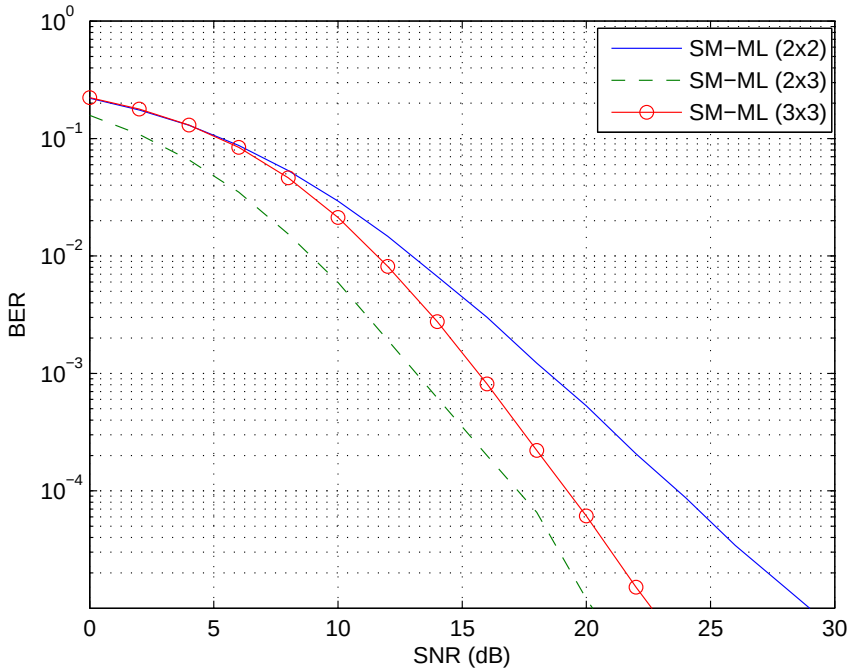

Figure 2.10: BER performance as a function of the SNR for different SM schemes with ML detection and QPSK modulation.

Several works [60–62] have focused on the performance assessing of the MIMO ML detection in terms of BER as a function of the SNR. An asymptotic union bound of the BER p_{eb} for Rayleigh MIMO channel with MLD is given in [60], and can be written as:

$$p_{eb} = \alpha SNR^{-N_r}, \tag{2.54}$$

where α is a parameter depending on the modulation type and the number of the transmit and receive antennas, and does not depend on the SNR. Hence, this implies that the diversity order of MLD is equal to the number of receive antennas N_r, independent of the number of transmit antennas N_t. Of course, there is an SNR penalty due to the increased number of transmit antennas N_t, because the parameter α grows with the increase of N_t [60]. Fig. 2.10 depicts the performance of MLD, in terms of the BER as a function of the SNR, with QPSK modulation and for different MIMO configurations. We can see that the curve slopes increase only with the growth of N_r. But, we also remark an SNR loss when the number of transmit antennas is increased.

2.1.3 Diversity-Multiplexing tradeoff

The previous sections highlight two methods for using multiple antennas to improve the performance of wireless systems. The first one exploits the different channel gains in order to obtain a very robust channel with high diversity gain. The second uses the different channels to increase the data rate by multiplexing different data streams onto these channels. This capacity gain is also referred to as a multiplexing gain. However, it is not necessary to use the antennas purely for diversity or multiplexing. Some of the space-time dimensions can be used for diversity gain, and the remaining dimensions used for multiplexing gain [13]. For finite space-time block lengths, it is not possible to achieve full diversity and full multiplexing gain simultaneously, in which case there is a tradeoff between these gains. The tradeoff between data rate and probability of error has been extensively studied in the literature [63–66]. A transmission scheme is said to achieve multiplexing gain r and diversity gain d if the data rate per unit Hertz $R(SNR)$ and the probability of error $P_e(SNR)$ as functions of SNR satisfy [64]:

$$\lim_{SNR\to+\infty} \frac{R(SNR)}{\log_2(SNR)} = r, \tag{2.55}$$

$$\lim_{SNR\to+\infty} \frac{\log(P_e(SNR))}{\log(SNR)} = -d. \tag{2.56}$$

For each r, we can define the optimal diversity gain $d_{opt}(r)$ as the maximum diversity order that we can achieve using any transmission scheme. The authors in [64] show that if the fading block length is larger than the total number of the transmit and receive antennas, then we have:

$$d_{opt}(r) = (N_t - r)(N_r - r), \qquad 0 \leq r \leq \min(N_t, N_r). \tag{2.57}$$

Therefore, we can adapt the diversity and multiplexing gains relative to channel conditions. Specifically, in poor channel states more antennas can be used for diversity gain, whereas in good states more antennas can be used for multiplexing [13].

2.2 Orthogonal frequency division multiplexing (OFDM)

The Orthogonal Frequency Division Multiplexing (OFDM) [67, 68] is the most widespread modulation among all the multicarrier modulations. In general, the idea of multicarrier modulation is to divide the transmitted bit stream into different substreams and send them, after mapping, over different orthogonal subchannels centered at different subcarrier frequencies f_k, with $k = 0, 1, ..., M-1$. The number M of substreams is chosen sufficiently large to insure that each subchannel has a bandwidth less than the coherence bandwidth of the channel. Equivalently, it makes the symbol time T on each substream much greater than the delay spread T_L of the channel. Hence, the substreams experience relatively flat fading. Thus, the ISI on each subchannel is small [13]. Fig. 2.11 illustrates a multicarrier transmitter.

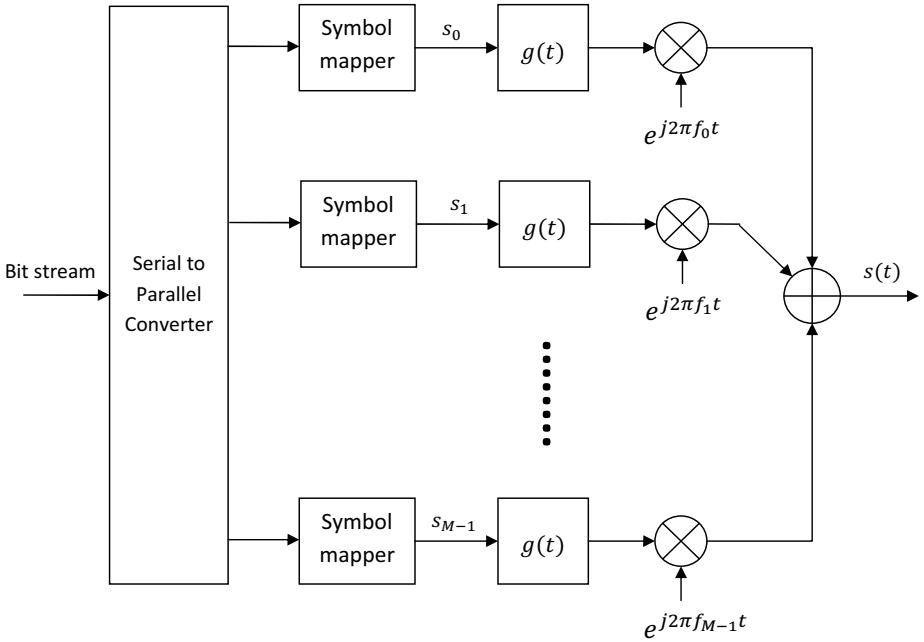

Figure 2.11: Multicarrier transmitter.

2.2.1 OFDM principle

In OFDM, the frequencies f_k are spaced by $\Delta f = \frac{1}{T}$, so $f_k = f_c + \frac{k}{T}$ where f_c is the carrier frequency. Let us assume $s_{k,n}$ is the data symbol to transmit on the kth subcarrier at instant nT. Then, the transmitted baseband signal can be written as [13]:

$$s(t) = \frac{1}{\sqrt{M}} \sum_{k=0}^{M-1} \sum_{n} s_{k,n} g(t - nT) e^{j2\pi \frac{kt}{T}}, \tag{2.58}$$

where the factor $\frac{1}{\sqrt{M}}$ is introduced for power normalization, and $g(t)$ is , in general, the rectangular window function:

$$g(t) = \begin{cases} 1 & 0 \leq t < T \\ 0 & \text{otherwise} \end{cases} \tag{2.59}$$

Assuming a distortion-free channel, perfect reconstruction of complex symbols is obtained thanks to the following complex orthogonality condition:

$$\int_{\mathbb{R}} g(t-nT)g(t-n'T)e^{j2\pi\frac{kt}{T}}e^{j2\pi\frac{k't}{T}}dt = \delta_{k,k'}\delta_{n,n'} \tag{2.60}$$

where $\delta_{k,k'} = 1$ if $k = k'$ and $\delta_{k,k'} = 0$ if $k \neq k'$.

In practice, $s(t)$ is the analog signal obtained from the discrete time samples $s[m] = s(mT_s)$ using the Nyquist sampling theorem [37, 42], where $T_s = \frac{T}{M}$ is the sampling period. Hence, the discrete time transmitted signal can be expressed as follows:

$$s[m] = \frac{1}{\sqrt{M}}\sum_{k=0}^{M-1}\sum_{n} s_{k,n}g[m-nM]e^{j2\pi\frac{km}{M}}. \tag{2.61}$$

The expression above is efficiently implemented using the Inverse Discrete Fourier Transform (IDFT). Let $x[m]$, $0 \leq m < M$, denote a discrete time sequence. The M-point DFT of $x[m]$ is defined as [69]:

$$X[k] = \frac{1}{\sqrt{M}}\sum_{m=0}^{M-1} x[m]e^{-j2\pi\frac{mk}{M}}, \quad 0 \leq k < M. \tag{2.62}$$

The DFT is the discrete-time equivalent to the continuous-time Fourier transform. Both the continuous-time Fourier transform and the DFT are based on the fact that complex exponentials are eigenfunctions for any linear system [13]. The sequence $x[m]$ can be recovered from its DFT using the IDFT:

$$x[m] = \frac{1}{\sqrt{M}}\sum_{k=0}^{M-1} X[k]e^{j2\pi\frac{km}{M}}, \quad 0 \leq m < M. \tag{2.63}$$

The DFT and its inverse are typically performed in hardware using the fast Fourier transform (FFT) algorithm [70].

For a given time index $n = n_0$, the expression of the transmitted signal $s[m]$, given by (2.61), becomes:

$$s_{n_0}[m] = \frac{1}{\sqrt{M}}\sum_{k=0}^{M-1} s_{k,n_0}e^{j2\pi\frac{km}{M}}, \quad n_0M \leq m < (n_0+1)M. \tag{2.64}$$

Substituting m by $m + n_0M$, it yields:

$$s_{n_0}[m] = \frac{1}{\sqrt{M}}\sum_{k=0}^{M-1} s_{k,n_0}e^{j2\pi\frac{km}{M}}, \quad 0 \leq m < M. \tag{2.65}$$

According to the definition of the IDFT given by (2.63), we conclude that the n_0th transmitted sequence block $s_{n_0}[m]$ is the IDFT of the data sequence s_{k,n_0}, $0 \leq k < M$. Therefore, the whole transmitted signal $s[m]$, given in (2.61), can be seen as a succession of blocks obtained by performing the IDFT on data blocks $\{s_{k,n}, \quad 0 \leq k < M\}$. Fig. 2.12 depicts the basic transmitter architecture of OFDM.

It is also straightforward to show that the OFDM transmitter can be represented by a simple matrix multiplication. Let $\mathbf{s}_n = [s_{0,n} \quad s_{1,n} \quad ... \quad s_{M-1,n}]^T$ be a vector whose

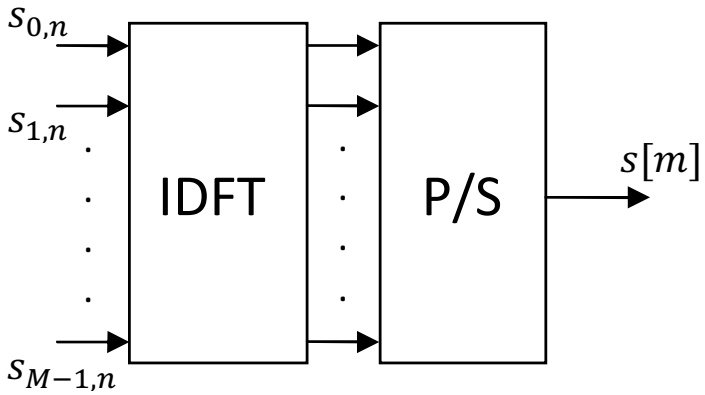

Figure 2.12: Basic OFDM transmitter architecture

elements are the data symbols in the nth block, and $\bar{\mathbf{s}}_n = [s_n[0] \quad s_n[1] \quad ... \quad s_n[M-1]]^T$ be the M-point IDFT of the vector $\mathbf{s}_n$. Then, we can write in the matrix form [13]:

$$\bar{\mathbf{s}}_n = \mathbf{W}^H \mathbf{s}_n \tag{2.66}$$

where $\mathbf{W}$ is the $M \times M$ DFT matrix given by:

$$\mathbf{W} = \frac{1}{\sqrt{M}} \begin{bmatrix} 1 & 1 & 1 & \cdots & 1 \\ 1 & w_M & w_M^2 & \cdots & w_M^{M-1} \\ \vdots & \vdots & \vdots & \ddots & \vdots \\ 1 & w_M^{M-1} & w_M^{2(M-1)} & \cdots & w_M^{(M-1)^2} \end{bmatrix}, \tag{2.67}$$

with $w_M = e^{-j\frac{2\pi}{M}}$. It is worth noticing that $\mathbf{W}$ is a unit matrix, so $\mathbf{W}^H\mathbf{W} = \mathbf{I}_M$ where $\mathbf{I}_M$ is the $M \times M$ identity matrix.

When the time-invariant channel is flat fading, *i.e.* it is represented by a single complex tap $h[0]$, the received discrete baseband signal is written as:

$$y[m] = h[0]s[m] = \frac{h[0]}{\sqrt{M}} \sum_n \sum_{k=0}^{M-1} s_{k,n} g[m - nM] e^{j2\pi \frac{km}{M}} + \gamma[m], \tag{2.68}$$

where $\gamma[m]$ denotes a complex AWGN term with variance σ^2. Assuming coherent demodulation and perfect synchronization, the signal at the demodulator output can be given by:

$$r_{k,n} = \frac{1}{\sqrt{M}} \sum_{m=-\infty}^{+\infty} y[m] g[m - nM] e^{-j2\pi \frac{km}{M}} \tag{2.69}$$

$$= \frac{1}{\sqrt{M}} \sum_{m=nM}^{(n+1)M-1} y[m] e^{-j2\pi \frac{km}{M}} \tag{2.70}$$

$$= \frac{1}{\sqrt{M}} \sum_{m=0}^{M-1} y[m + nM] e^{-j2\pi \frac{km}{M}} \tag{2.71}$$

According to the definition given in (2.62), the last expression corresponds to the DFT operation on the nth received M-point block starting from $m = nM$ and ending at $m = (n+1)M - 1$. Now, substituting (2.68) into (2.71), we obtain:

$$r_{k,n} = \frac{h[0]}{M} \sum_{m=0}^{M-1} \sum_{n'} \sum_{k'=0}^{M-1} s_{k',n'} g[m-(n'-n)M] e^{j2\pi \frac{(k'-k)m}{M}} + \acute{\gamma}_{k,n} \tag{2.72}$$

$$= \frac{h[0]}{M} \sum_{k'=0}^{M-1} s_{k',n} \sum_{m=0}^{M-1} e^{j2\pi \frac{(k'-k)m}{M}} + \acute{\gamma}_{k,n} \tag{2.73}$$

$$= h[0] s_{k,n} + b_{k,n} \tag{2.74}$$

where $\acute{\gamma}_{k,n} = \frac{1}{\sqrt{M}} \sum_{m=0}^{M-1} \gamma[m+nM] e^{-j2\pi \frac{km}{M}}$ which is also an AWGN with the same variance σ^2. Thus, the data symbol can be recovered as $\hat{s}_{k,n} = r_{k,n}/h[0]$. From a matrix point of view, since the demodulation can be obtained by using the DFT, as shown in (2.71), we can write the nth demodulated vector as:

$$\mathbf{r}_n = \begin{bmatrix} r_{0,n} \\ r_{1,n} \\ \vdots \\ r_{M-1,n} \end{bmatrix} = \mathbf{W} \begin{bmatrix} y[nM] \\ y[nM+1] \\ \vdots \\ y[(n+1)M-1] \end{bmatrix} \tag{2.75}$$

$$= h[0]\mathbf{W}\bar{\mathbf{s}}_n + \mathbf{b}_n = h[0]\mathbf{W}\mathbf{W}^H\mathbf{s}_n + \mathbf{b}_n$$

$$= h[0]\mathbf{s}_n + \mathbf{b}_n \tag{2.76}$$

where $\mathbf{b}_n = \begin{bmatrix} b_{0,n} & b_{1,n} & \dots & b_{(n+1)M-1,n} \end{bmatrix}^T$ is the AWGN vector at the demodulator output. Again, the estimated transmitted vector $\hat{\mathbf{s}}_n$ can be obtained as $\hat{\mathbf{s}}_n = \mathbf{r}_n/h[0]$.

2.2.2 OFDM in frequency selective channel

In the case where the time-invariant channel is frequency-selective, the channel is represented by its finite impulse response (FIR) $h[m], \quad 0 \leq m < L$. The received discrete-time baseband signal at the demodulator input is given by:

$$y[m] = h[m] * s[m] = \sum_{l=0}^{L-1} h[m]s[m-l] + n[m]. \tag{2.77}$$

As aforementioned, the transmitted signal $s[m]$ can be seen as a sequence of contiguous and disjoint signal blocks. However, these signal blocks are overlapped due to the multipath effect of the channel. As long as we assume that $M > L$, only each two consecutive blocks interfere with each other. Any output sequence of a FIR filter can be represented in a matrix form. Let us arrange the nth block of the channel output sequence in an $M \times 1$ vector as $\mathbf{y}_n = [y[nM] \quad y[nM+1] \quad \dots \quad y[(n+1)M-1]]^T$. Then, we can rewrite (2.77) in

the matrix form as:

$$\mathbf{y}_n = \begin{bmatrix} h[L-1] & h[L-2] & \cdots & h[0] & 0 & \cdots & 0 \\ 0 & h[L-1] & h[L-2] & \cdots & h[0] & \ddots & \vdots \\ \vdots & \ddots & \ddots & \ddots & & \ddots & 0 \\ 0 & \cdots & 0 & h[L-1] & h[L-2] & \cdots & h[0] \end{bmatrix} \begin{bmatrix} s[nM-L+1] \\ s[nM-L+2] \\ \vdots \\ s[nM-1] \\ s[nM] \\ \vdots \\ s[(n+1)M-1] \end{bmatrix} + \mathbf{n}_n \tag{2.78}$$

where $\mathbf{n}_n = [n[nM] \quad n[nM+1] \quad ... \quad n[(n+1)M-1]]^T$ is the noise vector. We notice that the elements $s[nM-L+1]$, $s[nM-L+2]$, ..., $s[nM-1]$ belong to the previous data block $\{s[(n-1)M], ..., s[nM-1]\}$. Therefore, the elements in $\mathbf{y}_n$ are linear combinations of elements in $\bar{\mathbf{s}}_n$ and $\bar{\mathbf{s}}_{n-1}$. Thus, as there is inter-bock interference in $\mathbf{y}_n$, the detection of $\mathbf{s}_n$ will require a complex equalization. To avoid inter-block interference, it has been proposed to add a guard interval, sufficiently large, in order to separate the data blocks. This could be done by adding zeros at the beginning of each vector $\bar{\mathbf{s}}_n$, which leads to the so-called Zero-Padding OFDM (ZP-OFDM) [71]. One tap equalization per subcarrier is ensured by adding a Cyclic Prefix (CP) [14, 15] to each vector $\bar{\mathbf{s}}_n$ leading to what is called CP-OFDM. In CP-OFDM, we add to $\bar{\mathbf{s}}_n$ given in (2.66) a duplication of its $L' \geq L-1$ last elements at its beginning, leading to the vector:

$$\tilde{\mathbf{s}}_n = \left.\begin{bmatrix} s[(n+1)M-L'] \\ s[(n+1)M-L'+1] \\ \vdots \\ \vdots \\ s[(n+1)M-1] \\ s[nM] \\ s[nM+1] \\ \vdots \\ s[(n+1)M-1] \end{bmatrix}\right\} \text{The } L' \text{ elements of the CP} \tag{2.79}$$

Hence, it is worth noticing that the transmitted blocks contain now $M+L'$ elements instead of M. Therefore, To take into account this change, the expression of $s[m]$ in (2.61) is slightly modified as:

$$s[m] = \frac{1}{\sqrt{M}} \sum_{k=0}^{M-1} \sum_{n} s_{k,n} \acute{g}[m - n(M+L')] e^{j2\pi \frac{km}{M}}. \tag{2.80}$$

where $\acute{g}[m]$ is now given by:

$$\acute{g}[m] = \begin{cases} 1 & -L' \leq m < M \\ 0 & \text{otherwise} \end{cases} \tag{2.81}$$

Since the cyclic prefix is introduced to absorb the multipath channel effect and separate the data blocks, the cyclic prefix is discarded at the receiver side. Then, the $M \times 1$ vector

$\mathbf{y}_n$ used for demodulation is now given by

$$\mathbf{y}_n = \begin{bmatrix} y[n(M+L')] & y[n(M+L')+1] & \dots & y[n(M+L')+M-1] \end{bmatrix}^T \tag{2.82}$$

and is expressed as:

$$\mathbf{y}_n = \begin{bmatrix} \overbrace{\begin{matrix} 0 & \cdots & 0 & h[L-1] & h[L-2] & \cdots & h[0] \\ 0 & \cdots & \cdots & 0 & h[L-1] & h[L-2] & \cdots \\ \vdots & \vdots & \vdots & \vdots & \ddots & \ddots & \ddots \\ 0 & \cdots & \cdots & 0 & \cdots & 0 & h[L-1] \end{matrix}}^{L' \text{ elements}} & \begin{matrix} 0 & \cdots & 0 \\ h[0] & \ddots & \vdots \\ & \ddots & 0 \\ h[L-2] & \cdots & h[0] \end{matrix} \end{bmatrix}_{M \times (M+L')} \times$$

$$\begin{bmatrix} s[(n+1)M-L'] \\ s[(n+1)M-L'+1] \\ \vdots \\ s[(n+1)M-1] \\ s[nM] \\ s[nM+1] \\ \vdots \\ s[(n+1)M-1] \end{bmatrix} + \underbrace{\begin{bmatrix} \gamma[n(M+L')] \\ \gamma[n(M+L')+1] \\ \vdots \\ \gamma[n(M+L')+M-1] \end{bmatrix}}_{\gamma_n} \tag{2.83}$$

First, we simplify this equation by omitting the first $L'-L$ null columns in the channel matrix and their $L'-L$ corresponding elements in the vector $\tilde{\mathbf{s}}_n$. This simplification proofs that it is sufficient to choose $L'=L$. Then, we obtain:

$$\mathbf{y}_n = \begin{bmatrix} h[L-1] & h[L-2] & \cdots & h[0] & 0 & \cdots & 0 \\ 0 & h[L-1] & h[L-2] & \cdots & h[0] & \ddots & \vdots \\ \vdots & \ddots & \ddots & \ddots & & \ddots & 0 \\ 0 & \cdots & 0 & h[L-1] & h[L-2] & \cdots & h[0] \end{bmatrix} \begin{bmatrix} s[(n+1)M-L] \\ s[(n+1)M-L+1] \\ \vdots \\ s[(n+1)M-1] \\ s[nM] \\ s[nM+1] \\ \vdots \\ s[(n+1)M-1] \end{bmatrix} + \gamma_n \tag{2.84}$$

The expression above can be rewritten based on the vector $\bar{\mathbf{s}}_n$ as:

$$\mathbf{y}_n = \underbrace{\begin{bmatrix} h[0] & 0 & \cdots & 0 & h[L-1] & \cdots & h[1] \\ h[1] & \ddots & \ddots & \ddots & \ddots & \ddots & \vdots \\ \vdots & \ddots & \ddots & \ddots & \ddots & \ddots & h[L-1] \\ h[L-1] & \cdots & h[1] & h[0] & 0 & \cdots & 0 \\ 0 & \ddots & \ddots & \ddots & \ddots & \ddots & \vdots \\ \vdots & \ddots & \ddots & \ddots & \ddots & \ddots & 0 \\ 0 & \cdots & 0 & h[L-1] & \cdots & h[1] & h[0] \end{bmatrix}}_{\mathbf{H}} \underbrace{\begin{bmatrix} s[nM] \\ s[nM+1] \\ \vdots \\ s[(n+1)M-1] \end{bmatrix}}_{\bar{\mathbf{s}}_n} + \gamma_n. \tag{2.85}$$

Hence, thanks to the cyclic prefix, $\mathbf{H}$ is an $M \times M$ circulant matrix, *i.e.* the rows are cyclic shifts of each other. Therefore, the matrix $\mathbf{H}$ has a singular value decomposition in the Fourier basis, *i.e.* there is a diagonal matrix $\bar{\mathbf{H}}$ such that $\bar{\mathbf{H}} = \mathbf{W}\mathbf{H}\mathbf{W}^H$, whose diagonal entries are given by:

$$\bar{\mathbf{H}}_{k,k} = h_k = \sum_{l=0}^{M-1} h[l] e^{-2\pi \frac{kl}{M}}. \tag{2.86}$$

Therefore, the vector $\mathbf{y}_n$ can be expressed as:

$$\begin{aligned} \mathbf{y}_n &= \mathbf{W}^H \bar{\mathbf{H}} \mathbf{W} \bar{\mathbf{s}}_n + \gamma_n \\ &= \mathbf{W}^H \bar{\mathbf{H}} \mathbf{s}_n + \gamma_n \end{aligned} \tag{2.87}$$

Then, the demodulated received vector is:

$$\mathbf{r}_n = \mathbf{W}\mathbf{y}_n = \bar{\mathbf{H}}\mathbf{s}_n + \underbrace{\mathbf{W}\gamma_n}_{\gamma'_n}. \tag{2.88}$$

As $\mathbf{W}$ is a unit matrix, the statistics of γ_n and $\acute{\gamma}_n$ are the same. Thus, the kth element of vector $\mathbf{r}_n$, denoted by $r_{k,n}$, is written as:

$$r_{k,n} = h_k s_{k,n} + \acute{\gamma}_{k,n}, \tag{2.89}$$

where $s_{k,n}$ and $\acute{\gamma}_{k,n}$ are respectively the kth elements of $\mathbf{s}_n$ and $\acute{\gamma}_n$. The integer k is generally referred as the subcarrier index. Then, each transmitted symbol $s_{n,k}$ undergos an equivalent flat fading channel, and a simple one-tap equalization per subcarrier is sufficient to recover the transmitted data.

We can also verify the expression (2.89) using (2.80), (2.77) and the fact that the demodulation is given by:

$$r_{k,n} = \frac{1}{\sqrt{M}} \sum_{m=-\infty}^{+\infty} y[m] g(m - n(M + L')) e^{-j2\pi \frac{mk}{M}} \tag{2.90}$$

$$\begin{aligned} &= \frac{1}{M} \sum_{l=0}^{L-1} h[l] \sum_{k'=0}^{M-1} e^{-j2\pi \frac{k'l}{M}} \sum_{n'} s_{k',n'} C_{k,k',l,n,n'} \\ &\quad + \frac{1}{\sqrt{M}} \sum_{m=-\infty}^{+\infty} \gamma[m] g(m - n(M + L')) e^{-j2\pi \frac{mk}{M}}, \end{aligned} \tag{2.91}$$

where $C_{k,k',l,n,n'} = \sum_{m=-\infty}^{+\infty} \acute{g}[m-l-n'(M+L')]g[m-n(M+L')]e^{j2\pi\frac{(k'-k)m}{M}}$. According to the definitions of $g[m]$ and $\acute{g}[m]$ given respectively in (2.59) and (2.81), $C_{k,k',l,n,n'}$ can be simplified by:

$$\begin{aligned} C_{k,k',l,n,n'} &= \delta_{n',n} \sum_{m=n(M+L')}^{n(M+L')+M-1} e^{j2\pi\frac{(k'-k)m}{M}} \\ &= M\delta_{n',n}\delta_{k',k} \end{aligned} \tag{2.92}$$

Hence, Equation (2.91) becomes:

$$\begin{aligned} r_{k,n} &= \sum_{l=0}^{L-1} h[l]e^{-j2\pi\frac{kl}{M}} \times s_{k,n} + \underbrace{\frac{1}{\sqrt{M}} \sum_{m=n(M+L')}^{n(M+L')+M-1} \gamma[m]e^{-j2\pi\frac{mk}{M}}}_{\acute{\gamma}_{k,n}} \\ &= h_k s_{k,n} + \acute{\gamma}_{k,n}, \end{aligned} \tag{2.93}$$

where $h_k = \sum_{l=0}^{L-1} h[l]e^{-j2\pi\frac{kl}{M}} = \sum_{l=0}^{M-1} h[l]e^{-j2\pi\frac{kl}{M}}$ since $L < M$. Hence, we obtain the same expression as (2.89).

The possibility of a one-tap equalization is undoubtedly an important advantage of CP-OFDM. The fact that the DFT demodulation (Resp. the IDFT modulation) can take advantage of the Fast Fourier Transform (FFT) algorithms (Resp. IFFT) is another recognized interest for CP-OFDM. However, there is a loss of spectral efficiency as the CP only contains redundant information. Another drawback is related to the rectangular pulse shaping which leads to a poor frequency localization [17]. Therefore, it is fair to say that OFDM can only achieve a symbol density of less than one, and the symbol density one can only be thought as an unachievable upper limit.

2.2.3 OFDM with MIMO systems

We have seen that when the cyclic prefix (CP) is longer than the delay of the channel impulse response, the OFDM system model is equivalent to a flat fading one as obtained in (2.89). Therefore, MIMO systems can be perfectly associated to OFDM modulation. Let $s_{k,n}^{(j)}$, $j = 1, ..., N_t$, be the data symbols to be transmitted at the jth antenna. After IDFT operation and CP insertion, each antenna "j" transmits a signal $s_j[m]$ according to (2.80). Each transmitted signal $s_i[m]$ passes through a different multipath channel $h_{ij}[m]$ from the transmit antenna "j" to the ith receive antenna. Then, at the receiver side, each antenna "i" collects the following signal:

$$r_i[m] = \sum_{j=1}^{N_t} h_{ij}[m] * s_j[m] + w_i[m], \tag{2.94}$$

where $w_i[m]$ is the noise term at the "i"th antenna. Assuming that the CP size is longer than the channel delays, the expression of the signals after OFDM demodulation at each receive antenna "i" is given by:

$$r_{k,n}^{(i)} = \sum_{j=1}^{N_t} h_{k,n}^{(ij)} s_{k,n}^{(j)} + \gamma_{k,n}^{(i)}, \tag{2.95}$$

where $\gamma_{k,n}^{(i)}$ is the noise term at the demodulator output, and $h_{k,n}^{(ij)} = \sum_{l=0}^{L-1} h_{ij}[l] e^{-j2\pi \frac{kl}{M}}$. We should note that the expression above is true because OFDM modulation and demodulation are linear operations. Finally, we can rewrite the latter equation in a matrix form as:

$$\begin{bmatrix} r_{k,n}^{(1)} \\ \vdots \\ r_{k,n}^{(N_r)} \end{bmatrix} = \underbrace{\begin{bmatrix} h_{k,n}^{(11)} & \cdots & h_{k,n}^{(1N_t)} \\ \vdots & \ddots & \vdots \\ h_{k,n}^{(N_r1)} & \cdots & h_{k,n}^{(N_rN_t)} \end{bmatrix}}_{\mathbf{H}_{k,n}} \begin{bmatrix} s_{k,n}^{(1)} \\ \vdots \\ s_{k,n}^{(N_t)} \end{bmatrix} + \begin{bmatrix} \gamma_{k,n}^{(1)} \\ \vdots \\ \gamma_{k,n}^{(N_r)} \end{bmatrix}. \tag{2.96}$$

2.3 FBMC/OQAM modulation

To overcome some CP-OFDM shortcoming such as the poor spectrum localization, we have to use a finite pulse shape filter (or prototype filter) $g[m]$ different from the rectangular one with smooth edges [72]. This leads to the filtered OFDM [73] and the filter-bank multicarrier (FBMC) systems [9,23,27]. On the other hand, any guard interval use leads to a spectral efficiency loss (*i.e.* symbol density $\rho < 1$), like in OFDM due to the CP. Hence, to avoid this drawback, we have to choose a multicarrier scheme with symbol density of one ($\rho = 1$). However, it is theoretically proven with the Balian Low theorem, see [74], that it is not possible to get a prototype function being well-localized in time and frequency, and satisfying in the meantime the orthogonality condition and a symbol density of one ($\rho = 1$).

Therefore, in order to meet these objectives, we must relax the orthogonality condition and restrict it to the real field. Then, to be able to recover the data at the receiver side, the transmitted data must be real-valued (or purely imaginary) chosen from a PAM constellation instead of a QAM one. But to maintain the same desired data rate, we should choose a symbol density of two real-valued symbols (to be equivalent to the one complex-valued symbol) per area unit of the time-frequency plane [72].

2.3.1 FBMC/OQAM principle

The main idea in FBMC/OQAM is to transmit offset QAM symbols instead of conventional QAM ones. Indeed, at the transmitter side each complex data symbol $s_{k,n}$, $k = 0, 1, ..., M-1$, carried at rate $F = 1/T$ by the kth substream, is divided into its in-phase (real part) $s_{k,n}^I$ and quadrature (imaginary part) $s_{k,n}^Q$ components. These may be thought of as the elements of a pair of PAM sequences that are then transmitted with a time offset $T/2$. Any pair of adjacent PAM symbols, along the time and frequency axes, are transmitted with a phase shift of $\pm\pi/2$.

Let us now denote by $a_{k,n}$ the transmitted PAM symbol, at the kth subcarrier and $nT/2$ time instant, which is either the in-phase or the quadrature component of a QAM (complex) symbol. Also, let $g[m]$ be a causal prototype filter with length $L_g = KM$, where K is referred by the overlapping factor [29] and M is the total subcarriers number. The discrete-time baseband transmitted signal in FBMC/OQAM can be written as [10]:

$$s[m] = \sum_{k=0}^{M-1} \sum_{n=-\infty}^{+\infty} a_{k,n} g[m - nM/2] e^{j\frac{2\pi k}{M}(m - D/2)} e^{j\phi_{k,n}}, \tag{2.97}$$

where $D/2$ is a delay term that depends on L_g the length of the prototype filter. We have $D = L_g - 1 = KM - 1$. The phase term $\phi_{k,n}$ is to insure the phase shift of $\pm\pi/2$ between

adjacent transmitted PAM symbols along the time and frequency axes, and can be given by [17]:

$$\phi_{k,n} = \frac{\pi}{2}(n+k) + \epsilon\pi kn \tag{2.98}$$

where ϵ can take one of the values in $\{-1, 0, 1\}$. In this thesis, we take $\epsilon = -1$ as in [10]. The expression above can thus be written in a simpler manner as:

$$s[m] = \sum_{k=0}^{M-1} \sum_{n} a_{k,n} g_{k,n}[m], \tag{2.99}$$

where $g[m]$ is defined by

$$g_{k,n}[m] = g[m - nM/2] e^{j\frac{2\pi k}{M}(m - D/2)} e^{j\phi_{k,n}}. \tag{2.100}$$

Assuming a noiseless and distortion-free channel, the demodulated symbol over the kth subcarrier and the nth instant can be determined using the inner product of $s[m]$ and $g_{k,n}[m]$:

$$\begin{aligned} r_{k,n} = \langle s, g_{k,n} \rangle &= \sum_{m=-\infty}^{+\infty} s[m] g^*_{k,n}[m] \\ &= \sum_{k'=0}^{M-1} \sum_{n'=-\infty}^{+\infty} a_{k',n'} \sum_{m=-\infty}^{+\infty} g_{k',n'}[m] g^*_{k,n}[m]. \end{aligned} \tag{2.101}$$

If we assume that only a unit impulse is transmitted in a frequency-time position (k_0, n_0), we then obtain from the equation above the expression of the transmultiplexer impulse response:

$$\begin{aligned} r_{k,n} &= \sum_{m=-\infty}^{+\infty} g_{k_0,n_0}[m] g^*_{k,n}[m] \\ &= \sum_{m=-\infty}^{+\infty} g[m] g[m - \Delta n M/2] e^{j\frac{2\pi}{M}\Delta k(\frac{D}{2} - m)} e^{j\pi(\Delta k + k_0)\Delta n} e^{-j\frac{\pi}{2}(\Delta k + \Delta n)}, \end{aligned} \tag{2.102}$$

where $\Delta k = k - k_0$ and $\Delta n = n - n_0$. Then, the transmultiplexer impulse response depends strongly on the used prototype filter $g[m]$. The prototype filter must be designed such that it satisfies the orthogonality condition restricted to the real field:

$$\Re\left\{ \sum_{m=-\infty}^{+\infty} g_{k',n'}[m] g^*_{k,n}[m] \right\} = \delta_{k,k'} \delta_{n,n'}. \tag{2.103}$$

Consequently, we can rewrite (2.101) as

$$r_{k,n} = a_{k,n} + \underbrace{\sum_{(k',n') \neq (k,n)} a_{k',n'} \sum_{m=-\infty}^{+\infty} g_{k',n'}[m] g^*_{k,n}[m]}_{I_{k,n}} \tag{2.104}$$

where $I_{k,n}$ represents the inherent intersymbol interference of an FBMC/OQAM system. Since all the transmitted symbols $a_{k',n'}$ are PAM symbols (real-valued symbols) and owing the real orthogonality condition (2.103), then the ISI term $I_{k,n}$ is a purely imaginary

quantity, *i.e.* $I_{k,n} = ju_{k,n}$ with $u_{k,n}$ is real-valued. Therefore, equation (2.104) is rewritten as:

$$r_{k,n} = a_{k,n} + ju_{k,n}, \tag{2.105}$$

and the transmitted PAM symbol $a_{k,n}$ is recovered just by retrieving the real part of the received demodulated signal $r_{k,n}$:

$$\hat{a}_{k,n} = \Re\{r_{k,n}\} = a_{k,n}. \tag{2.106}$$

2.3.2 FBMC/OQAM in multipath channel

For transmission over a realistic channel, the orthogonality property in (2.103) would be lost. As FBMC/OQAM does not introduce any guard interval, successive transmitted symbols will overlap due to the multipath channel effect.

For derivation simplicity, we assume that the channel is time-invariant. It is also assumed, as in the case of CP-OFDM, that the number of subcarriers M is sufficiently large, *i.e.* $L_h \ll M$ where L_h is the length of the discrete channel response, so that the channel is seen as a flat fading at each subchannel. After passing through the multipath channel, the baseband version of the received signal, noise taken apart, can be written in discrete time as follows:

$$\begin{aligned} r[m] &= (h * s)[m] \\ &= \sum_{l=0}^{L_h-1} h[l]s[m-l] \\ &= \sum_{n=-\infty}^{+\infty} \sum_{k=0}^{M-1} a_{k,n} \sum_{l=0}^{L_h-1} h[l]g_{k,n}[m-l] \\ &= \sum_{n=-\infty}^{+\infty} \sum_{k=0}^{M-1} a_{k,n} e^{j\frac{2\pi k}{M}(m-D/2)} e^{j\phi_{k,n}} \underbrace{\sum_{l=0}^{L_h-1} h[l]g\left[m-l-nM/2\right] e^{-j2\pi\frac{kl}{M}}}_{\Theta} \end{aligned} \tag{2.107}$$

Looking at the last term Θ, we notice that the exponential term $e^{-j2\pi\frac{kl}{M}}$ has fast variations for $l \in \{0, ..., L_h - 1\}$ and cannot be considered as being constant over this set (or interval $[0, L_h[$). However, $g[m - l - nM/2]$ may have only relatively slow variations when $l \in \{0, ..., L_h - 1\}$. Indeed, compared to the coherence bandwidth, the filter bandwidth is small ($L_h \ll L_g = KM$), which also means that time variations of g are necessarily very limited [17]. Therefore, we can assume that $g[m - l - nM/2] \approx g[m - nM/2]$ for $l \in \{0, ..., L_h - 1\}$. Then, Θ can be approximated by:

$$\Theta \approx g[m - nM/2] \sum_{l=0}^{L_h-1} h[l]e^{-j2\pi\frac{kl}{M}}. \tag{2.108}$$

Setting

$$h_{k,n} = \sum_{l=0}^{L_h-1} h[l]e^{-j2\pi\frac{kl}{M}}, \tag{2.109}$$

where $h_{k,n}$ is the channel frequency response at subcarrier k and at time index n, and taking into account the presence of an AWGN term, we can simplify (2.107) as:

$$\begin{aligned} r[m] &\approx \sum_{n=-\infty}^{+\infty} \sum_{k=0}^{M-1} h_{k,n} a_{k,n} g[m - nM/2] e^{j\frac{2\pi k}{M}(m-D/2)} e^{j\phi_{k,n}} + \gamma[m] \\ &\approx \sum_{n=-\infty}^{+\infty} \sum_{k=0}^{M-1} h_{k,n} a_{k,n} g_{k,n}[m] + \gamma[m] \end{aligned} \tag{2.110}$$

where $\gamma[m]$ is the AWGN term with variance σ^2.

The demodulation of the received signal at time-frequency position (k, n) provides a complex symbol denoted by $r_{k,n}$ and given by:

$$\begin{aligned} r_{k,n} &= \sum_{m=-\infty}^{+\infty} r[m] g^*_{k,n}[m] \\ &= \sum_{n'=-\infty}^{+\infty} \sum_{k'=0}^{M-1} h_{k',n'} a_{k',n'} \underbrace{\sum_{m=-\infty}^{+\infty} g_{k',n'}[m] g^*_{k,n}[m]}_{\langle g_{k',n'}, g_{k,n}\rangle} + \underbrace{\sum_{m=-\infty}^{+\infty} \gamma[m] g^*_{k,n}[m]}_{\gamma_{k,n}}, \end{aligned} \tag{2.111}$$

where $\gamma_{k,n}$ is a noise term at the demodulator output. According to the real orthogonality condition (2.103), then we can write:

$$r_{k,n} = h_{k,n} a_{k,n} + \underbrace{\sum_{(k',n') \neq (k,n)} h_{k',n'} a_{k',n'} \langle g_{k',n'}, g_{k,n}\rangle}_{\bar{I}_{k,n}} + \gamma_{k,n}, \tag{2.112}$$

where $\bar{I}_{k,n}$ is now a complex interference term as $h_{k',n'}$ are complex coefficients. The prototype filter $g[m]$ is supposed to be well-localized in time-frequency domain, which means that it exists a finite set $\Omega_{k,n}$ of neighboring positions around the considered one which can be defined as $\Omega_{k,n} = \{(k', n')/(k', n') \notin \Omega_{k,n} \Rightarrow \langle g_{k',n'}, g_{k,n}\rangle = 0\}$. Then, we notice that the size of $\Omega_{k,n}$ depends only on how the prototype filter $g[m]$ is designed. Setting $\Omega^*_{k,n} = \Omega_{k,n} - (k, n)$, we can rewrite the complex interference term $\bar{I}_{k,n}$ as:

$$\bar{I}_{k,n} = \sum_{(k',n') \in \Omega^*_{k,n}} h_{k',n'} a_{k',n'} \langle g_{k',n'}, g_{k,n}\rangle. \tag{2.113}$$

Then, The objective is to design a filter so conveniently well-localized that we can consider the channel coefficients $h_{k,n}$ as constant within $\Omega_{k,n}$. That is, $(k', n') \in \Omega_{k,n} \Rightarrow h_{k',n'} \approx h_{k,n}$. In this case, we can write:

$$\begin{aligned} \bar{I}_{k,n} &\approx h_{k,n} \sum_{(k',n') \in \Omega^*_{k,n}} a_{k',n'} \langle g_{k',n'}, g_{k,n}\rangle \\ &\approx j h_{k,n} u_{k,n}, \end{aligned}$$

where the last equality is obtained according to (2.103), and $u_{k,n}$ is a real-valued interference term. Finally, substituting this last expression into (2.112), we obtain the demodulated signal expressed as:

$$r_{k,n} \approx h_{k,n}(a_{k,n} + j u_{k,n}) + \gamma_{k,n}. \tag{2.114}$$

2.3.3 Efficient digital implementation

Efficient digital implementation of the FBMC/OQAM system through polyphase structures and DFT was first introduced by Bellanger [75] and later studied by Hirosaki [30].

Efficient digital implementation of the transmitter

The transmitted signal $s[m]$ in (2.97) can be split into two signals as:

$$\begin{aligned} s[m] &= \dot{s}[m] + \ddot{s}[m - M/2] \\ &= \sum_n \sum_{k=0}^{M-1} a_{k,2n} g[m - nM] e^{j\frac{2\pi k}{M}(m - D/2)} e^{j\phi_{k,2n}} \\ &\quad + \sum_n \sum_{k=0}^{M-1} a_{k,2n+1} g[m - nM - M/2] e^{j\frac{2\pi k}{M}(m - \frac{M+D}{2})} e^{j\pi k} e^{j\phi_{k,2n+1}} \\ &= \sum_n \sum_{k=0}^{M-1} \dot{a}_{k,n} g[m - nM] e^{j\frac{2\pi k}{M}(m - D/2)} e^{j\dot{\phi}_{k,n}} \\ &\quad + \sum_n \sum_{k=0}^{M-1} \ddot{a}_{k,n} g[m - M/2 - nM] e^{j\frac{2\pi k}{M}(m - \frac{M+D}{2})} e^{j\ddot{\phi}_{k,n}} \end{aligned} \tag{2.115}$$

where $\dot{\phi}_{k,n} = \pi n + \frac{\pi}{2}k$ and $\ddot{\phi}_{k,n} = \pi n + \frac{\pi}{2}k + \frac{\pi}{2}$, according to (2.98). $\dot{a}_{k,n}$ and $\ddot{a}_{k,n}$ are, for a fixed k, two interleaved sequences, each one transmitted with a rate of $T = MT_s$. From the last term of the equation above, we can conclude the expression of $\ddot{s}[m]$ as:

$$\ddot{s}[m] = \sum_n \sum_{k=0}^{M-1} \ddot{a}_{k,n} g[m - nM] e^{j\frac{2\pi k}{M}(m - D/2)} e^{j\ddot{\phi}_{k,n}} \tag{2.116}$$

which has the same expression form as $\dot{s}[m]$. Now, setting $m = k' + pM$ with $k' \in \{0, ..., M\}$ and $p \in \mathbb{Z}$, we can write the first signal term $\dot{s}[m]$ as:

$$\begin{aligned} \dot{s}[k' + pM] &= \sum_n \underbrace{\sum_{k=0}^{M-1} \dot{a}_{k,n} e^{j\dot{\phi}_{k,n}} e^{-j\frac{\pi D k}{M}} e^{j\frac{2\pi k k'}{M}}}_{\dot{b}_{k'}[n]} g[k' + (p - n)M] \\ &= \sum_n \dot{b}_{k'}[n] g[k' + (p - n)M] \end{aligned} \tag{2.117}$$

where $\dot{b}_{k'}[n]$, $k' \in \{0, ..., M-1\}$, can be seen as the outputs of an M-IDFT blocks whose the inputs are $\dot{a}_{k,n} e^{j(\dot{\phi}_{k,n} - \frac{\pi D k}{M})}$, $k \in \{0, ..., M-1\}$. In the same way, we can write the signal $\ddot{s}[m]$ as:

$$\ddot{s}[k' + pM] = \sum_n \ddot{b}_{k'}[n] g\left[k' + (p - n)M\right] \tag{2.118}$$

where $\ddot{b}_{k'}[n]$, $k' \in \{0, ..., M-1\}$, are the outputs of an M-IDFT blocks whose the inputs are $\ddot{a}_{k,n} e^{j(\ddot{\phi}_{k,n} - \frac{\pi D k}{M})}$, $k \in \{0, ..., M-1\}$.

Therefore, considering the the polyphase components $g_{k'}[p]$, which operates at a rate of $1/(MT_s)$, of the prototype filter $g[m]$ as:

$$g_{k'}[p] = g[k' + pM], \qquad k' \in \{0, ..., M-1\}, \tag{2.119}$$

we obtain:

$$\begin{cases} \dot{s}[k' + pM] = \sum_n \dot{b}_{k'}[n] g_{k'}[p-n] \\ \ddot{s}[k' + pM] = \sum_n \ddot{b}_{k'}[n] g_{k'}[p-n] \end{cases} \tag{2.120}$$

It follows that each sample of the signals $\dot{s}[m]$ or $\ddot{s}[m]$ can be obtained by convolving each kth IDFT output signal with the kth polyphase component $g_k[n]$, and then multiplexing all the resulting sequences of the M branches into one sequence by using a parallel-to-serial converter (P/S). Fig. 2.13 depicts the implementation scheme of the IDFT and the polyphase network generating $\dot{s}[m]$, where $G_k(z)$ is the Z transform of $g_k[n]$. Hence, because

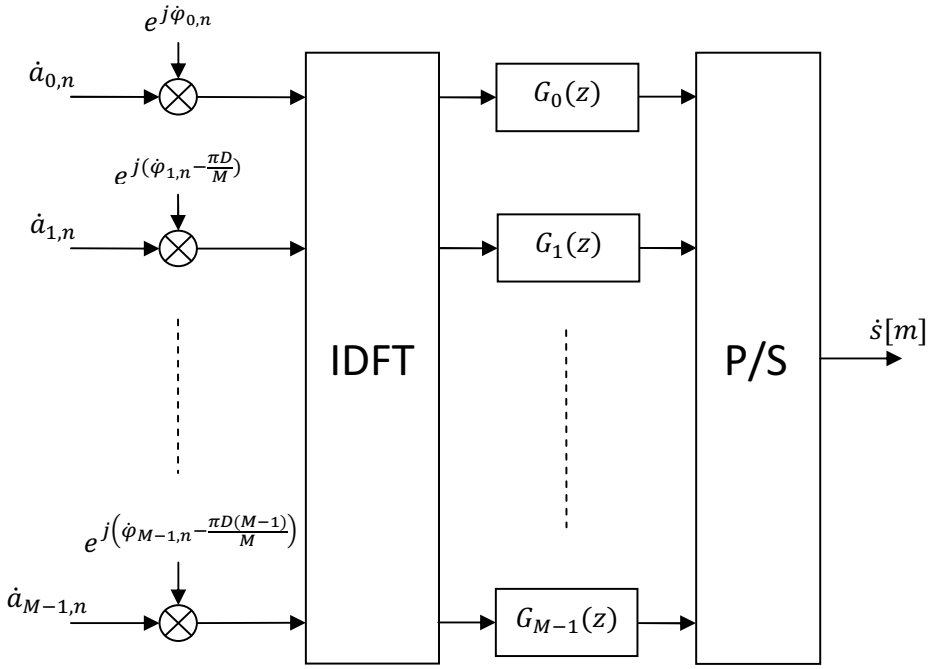

Figure 2.13: Implementation scheme of the IDFT and the polyphase network for a single chain

the transmitted signal is $s[m] = \dot{s}[m] + \ddot{s}[m - M/2]$, the direct implementation of IDFT-PPN approach for the transmitter requires two chains, or a single IDFT running at rate $2/(MT_s)$ and two identical PPN devices as shown in Fig. 2.14 [76].

Nevertheless, Both PPN devices can be grouped into a single PPN as follows. The P/S converter of size M is equivalent to a system in which the signal in each branch is first oversampled by M, then each kth branch is delayed by k samples (z^{-k}) and all the resulting signals are summed. Fig. 2.15 depicts the equivalent scheme of a P/S converter. Hence, denoting by $\dot{B}_{k'}(z)$ and $\ddot{B}_{k'}(z)$ the Z-transforms, respectively, of $\dot{b}_{k'}[n]$ and $\ddot{b}_{k'}[n]$, we can

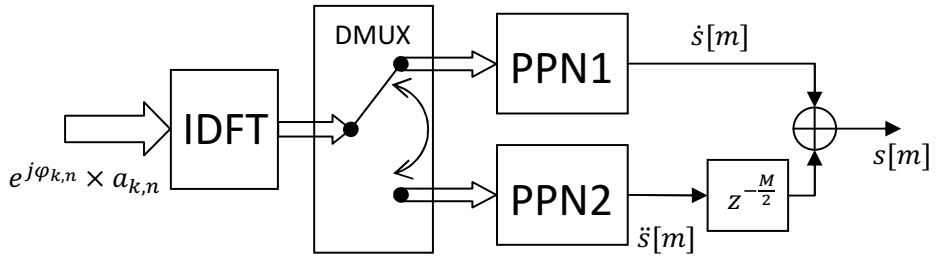

Figure 2.14: Implementation scheme of the FBMC/OQAM transmitter using one IDFT and two polyphase networks

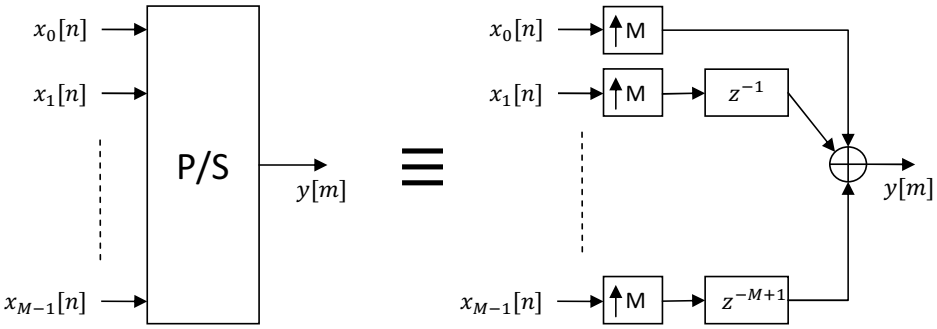

Figure 2.15: Equivalent scheme of a Parallel-to-Serial converter

write the Z-transform of $s[m]$ as:

$$\begin{aligned} S(z) &= \sum_{k'=0}^{M-1} z^{-k'} G_{k'}(z^M)\dot{B}_{k'}(z^M) + z^{-\frac{M}{2}} \sum_{k'=0}^{M-1} z^{-k'} G_{k'}(z^M)\ddot{B}_{k'}(z^M) \\ &= \sum_{k'=0}^{M-1} z^{-k'} G_{k'}(z^M) \left(\dot{B}_{k'}(z^M) + z^{-\frac{M}{2}} \ddot{B}_{k'}(z^M)\right) \\ &= \sum_{k'=0}^{M-1} z^{-k'} Y_{k'}(z^{\frac{M}{2}}), \end{aligned} \tag{2.121}$$

where

$$Y_{k'}(z) = G_{k'}(z^2) \left(\dot{B}_{k'}(z^2) + z^{-1}\ddot{B}_{k'}(z^2)\right).$$

Since $\dot{b}_{k'}[n]$ and $\ddot{b}_{k'}[n]$ are the IDFT outputs according to their definitions in (2.117) and (2.118), we can write $Y_{k'}(z)$ as:

$$\begin{aligned} Y_{k'}(z) &= G_{k'}(z^2) \left(\sum_{k=0}^{M-1} \dot{A}_k(z^2) e^{j2\pi \frac{kk'}{M}} + z^{-1} \sum_{k=0}^{M-1} \ddot{A}_k(z^2) e^{j2\pi \frac{kk'}{M}} \right) \\ &= G_{k'}(z^2) \sum_{k=0}^{M-1} \left(\dot{A}_k(z^2) + z^{-1}\ddot{A}_k(z^2)\right) e^{j2\pi \frac{kk'}{M}}. \end{aligned} \tag{2.122}$$

where $\ddot{A}_k(z)$ and $\dot{A}_k(z)$ are the Z-transform of the data sequences (including the phase terms) at the IDFT input. This last expression shows that both data chains (odd and even)

can share a single IDFT-PPN device to generate the transmitted signal $s[m]$. Consequently, The Z-transform of the signal at the unique IDFT input is given by $\dot{A}_k(z^2) + z^{-1}\ddot{A}_k(z^2)$.

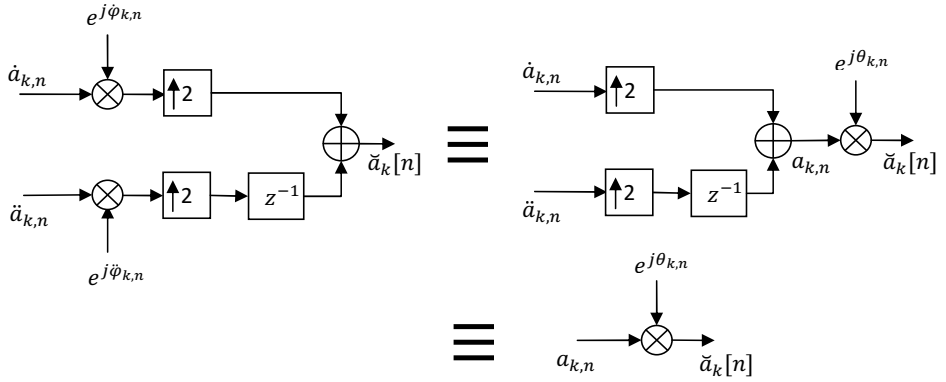

Figure 2.16: the implementation scheme of the IDFT input, for a given k value, and its simplified equivalent implementation

Fig. 2.16 illustrates the implementation scheme of the IDFT input, for a given k value, and its simplified equivalent implementation. Indeed, we can write the signal at the input IDFT for a given value of k, as:

$$\begin{aligned}\breve{a}_k[n] &= e^{-j\frac{\pi Dk}{M}} \begin{cases} \dot{a}_{k,\frac{n}{2}} e^{j\dot{\phi}_{k,\frac{n}{2}}} & n \text{ even} \\ \ddot{a}_{k,\frac{n-1}{2}} e^{j\ddot{\phi}_{k,\frac{n-1}{2}}} & n \text{ odd} \end{cases} \\ &= e^{j(\frac{\pi}{2}(k+n)-\frac{\pi Dk}{M})} \begin{cases} \dot{a}_{k,\frac{n}{2}} & n \text{ even} \\ \ddot{a}_{k,\frac{n-1}{2}} & n \text{ odd} \end{cases} \\ &= a_{k,n} e^{j(\frac{\pi}{2}(k+n)-\frac{\pi Dk}{M})} \end{aligned} \tag{2.123}$$

Then, we can set $\theta_{k,n} = \frac{\pi}{2}(k+n) - \frac{\pi Dk}{M}$. The complete implementation scheme of the transmitter is shown in Fig. 2.17.

Efficient digital implementation of the receiver

Similarly, an efficient realization of the demodulator can be designed using the polyphase components of the prototype filter. We have seen that if $r[m]$ denotes the input of the demodulator, the output signal on the kth subband is given by:

$$r_{k,n} = \sum_{m=-\infty}^{\infty} r[m]g[m - nM/2]e^{-j\frac{2\pi k}{M}(m-\frac{D}{2})}e^{-j\phi_{k,n}}.$$

Using the fact that $g[m] = g[KM - m]$, we can rewrite the output signal as:

$$r_{k,n} = \sum_{m=-\infty}^{\infty} r[m]g[KM - m + nM/2]e^{-j\frac{2\pi k}{M}(m-\frac{D}{2})}e^{-j\phi_{k,n}}. \tag{2.124}$$

In order to illustrate the analogy with the transmitter, this equation can be rewritten, making a reconstruction delay appear, as:

$$r_{k,n-2(K-1)} = \sum_{m=-\infty}^{\infty} r[m]g[nM/2 - m + M]e^{-j\frac{2\pi k}{M}(m-\frac{D}{2})}e^{-j\phi_{k,n-2(K-1)}}. \tag{2.125}$$

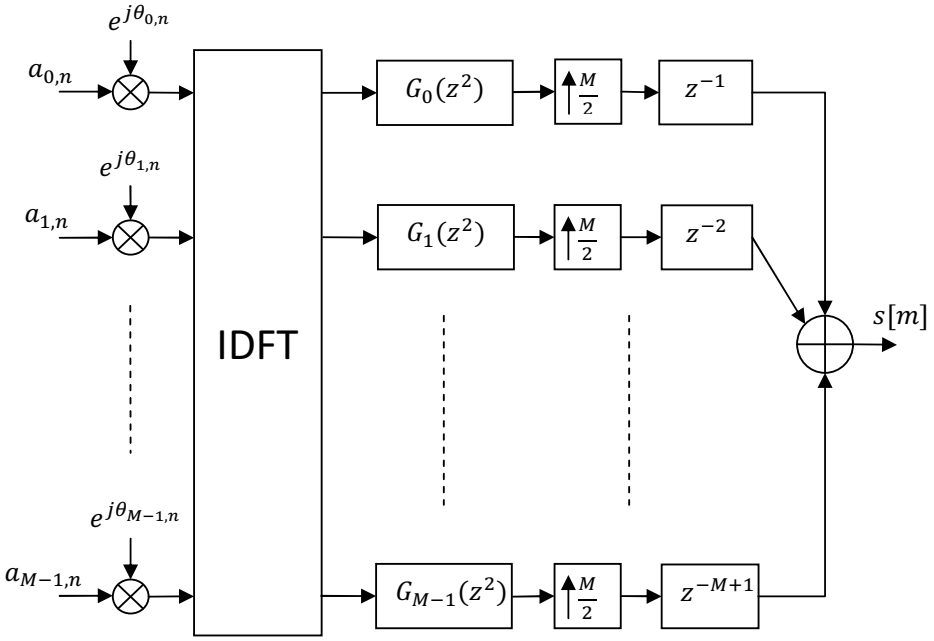

Figure 2.17: Implementation scheme of the transmitter in FBMC/OQAM system

For notation simplicity, let us set $r'_{k,n} = r_{k,n-2(K-1)}$ and $\phi_{k,n-2(K-1)} = \phi'_{k,n}$. Then, setting $m = k' + pM$ with $p \in \mathbb{Z}$ and $k' \in \{0, 1, ..., M-1\}$, the even demodulated signals $r'_{k,2n}$ are obtained as:

$$\begin{aligned} r'_{k,2n} &= \sum_{k'=0}^{M-1} \sum_{p} r[k' + pM] g[(1 + n - p)M - k'] e^{-j\frac{2\pi k k'}{M}} e^{-j\phi'_{k,2n}} e^{j\frac{\pi k D}{M}} \\ &= e^{-j\phi'_{k,2n}} e^{j\frac{\pi k D}{M}} \times \sum_{k'=0}^{M-1} \left(\sum_{p} r_{k'}[p] \tilde{g}_{k'}[n-p] \right) e^{-j\frac{2\pi k k'}{M}}, \end{aligned} \tag{2.126}$$

where $r_{k'}[p] = r[k' + Mp]$ is the k'th output sequence of an S/P converter, and $\tilde{g}_{k'}[p]$ is a FIR filter obtained by $\tilde{g}_{k'}[p] = g[(p+1)M - k']$. According to the equation obtained above, the M signals $r_{k'}[p]$ are filtered in parallel by M FIR filters $\tilde{g}_{k'}[p]$, and then the obtained signals are applied to an M-FFT block. After that, the samples $r'_{k,2n}$ are obtained by multiplying the M-FFT outputs by the phase terms $e^{j(\frac{\pi k D}{M} - \phi'_{k,2n})}$. Fig. 2.18 depicts the polyphase implementation of the even demodulator.

As for the odd demodulator, we consider the delayed signal $\dot{r}[m] = r[m - M/2]$. Therefore, we can rewrite equation (2.125) as:

$$r'_{k,n} = \sum_{m=-\infty}^{\infty} \dot{r}[m] g[nM/2 - m + M + M/2] e^{-j\frac{2\pi k}{M}(m - \frac{D}{2})} e^{-j\phi'_{k,n}} e^{j\pi k}. \tag{2.127}$$

Hence, the odd samples $r'_{k,2n-1}$ are given by:

$$r'_{k,2n-1} = \sum_{m=-\infty}^{\infty} \dot{r}[m] g[nM - m + M] e^{-j\frac{2\pi k}{M}(m - \frac{D}{2})} e^{-j\phi'_{k,2n-1}} e^{j\pi k}. \tag{2.128}$$

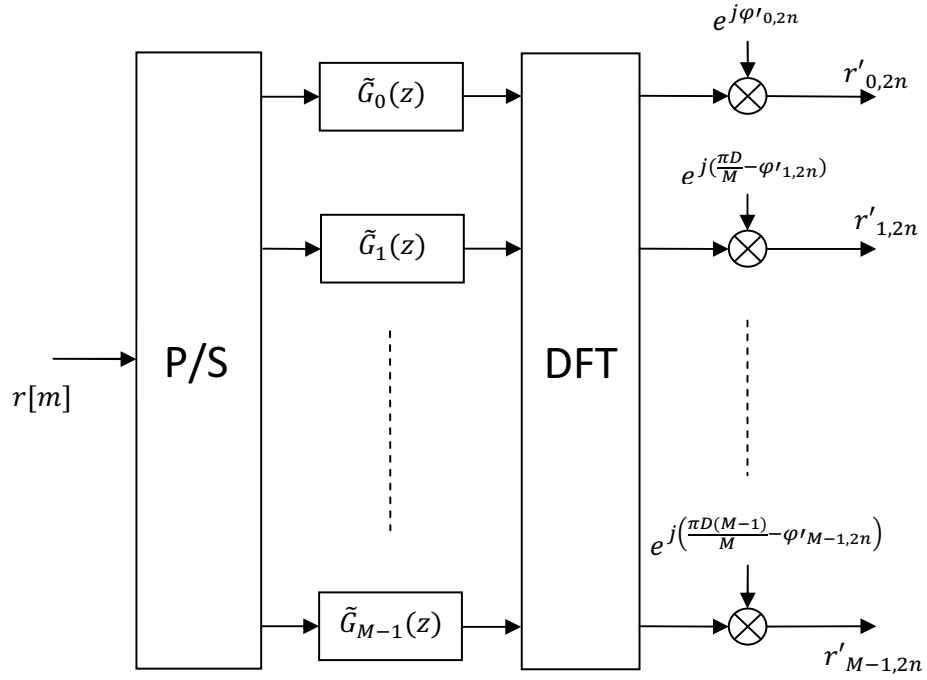

Figure 2.18: Implementation scheme of the DFT and the polyphase network of the even demodulator.

Setting $m = k' + pM$ with $p \in \mathbb{Z}$ and $k' \in \{0, 1, ..., M-1\}$, we obtain:

$$\begin{aligned} r'_{k,2n-1} &= \sum_{k'=0}^{M-1} \sum_{p} \dot{r}[k'+pM] g[(1+n-p)M - k'] e^{-j\frac{2\pi kk'}{M}} e^{-j\phi'_{k,2n-1}} e^{j\frac{\pi kD}{M}} e^{j\pi k} \\ &= e^{-j\phi'_{k,2n-1}} e^{j\frac{\pi kD}{M}} e^{j\pi k} \times \sum_{k'=0}^{M-1} \left(\sum_{p} \dot{r}_{k'}[p] \tilde{g}_{k'}[n-p] \right) e^{-j\frac{2\pi kk'}{M}}. \end{aligned} \tag{2.129}$$

Hence, we remark that the same operations as in the even chain are applied in the odd even on the delayed signal $\dot{r}[m] = r[m - M/2]$, except for the additional phase term $e^{j\pi k}$.

2.3.4 Prototype filters

In the literature, various prototype filters $g[m]$ are designed for their corresponding applications. The study of prototype functions and filters is of a particular interest for FBMC/OQAM because it represents an important degree of freedom with respect to what is possible with OFDM [17]. Furthermore, these prototypes can be built to satisfy some target objective, *e.g.* frequency selectivity or time-frequency localization. Let us look at some examples of prototype filters.

Rectangular window

The time-discrete rectangular window function can be defined as:

$$g[m] = \begin{cases} 1 & m \in \{0, 1, ..., M-1\} \\ 0 & \text{otherwise} \end{cases} \tag{2.130}$$

This prototype filter is the same as the one used in OFDM. its time and frequency representations are given respectively in Fig. 2.19 and Fig. 2.20.

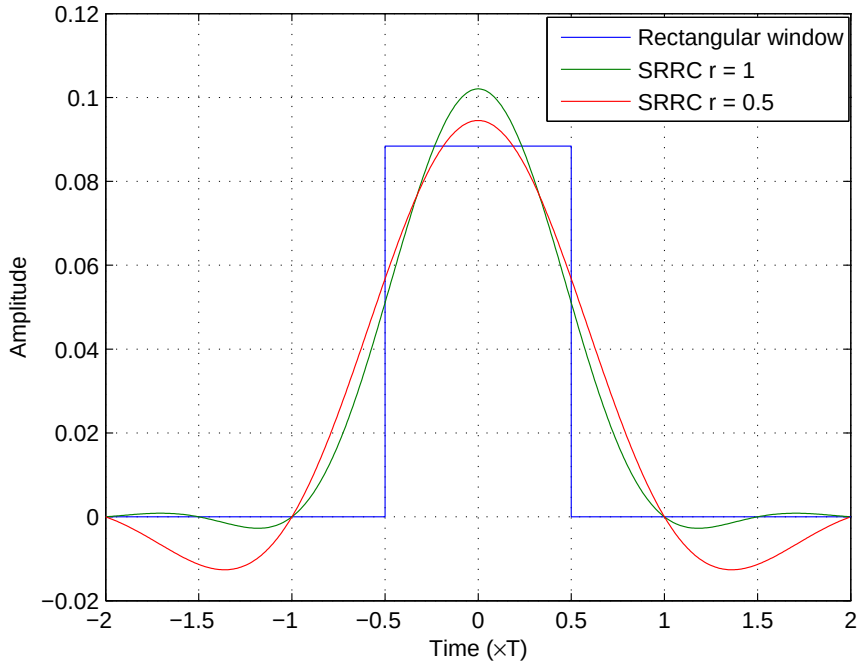

Figure 2.19: Time representation of the rectangular window and the SRRC filter response with $r = 1$ and $r = 0.5$.

The square root raised cosine (SRRC) filter

The square root raised cosine (SRRC) filter is a well known reference filter in digital communication. For a transmission rate of $F = 1/T$, the SRRC filter is defined in the frequency domain by [77]:

$$G(f) = \begin{cases} \sqrt{T} & |f| \leq (1-r)\frac{1}{2T} \\ \sqrt{T}\cos\left(\frac{\pi}{2r}\left(T|f| - \frac{1-r}{2}\right)\right) & (1-r)\frac{1}{2T} < |f| \leq (1+r)\frac{1}{2T} \\ 0 & (1+r)\frac{1}{2T} < |f| \end{cases} \tag{2.131}$$

where r is the roll-off parameter ($0 \leq r \leq 1$). Then, this filter has a frequency response more interesting since it is limited in frequency. The impulse response of the SRRC filter in

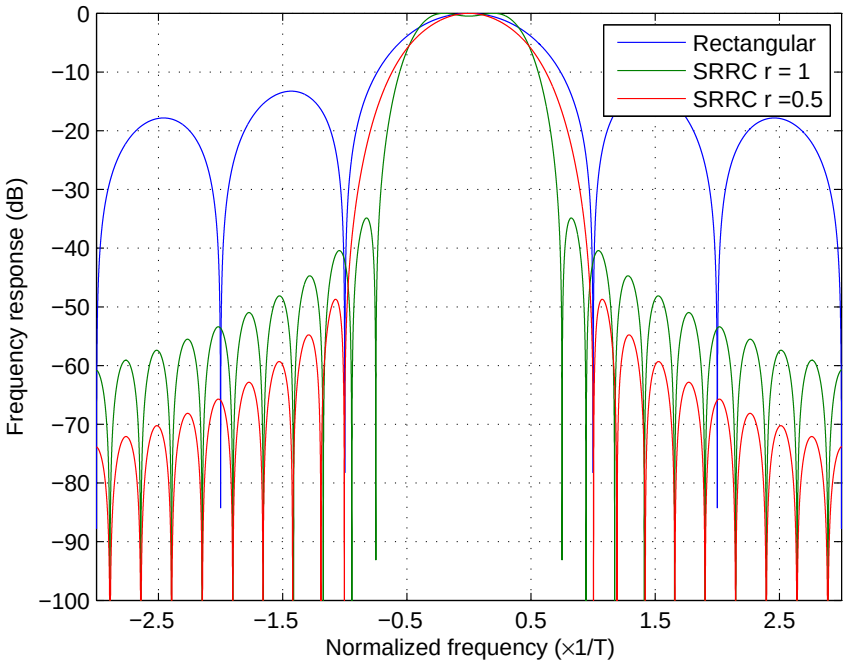

Figure 2.20: Frequency representation of the rectangular window and the SRRC filter response with $r = 1$ and $r = 0.5$.

continuous time is given by [72, 77]:

$$g(t) = \frac{\sin\left((1-r)\frac{\pi t}{T}\right) + \frac{4rt}{T}\cos\left((1+r)\frac{\pi t}{T}\right)}{\frac{\pi t}{T}\left(1-\left(\frac{4rt}{T}\right)^2\right)}. \tag{2.132}$$

The discrete-time impulse response of the SRRC filter is obtained by truncation and sampling the continuous-time function $g(t)$. However, discretization can lead to a discrete prototype filter being only nearly orthogonal [10]. Fig. 2.19 and Fig. 2.20 give the SRRC representation with roll-off $r = 1/2$ and $r = 1$, in time and frequency, respectively. We observe that the SRRC prototype presents a significant improvement compared to the rectangular window prototype in terms of frequency selectivity.

Isotropic orthogonal transform algorithm (IOTA) prototype filter

According to the Heisenberg-Gabor uncertainty principle [78], the most well-localized pulse shape in the time-frequency domain is the Gaussian pulse $f(t) = e^{-\pi t^2}$, which has an interesting property as it is invariant through the Fourier transform. However, it does not satisfy the real orthogonality condition. Therefore, an algorithm was introduced by Alard in [79, 80] converting the Gaussian pulse to an orthogonalized pulse. This obtained orthogonalized pulse shape is called IOTA (Isotropic Orthogonal Transform Algorithm) prototype function.

IOTA prototype function is also considered as a special case of the Extended Gaussian

Functions (EGF) defined in time domain by [81]:

$$z_{\alpha,\nu,\tau}(t) = \frac{1}{2}\sum_{k=0}^{+\infty} d_{k,\alpha,\nu}\left[f_\alpha\left(t+\frac{k}{\nu}\right)+f_\alpha\left(t-\frac{k}{\nu}\right)\right]\sum_{l=0}^{+\infty} d_{l,1/\alpha,\tau}\cos\left(2\pi\frac{lt}{\tau}\right), \qquad (2.133)$$

where α is a real-valued number, $d_{k,\alpha,\nu}$ are some real-valued coefficients which can be computed via the rules described in [81], and f_α is the Gaussian function $g_\alpha(t) = (2\alpha)^{\frac{1}{4}}e^{-\pi\alpha t^2}$. Then, IOTA prototype function is obtained by setting $g(t) = z_{1,\frac{1}{\sqrt{2}},\frac{1}{\sqrt{2}}}(t)$. Note that the IOTA prototype function is identical to its Fourier transform [80]. So IOTA is equally localized in time and frequency. Its excellent time localization implies that it is less sensitive than the SRRC to time truncation [10]. Fig. 2.21 and Fig. 2.22 give the IOTA prototype filter representations in the time and frequency domains, respectively.

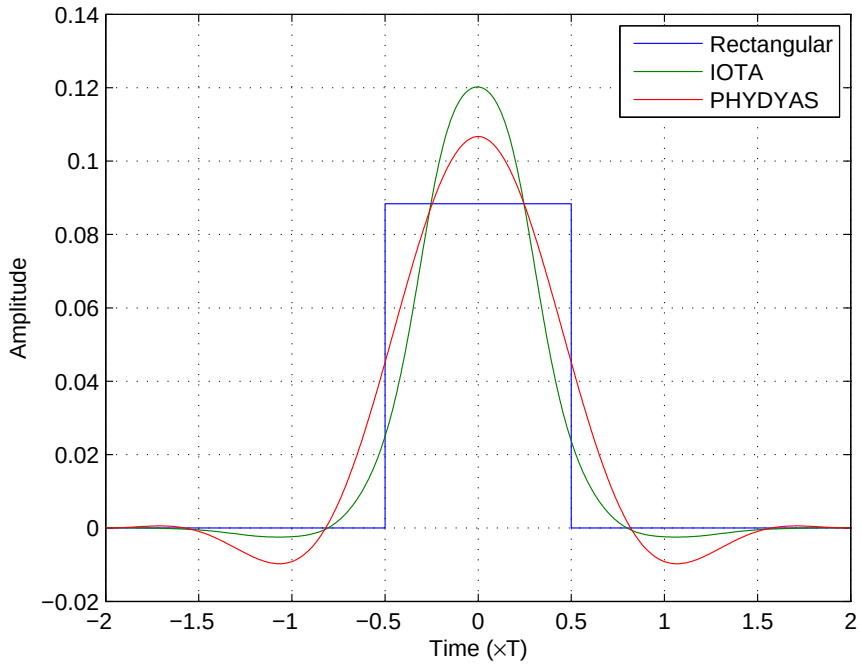

Figure 2.21: Time representation of the IOTA and PHYDYAS prototype filter compared to the rectangular window.

Since we have the expression of the prototype filter, we can calculate the coefficients of the transmultiplexer impulse response from (2.102) for IOTA prototype filter. The coefficients are depicted in Table 2.1.

PHYDYAS prototype filter

The PHYDYAS prototype filter is the one adopted in the **phy**sical layer for **dy**namic spectrum **a**cces**s** and cognitive radio (PHYDYAS) European project [82]. This prototype filter was introduced by Bellanger in [29]. The prototype filter is designed using the frequency sampling technique [83]. The idea of this technique is first to determine the continuous frequency response $G(f)$ via the interpolation formula of the desired frequency response

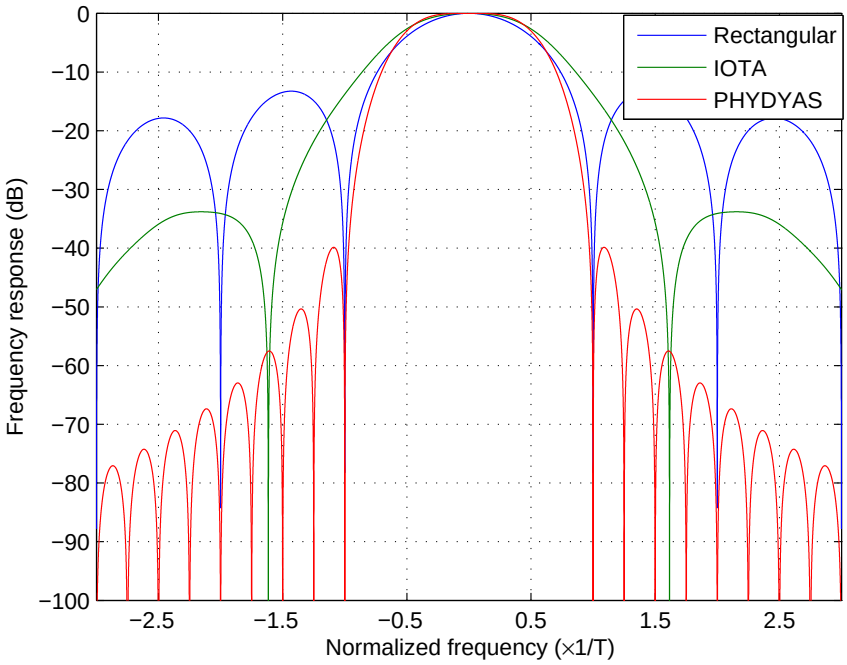

Figure 2.22: Frequency representation of the IOTA and PHYDYAS prototype filter compared to the rectangular window.

samples G_k, that are uniformly spaced at the frequency points $f_k = \frac{k}{KT}$ where K is the overlapping factor and T is the symbol period. That is:

$$G(f) = \sum_k G_k \frac{\sin\left(\pi(KTf - k)\right)}{\pi(KTf - k)} \tag{2.134}$$

Then, the continuous impulse response of the prototype filter is obtained by the inverse Fourier transform of $G(f)$, which is:

$$g(t) = \sum_k G_k e^{j2\pi \frac{kt}{KT}} \qquad \text{for } |t| \leq KT. \tag{2.135}$$

For the PHYDYAS prototype filter, the overlapping factor is chosen to be $K = 4$, and the frequency coefficients G_k are chosen according to the Nyquist theory and are optimized to offer the maximum frequency selectivity and minimize the total interference that originates from the filter bank structure [84]. Thus, the frequency coefficients G_k chosen for the PHYDYAS filter are given by [29]:

$$\begin{cases} G_0 = 1, \quad G_1 = 0.971960, \quad G_2 = \frac{1}{\sqrt{2}}, \quad G_3 = \sqrt{1 - G_1^2} = 0.235147 \\ G_k = 0 \quad \text{for } k > 3 \\ G_k = G_{-k} \quad \text{for } k < 0 \text{ (To obtain a real-valued filter)} \end{cases} \tag{2.136}$$

Therefore, the time-continuous impulse response of the PHYDYAS prototype filter is given

Table 2.1: Transmultiplexer impulse response using IOTA filter

	n_0-3	n_0-2	n_0-1	n_0	n_0+1	n_0+2	n_0+3
k_0-2	$-0.0016j$	0	$-0.0381j$	0	$0.0381j$	0	$0.0016j$
k_0-1	$0.0103j$	$0.0381j$	$0.228j$	$0.4411j$	$0.228j$	$0.0381j$	$0.0103j$
k_0	$-0.0182j$	0	$-0.4411j$	1	$0.4411j$	0	$0.0182j$
k_0+1	$+0.0103j$	$-0.0381j$	$0.228j$	$-0.4411j$	$0.228j$	$-0.0381j$	$0.0103j$
k_0+2	$-0.0016j$	0	$-0.0381j$	0	$0.0381j$	0	$0.0016j$

by:

$$g(t) = 1 + 2\sum_{k=1}^{3} G_k \cos\left(\pi \frac{kt}{2T}\right) \qquad \text{for } |t| \leq 4T. \tag{2.137}$$

where G_k, $k \in \{1,2,3\}$, are given in (2.136). Finally, Fig. 2.21 and Fig. 2.22 give the PHYDYAS prototype filter representations in time and frequency domains, respectively. As for the transmultiplexer impulse response of PHYDYAS filter, its main coefficients are calculated by using (2.102) and are depicted in Table 2.2.

Table 2.2: Transmultiplexer impulse response (main part) using PHYDYAS filter

	$n-3$	$n-2$	$n-1$	n	$n+1$	$n+2$	$n+3$
$k-1$	$0.043j$	$0.125j$	$0.206j$	$0.239j$	$0.206j$	$0.125j$	$0.043j$
k	$-0.067j$	0	$-0.564j$	1	$0.564j$	0	$0.067j$
$k+1$	$0.043j$	$-0.125j$	$0.206j$	$-0.239j$	$0.206j$	$-0.125j$	$0.043j$

2.3.5 FBMC/OQAM with MIMO systems

In this section, we try to apply different well-known multi-antennas architectures to FBMC, while comparing them with those used in CP-OFDM. Both MIMO spatial multiplexing and Space Time Block Coding (STBC) Alamouti schemes are considered when combined with FBMC/OQAM. In section 2.3.2, we have shown for FBMC/OQAM systems that in the case of a SISO transmission between an antenna j and a received antenna i, if $a_{k,n}^{(j)}$ is the transmitted real data at time n and at frequency k then the demodulated signal $r_{k,n}^{(i)}$ is given by:

$$r_{k,n}^{(i)} \approx h_{k,n}^{(ij)}(a_{k,n}^{(j)} + ju_{k,n}^{(j)}) + \gamma_{k,n}^{(i)}, \tag{2.138}$$

where $h_{k,n}^{(ij)}$ is the channel coefficient from the transmit antenna j to the receive antenna i at frequency k and time instant n. $\gamma_{k,n}^{(i)}$ is the noise component at antenna i and at time-frequency (n,m). $u_{k,n}^{(j)}$ is the interference term as given in (2.104). Therefore, In the MIMO

context, when N_t antennas are used to transmit N_t real data symbols and N_r antennas are used to collect the transmitted signals, the FBMC demodulated signal at the jth receive antenna and at a given time-frequency position (k,n) is expressed by:

$$r_{k,n}^{(j)} = \sum_{i=1}^{N_t} h_{k,n}^{(ji)}(a_{k,n}^{(i)} + ju_{k,n}^{(i)}) + \gamma_{k,n}^{(j)}, \tag{2.139}$$

Finally, the matrix formulation of the system can be expressed as:

$$\underbrace{\begin{bmatrix} r_{k,n}^{(1)} \\ \vdots \\ r_{k,n}^{(N_r)} \end{bmatrix}}_{\mathbf{r}_{k,n}} = \underbrace{\begin{bmatrix} h_{k,n}^{(11)} & \cdots & h_{k,n}^{(1N_t)} \\ \vdots & \ddots & \vdots \\ h_{k,n}^{(N_r1)} & \cdots & h_{k,n}^{(N_rN_t)} \end{bmatrix}}_{\mathbf{H}_{k,n}} \underbrace{\begin{bmatrix} a_{k,n}^{(1)} + ju_{k,n}^{(1)} \\ \vdots \\ a_{k,n}^{(N_t)} + ju_{k,n}^{(N_t)} \end{bmatrix}}_{\mathbf{a}_{k,n}+j\mathbf{u}_{k,n}} + \underbrace{\begin{bmatrix} \gamma_{k,n}^{(1)} \\ \vdots \\ \gamma_{k,n}^{(N_r)} \end{bmatrix}}_{\gamma_{k,n}}, \tag{2.140}$$

which yields:

$$\mathbf{r}_{k,n} = \mathbf{H}_{k,n}(\mathbf{a}_{k,n} + j\mathbf{u}_{k,n}) + \gamma_{k,n}, \tag{2.141}$$

where $\mathbf{H}_{k,n}$ is an $(N_r \times N_t)$ channel matrix.

ZF and MMSE equalizers

Linear equalization as ZF and MMSE in SM system in FBMC/OQAM context can be performed as described in [11] where a virtually transmitted vector $\mathbf{c}_{k,n}$ is considered instead of the effective one and defined as:

$$\mathbf{c}_{k,n} = \mathbf{a}_{k,n} + j\mathbf{u}_{k,n}. \tag{2.142}$$

The vector $\mathbf{r}_{k,n}$ represents the input of the equalizer having as output the equalized virtually transmitted vector $\tilde{\mathbf{c}}_{k,n}$:

$$\tilde{\mathbf{c}}_{k,n} = \mathbf{G}_{k,n}^H \mathbf{r}_{k,n}, \tag{2.143}$$

where $\mathbf{G}_{k,n}$ is the equalization matrix based on the ZF or MMSE criterion as presented in section 2.1.2. Then, the real part retrieval of $\tilde{\mathbf{c}}_{k,n}$ yields the real equalized data vector $\tilde{\mathbf{a}}_{k,n}$ [11].

Alamouti scheme

The application of Alamouti coding in a straightforward manner to the FBMC makes an inherent interference appear, and it cannot be easily removed [17]. The difficulty to apply Alamouti scheme with FBMC can be conceptually explained by the fact that the Alamouti scheme relies on a complex orthogonality whereas FBMC technique has only a real orthogonality that cannot lead to the same type of equations [17]. To tackle this drawback, some works have been carried out on this topic such as [35] where the authors show that Alamouti coding can be performed when it is combined with code division multiple access (CDMA) [85]. Indeed the authors in [35] showed that it is possible to have a complex orthogonality with FBMC thanks to CDMA WH (Walsh-Hadamard) codes. Another work was carried out in [36] where a pseudo-Alamouti scheme was proposed. But this last solution requires the appending of the cyclic prefix (CP) to the FBMC signal as introduced in [86].

Renfors *et al.* in [12] have proposed a solution to combine the Alamouti scheme with FBMC, where the Alamouti coding is performed in a block-wise manner inserting gaps (zero-symbols and pilots) in order to isolate the blocks. This solution is feasible when the FBMC transmultiplexer impulse response (let us denote it by $\mathbf{T}$) is conjugate symmetric along the time axis. Indeed, this corresponds to the FBMC model considering the phase term $\phi = \pi kn$ in (2.98) and the data signal $a_{k,n}$ is alternatively purely imaginary and purely real. Let $\mathbf{a_1}$ and $\mathbf{a_2}$ be two data symbol blocks in the time-frequency domain simultaneously transmitted from antenna 1 and antenna 2, respectively. After that, the first antenna transmits $-\overleftarrow{\mathbf{a_2}}^*$ whereas the second one transmits $\overleftarrow{\mathbf{a_1}}^*$. The left arrow on top of a variable denotes the time-reversal version of the corresponding sequence [12, 87]. Assuming that the channels h_1 and h_2 are invariant during the transmission of both symbol blocks, the first signal block collected at the receive antenna can be written as:

$$\mathbf{r_1} = h_1\mathbf{T} \otimes \mathbf{a_1} + h_2\mathbf{T} \otimes \mathbf{a_2} + \mathbf{n_1}, \tag{2.144}$$

where $\otimes$ operation stands for the 2D convolution, and $\mathbf{n_1}$ is a block of the noise terms. The second received signal block is:

$$\mathbf{r_2} = h_2\mathbf{T} \otimes \overleftarrow{\mathbf{a_1}}^* - h_1\mathbf{T} \otimes \overleftarrow{\mathbf{a_2}}^* + \mathbf{n_2}. \tag{2.145}$$

Then, we have:

$$\begin{aligned} \overleftarrow{\mathbf{r_2}}^* &= h_2^*\overleftarrow{\mathbf{T}}^* \otimes \mathbf{a_1} - h_1^*\overleftarrow{\mathbf{T}}^* \otimes \mathbf{a_2} + \overleftarrow{\mathbf{n_2}}^* \\ &= h_2^*\mathbf{T} \otimes \mathbf{a_1} - h_1^*\mathbf{T} \otimes \mathbf{a_2} + \overleftarrow{\mathbf{n_2}}^*. \end{aligned} \tag{2.146}$$

The last equality stands thanks to the fact that $\mathbf{T}$ is conjugate symmetric along the time axis ($\overleftarrow{\mathbf{T}}^* = \mathbf{T}$). Therefore, applying the Alamouti decoding [34] we have:

$$\mathbf{y_1} = \frac{h_1^*\mathbf{r_1} + h_2\overleftarrow{\mathbf{r_2}}^*}{|h_1|^2 + |h_2|^2} = \mathbf{T} \otimes \mathbf{a_1} + \frac{h_1^*\mathbf{n_1} + h_2\overleftarrow{\mathbf{n_2}}^*}{|h_1|^2 + |h_2|^2}, \tag{2.147}$$

and

$$\mathbf{y_2} = \frac{h_2^*\mathbf{r_1} - h_1\overleftarrow{\mathbf{r_2}}^*}{|h_1|^2 + |h_2|^2} = \mathbf{T} \otimes \mathbf{a_2} + \frac{h_2^*\mathbf{n_1} - h_1\overleftarrow{\mathbf{n_2}}^*}{|h_1|^2 + |h_2|^2}. \tag{2.148}$$

The term $\mathbf{T} \otimes \mathbf{a}$ contains the transmitted data symbols and also the inherent interference. We can write it as in [87]:

$$\mathbf{T} \otimes \mathbf{a} = \mathbf{a} + \mathbf{u}, \tag{2.149}$$

where $\mathbf{u}$ is the block of the interference terms. When a data symbol in $\mathbf{a}$ is purely real, its corresponding interference term in $\mathbf{u}$ is purely imaginary and vice versa. Then, the transmitted data symbols are easily estimated by a simple real or imaginary part retrieval.

Maximum likelihood detection in spatial multiplexing

To the best of our knowledge, there is no work until now addressing the association of the FBMC modulation to the spatial multiplexing with Maximum Likelihood (ML) detection. Indeed, the presence of the interference vector term $\mathbf{u}_{k,n}$ in (2.141) prevents the application of ML separately at each time-frequency position (k, n). This is because the interference

terms take their values in a large set and depend on the transmitted data symbols in the neighborhood around the considered position (k, n).

The global ML decoder is the one that considers all the transmitted data symbols within a frame. Let us consider a data frame $\mathbf{a}$ with L multicarrier symbols. Then, $\mathbf{a}$ contains $(M \times L)$ elements (M is the subcarrier number) and each element $\mathbf{a}_{k,n}$ is a $(N_t \times 1)$ real vector. At the receiver side, we also obtain a $(M \times L)$ frame $\mathbf{r}$ whose elements $\mathbf{r}_{k,n}$ are $(N_r \times 1)$ complex vectors. The global ML method consists in finding the frame $\mathbf{a}$ among all the possible ones that maximizes the probability of receiving frame $\mathbf{r}$ assuming that $\mathbf{a}$ is transmitted [13], we can write:

$$\hat{\mathbf{a}} = \underset{\mathbf{a}}{argmax} \left\{ P(\mathbf{r}/\mathbf{a}) \right\}. \tag{2.150}$$

Obviously, a such receiver implementation is by far impractical due to its huge complexity. If we consider BPSK modulation, then we have $2^{N_t \times M \times L}$ possible and different data frame $\mathbf{a}$.

The received FBMC signal can be seen as a 2D convolution of the transmitted data frame $\mathbf{a}$ with the transmultiplexer impulse response weighted by the channel matrix. Therefore, a 2D-Viterbi algorithm deserves to be considered. Many works were carried out on 2D-Viterbi algorithm in different study fields such as in optical and magnetic data storage [88, 89]. Commonly, a 2D Viterbi detector performs joint symbol detection on all the subcarriers [90, 91]. To reduce the complexity of a full-fledged 2D Viterbi detector (VD), the VD is divided into smaller processing units (called stripe VD). Each stripe VD covers a limited number of subcarriers. This detection configuration is called a stripe-wise Viterbi detector (SWVD) [91, 92]. Some other techniques, such as decision feedback equalization VD (DFE-VD) [93] and fixed delay tree search with decision feedback VD (FDTS/DF-VD) [94], have been reported in the literature to further reduce the complexity of 2D VD. In the next chapter, we address the problem of performing ML detection in spatial multiplexing with FBMC modulation. We propose to examine solutions based on interference estimation and cancellation.

Chapter 3

Interference cancelation and ML detection in spatial multiplexing with FBMC

We have seen in the previous chapter that the presence of the inherent interference in FBMC causes problems to apply the ML detector in the MIMO spatial multiplexing scheme. By using Viterbi algorithm [95], full maximum likelihood receivers, in principle, offer the best possible performance but require an impractically high complexity when the impulse response is long. Moreover, the intrinsic interference in FBMC is two-dimensional which further complicates the detection task in maximum likelihood sense. In this chapter, we analyze the possibility to cancel the interference before applying ML detection. Indeed, the interference cancellation approaches generally offer the possibility of removing interference with low complexity increase and without enhancing the level of noise already present in the received signal. This chapter is organized as follows. First, we give a brief overview on interference cancellation technique. In light of this background, we derive conditions for optimal interference cancellation scheme in the FBMC context. Then, we present the performance results obtained by simulation in both uncoded and coded cases. After that, we analyze another cancellation approach based on partially interference cancellation. Finally, we finish the chapter by a conclusion where the main results are summarized.

3.1 Motivation of the interference cancellation

In this section, we will highlight the potential SNR gain over OFDM that FBMC could offer in spatial multiplexing if the interference were completely removed. This potential gain motivates us to study in depth the interference cancellation methods.

In CP-OFDM, when the CP length is large enough, the system is equivalent to the

narrowband single carrier configuration regardless of the efficiency loss due to the CP. In MIMO context, the system is modeled as:

$$\mathbf{y} = \mathbf{H}\mathbf{s} + \mathbf{n}, \tag{3.1}$$

where $s_k \in \mathbb{A}$ is the transmitted symbol at the kth antenna with average symbol energy E_s and $\mathbb{A}$ is the square M-QAM constellation set with size M. $\mathbf{H}$ is an $N_r \times N_t$ channel gain matrix, whose elements are independent zero-mean complex Gaussian random variables with unit variance, and the N_r elements of vector n are samples of independent complex white Gaussian noise with single-side power spectral density N_0. Performance analysis of ML detection in this context was treated in [18] and a union bound expression was developed. Let $\{\mathbf{s}\}$ denote the set of all M^{N_t} possible transmitted symbol vectors. We define $\{\mathbf{s}_j\}$ with size M^{N_t-1} as a subset of $\{\mathbf{s}\}$ in which vectors have s_m as their first element. We also define $\{\mathbf{s}_i\}$ as the set of vectors that differ in their first element from $\{\mathbf{s}_j\}$ so that there are a total of $(M^{N_t} - M^{N_t-1})$ such vectors. Assuming Gray coding and perfect Channel State Information (CSI) at the receiver side, an asymptotical expression of the BER is given by [18]:

$$P(\gamma_c) = \frac{\alpha}{b}\left(\frac{1}{2\gamma_c}\right)^{N_r}\begin{pmatrix} 2N_r - 1 \\ N_r - 1 \end{pmatrix}, \tag{3.2}$$

where $\alpha = M^{-N_t}\sum_m \sum_j \sum_i a_{s_m,ij}^{-N_r}$ and $a_{s_m,ij} = \|\mathbf{d}_i - \mathbf{d}_j\|^2/2E_s$. $b = \log_2(M)$ is the number of bits per symbol and $\gamma_c = E_s/N_0$ denotes the average symbol SNR per diversity branch. The relationship between E_b/N_0 and γ_c is given by [18, 96]:

$$E_b/N_0 = \frac{N_r E_s}{bN_0} = \frac{N_r}{b}\gamma_c. \tag{3.3}$$

Let us consider now the FBMC system model. Assuming perfect interference cancellation, we can rewrite equation (2.141) as:

$$\mathbf{y} = \mathbf{H}\mathbf{a} + \mathbf{n}. \tag{3.4}$$

We recall that the symbol a is real-valued and $a \in \mathbb{A}_r$ which is the orthogonal projection of $\mathbb{A}$ on the real axis. Therefore, the energy of each transmitted symbol a is $\mathbb{E}\{a^2\} = E_s/2$, and the number of bits per symbol a is $b' = \log_2(\sqrt{M}) = b/2$. According to the above equations, we can derive in this context the asymptotical BER expression as:

$$P'(\gamma_c) = \frac{2\alpha'}{b}\left(\frac{1}{2\gamma_c'}\right)^{N_r}\begin{pmatrix} 2N_r - 1 \\ N_r - 1 \end{pmatrix}, \tag{3.5}$$

with $\alpha' = M^{-\frac{N_t}{2}}\sum_m \sum_j \sum_i a_{s_m,ij}^{-N_r}$ and $\gamma_c' = \frac{\mathbb{E}\{a^2\}}{N_0} = \gamma_c/2$. The signal-to-noise ratio per bit expression in this context is similar to equation (3.3) because we have:

$$E_b/N_0 = \frac{N_r(\frac{E_s}{2})}{(\frac{b}{2})N_0} = \frac{N_r}{b}\gamma_c.$$

In order to determine the SNR gap in the performance between both systems, let us resolve the equation $P'(\gamma_{c_1}) = P(\gamma_{c_2})$. Starting from (3.2) and (3.5) we have:

$$\frac{2\alpha'}{b}\left(\frac{1}{\gamma_{c_1}}\right)^{N_r} = \frac{\alpha}{b}\left(\frac{1}{2\gamma_{c_2}}\right)^{N_r}, \tag{3.6}$$

which yields the following expression:

$$\frac{\gamma_{c_2}}{\gamma_{c_1}} = \frac{1}{2} \sqrt[N_r]{\frac{\alpha}{2\alpha'}}. \tag{3.7}$$

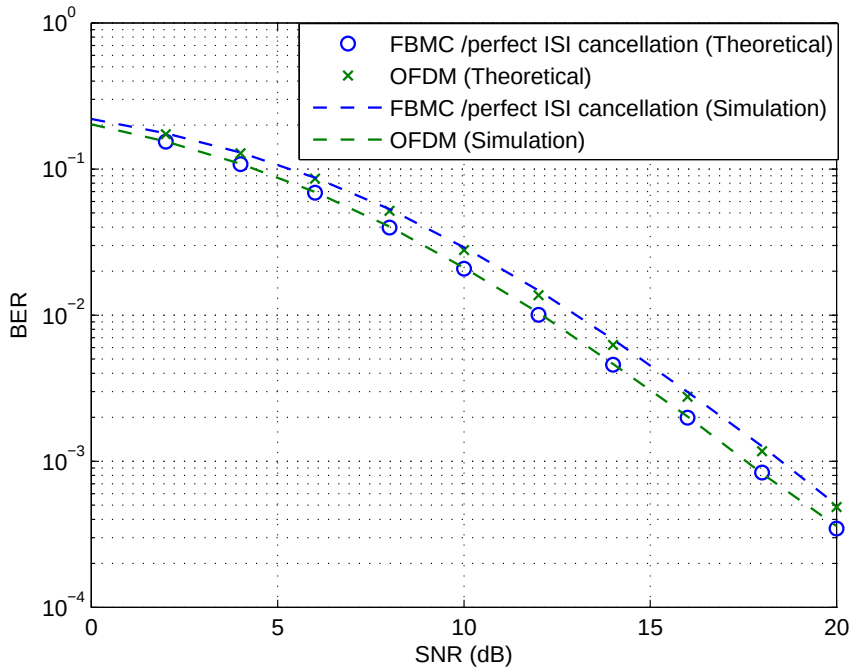

Figure 3.1: Illustation of the potential SNR gain of the FBMC over OFDM in 2×2 SM system

For QPSK modulation and $N_r = N_t = 2$, we have $\alpha = \frac{541}{144}$ and $\alpha' = \frac{5}{16}$, so the performance gain between both systems is $G = 10\log_{10}(\frac{\gamma_{c_2}}{\gamma_{c_1}}) \approx 0.88\ dB$. Fig. 3.1 depicts the BER performance obtained by simulation of OFDM and FBMC with perfect ISI cancellation in a 2×2 SM. We observe clearly that FBMC provides an SNR gain of about 1 dB over OFDM when the FBMC interference is perfectly removed. The theoretical curves plotted in the figure are obtained using the method described in [62]. In the rest of this chapter, we will propose some different solutions to cope with the FBMC interference.

3.2 FBMC interference estimation by using linear equalizer

We have seen in Section 2.3.5 that the MIMO linear equalizers such as ZF and MMSE equalizers are straightforwardly applicable to the FBMC spatial multiplexing systems. To be able to apply ML detection, we propose in this section a receiver proceeding by interference estimation and cancellation where the interference is estimated using a MIMO linear equalizer. The proposed receiver scheme is depicted in Fig. 3.2. We have used only the MMSE equalizer as it outperforms the ZF one with almost the same computational complexity. We refer to this receiver as MMSE-ML receiver since we combine MMSE equalizer and

ML detector. As we have seen, the MMSE equalizer provides an estimation of the virtual transmitted symbol vector $\mathbf{c}_{k,n} = \mathbf{a}_{k,n} + j\mathbf{u}_{k,n}$. Therefore, an evaluation of the interference terms are available by taking only the imaginary part of $\tilde{\mathbf{c}}_{k,n}$. This estimation is used to cancel the interference contribution from the received vector $\mathbf{r}_{k,n}$. Hence, we obtain a vector $\mathbf{y}_{k,n}$ expressed as:

$$\begin{aligned}\mathbf{y}_{k,n} &= \mathbf{r}_{k,n} - j\mathbf{H}_{k,n}\tilde{\mathbf{u}}_{k,n}, \\ &= \mathbf{H}_{k,n}(\mathbf{a}_{k,n} + j(\mathbf{u}_{k,n} - \tilde{\mathbf{u}}_{k,n})) + \mathbf{n}_{k,n}, \\ &= \mathbf{H}_{k,n}(\mathbf{a}_{k,n} + j\epsilon_{k,n}) + \mathbf{n}_{k,n}, \end{aligned} \tag{3.8}$$

where $\tilde{\mathbf{u}}_{k,n}$ is the estimated interference vector given by $\tilde{\mathbf{u}}_{k,n} = \mathfrak{Im}\{\tilde{\mathbf{c}}_{k,n}\}$. The interference estimation error $\epsilon_{k,n}$ is considered as an additional noise term. Its statistical parameters depend especially on the channel matrix $\mathbf{H}_{k,n}$, since the reliability of $\tilde{\mathbf{u}}_{k,n}$ depends on the MMSE equalization matrix.

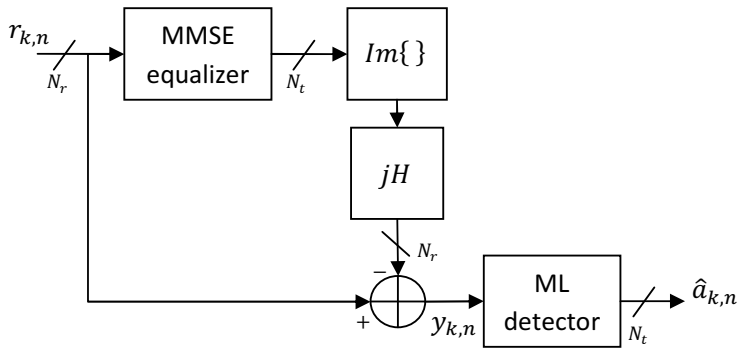

Figure 3.2: Basic scheme of the MMSE-ML receiver

Assuming almost perfect interference estimation, that is $\epsilon_{k,n} \approx \mathbf{0}$, we consider that the vector $\mathbf{y}_{k,n}$ at the output of the interference canceller is free of interference. Thus, ignoring the presence of $\epsilon_{k,n}$ term, we perform a simple conventional ML detector. One of the advantages of this receiver is the fact that it does not introduce any processing delay in the system; the interference is estimated from the current received vector and is immediately removed. However, this receiver is based on the assumption that $\mathbf{y}_{k,n}$ is free of interference. But unfortunately, the error term in equation (3.8) is obviously non-zero ($\epsilon_{k,n} \neq 0$). Consequently, it is clear that we cannot reach the optimal bit-error-rate performance as if there is no interference.

Fig. 3.3 shows the BER performance of the proposed MMSE-ML receiver in 2×2 and 4×4 SM configurations, which is compared to the MMSE equalizer and to the Genie-Aided optimal performance. The number of subcarriers is $M = 512$, and the data symbols are QPSK modulated (*i.e*, twice BPSK for FBMC). The sampling frequency is $f_s = 10\ MHz$. We assume perfect channel knowledge at the receiver side. The different channels between the antennas are spatially uncorrelated, and the channel model used for simulation is the Pedestrian-A (Ped-A) channel model [97] where the parameters are given by:

- Delays = [0 110 190 410] ns,

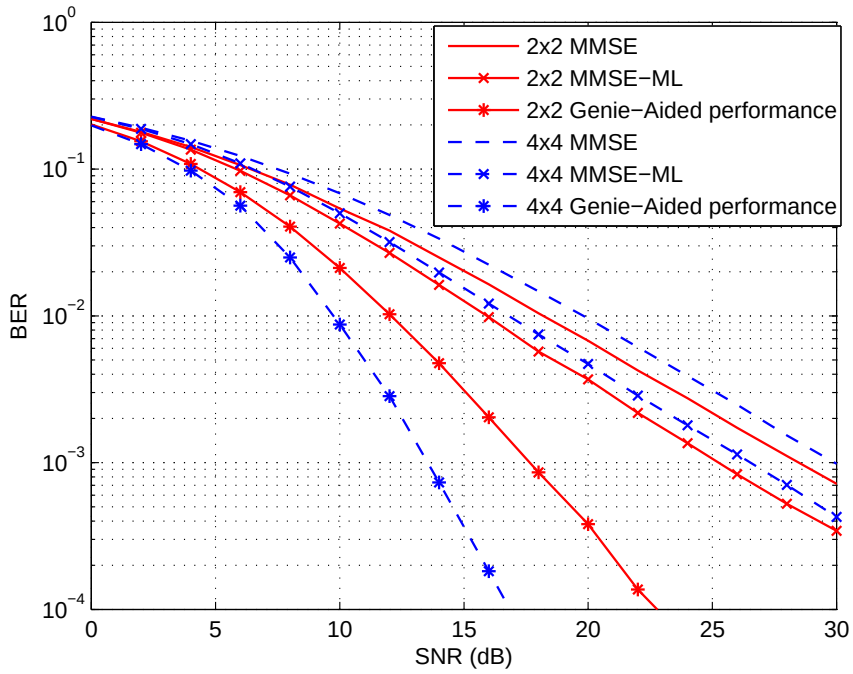

Figure 3.3: BER performance of the MMSE-ML receiver compared to MMSE equalizer and to the Genie-Aided in a 2×2 SM system

- Powers = [0 -9.7 -19.2 -22.8] dB.

Solid curves represent the performance in a 2×2 SM, whereas 4×4 SM configuration is depicted by dash curves. We notice that MMSE-ML receiver outperforms the MMSE equalizer in both SM configurations. We can note almost the same SNR gain of about 2 dB at $BER = 10^{-2}$. However, the performance of the MMSE-ML receiver is still far from the optimum one. This performance limitation is explained by the fact that the interference is not perfectly canceled. Further, we observe that the SNR gap between MMSE-ML performance and Genie-Aided one is more important in the case of 4×4 SM configuration. This is due to the diversity limitation of the MMSE equalizer compared to the ML detector. Indeed, the ML detector provides a diversity order of 2 in the case of 2×2 SM, and a diversity order of 4 in the case of 4×4 SM, whereas the MMSE equalizer has a diversity order of 1 in both cases.

3.3 Intersymbol interference cancellation

3.3.1 Background on ISI cancellation

ISI cancellation scheme is essentially based on using preliminary decisions to estimate and cancel the interference. The idea of using preliminary decisions to generate an intermediate estimate of the transmitted data signal was independently proposed by various investigators. Proakis, in [98], proposed the cancellation scheme where the canceller attempts to remove the

ISI directly from the received signal. This approach does not achieve improved performance over linear equalization if there is a phase distortion [99]. Then, Gersho and Lim described, in [99], a linear canceller structure where the received signal is first filtered by a transversal filter $\underline{W}$ before attempting to remove the ISI estimated by using a canceller filter $\underline{C}$. Fig. 3.4 shows the basic scheme of the ISI canceller as described in [99].

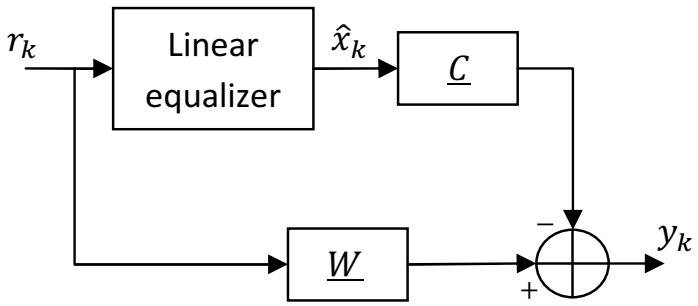

Figure 3.4: Basic scheme of an interference cancellation receiver

Let us consider r_k as the baseband equivalent received signal x_k corrupted by a linear dispersive channel h_k and additive gaussian noise n_k. That is:

$$r_k = \sum_l h_l x_{k-l} + n_k. \tag{3.9}$$

Suppose a separate linear equalizer operating on the received signal r_k. If optimally designed, it will have a modest error rate, and we can use its decisions $\hat{x}_k$ as preliminary or tentative decisions for the purpose of constructing an estimate of the total ISI. On the other hand, the received signal is also fed to the filter $\underline{W}$. Whereas, the input of the canceller filter $\underline{C}$ is the preliminary decision sequence, and its output sequence is subtracted form the output of the filter $\underline{W}$. This difference, producing y_k, may be viewed as a linear estimator of the data symbol x_k [99]. Hence, the output y_k of the receiver is described by the equation

$$y_k = \sum_j w_j r_{k-j} - \sum_{j \neq 0} c_j \hat{x}_{k-j}, \tag{3.10}$$

where $\hat{x}_k$ are preliminary decisions. We make the constraint that the center tap of the cancellation filter is zero $c_0 = 0$, this restricts the role of the canceller to removing ISI and prevents the canceller from making use of the current data symbol which must be estimated by the output signal from the filter $\underline{W}$ [99].

To determine the optimal pair of filters $\underline{W}$ and $\underline{C}$ for the cancellation scheme, we make the simplifying assumption that the preliminary decisions $\hat{x}_k$ available from the linear equalizer are correct [99]. Then, we consider the structure shown in Fig. 3.5 where the canceller $\underline{C}$ is fed directly by the true transmitted data symbols since the tentative decisions are assumed to be correct. Therefore, the goal is to determine the filters $\underline{W}$ and $\underline{C}$ that minimize the mean square error:

$$E_k = \mathbb{E}\{|\epsilon_k|^2\}, \tag{3.11}$$

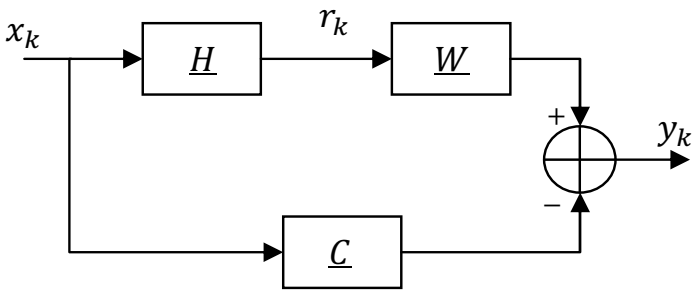

Figure 3.5: Model of a linear canceller

where $\epsilon_k = y_k - x_k$.

Gersho and Lim showed that the optimal coefficients of the filters $\underline{W}$ and $\underline{C}$, based on the mean square error criterion, assuming that the noise samples are not correlated and the mean square value of data symbols is equal to 1, are given by:

$$\begin{aligned} w_k &= \frac{1}{E_h + \sigma^2} h^*(-k), \quad \forall k \\ c_k &= \frac{1}{E_h + \sigma^2} R_h(k), \quad \forall k \neq 0 \end{aligned} \tag{3.12}$$

where E_h is the energy of the channel impulse response and $R_h(k)$ is its autocorrelation function. σ^2 is the variance of the additive noise. Whereas, in the case where the noise is correlated, the optimal filter coefficients are given by their Fourier transforms:

$$\begin{aligned} W(\omega) &= \frac{H(-\omega)}{(1+\xi)S_n(-\omega)}, \\ C(\omega) &= \frac{|H(-\omega)|^2}{(1+\xi)S_n(-\omega)}, \end{aligned} \tag{3.13}$$

with

$$\xi = \frac{T}{4\pi} \int_{\frac{-2\pi}{T}}^{\frac{2\pi}{T}} \frac{|H(-\omega)|^2}{S_n(-\omega)} d\omega \tag{3.14}$$

where $H(\omega)$ is the Fourier transform of the channel-sampled impulse response, $S_n(\omega)$ is the sampled noise spectrum, and T is the sampling period.

3.3.2 Interference cancellation in FBMC

In this section, we propose to design an interference cancellation receiver for the FBMC system based on the principle presented in Section 3.3.1. The goal is to obtain signal samples as if the data symbols were transmitted in isolation. That is, the first stage of the receiver does not equalize the channel but attempts only to cancel the FBMC interference. Then, in the context of the spatial multiplexing system, the ML detector is applied after the ISI cancellation. Because of the nature of the FBMC interference, the filters $\underline{W}$ and $\underline{C}$ should be two-dimensional. Moreover, we have to take into account the fact that the

transmultiplexer impulse response depends on the subcarrier index k as aforementioned in the previous chapter.

According to (2.101) and (2.102), we can write the received signal, in the case of an AWGN channel, as:

$$r(k,n) = \sum_{p=-P}^{P} \sum_{q=-Q}^{Q} a(k-p,n-q) f(p,q) (-1)^{q(k-p)} + \gamma(k,n), \tag{3.15}$$

where $a(k,n)$ is the real-valued transmitted data symbols, $\gamma(k,n)$ is the noise term at the demodulator output, and $f(p,q)$ is given by:

$$f(p,q) = \sum_{m=-\infty}^{+\infty} g[m] g[m - qM/2] e^{j\frac{2\pi}{M}p(\frac{D}{2}-m)} e^{-j\frac{\pi}{2}(p+q)} e^{j\pi pq}. \tag{3.16}$$

The noise term $\gamma(k,n)$ in (3.15) is a colored noise and given by

$$\gamma(k,n) = \sum_{m=-\infty}^{+\infty} b[m] g[m - n\frac{M}{2}] e^{j\frac{2\pi}{M}k(\frac{D}{2}-m)} e^{-j\phi_{k,n}}, \tag{3.17}$$

where $b[m]$ is the AWGN with variance σ^2. We show in Appendix A.1 that the noise autocorrelation is given by

$$\mathbb{E}\{\gamma^*(k',n')\gamma(k,n)\} = \sigma^2 f(k-k', n-n')(-1)^{(n-n')k'}. \tag{3.18}$$

When the spatial multiplexing configuration is considered, the received signal at the demodulator output of the ith receive antenna is written as:

$$r^{(i)}(k,n) = \sum_{j=1}^{N_t} \sum_{p=-P}^{P} \sum_{q=-Q}^{Q} h_{k,n}^{(ij)} a^{(j)}(k-p,n-q) f(p,q) (-1)^{q(k-p)} + \gamma^{(i)}(k,n). \tag{3.19}$$

where $h_{k,n}^{(ij)}$ is the Rayleigh channel coefficient between the jth transmit antenna and the ith received one. Hence, one can rewrite:

$$r^{(i)}(k,n) = \sum_{p=-P}^{P} \sum_{q=-Q}^{Q} \left(\sum_{j=1}^{N_t} h_{k,n}^{(ij)} a^{(j)}(k-p,n-q) \right) f(p,q) (-1)^{q(k-p)} + \gamma^{(i)}(k,n). \tag{3.20}$$

The quantity in brackets can be seen as a virtual transmitted symbol. Therefore, the same ISI cancellation scheme is applied on each receive antenna branch. Thus, the output of the whole ISI canceller is assumed to be free of interference and considered as the output of a conventional spatial multiplexing channel. Fig. 3.6 depicts the basic scheme of the proposed receiver. We should note that the outputs of the preliminary estimator block in Fig. 3.6 are estimations of the quantity in brackets in equation (3.20). That is, the N_r-vector fed to the canceller filter $\underline{C}$ is:

$$\hat{\mathbf{r}}_{k,n} = \mathbf{H}_{k,n} \tilde{\mathbf{a}}_{k,n}, \tag{3.21}$$

where the N_t-vector $\tilde{\mathbf{a}}_{k,n}$ is a preliminary decision of the transmitted data vector $\mathbf{a}_{k,n}$. Since the same cancellation scheme is applied on each receive antenna branch, we can make use of equation (3.15) to derive the optimum coefficients of the filters $\underline{W}$ and $\underline{C}$.

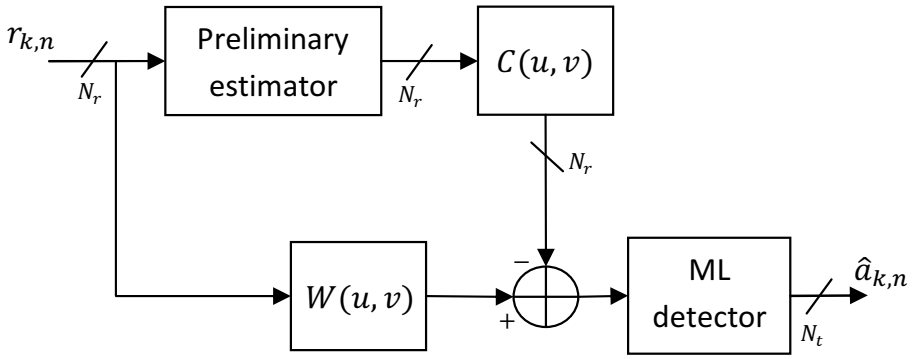

Figure 3.6: Basic scheme of interference cancellation MIMO receiver

Derivation of the coefficients of the filters $\underline{\mathbf{W}}$ and $\underline{\mathbf{C}}$

To determine the optimal pair of filters $\underline{W}$ and $\underline{C}$ in the mean-square sense, we make as in [99] the simplifying assumption that the preliminary decisions are correct. Let $\mathfrak{U}(k,n)$ and $\mathfrak{V}(k,n)$ denote the output sequences of the filters $\underline{W}$ and $\underline{C}$ respectively. Then, we can write

$$\mathfrak{U}(k,n) = \sum_{y=-Y}^{Y} \sum_{z=-Z}^{Z} W(y,z) r(k-y, n-z) \tag{3.22}$$

$$\mathfrak{V}(k,n) = \sum_{u=-U}^{U} \sum_{v=-V}^{V} C(u,v) a(k-u, n-v) \tag{3.23}$$

Notice that the true data sequence $a(k,n)$ is involved in this last equation as we have assumed the tentative decisions are correct. Then, the estimation of the symbol $a(k,n)$ is obtained by subtracting $\mathfrak{V}(k,n)$ from $\mathfrak{U}(k,n)$. The goal is to determine the filters $\underline{W}$ and $\underline{C}$ that minimize the mean-square error (MSE):

$$E(k,n) = \mathbb{E}\{|\epsilon(k,n)|^2\}, \tag{3.24}$$

where $\epsilon(k,n) = \mathfrak{U}(k,n) - \mathfrak{V}(k,n) - a(k,n)$.

To do this, we differentiate $E(k,n)$ with respect to the complex tap weights $\{C(u,v)\}$ and $\{W(y,z)\}$ and set the derivatives to zero. Using (3.23) and (3.22), we obtain:

$$\begin{aligned}
\frac{\partial |\epsilon(k,n)|^2}{\partial W(y,z)} &= \epsilon^*(k,n) \frac{\partial \epsilon(k,n)}{\partial W(y,z)} = \epsilon^*(k,n) \frac{\partial \mathfrak{U}(k,n)}{\partial W(y,z)} \\
&= \epsilon^*(k,n) \sum_{y'=-Y}^{Y} \sum_{z'=-Z}^{Z} \frac{\partial W(y',z')}{\partial W(y,z)} r(k-y', n-z') \\
&= \epsilon^*(k,n) r(k-y, n-z)
\end{aligned} \tag{3.25}$$

and

$$\begin{aligned}\frac{\partial|\epsilon(k,n)|^2}{\partial C(u,v)} &= \epsilon^*(k,n)\frac{\partial\epsilon(k,n)}{\partial C(u,v)} = -\epsilon^*(k,n)\frac{\partial\mathfrak{V}(k,n)}{\partial C(u,v)} \\ &= -\epsilon^*(k,n)\sum_{\substack{u'=-U\\u'\neq 0}}^{U}\sum_{\substack{v'=-V\\v'\neq 0}}^{V}\frac{\partial C(u',v')}{\partial C(u,v)}a(k-u',n-v') \\ &= -\epsilon^*(k,n)a(k-u,n-v) \qquad (u,v)\neq(0,0) \end{aligned} \tag{3.26}$$

Hence, setting the derivatives of $E(k,n)$ to zero yields the following expressions:

$$\mathbb{E}\{\epsilon^*(k,n)a(k-u,n-v)\} = 0 \quad (u,v)\neq(0,0), \tag{3.27}$$

$$\mathbb{E}\{\epsilon^*(k,n)r(k-y,n-z)\} = 0 \quad \forall(y,z). \tag{3.28}$$

Thus, these optimality conditions require that the error signal $\epsilon(k,n)$ is orthogonal to the observable inputs of the $\underline{C}$ and $\underline{W}$ filters, namely, $a(k,n)$ and $r(k,n)$ [99].

In Appendix A.2, we develop the conditions (3.27) and (3.28), and we obtain that equation (3.27) yields:

$$C^*(u,v) = \sum_{y=-Y}^{Y}\sum_{z=-Z}^{Z}W^*(y,z)f^*(u-y,v-z)(-1)^{(v-z)(k-u)}, \quad \forall(u,v)\neq(0,0) \tag{3.29}$$

and equation (3.28) gives:

$$\begin{aligned}&\sigma_a^2\sum_{z'=-Z}^{Z}\sum_{y'=-Y}^{Y}W^*(y',z')\sum_{p=-P}^{P}\sum_{q=-Q}^{Q}f^*(p,q)f(p+y'-y,q+z-z')(-1)^{(z'-z)(k-y'-p)} \\ &+\sum_{z'=-Z}^{Z}\sum_{y'=-Y}^{Y}W^*(y',z')\mathbb{E}\{\gamma^*(k-y',n-z')\gamma(k-y,n-z)\} \\ &=\sigma_a^2 f(-y,-z)(-1)^{-zk}+\sigma_a^2\sum_{u=-U}^{U}\sum_{v=-V}^{V}C^*(u,v)f(u-y,v-z)(-1)^{(v-z)(k-u)}\end{aligned} \tag{3.30}$$

where $\sigma_a^2 = \mathbb{E}\{|a(k,n)|^2\}$ is variance of the signal $a(k,n)$.

Hence, we obtained two equations with two unknowns $C(u,v)$ and $W(y,z)$. By substituting (3.29) into (3.31), we attempt to retrieve $W(y,z)$, then we have:

$$\begin{aligned}&\sigma_a^2\sum_{z'=-Z}^{Z}\sum_{y'=-Y}^{Y}W^*(y',z')\sum_{p=-P}^{P}\sum_{q=-Q}^{Q}f^*(p,q)f(p+y'-y,q+z-z')(-1)^{(z'-z)(k-y'-p)} \\ &+\sum_{z'=-Z}^{Z}\sum_{y'=-Y}^{Y}W^*(y',z')\mathbb{E}\{\gamma^*(k-y',n-z')\gamma(k-y,n-z)\}=\sigma_a^2 f(-y,-z)(-1)^{-zk} \\ &+\sigma_a^2\sum_{z'=-Z}^{Z}\sum_{y'=-Y}^{Y}W^*(y',z')\sum_{\substack{u=-U\\u\neq 0}}^{U}\sum_{\substack{v=-V\\v\neq 0}}^{V}f^*(u-y',v-z')f(u-y,v-z)(-1)^{(z+z')(u-k)}.\end{aligned} \tag{3.31}$$

Then, we can rewrite

$$\sum_{z'=-Z}^{Z}\sum_{y'=-Y}^{Y} W^*(y',z')T^{(k)}_{y,y',z,z'} + \frac{1}{\sigma_a^2}\sum_{z'=-Z}^{Z}\sum_{y'=-Y}^{Y} W^*(y',z')\mathbb{E}\{\gamma^*(k-y',n-z')\gamma(k-y,n-z)\}$$
$$= f(-y,-z)(-1)^{-zk} - \sum_{z'=-Z}^{Z}\sum_{y'=-Y}^{Y} W^*(y',z')f^*(-y',-z')f(-y,-z)(-1)^{-k(z+z')}, \quad (3.32)$$

where

$$T^{(k)}_{y,y',z,z'} = \sum_{p=-P}^{P}\sum_{q=-Q}^{Q} f^*(p,q)f(p+y'-y,q+z-z')(-1)^{(z'-z)(k-y'-p)}$$
$$- \sum_{u=-U}^{U}\sum_{v=-V}^{V} f^*(u-y',v-z')f(u-y,v-z)(-1)^{(z+z')(u-k)}. \quad (3.33)$$

In the following, we show that the term $T^{(k)}_{y,y',z,z'}$ is zero. Let us substitute u by $p+y'$ and v by $q+z'$, Hence we obtain

$$T^{(k)}_{y,y',z,z'} = \sum_{p=-P}^{P}\sum_{q=-Q}^{Q} f^*(p,q)f(p+y'-y,q+z-z')(-1)^{(z'-z)(k-y'-p)}$$
$$- \sum_{p=-U-y'}^{U-y'}\sum_{q=-V-z'}^{V-z'} f^*(p,q)f(p+y'-y,q+z'-z)(-1)^{(z+z')(k-p-y')}. \quad (3.34)$$

We know that $f^*(p,q)=0$ when $(p,q)\notin\{-P,...,P\}\times\{-Q,...,Q\}$. Then, we set $|U-y'|\geq P$ and $|V-z'|\geq Q$ for all $(y',z')\in\{-Y,...,Y\}\times\{-Z,...,Z\}$. That means that we have to set $U\geq P+Y+1$ and $V\geq Q+Z+1$. Therefore, we can write

$$T^{(k)}_{y,y',z,z'} = \sum_{p=-P}^{P}\sum_{q=-Q}^{Q} f^*(p,q)f(p+y'-y,q+z-z')\left((-1)^{(z'-z)(k-y'-p)} - (-1)^{(z+z')(k-y'-p)}\right)$$
$$= 0. \quad (3.35)$$

Consequently, (3.32) is simplified as

$$\frac{1}{\sigma_a^2}\sum_{z'=-Z}^{Z}\sum_{y'=-Y}^{Y} W^*(y',z')\mathbb{E}\{\gamma^*(k-y',n-z')\gamma(k-y,n-z)\}$$
$$= \Bigg(1 - \underbrace{\sum_{z'=-Z}^{Z}\sum_{y'=-Y}^{Y} W^*(y',z')f^*(-y',-z')(-1)^{-kz'}}_{\beta_k}\Bigg) f(-y,-z)(-1)^{-kz}, \quad (3.36)$$

where β_k is a constant depending only on the parity of k. It is worth noticing that the solution of this equation depends significantly on the autocorrelation of the noise $\gamma(k,n)$. If the noise were uncorrelated, the solution of (3.36) would be trivial. Unfortunately, the noise term $\gamma(k,n)$ is correlated and its autocorrelation function is given by (3.18). Therefore, equation (3.36) becomes:

$$\frac{\sigma^2}{\sigma_a^2}\sum_{z'=-Z}^{Z}\sum_{y'=-Y}^{Y} W^*(y',z')f(y'-y,z'-z)(-1)^{(z-z')y'+kz'} = (1-\beta_k)f(-y,-z). \quad (3.37)$$

This equation above represents a system of linear equations. To be able to resolve it, we rewrite (3.37) in a matrix form.

Let $\underline{\mathbf{f}}$ and $\underline{\mathbf{w}}$ be $(2Z+1)(2Y+1)\times 1$ vectors and $\underline{\mathbf{F}}_k$ be a $(2Z+1)(2Y+1)\times(2Z+1)(2Y+1)$ matrix such that:

$$\underline{\mathbf{f}}(p+(2Y+1)q) = f(Y-p, Z-q), \tag{3.38}$$

$$\underline{\mathbf{w}}(p+(2Y+1)q) = W^*(p-Y, q-Z), \tag{3.39}$$

and

$$\underline{\mathbf{F}}_k(p+(2Y+1)q, p'+(2Y+1)q') = f(p'-p, q'-q)(-1)^{(p'-Y)(q-q')}(-1)^{k(q'-Z)}, \tag{3.40}$$

with $(p,p') \in \{0,...,2Y\}^2$ and $(q,q') \in \{0,...,2Z\}^2$. Therefore, we can express (3.37) in a matrix form as

$$\underline{\mathbf{F}}_k\underline{\mathbf{w}} = \frac{\sigma_a^2}{\sigma^2}(1-\beta_k)\underline{\mathbf{f}}. \tag{3.41}$$

We notice that the column of index $Y+Z(2Y+1)$ (the central one) of the matrix $\underline{\mathbf{F}}_k$ equals the vector $\underline{\mathbf{f}}$. Hence, the trivial solution of (3.41) is

$$\underline{\mathbf{w}} = \frac{\sigma_a^2}{\sigma^2}(1-\beta_k)\underline{\mathbf{e}}_l, \tag{3.42}$$

where the vector $\underline{\mathbf{e}}_l$ has the same size as $\underline{\mathbf{w}}$, and contains zeros except the position $l = Y+Z(2Y+1)$ that is set to 1. Then, according to (3.39), all the coefficients $W^*(y,z)$ are zeros except for $W^*(0,0) = \frac{\sigma_a^2}{\sigma^2}(1-\beta_k)$. Thus, we can write

$$W^*(y,z) = \frac{\sigma_a^2}{\sigma^2}(1-\beta_k)\delta(y,z), \tag{3.43}$$

where $\delta(y,z)$ is the kronecker delta function. Now, to determine β_k we make use of its definition given in (3.36), thus we obtain:

$$\beta_k = \frac{\sigma_a^2}{\sigma^2}(1-\beta_k)f^*(0,0) \tag{3.44}$$

which yields

$$\beta_k = \frac{\sigma_a^2 f^*(0,0)}{\sigma^2+\sigma_a^2 f^*(0,0)}. \tag{3.45}$$

Finally, plugging (3.45) into (3.43) we obtain

$$W(y,z) = \frac{\sigma_a^2}{\sigma^2+\sigma_a^2 f(0,0)}\delta(y,z). \tag{3.46}$$

Whatever the used prototype filter, we have $f(0,0) = 1$. Hence, we can simplify the last equation as:

$$W(y,z) = \frac{\sigma_a^2}{\sigma^2+\sigma_a^2}\delta(y,z). \tag{3.47}$$

Now, we substitute (3.47) into (3.29), we obtain:

$$C(u,v) = \frac{\sigma_a^2}{\sigma^2+\sigma_a^2}f(u,v)(-1)^{v(k-u)}, \quad \forall (u,v) \neq (0,0). \tag{3.48}$$

Application and simulation results

According to the results obtained in the previous subsection, the filter $\underline{W}$ is just a one tap coefficient $\frac{\sigma_a^2}{\sigma^2+\sigma_a^2}$, and the canceller filter $\underline{C}$ has the same impulse response as the FBMC transmultiplexer scaled by $\frac{\sigma_a^2}{\sigma^2+\sigma_a^2}$ except for the center tap which is zero. One can check this latter by comparing equations (3.48) and (3.15). Hence, if the interference cancellation is perfect, the input vector to the ML detector is:

$$\tilde{\mathbf{r}}_{k,n} = \frac{\sigma_a^2}{\sigma^2+\sigma_a^2}\mathbf{r}_{k,n}. \tag{3.49}$$

The ML detector applied on vector $\tilde{\mathbf{r}}_{k,n}$ has to take into account the scaling factor $\frac{\sigma_a^2}{\sigma^2+\sigma_a^2}$. Therefore, the ML detector selects the data vector $\hat{\mathbf{a}}_{k,n}$ that minimizes the Euclidean distance as follows:

$$\hat{\mathbf{a}}_{k,n} = \underset{\mathbf{a}_{k,n}}{\arg\min}\left\{\left\|\tilde{\mathbf{r}}_{k,n} - \frac{\sigma_a^2}{\sigma^2+\sigma_a^2}\mathbf{H}_{k,n}\mathbf{a}_{k,n}\right\|^2\right\}, \tag{3.50}$$

where $\mathbf{H}_{k,n}$ is the MIMO-SM channel matrix. We notice that this metric minimization is absolutely equivalent to the following one:

$$\hat{\mathbf{a}}_{k,n} = \underset{\mathbf{a}_{k,n}}{\arg\min}\left\{\left\|\mathbf{r}_{k,n} - \mathbf{H}_{k,n}\mathbf{a}_{k,n}\right\|^2\right\}. \tag{3.51}$$

Hence, for the sake of the receiver simplicity, we can set the filters $\underline{W}$ and $\underline{C}$ as:

$$W(y,z) = \delta(y,z), \tag{3.52}$$

$$C(u,v) = \begin{cases} f(u,v)(-1)^{v(k-u)}, & \forall (u,v) \neq (0,0) \\ 0 & (u,v) = (0,0) \end{cases} \tag{3.53}$$

and the ML detector makes use of the metric given in (3.51). Since the interference is estimated by involving the preliminary decisions of some postcursor symbols, a processing delay is then introduced in the system.

As for the tentative equalizer providing preliminary decisions $\tilde{\mathbf{a}}_{k,n}$, we can use the simple MMSE equalizer. According to (3.21) the input signal of the canceller filter $\underline{C}$ in the receive antenna branch i is:

$$\hat{r}_{k,n}^{(i)} = \sum_{j=1}^{N_t} h_{k,n}^{(ij)}\tilde{a}_{k,n}^{(j)}. \tag{3.54}$$

Therefore, the MMSE equalizer has to be followed by a reconstruction operation of vector $\hat{\mathbf{r}}_{k,n}$ by using the channel matrix $\mathbf{H}_{k,n}$. The basic scheme of the whole proposed receiver is depicted in fig. 3.7. We call this receiver IC-ML. It is worth noticing that the difference between the IC-ML receiver and the MMSE-ML one lies in the interference estimation method; in MMSE-ML the interference is estimated directly by taking the imaginary part of the MMSE outputs, whereas in IC-ML the interference is calculated through the MMSE decided symbols around the considered symbol. In the latter, a processing delay is then introduced.

We have tested this receiver in a 2×2 SM system with the Ped-A channel model [97]. The number of subcarrier is $M = 512$, and the frequency sampling is $f_s = 10\ MHz$. Fig.

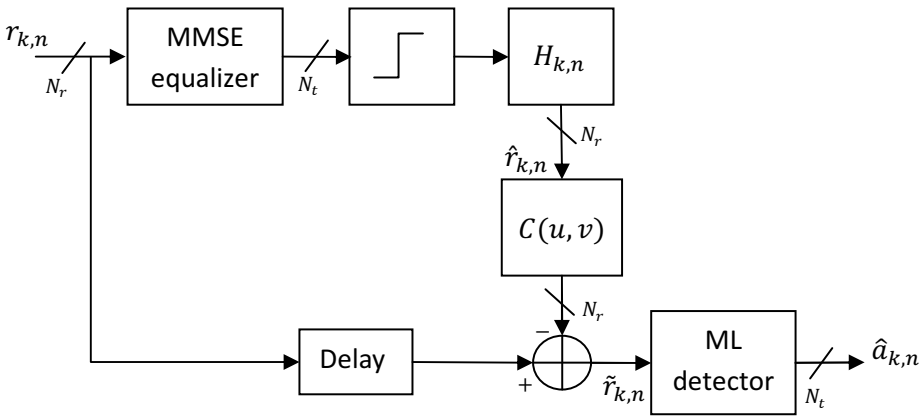

Figure 3.7: Basic scheme of the MIMO IC-ML receiver

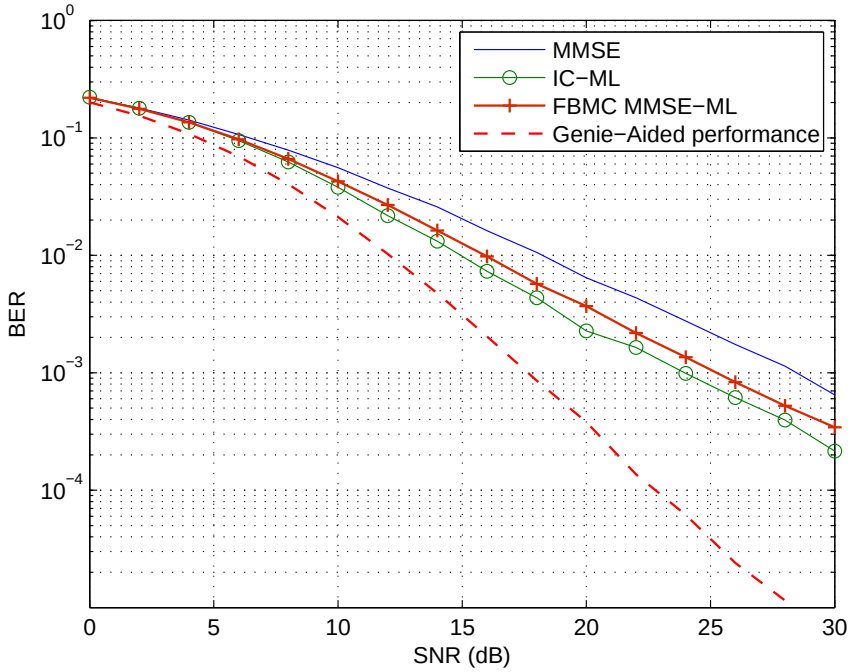

Figure 3.8: BER performance comparison of IC-ML receiver with MMSE-ML and the Genie-Aided one in a 2×2 SM system

3.8 shows the BER performance of the proposed IC-ML receiver, which is compared to the optimal detection and to the MMSE-ML one presented in section 3.2. We remark that we obtain better BER performance than the MMSE-ML one; we note an SNR gain of about 1 dB with respect to MMSE-ML. But the performance of IC-ML still remains far from the optimum one. This performance limitation is certainly due to the reliability level of the MMSE equalizer. In order to improve the BER performance, we can exploit the outputs of the ML detector, and use them as tentative decisions to estimate again the interference. However, the drawback of this last receiver proposal is that the processing delay is doubled.

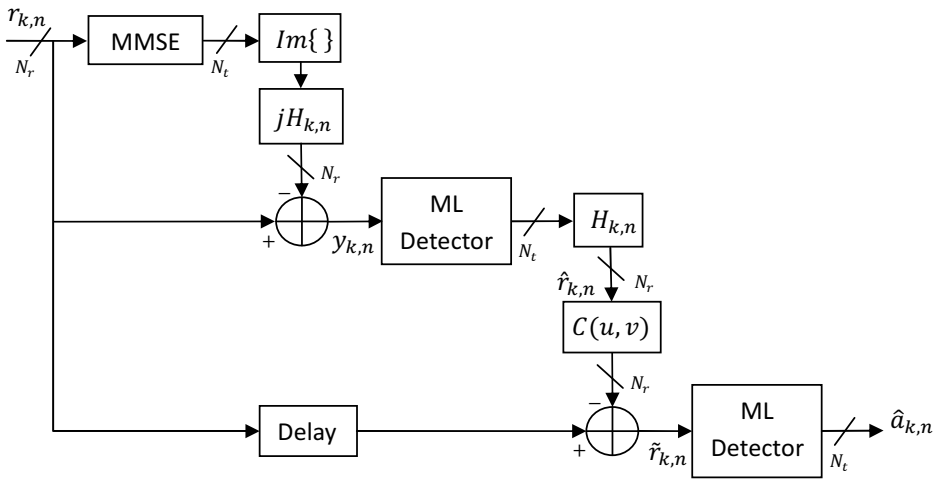

Figure 3.9: Basic scheme of the Rec-ML receiver

In order to improve the interference cancellation scheme without increasing the processing delay, we propose to replace the tentative MMSE equalizer by the MMSE-ML detector presented in 3.2. We call this receiver Rec-ML (Recursive ML). Fig 3.9 depicts the basic scheme of the Rec-ML receiver. The advantage of this receiver is that the tentative decisions are now more reliable. The BER performance of the Rec-ML receiver is depicted in Fig. 3.10, where it is compared to the MMSE-ML and the Genie-Aided performance (assuming perfect ISI cancellation). The size of the SM matrix channel is 2×2, and we used Ped-A channel model for simulation. We observe that Rec-ML receiver improves the BER performance compared to MMSE-ML. At $BER = 10^{-3}$ we have an SNR gain of about 3.5 dB with respect to MMSE-ML receiver. However, there is still a gap with respect to optimal detection, which stems from the decision and estimation errors on the data symbols involved in the calculation of the interference term. This gap can be reduced if error correction is introduced in the system. It is worth noting that exploiting the Rec-ML outputs to estimate again the interference does not improve the BER-performance. Indeed, we obtained by simulation the same performance as the Rec-ML one. This fact is due to the error propagation as we will see in section 3.4.

Reducing the processing delay

We have seen that the proposed Rec-ML receiver introduces a processing delay since some postcursor symbol decisions are involved in the interference cancellation. This processing

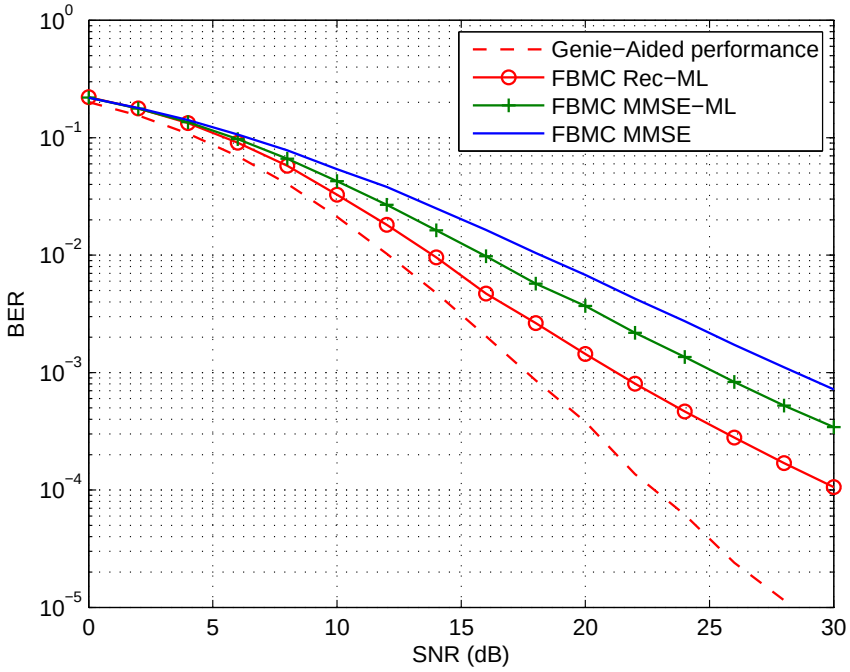

Figure 3.10: BER performance of the Rec-ML receiver compared to MMSE, MMSE-ML equalizers and to the Genie-Aided in a 2×2 SM system

delay depends in fact on the overlapping factor K of the FBMC system. Indeed, since two successive multicarrier symbols in FBMC are transmitted with an offset of $\frac{M}{2}$ samples, the last multicarrier symbol interfering with the current one is offset with respect to the latter by $(K - \frac{1}{2})M$ samples. Therefore, the processing delay introduced in the system is of $K - \frac{1}{2}$ multicarrier symbols. In our case $K = 4$, then Rec-ML has a processing delay of 3.5 multicarrier symbols. The delay might be critical and, in order to limit its value, it is interesting to use a small set of coefficients of the system impulse response. Of course, if an incomplete impulse response is used, a residual interference term remains, which introduces a floor in the BER versus received SNR curve. Three neighborhoods to the central unity term are considered, with 8, 12 and 18 coefficients respectively. For each one, the value of the residual interference power σ^2_{RI} is calculated. The results are given in Table 3.1, and the corresponding delays are indicated.

Table 3.1: residual interference power calculated with 3 sets of coefficients using PHYDYAS filter

Neighborhood	$\sigma^2_{\mathbf{RI}}$ (dB)	**Delay**
1	-11.03	$1/2$
2	-17.85	1
3	-38.70	$3/2$

Clearly, neighborhood 1 is likely to produce a high bit error rate, while neighborhood 3 is close to optimum, except for high SNR values. The BER performance is assessed by simulation in each of the 3 cases. That leads to results shown in Fig. 3.11.

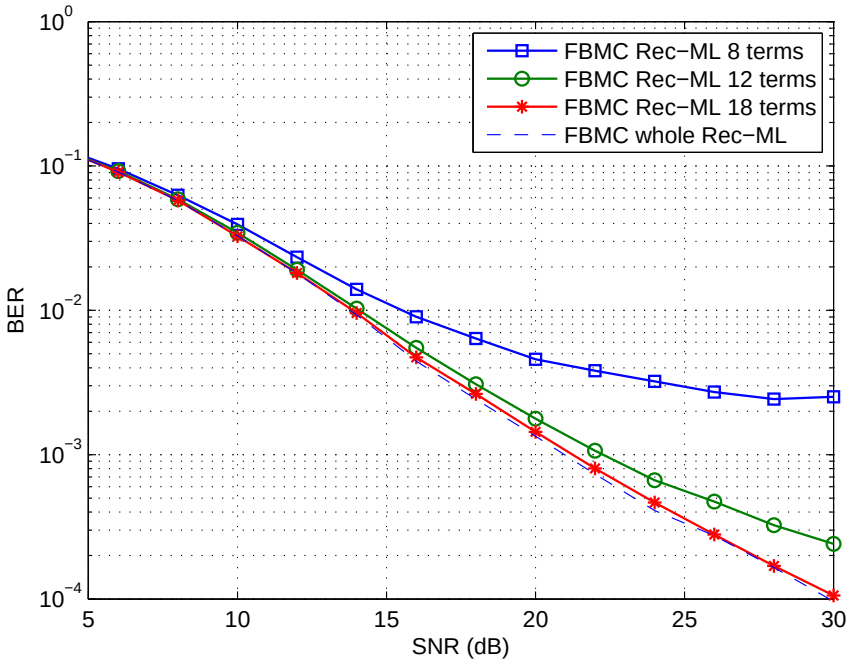

Figure 3.11: BER performance of the Rec-ML receiver using the 3 different neighborhoods in a 2×2 SM system

As expected, neighborhood 1 (8 coefficients) produces a high BER floor due to the high value of the residual interference. There is virtually no difference between neighborhoods 2 and 3 as long as the SNR at the receiver output does not exceed 20 dB. This means that the contribution of the residual interference is negligible, compared to the noise level. Further, with neighborhood 3, we obtain the same performance as the whole Rec-ML depicted in Fig. 3.10. Therefore, neighboring 3 or 2 are satisfactory compromises between performance and delay.

3.3.3 Interference cancellation in coded FBMC

We have seen in the previous sections that the interference cancellation in the proposed receiver schemes is not very effective due to the presence of erroneous tentative decisions. Indeed, it was shown by simulations that there is a BER-performance gap between the proposed receivers and the Genie-Aided performance obtained by perfect interference removing. Since the performance limitation is due to the tentative decision errors, error correction coding may significantly improve the interference cancellation. In this section, we test the proposed receivers in the context of encoded data.

At the transmitter side, the binary information enters a convolutional encoder to produce an encoded binary sequence which is bit-interleaved by a random interleaver. Then,

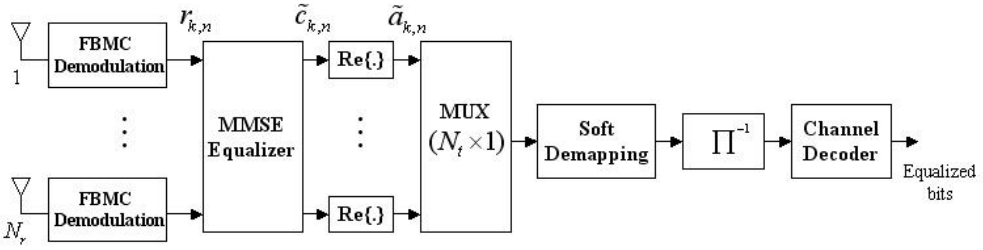

Figure 3.12: MMSE receiver for FBMC in $N_t \times N_r$ Spatial Data Multiplexing

the interleaved bits are mapped by a memoryless modulator into symbols belonging to a PAM constellation set $\mathbb{A}$ with cardinality of $2^{\frac{q}{2}}$, where $\frac{q}{2}$ is the bit number in the PAM symbol. After that, the PAM symbols are demultiplexed onto N_t branches (corresponding to N_t antennas). Over each branch the data are sent to the FBMC modulator and then transmitted through the radio channel. At the receiver side, the N_t transmitted signals are collected by N_r receive antennas. The signal in each receive antenna branch is FBMC demodulated, forming thus demodulated vectors $\mathbf{r}_{k,n} = [r_{k,n}^{(1)}, ..., r_{k,n}^{(N_r)}]^T$, where $r_{k,n}^{(i)}$ are the FBMC demodulator outputs at the ith receive antenna.

MMSE equalization

The implementation of the MMSE equalization in the considered context has been described in [11]. The demodulated vector $\mathbf{r}_{k,n}$ is fed to the MMSE equalizer having as output the equalized virtually transmitted vector:

$$\tilde{\mathbf{c}}_{k,n} = \mathbf{G}_{k,n}^H \mathbf{r}_{k,n}, \tag{3.55}$$

where $\mathbf{G}_{k,n}$ is the MMSE equalization matrix. Then, a real part retrieval of $\tilde{\mathbf{c}}_{k,n}$ yields the real equalized data vector $\tilde{\mathbf{a}}_{k,n}$. Inverting exactly the transmission operations, these symbols are multiplexed one by one, soft demapped and deinterleaved before being decoded to recover the transmitted data bits. This scheme is the non iterative MMSE receiver as referred in [11] and depicted on Fig. 3.12.

The soft demapping consists in calculating the bit reliability information in the form of Log-Likelihood Ratio (LLR). The LLRs are calculated separately for each layer. We can write each component of vector $\tilde{\mathbf{c}}_{k,n}$ as [100]:

$$\begin{aligned} \tilde{c}_{k,n}(i) &= \mathbf{g}_{k,n}^H(i)\mathbf{r}_{k,n} \\ &= \beta_{k,n}(i)c_{k,n}(i) + \omega_{k,n}(i), \quad i = 1, ..., N_t \end{aligned} \tag{3.56}$$

with $\beta_{k,n}(i)$ is a bias term given by:

$$\beta_{k,n}(i) = \mathbf{g}_{k,n}^H(i)\mathbf{h}_{k,n}(i), \tag{3.57}$$

where $\mathbf{h}_{k,n}(i)$ and $\mathbf{g}_{k,n}(i)$ are, respectively, the ith column of matrices $\mathbf{H}_{k,n}$ and $\mathbf{G}_{k,n}$. $\omega_{k,n}(i)$ in (3.56) is an interference-plus-noise term approximated as a zero-mean complex

Gaussian variable with variance given by [100, 101]:

$$\sigma^2_{\omega_i} = 2E_a(\beta_{k,n}(i) - \beta_{k,n}(i)^2), \tag{3.58}$$

where $E_a = \mathbb{E}\{|a_{k,n}(i)|^2\} = \mathbb{E}\{|c_{k,n}(i)|^2\}/2$. Since $\beta_{k,n}(i) \in]0,1[$ is real-valued [100], the real MMSE-equalized symbol expression is:

$$\tilde{a}_{k,n}(i) = \beta_{k,n}(i)a_{k,n}(i) + \mathfrak{Re}\{\omega_{k,n}(i)\}. \tag{3.59}$$

According to this expression, the LLR value corresponding to the lth bit b^l_i, $l \in \{1, ..., \frac{q}{2}\}$, in $a_{k,n}(i)$ is obtained as:

$$L(b^l_i) = \log\left(\frac{\sum_{a(i)\in\mathbb{A}^+_l} e^{-\frac{1}{\sigma^2_{\omega_i}}(\tilde{a}(i)-\beta(i)a(i))^2}}{\sum_{a(i)\in\mathbb{A}^-_l} e^{-\frac{1}{\sigma^2_{\omega_i}}(\tilde{a}(i)-\beta(i)a(i))^2}}\right), \tag{3.60}$$

where $\mathbb{A}^+_l$ and $\mathbb{A}^+_l$ denote the constellation subset whose lth bit equals $+1$ and -1, respectively. Using the Log-Sum approximation, the above expression becomes:

$$\begin{aligned} L(b^l_i) \approx & \frac{1}{\sigma^2_{\omega_i}} \min_{a(i)\in\mathbb{A}^-_l} (\tilde{a}(i) - \beta(i)a(i))^2 \\ & - \frac{1}{\sigma^2_{\omega_i}} \min_{a(i)\in\mathbb{A}^+_l} (\tilde{a}(i) - \beta(i)a(i))^2, \quad l \in \{1, ..., \frac{q}{2}\} \end{aligned} \tag{3.61}$$

It is worth pointing out that in case of QPSK modulation ($q = 2$, $a_{k,n}(i) = \frac{\pm 1}{\sqrt{2}}$), we can show that $L(b^1_i)$ is proportional to the quantity $\frac{\tilde{a}_{k,n}(i)}{1-\beta_{k,n}(i)}$, and as a consequence we can drop out the soft demapping bloc and consider this quantity as the soft input of the decoder in order to simplify the receiver.

Fig. 3.13 shows the BER performance comparison of MMSE equalizer between FBMC and OFDM in a 2×2 SM system. The performance comparison is done for two different channel models, namely, Ped-A and Vehicular-A (Veh-A) channel model [97]. We assumed perfect Channel State Information (CSI) at the receiver side. The simulation parameters for FBMC and OFDM are summarized in Table 3.2.

Table 3.2: Simulation parameters

	Pedestrian-A	**Vehicular-A**
Complex modulation	QPSK	QPSK
FFT size (M)	1024	1024
CP size for OFDM (Δ)	8	32
Convolutional code	$(171, 133)$	$(171, 133)$
Sampling frequency	10 MHz	10 MHz

Since the CP duration affects OFDM performance and in order to compare FBMC to the best OFDM configuration, we have chosen in table 3.2 the smallest possible CP size for each channel model. The system performance is assessed in terms of BER as function of the signal-to-noise ratio per bit (E_b/N_0). For CP-OFDM, we define E_b/N_0 by:

$$E_b/N_0 = \frac{M + \Delta}{M} \times \frac{N_r}{qR_sR_c} SNR, \tag{3.62}$$

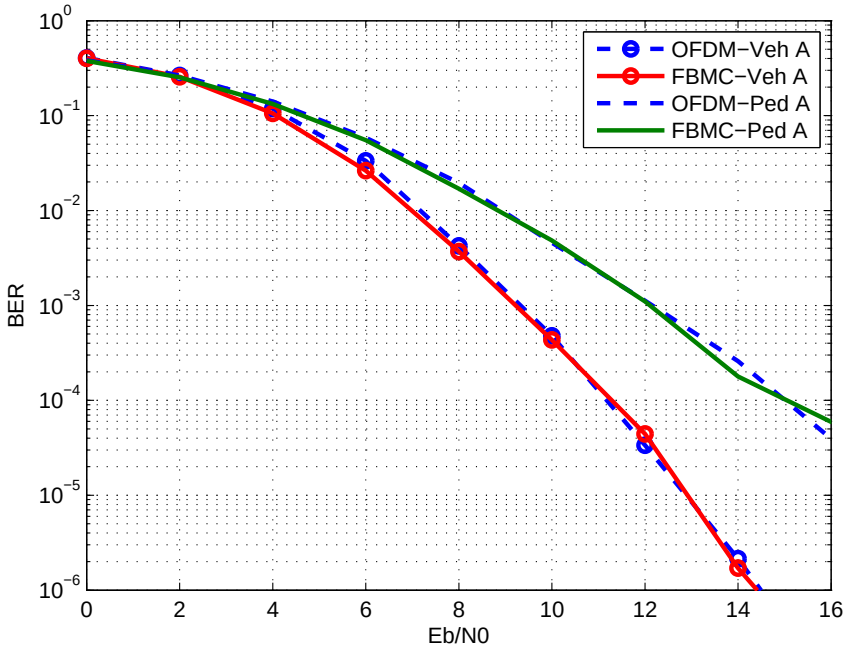

Figure 3.13: BER performance comparison between CP-OFDM and FBMC in 2×2 MIMO case over Ped. A and Veh. A channels with MMSE receiver

where M is the subcarrier number (FFT size), Δ is the cyclic prefix size, R_c is the channel coding rate, R_s is the space-time coding rate, q is the bit number in a complex QAM symbol ($q = 2$ for QPSK), and SNR is the Signal-to-Noise ratio. As for FBMC, the expression of E_b/N_0 is obtained by nulling the CP duration Δ, so we can write:

$$E_b/N_0 = \frac{N_r}{qR_sR_c} SNR. \tag{3.63}$$

As we can observe in Fig. 3.13, there is pratically no difference between FBMC and OFDM from BER performance point of view when using MMSE equalizer. The performance gain obtained in Veh-A channel model over the Ped-A one is due to the difference in the frequency diversity order that each channel model offers. This frequency diversity is exploited thanks to coding and bit interleaving.

MMSE-ML and Recursive-ML (Rec-ML) receivers

In MMSE-ML receiver which is presented in section 3.2, the MMSE equalizer is used to estimate the interference terms which are obtained by taking the imaginary parts of the MMSE outputs. Once the contribution of these interference terms are removed from the received signal vector $\mathbf{r}_{k,n}$, the resulting signal vector $\mathbf{y}_{k,n}$ is fed to a soft ML detector giving soft outputs in the form of LLR values. Then, these soft values are multiplexed, deinterleaved, and decoded to provide decision bits. Fig. 3.14 shows the basic scheme of the MMSE-ML receiver.

The received vector $\mathbf{r}_{k,n}$ is an observation of N_t transmitted PAM symbols $a_{k,n}^{(j)}$, $j \in \{1, ..., N_t\}$. Hence, there are $\frac{q}{2}N_t$ bits d_l involved in the received vector $r_{k,n}$. The soft ML

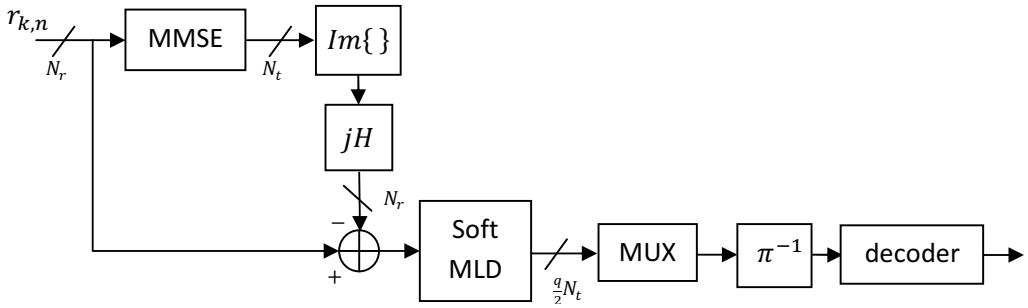

Figure 3.14: MMSE-ML scheme for FBMC in $N_t \times N_r$ Spatial Data Multiplexing

detector calculates the LLRs of the *a posteriori probability* (APP) of the encoded bits d_l being $+1$ or -1. The LLR values for the ML detector are defined as:

$$L_{APP}(d_l|\mathbf{y}_{k,n}) = \log\left(\frac{P(d_l=+1|\mathbf{y}_{k,n})}{P(d_l=-1|\mathbf{y}_{k,n})}\right), \quad l = 1, ..., \frac{q}{2}N_t \tag{3.64}$$

where $\frac{q}{2}$ is the number of bits that constitute the real symbol $a_{k,n}$. Then, in each subcarrier and half period $T/2$, we have $\frac{q}{2}N_t$ soft bits at the soft MLD output. By employing Bayes' theorem and assuming statistical independence and equiprobability among the bits d_l, the LLR can be written as [102, 103]:

$$L_{APP}(d_l|\mathbf{y}_{k,n}) = \log\left(\frac{\sum_{\mathbf{d}\in\mathbb{D}_k^+} p(\mathbf{y}_{k,n}|\mathbf{d})}{\sum_{\mathbf{d}\in\mathbb{D}_k^-} p(\mathbf{y}_{k,n}|\mathbf{d})}\right), \tag{3.65}$$

where the vector $\mathbf{d}$ contains all the bits corresponding to the transmitted symbols $a_{k,n}$ over all the antennas, and the set $\mathbb{D}_l^+$ (or $\mathbb{D}_l^-$) contains the vectors $\mathbf{d}$ having $d_l = +1$ (or $d_l = -1$). The likelihood density $p(\mathbf{y}_{k,n}|\mathbf{d})$ is given by:

$$p(\mathbf{y}_{k,n}|\mathbf{d}) = \frac{\exp\left(-\frac{1}{2\sigma^2}\|\mathbf{r}_{k,n} - \mathbf{H}_{k,n}\mathbf{a}_{k,n}(\mathbf{d})\|^2\right)}{(2\pi\sigma^2)^{N_r}}, \tag{3.66}$$

where $\mathbf{a}_{k,n}(\mathbf{d})$ is the transmitted real vector corresponding to the bit-vector $\mathbf{d}$. Substituting equation (3.66) in (3.65) and applying the Max-Log approximation, the LLR calculation is simplified by:

$$\begin{aligned} L_{APP}(d_l|\mathbf{y}_{k,n}) = &\frac{1}{2\sigma^2}\min_{\mathbf{d}\in\mathbb{D}_k^-}\|\mathbf{r}_{k,n} - \mathbf{H}_{k,n}\mathbf{a}_{k,n}(\mathbf{d})\|^2 \\ &- \frac{1}{2\sigma^2}\min_{\mathbf{d}\in\mathbb{D}_k^+}\|\mathbf{r}_{k,n} - \mathbf{H}_{k,n}\mathbf{a}_{k,n}(\mathbf{d})\|^2, \quad l \in \{1, ..., \frac{q}{2}N_t\} \end{aligned} \tag{3.67}$$

The obtained soft information at the ML output should be multiplexed, deinterleaved and fed into the soft-input decoder to recover the transmitted information source bits.

As for the Rec-ML receiver, we use the outputs of the MMSE-ML receiver to perform a second interference estimation. This time, the intrinsic interference is estimated by using the decided data bits (available at the MMSE-ML output) which are involved in the symbols $a_{k',n'}$ within the neighborhood of the considered frequency-time position (k, n). For this,

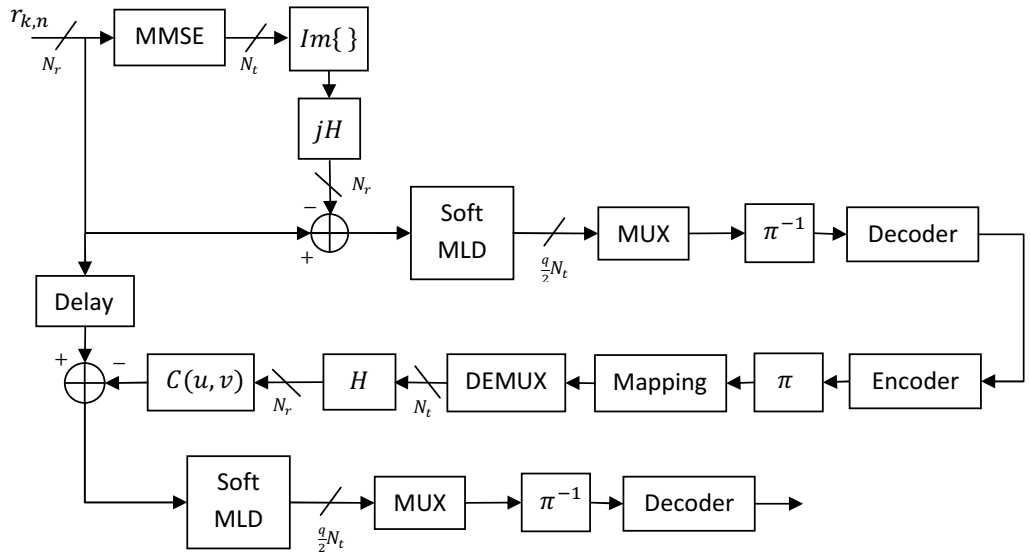

Figure 3.15: Recursive ML scheme for FBMC in $N_t \times N_r$ Spatial Data Multiplexing

the decided data bits are encoded with the same convolutional code used at the transmitter, interleaved, mapped and demultiplexed repeating exactly the same transmission operations to provide an estimation of the transmitted symbols $\hat{\mathbf{a}}_{k,n}$ which will serve to calculate an interference estimate. Thus, the interference estimation is improved since the information bits are encoded and some errors would be corrected. Once this interference is estimated, its contribution is canceled again from the received vector $\mathbf{r}_{k,n}$, and then, we perform once more the soft ML detection. The complete receiver scheme is depicted in Fig. 3.15.

In the following, we show the simulation results for MMSE-ML and Rec-ML receivers and compare their performance to OFDM. We consider a 2×2 spatial multiplexing scheme. Our objective is to test the proposed receiver schemes over a low and high frequency selective channels. For that purpose, we have chosen the Ped-A and the Veh-A channel models [97]. We should note that for both chosen channels, we have not considered the time selectivity. The simulation parameters are the same as the ones used for MMSE equalizer and are summarized in Table 3.2. We also assume perfect channel knowledge at the receiver side, and the performance is assessed in terms of BER as function of E_b/N_0 which is defined by (3.63) and (3.62) for OFDM and FBMC, respectively.

As in the uncoded case, we define the Genie-Aided performance as the fictional one obtained when the symbols serving to estimate the interference are identical to the transmitted ones (perfect interference estimation). We have shown in section 3.1 that even by neglecting the efficiency loss due to CP, the Genie-Aided receiver outperforms CP-OFDM by about 1 dB in a 2×2 SM with QPSK modulation. Hence, it is interesting to compare its performance to the OFDM and the proposed receivers when using convolutional coding.

Fig. 3.16 captures the performance of CP-OFDM with ML and that of FBMC with all the proposed receivers (including MMSE) over the Ped-A channel. The curves show that the MMSE-ML scheme outperforms the MMSE equalizer, but the performance is still far from the CP-OFDM with ML. The gain obtained by MMSE-ML with respect to MMSE equalizer

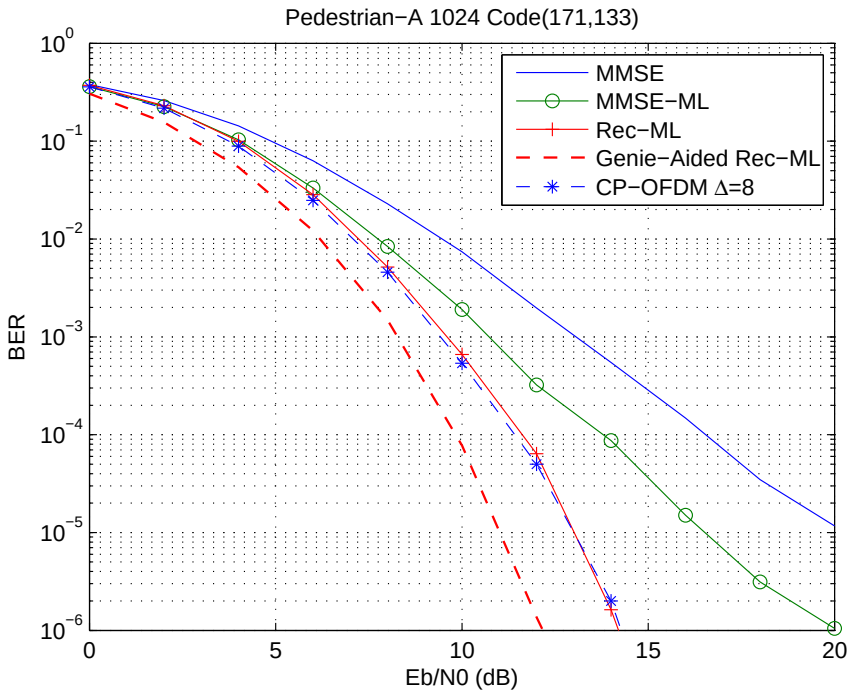

Figure 3.16: BER performance comparison between CP-OFDM and FBMC receivers in 2×2 MIMO case over Ped.-A channel

is about 2.5 dB at $BER = 10^{-4}$, whereas OFDM-ML provides a 5 dB SNR gain compared to MMSE. However, Rec-ML receiver exhibits almost the same performance as OFDM-ML. It is worth recalling that CP-OFDM performance is obtained with the smallest possible CP size ($\Delta = 8$). Increasing Δ yields a performance degradation for CP-OFDM, and thus, FBMC with Rec-ML receiver will outperform CP-OFDM. For example, as in IEEE 802.16e standard [104], if we set $\Delta = \frac{T}{8} = 128$, we obtain a degradation of about 0.48 dB.

Regarding the Veh-A channel, Fig. 3.17 shows the performance of the different receivers in this propagation channel. First, as in the Pedestrian-A channel case, we remark that a considerable SNR gain is obtained by MMSE-ML receiver compared to MMSE equalizer, we have a gain of about 2 dB at $BER = 10^{-4}$. Secondly, we can clearly observe that the obtained Rec-ML performance is slightly better than that obtained with CP-OFDM from $E_b/N_0 = 6$ dB, and tends to reach the Genie-Aided performance in high E_b/N_0 regime.

We notice that the potential SNR gain of FBMC over OFDM is not yet completely exploited, and that the interference is not fully removed even in the encoded case [105]. Therefore, further investigations on interference estimation are needed to improve the performance.

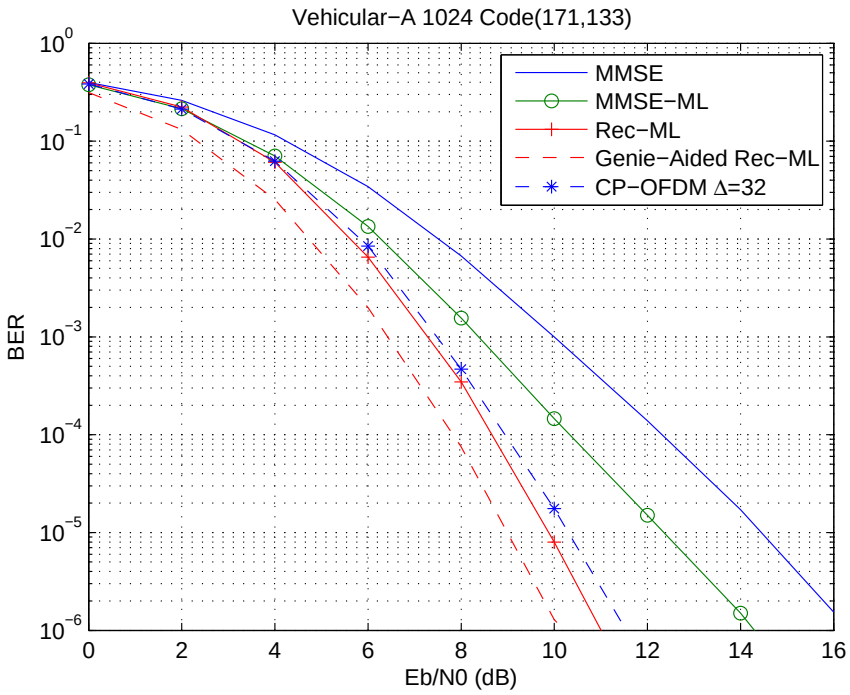

Figure 3.17: BER performance comparison between CP-OFDM and FBMC receivers in 2×2 MIMO case over Veh.-A channel

3.4 Viterbi detection and partial interference cancellation

We have seen in the previous sections that the proposed interference cancellation schemes are not totally effective due to the error propagation. In this section, we propose to study a receiver scheme based on partial ISI cancellation followed by a Viterbi detector instead of an ML detector. The tentative detector is first used to only partially cancel the intrinsic interference.

In order to counteract the error propagation and make the cancellation scheme effective, we were inspired by reference [106] where the authors have established the conditions under which the cancellation scheme is effective. We will show that satisfying these conditions allows our proposed iterative scheme to converge to OFDM performance.

We start in section 3.4.1 by giving a background on the use of tentative decisions to cancel the ISI, and we show how we apply it in the FBMC context.

3.4.1 Partial interference cancellation with Viterbi detection

In reference [106], the authors have considered the channel model depicted in Fig. 3.18, where $f_0(a_k, a_{k-1}, ..., a_{k-\delta+1})$ is a function of δ data symbols and represents the target response expected by the receiver. $f_1(a_{k+\gamma}, a_{k+\gamma-1}, ..., a_{k-\lambda+1})$ is a function of $\gamma+\lambda$ data symbols and represents a small channel perturbation.

It should be noted that, in general, both f_0 and f_1 may be nonlinear functions. The

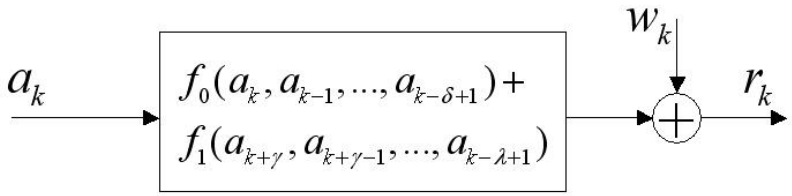

Figure 3.18: Channel model

samples of the signal at the input of the receiver are:

$$\begin{aligned} r_k =& f_0(a_k, a_{k-1}, ..., a_{k-\delta+1}) \\ &+ f_1(a_{k+\gamma}, a_{k+\gamma-1}, ..., a_{k-\lambda+1}) + w_k, \end{aligned} \tag{3.68}$$

where w_k is the noise contribution. The receiver is composed by a tentative detector producing tentative decisions, and a main viterbi detector which assumes that the channel is described only by f_0. Before performing the main Viterbi detector, the tentative decisions are used only to cancel the remaining ISI (RISI) represented by f_1. The receiver scheme is depicted in Fig. 3.19.

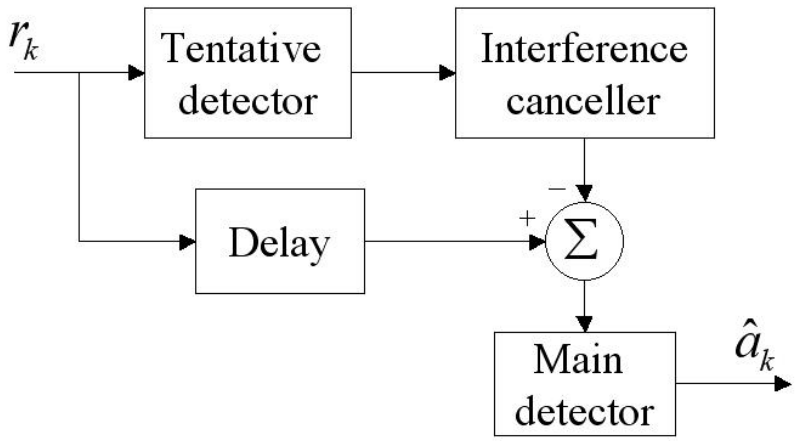

Figure 3.19: Receiver scheme with ISI cancellation using tentative decisions

Given the correct data sequence a_k, and a sequence $a_k^{(\epsilon)}$ for a given error event ϵ, let us define:

$$\begin{aligned} \Delta_k^{(\epsilon)} =& f_0(a_k^{(\epsilon)}, a_{k-1}^{(\epsilon)}, ..., a_{k-\delta+1}^{(\epsilon)}) \\ &- f_0(a_k, a_{k-1}, ..., a_{k-\delta+1}), \end{aligned} \tag{3.69}$$

$$\Phi(\epsilon) = [\Delta_0^{(\epsilon)}, \Delta_1^{(\epsilon)}, ..., \Delta_{K-1}^{(\epsilon)}]^T, \tag{3.70}$$

where K is assumed to be the total number of transmitted symbols. The authors in [106] classified the error events in terms of their distance $d_0(\epsilon)$ in the absence of RISI ($f_1 = 0$), which is given, in the presence of correlated noise, by:

$$d_0(\epsilon) = \frac{\|\Phi(\epsilon)\|^2}{\sqrt{\Phi^H(\epsilon)\mathbf{R}\Phi(\epsilon)}}, \tag{3.71}$$

where $\mathbf{R}$ is the normalized noise autocovariance matrix. The events whose distance $d_0(\epsilon)$ is minimum are called "first-order" error events. Similarly, events whose distance is the second smallest are called "second-order" error events, and so on [106].

The conditions for which RISI cancellation is satisfying are summarized as follows [106]:

1. Errors affecting the main (Viterbi detector) and the tentative detector must be statically independent.

2. The RISI (described by f_1) must be small enough to guarantee that the main Viterbi detector can make relatively reliable decisions even when the tentative detector makes a decision error, and such that the tentative detector also makes relatively reliable decisions in spite of the ISI.

3. The distance of second-order and higher-order error events that could cause error propagation must be significantly larger than that of first-order error events.

Now that the conditions for effective RISI cancellation are summarized, we will attempt to apply them to FBMC. Hence, the problem is, essentially, how to select the functions f_0 and f_1 such as these conditions are fulfilled. The intrinsic interference in FBMC is seen as a two-dimensional intersymbol interference (2D-ISI). An extension of the works of Agazzi and Seshadri [106] to 2D-ISI channels was treated in [90] assuming that the noise is uncorrelated (which is not the case in FBMC). Hence in general, the target response f_0 may also represent a 2D-ISI channel. Then, a 2D-Viterbi detector is required to match with f_0. Designing a 2D-Viterbi is quite challenging. Therefore, for simplicity reasons, we opted to set the additional constraint that the target response f_0 must be one-dimensional and that f_1 covers the rest of 2D-ISI.

Obviously the receiver complexity depends essentially on the complexity of the Viterbi detector. Therefore, we have to choose a configuration with the least complex Viterbi detector that meets the conditions for effective RISI cancellation. We will select three configurations with different sizes of the target response f_0. According to the second condition, f_0 must contain the largest coefficients ($\Gamma_{\delta k,\delta n}$) in each configuration. Hence, from Table 2.2, the selected target responses are [107]:

$$f_0^{(1)}(a_{k,n}) = a_{k,n}, \tag{3.72}$$

$$f_0^{(2)}(a_{k,n}, a_{k,n-1}) = a_{k,n} + \Gamma_{0,-1} \times a_{k,n-1}, \tag{3.73}$$

and

$$f_0^{(3)}(a_{k,n+1}, a_{k,n}, a_{k,n-1}) = \Gamma_{0,1} a_{k,n+1} + a_{k,n} + \Gamma_{0,-1} a_{k,n-1}. \tag{3.74}$$

The first configuration ($f_0^{(1)}$) corresponds to the whole ISI cancellation which has been studied in the previous section. Since, in FBMC, we have $\sum_{p,q} |\Gamma_{p,q}|^2 = 2$ [108], it is easy to calculate the power of the RISI (represented by f_1) for each configuration.

Regarding the first condition, it is easily satisfied when the tentative detector is different from the main one (Viterbi) [106]. We recall that we consider the case of spatial multiplexing system. Then, we chose the MMSE equalizer as the tentative detector.

The third condition concerns the spectrum distances $d_0(\epsilon)$ defined by (3.71). Hence, for each configuration ($f_0^{(i)}$, $i \in \{1, 2, 3\}$), we compare the non-minimum distances to the minimum one. Then, according to (3.71), we have to determine the matrix $\mathbf{R}$. Since we consider that the target responses are one-dimensional and Viterbi algorithm is performed on each subcarrier "k", the matrix $\mathbf{R}$ is composed only by the coefficients $\Gamma_{0,q}$, $q \in \mathbb{Z}$ (see equations (3.18) and (3.15)) and is given by:

$$\mathbf{R} = \begin{bmatrix} 1 & \Gamma_{0,1} & \Gamma_{0,2} & \cdots \\ \Gamma_{0,-1} & 1 & \Gamma_{0,1} & \cdots \\ \Gamma_{0,-2} & \Gamma_{0,-1} & 1 & \cdots \\ \vdots & \vdots & \vdots & \ddots \end{bmatrix}_{K \times K} \tag{3.75}$$

In Table 3.3, we summarize the values of the first, second, and third order distances obtained by using (3.71), and also the power of the RISI for the three considered configurations. We remark that the difference between the second-order and the first-order distances is almost the same for all the configurations (0.8 ± 0.03), so we consider (as considered in [106]) that the higher-order distances are sufficiently larger than the minimum distance for each configuration. Hence, condition 3) is fulfilled for the three configurations.

Table 3.3: Spectrum distances and RISI power

	First Configuration ($f_0^{(1)}$)	Second Configuration ($f_0^{(2)}$)	Third Configuration ($f_0^{(3)}$)
First-order distance	2	1.8857	1.9189
Second-order distance	$2\sqrt{2}$	2.6668	2.7137
Third-order distance	$2\sqrt{3}$	3.4596	3.2728
Power of the RISI	1	0.6819	0.3638

Now, we have only to determine the configuration(s) for which the second condition is satisfied. Unfortunately, the determination of the RISI power for which the cancellation starts to be effective (or equivalently, error propagation ceases) is not trivial and depends also on the noise variance σ^2 [106]. We will show in the following (by simulations) that only the third configuration ($f_0^{(3)}$) allows to obtain effective RISI cancellation.

As for the receiver complexity, it strongly depends on that of the Viterbi detector. When we consider a spatial multiplexing system with N_t transmit antennas, the Viterbi detector has to compute $q^{i \times N_t}$ branch metrics, where q is the number of all possible symbols $a_{k,n}$ (constellation size) and $i \in \{1, 2, 3\}$ is the number of the taps in $f_0^{(i)}$. In order to reduce the receiver complexity, we can replace the Viterbi detection algorithm by the M-Algorithm [109] which keeps only a fixed number (J) of inner states instead of all the inner states ($q^{(i-1) \times N_t}$). Hence, the M-algorithm has to compute only $J \times q^{N_t}$ branch metrics.

3.4.2 Simulation results

In the following, we provide the simulation results concerning the three configurations treated above. Since the motivation of this work is to address the problem of optimum detection in spatial multiplexing with FBMC, we have considered the simple 2×2 spatial multiplexing scheme. We assume perfect channel knowledge at the receiver side, and the four Rayleigh sub-channels are spatially non-correlated. The complex data symbols are QPSK modulated ($q = 2$). The system performance is assessed in terms of BER as function of SNR and is compared to that of the conventional OFDM with ML detector.

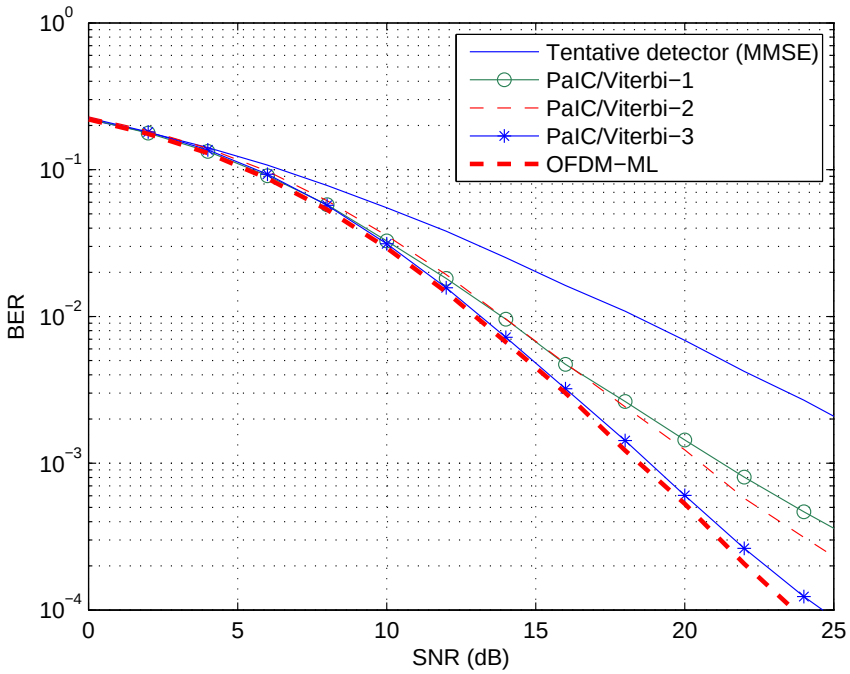

Figure 3.20: Performance of PaIC/Viterbi receivers for 2×2 spatial multiplexing

We call the proposed receivers "PaIC/Viterbi" (for Partial Interference Cancellation with Viterbi detector) followed by an index indicating the considered configuration. Fig. 3.20 depicts the performance of the MMSE equalizer (which is our tentative detector) and of the PaIC/Viterbi for the three considered configurations. We clearly notice that PaIC/Viterbi-3 exhibits almost the same performance as OFDM, and that the RISI cancellation is effective. Hence, the value of the RISI power given in Table 3.3 for the third configuration is sufficiently small so that condition 2) is satisfied. However, a slight degradation of the PaIC/Viterbi-3 performance compared to OFDM is observed beyond 22 dB. Indeed, as we have mentioned at the end of the previous section, the threshold of the RISI power from which the error propagation begins (ineffectiveness of the RISI cancellation) depends on the noise variance σ^2. As shown -for a specific example- in [106], the threshold lowers with the SNR increase. As for the first and second configurations, the performance degradation compared to OFDM begins from about 12 dB. This relatively high degradation is due to the high values of the corresponding RISI powers causing error propagation.

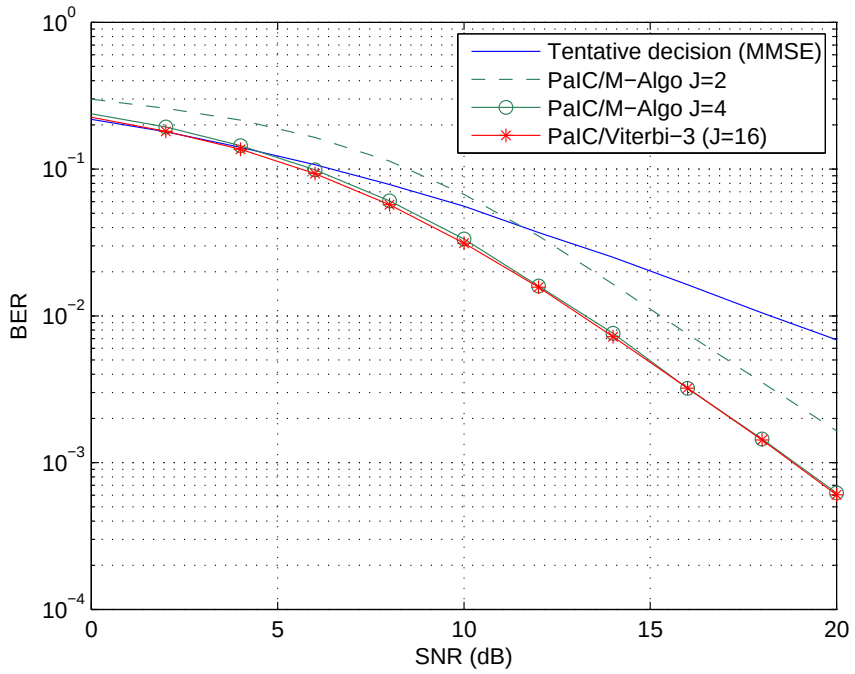

Figure 3.21: Performance of PaIC/M-Algo receiver for 2×2 spatial multiplexing

Now we consider only the third configuration ($f_0^{(3)}$) since the RISI cancellation is effective, and we assess the BER performance when using M-Algorithm instead of the Viterbi one in order to reduce the complexity. In Fig. 3.21, we show the obtained performance of the M-Algorithm with two different values of J ($J = 2$, and $J = 4$). We notice that with $J = 2$ we have an SNR loss of about 2.5 dB compared to PaIC/Viterbi-3. This SNR loss is due to the suboptimality of the M-Algorithm when J is small. Moreover, PaIC/M-Algo with $J = 2$ provides a performance worse than the one provided by the tentative detector (MMSE) as long as the SNR is less than 12 dB. However, with $J = 4$, we can observe that PaIC/M-Algo exhibits almost the same performance as PaIC/Viterbi-3 but with much lower algorithm complexity (4 inner states instead of 16).

To conclude, the intrinsic interference in FBMC is a 2D-ISI in the time-frequency plan. In order to avoid a full 2D-Viterbi detector, a receiver based on ISI cancellation is proposed. However, the ISI cancellation is effective only under some strict conditions. One of these conditions is that the ISI must be sufficiently small. Unfortunately, the intrinsic interference, in FBMC, has the same power as the desired symbol. Hence, we have proposed a trade-off between a whole ISI cancellation (Rec-ML) and a full 2D-Viterbi detection. The proposed receiver is composed by a tentative detector giving decisions which serve to partially cancel the interference, followed by a Viterbi detector matching to the non-canceled ISI. Three configurations were treated. The first one is called PaIC/Viterbi-1 (or Rec-ML) and correspond to the whole ISI cancellation. The second one is PaIC/Viterbi-2, where the Viterbi detector matches with the two largest coefficients of the transmultiplexer impulse response. The third one is PaIC/Viterbi-3 and the Viterbi detector matches with the three largest

coefficients. We have shown, by simulations, that only the PaIC/Viterbi-3 receiver gives the same performance as OFDM. The two other configurations suffer from error propagation because their RISI are not sufficiently small. We have also proposed to replace the Viterbi detector by another based on M-Algorithm in order to reduce the receiver complexity. Indeed, we have shown that using the M-Algorithm with $J = 4$, we obtain exactly the same BER performance as PaIC/Viterbi-3 with much lower complexity.

3.5 Conclusion

We have addressed in this chapter the problem of the ML detection in spatial multiplexing system using FBMC/OQAM modulation. In the first part of this chapter, we proposed different receivers based on interference estimation and cancellation. We have seen that the proposed MMSE-ML receiver which estimates the interference terms using the MMSE equalization provides a slight performance improvement compared to the MMSE performance. An advantage of the MMSE-ML receiver is the fact that the interference is estimated and canceled immediately from the received signals and does not introduce any processing delay in the system. The second proposed receiver is the Rec-ML receiver which makes use of the MMSE-ML as the tentative detector. Then, the whole interference is estimated by using the decided symbols within the neighboring positions in the time-frequency domain around the considered position. The drawback of this receiver is the introduced additional processing delay. A performance improvement is obtained with Rec-ML receiver compared to MMSE-ML one, but there is still a performance gap with respect to the OFDM and Genie-Aided performance. We have also seen that the performance gap with respect to OFDM can be removed when error correcting codes are used.

In the second part of the chapter, we have proposed receivers schemes based on Viterbi algorithm and partial interference cancellation that we have called PaIC-Viterbi receivers. This technique allows to reduce the interference power concerned by the interference cancellation, and thus, it reduces the error propagation effect. We have shown by simulation that when the three largest coefficients of the transmultiplexer response are involved in the Viterbi algorithm, the interference cancellation is effective and PaIC-Viterbi-3 receiver exhibits almost similar BER performance as OFDM-ML.

Chapter 4

Interference cancellation in FBMC/QAM

The transmitted data symbols in conventional FBMC are OQAM (Offset QAM) modulated, and the received data symbols are corrupted by inherent interference terms which complicate the detection in a maximum likelihood (ML) sense in the spatial multiplexing scheme. We have seen in the previous chapter that detection schemes with ISI estimation and cancellation are not always effective due to the error propagation. Therefore, the challenge in ISI estimation and cancellation is mitigating the error propagation through iterations.

We have also seen that in order to counteract the error propagation and make the cancellation scheme effective, the authors in [106] showed that a necessary condition to avoid the error propagation is to hold the interference power under a certain threshold, *i.e.* the interference cancellation technique is effective only when the ISI power is small enough and less than a certain amount. Unfortunately, this threshold is depending on the SNR and it is not trivial to obtain a closed form of the ISI power threshold [106]. Nevertheless, the authors showed -in a specific example- that the threshold lowers with the SNR increase. In other words, removing completely the ISI effects becomes more difficult in high SNR.

On the other hand, the interference in FBMC is inherent, thus it does not depend on the noise variance or SNR. Hence, the ISI power in FBMC is constant whatever the value of SNR. Consequently, the error propagation will appear from a certain amount of SNR (denoted by SNR_0) when the ISI power threshold falls below the inherent interference power. Therefore, the interference cancellation is effective only when the SNR is less than SNR_0 for which the ISI power threshold is equal to the FBMC inherent interference. Fig. 4.1 depicts in qualitative manner the curves of the ISI power threshold and the inherent FBMC interference as function of the SNR. Therefore, if we decrease the inherent FBMC interference, then the value of SNR_0 increases.

In this chapter, we propose to modify the conventional FBMC system by transmitting

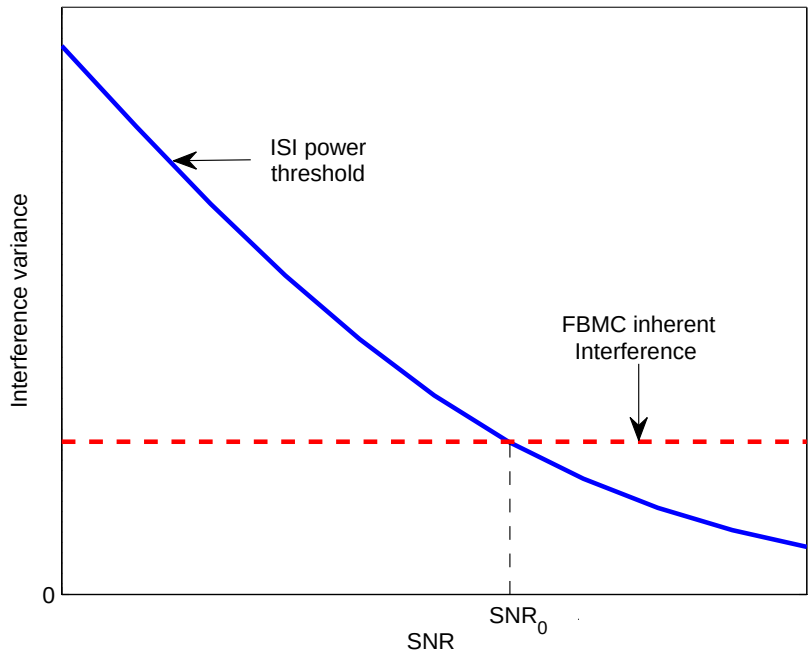

Figure 4.1: Qualitative representation of the curves of the ISI power threshold and the FBMC inherent interference.

QAM data symbols instead of OQAM ones in order to reduce the inherent interference [19]. Then, we apply a receiver based on ISI estimation and cancellation where a simple tentative detector is first used to attempt to cancel the ISI before applying the ML detection. We will show that using QAM modulated symbols instead of OQAM allows us to reduce the inherent interference power and allows -in some cases- our proposed iterative scheme to converge to OFDM performance.

4.1 FBMC/QAM proposal

We propose an FBMC configuration where QAM symbols are transmitted at each one period T instead of transmitting OQAM (real-valued) symbols at each half a period $T/2$. We note that in this proposed scheme the orthogonality condition (2.103) is lost. The expression of the transmitted signal $s[m]$ given in (2.97) becomes

$$s[m] = \sum_{k=0}^{M-1} \sum_{n \in \mathbf{Z}} s_{k,n} g[m - nM] e^{j\frac{2\pi k}{M}(m-\frac{D}{2})} e^{j\phi_{k,2n}}, \tag{4.1}$$

where $s_{k,n}$ are now complex QAM symbols. We note that the phase term $\phi_{k,2n}$ can also be aborted, as we dropped the real orthogonality condition.

The transmultiplexer impulse response of the proposed FBMC/QAM system can be derived from the impulse response given in Table 2.2 or Table 2.1 by decimation by a factor of 2 in time axis. That yields the coefficients depicted in Table 4.1 and Table 4.2 for PHYDYAS and IOTA filter respectively.

Table 4.1: Transmultiplexer impulse response of the FBMC/QAM using PHYDYAS filter

	$n-1$	n	$n+1$
$k-1$	$0.125j$	$0.239j$	$0.125j$
k	0	1	0
$k+1$	$-0.125j$	$-0.239j$	$-0.125j$

Table 4.2: Transmultiplexer impulse response of the FBMC/QAM using IOTA filter

	$n-1$	n	$n+1$
$k-1$	$0.0381j$	$0.4411j$	$0.0381j$
k	0	1	0
$k+1$	$-0.0381j$	$-0.4411j$	$-0.0381j$

When we consider the MIMO spatial multiplexing system, the matrix equation (2.140) becomes in FBMC/QAM as:

$$\underbrace{\begin{bmatrix} r_{k,n}^{(1)} \\ \vdots \\ r_{k,n}^{(N_r)} \end{bmatrix}}_{\mathbf{r}_{k,n}} = \underbrace{\begin{bmatrix} h_{k,n}^{(11)} & \cdots & h_{k,n}^{(1N_t)} \\ \vdots & \ddots & \vdots \\ h_{k,n}^{(N_r1)} & \cdots & h_{k,n}^{(N_rN_t)} \end{bmatrix}}_{\mathbf{H}_{k,n}} \underbrace{\begin{bmatrix} s_{k,n}^{(1)} + I_{k,n}^{(1)} \\ \vdots \\ s_{k,n}^{(N_t)} + I_{k,n}^{(N_t)} \end{bmatrix}}_{\mathbf{s}_{k,n}+\mathbf{I}_{k,n}} + \underbrace{\begin{bmatrix} b_{k,n}^{(1)} \\ \vdots \\ b_{k,n}^{(N_r)} \end{bmatrix}}_{\mathbf{b}_{k,n}}, \tag{4.2}$$

where the entries of the interference vector $\mathbf{I}_{k,n}$ are complex-valued because the transmitted data $s_{k,n}$ are now complex. The expression of $I_{k,n}$ is given by:

$$I_{k,n} = \sum_{(k',n')\in\Omega_{k,n}^{*}} \acute{\Gamma}_{\delta k,\delta n} s_{k',n'}, \tag{4.3}$$

where $\acute{\Gamma}_{k',n'}$ are the coefficients given in Table 4.1 or Table 4.2, $\delta k = k'-k$, and $\delta n = n'-n$.

It is shown in [108] that, in FBMC/OQAM, we have $\sum_{p,q} |\Gamma_{p,q}|^2 = 2$ where $\Gamma_{p,q}$ are the coefficients given in Table 2.2 (or Table 2.1). Hence, the ISI variance in conventional FBMC (FBMC/OQAM) for both prototype filters is

$$\begin{aligned} \acute{\sigma}_{ISI}^2 &= \sum_{(p,q)\neq(0,0)} |\Gamma_{p,q}|^2 \\ &= \sum_{p,q} |\Gamma_{p,q}|^2 - |\Gamma_{0,0}|^2 = 1. \end{aligned} \tag{4.4}$$

Therefore, in FBMC/OQAM, the power of ISI has the same value as the transmitted data variance. Whereas, the ISI variance in the proposed FBMC/QAM system, using PHYDYAS filter, is given by

$$\begin{aligned} \sigma_{ISI}^2 &= \sum_{(p,q)\neq(0,0)} |\Gamma_{p,2q}|^2 \\ &= \sum_{p,q} |\Gamma_{p,2q}|^2 - 1 = 0.1771. \end{aligned} \tag{4.5}$$

Hence, thanks to the proposed scheme we have reduced the ISI power to 17.7%. If the IOTA filter is used, we can show that the inherent interference variance in FBMC/QAM is $\sigma_{ISI}^2 = 0.3956$. We remark that the variance of the interference when using IOTA filter is more than twice the interference variance when using PHYDYAS filter. Therefore, it is natural to expect smaller values of SNR_0 in the case of IOTA compared to the PHYDYAS case. Consequently, the error propagation effect begins to occur in the IOTA case before it appears in the case where PHYDYAS filter is used.

4.2 Iterative interference cancelation in FBMC/QAM

In FBMC/QAM case, we opted to use MMSE equalizer as the tentative detector, and the main detector is a simple ML one. Hence, MMSE equalizer provides tentative estimations of the data vectors $\mathbf{s}_{k,n}$. Then, basing on these tentative estimates, the interference canceler calculates an estimation of the the whole interference vector that should be removed from the received vector $\mathbf{r}_{k,n}$. It is worth pointing out that the performance of MMSE equalizer in the case of FBMC/QAM is significantly depending on the interference variance because both useful and interference signals ($s_{k,n}$ and $I_{k,n}$) are complex-valued. We nominate this receiver by IIC-ML (Iterative Interference Cancelation). Fig. 4.2 depicts the principal blocks of the proposed IIC-ML receiver.

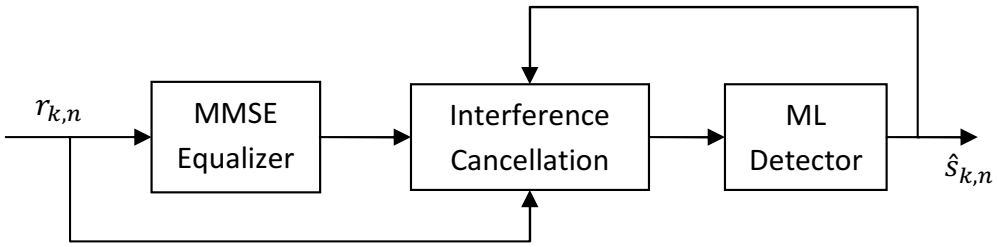

Figure 4.2: Block scheme of the IIC-ML receiver

In the following, we provide simulation results of the proposed FBMC/QAM scheme compared to OFDM and also to FBMC/OQAM. The number of subcarriers is set to $M = 512$. According to the IEEE 802.16e standard [104], the CP duration for OFDM is set to $\Delta = \frac{M}{8} = 64$. We assume perfect channel knowledge at the receiver side, and we use the Veh-A channel model [97] to generate the channels. The complex data symbols are QPSK modulated for OFDM and the proposed FBMC/QAM. However, since the conventional FBMC uses OQAM modulation, each transmitted symbol, on each $T/2$, is 2-PAM modulated. The system performance is assessed in terms of BER as function of the SNR. For FBMC/OQAM and FBMC/QAM, we define the SNR as

$$SNR = \frac{N_t \sigma_s^2}{\sigma^2},$$

where σ_s^2 is the signal variance on each transmit antenna, and σ^2 is the noise variance on each receive antenna. However, for OFDM, the expression of the SNR is defined so that it

takes into account the SNR loss due to the CP:

$$SNR = \frac{M + \Delta}{M} \frac{N_t \sigma_s^2}{\sigma^2}.$$

Before considering MIMO systems, we will first test the proposed receiver in the SISO case. The tentative detector in this case is the simple one tap ZF equalizer. Since ZF and ML have the same BER performance, it is also worth replacing the ML detector by the linear ZF equalizer. In Fig. 4.3 we present the BER performance of the IIC receiver with IOTA filter for different numbers of iterations. For comparison we also depict the performance of ZF and the Genie-Aided one. The "Genie-Aided" performance is defined as the performance obtained by assuming a perfect interference estimation, *i.e* the exact transmitted symbols are involved to estimate the interference. According to the simulation results presented in the figure, the performance of IIC receivers with 3, 4 and 5 iterations provide the same BER performance. Hence, the IIC performance converges from the third iteration, but the interference is not successfully removed. We notice that the IIC receiver does not reach the Genie-Aided performance; we can observe an SNR gap of about 5 dB at $BER = 10^{-2}$. Therefore, we conclude that the interference cancellation is not effective in SISO-FBMC/QAM using IOTA filter, and the proposed IIC receiver suffers considerably from the error propagation. This is explained by the relatively high interference variance $\sigma^2_{ISI} = 0.3956$ in IOTA case.

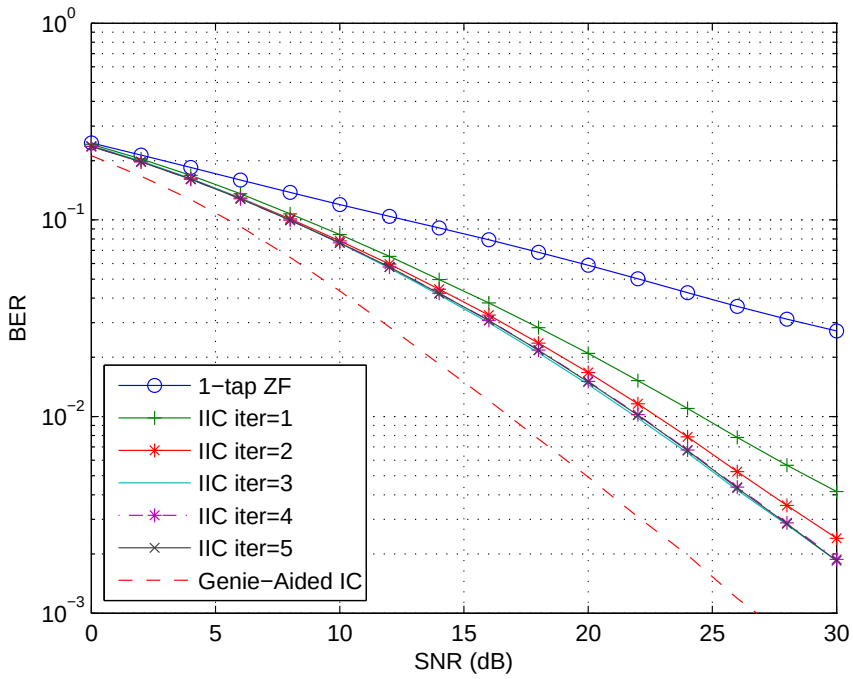

Figure 4.3: Performance of IC receiver with FBMC/QAM system using IOTA filter in SISO system

Fig. 4.4 concerns the case where PHYDYAS filter is used. In this case, we notice that the performance of IIC receiver converges at the second iteration since IIC receivers with

2 and 3 iterations exhibit the same BER performance. Moreover, we remark that with one iteration we obtain almost the same performance as obtained with 2 or 3 iterations. That means that we can be satisfied with only one iteration in order to limit the computational complexity. Further, we notice that the SNR gap between the IIC performance and the Genie-Aided one is small enough. We observe an SNR gap of about 0.5 dB in the whole considered SNR region. It is also worth pointing out the impact of the prototype filter choice on the BER performance of the ZF equalizer in FBMC/QAM; according to fig. 4.3 and Fig. 4.4 we remark that the ZF performance with IOTA filter is worse than the one obtained with PHYDYAS. This is due to the difference of in interference variance values for each case (namely $\sigma^2_{ISI} \approx 0.18$ for PHYDYAS, $\sigma^2_{ISI} \approx 0.40$ for IOTA).

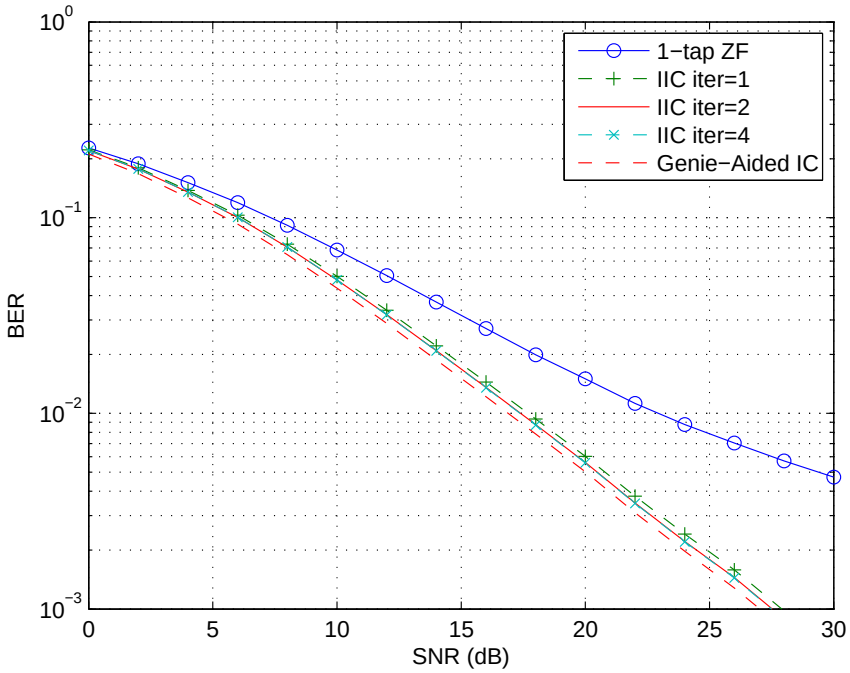

Figure 4.4: Performance of IC receiver in FBMC/QAM system using PHYDYAS filter in SISO system

Regarding MIMO, we have considered the 2×2 spatial multiplexing scheme. The Rayleigh spatial sub-channels are spatially non-correlated. Fig. 4.5 depicts the obtained BER performance of the proposed FBMC/QAM using PHYDYAS filter with MMSE equalizer, which is now our tentative detector. We also show in this figure the performance obtained using IIC-ML for different values of iterations and compare them to the optimum performance obtained with the Genie-Aided. We notice that increasing the number of iterations of IIC-ML improves the BER performance and almost converges to the optimum one after 5 iterations, *i.e.* there is practically no improvement beyond 5 iterations. Hence, IIC-ML receiver performs correctly with 5 iterations. However, as in the SISO case, we observe a slight SNR loss less than 0.5 dB compared to the Genie-Aided performance.

In Fig. 4.6 we compare the performance of IIC-ML in FBMC/QAM with the Rec-ML one in FBMC/OQAM using -for both of them- the PHYDYAS filter. We also show the

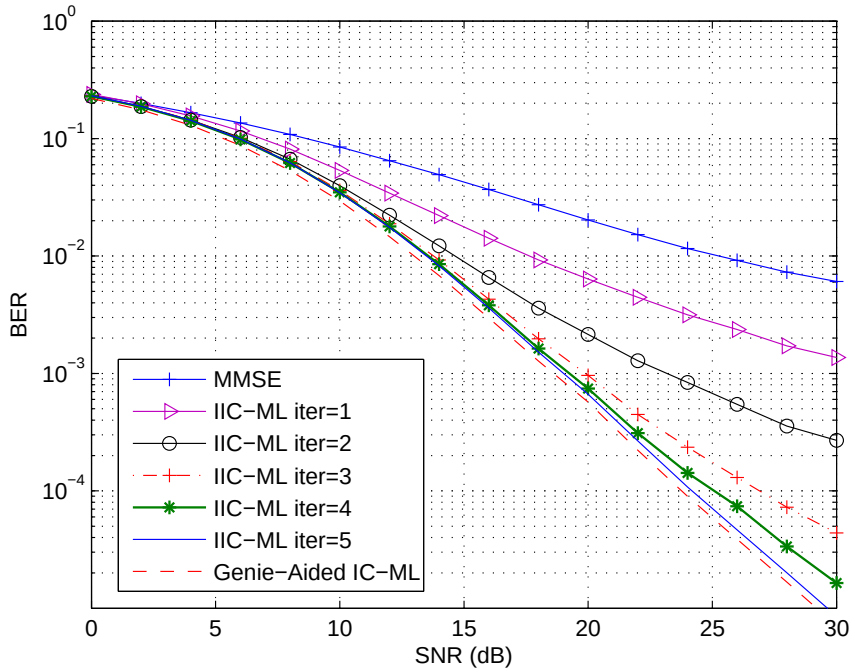

Figure 4.5: Performance of IIC-ML receiver in FBMC/QAM system using PHYDYAS filter for 2×2 spatial multiplexing

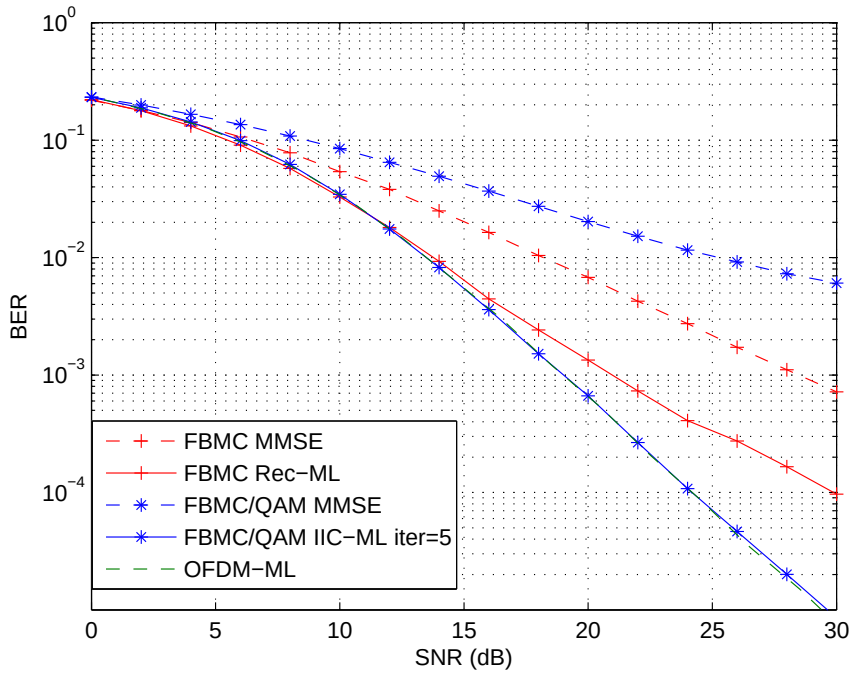

Figure 4.6: Performance comparison between Rec-ML in FBMC/OQAM and IIC-ML in FBMC/QAM using PHYDYAS filter in 2×2 SM

BER performance of the OFDM using ML detector. For FBMC/QAM, we present only the performance of the MMSE equalizer (tentative detector) and the performance of the IIC-ML after 5 iterations. As for classical FBMC, we show the performance of MMSE and the performance of Rec-ML. First of all, one can notice that MMSE equalizer for FBMC/QAM exhibits worse BER performance compared to FBMC/OQAM. This is explained by the fact that the inherent ISI term in FBMC/QAM is complex as the transmitted data symbols, whereas in FBMC the interference terms are pure imaginary and the data symbols are real-valued (real orthogonality). However, the situation is different with IIC-ML and Rec-ML receivers, we clearly notice that Rec-ML with conventional FBMC suffers from the error propagation effect and the BER performance converges to a suboptimal one, whereas the ISI cancellation is effective with IIC-ML in FBMC/QAM system, where we obtain almost the same performance as OFDM-ML.

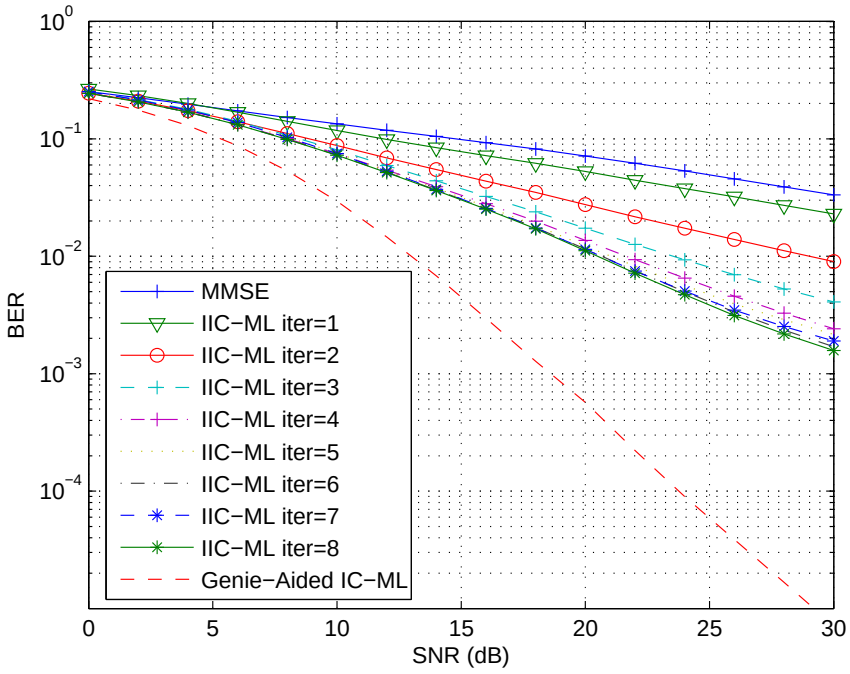

Figure 4.7: Performance of IIC-ML receiver with FBMC/QAM system using IOTA filter for 2×2 spatial multiplexing

When IOTA filter is used, we notice in Fig 4.7 that the BER performance of the IIC-ML receiver does not converge to the optimum performance. That is, the interference cancellation is not effective and the receiver suffers from error propagations. This is due to the high value of the interference variance which is equal to $\sigma^2_{ISI} = 0.3956$. We observe that the IIC-ML performance converges starting from the fifth iteration. IIC-ML receivers with 5 to 8 iterations exhibit the same BER performance. We can note an SNR loss for the IIC-ML performance with respect to the optimum one of about 7 dB at $BER = 10^{-2}$. Therefore, the proposed IIC-ML receiver can not be performed in FBMC/QAM using IOTA prototype filter.

4.3 PaIC/Viterbi receivers in FBMC/QAM

Regarding PaIC/Viterbi receivers, only a part of the interference is concerned by the cancellation and the main detector uses the Viterbi algorithm. The main principle of the receiver remains the same as for conventional FBMC presented in Section 3.4. However, the configuration of the PaIC/Viterbi receiver has to be adapted to the new FBMC/QAM context. Indeed, we have seen that the function f_0 that matches the Viterbi detector must contain the largest coefficients $\acute{\Gamma}_{p,q}$. According to the transmultiplexer impulse responses depicted in Table 4.1 and Table 4.2, the three largest coefficients ($\{1, \pm 0.239j\}$ for PHYDYAS, and $\{1, \pm 0.4411j\}$ for IOTA) in each table are aligned with the direction of the frequency axis. Therefore, we can select the following three functions $f_0^{(i)}$, $i = 1, 2, 3$ that determine the Viterbi target responses:

$$f_0^{(1)}(s_{k,n}) = s_{k,n}, \tag{4.6}$$

$$f_0^{(2)}(s_{k,n}, s_{k-1,n}) = s_{k-1,n} + \acute{\Gamma}_{-1,0} \times s_{k,n-1}, \tag{4.7}$$

and

$$f_0^{(3)}(s_{k+1,n}, s_{k,n}, s_{k-1,n}) = \acute{\Gamma}_{1,0} s_{k+1,n} + s_{k,n} + \acute{\Gamma}_{-1,0} s_{k-1,n}, \tag{4.8}$$

where $f_0^{(1)}$ obviously corresponds to the IIC-ML receiver where the whole interference cancellation is performed. Hence, the advantage for PaIC/Viterbi receivers in FBMC/QAM lies in the fact that the Viterbi algorithms are performed in the frequency axis direction. Whereas in FBMC/OQAM they are performed in the time axis direction. Consequently, from an implementation point of view, the PaIC/Viterbi receivers are less complicated for implementation in FBMC/QAM than in the conventional FBMC, because only one Viterbi algorithm has to be performed for each one received multicarrier symbol, whereas in FBMC/OQAM we need to perform a Viterbi detector simultaneously for each subcarrier.

We have seen in section 3.4 that the performance of PaIC/Viterbi receivers depend on the power of the residual ISI which is concerned by the interference cancellation, and also depend on the values of the spectrum distances $d_0(\epsilon)$ given by (3.71). To calculate the values of $d_0(\epsilon)$, we need first to determine the normalized autocovariance matrix of the noise $\mathbf{R}$. Since the Viterbi algorithm is performed in the direction of the frequency axis, the matrix $\mathbf{R}$ is given this time by:

$$\mathbf{R} = \begin{bmatrix} 1 & \acute{\Gamma}_{1,0} & \acute{\Gamma}_{2,0} & \cdots & \acute{\Gamma}_{M-1,0} \\ \acute{\Gamma}_{-1,0} & 1 & \acute{\Gamma}_{1,0} & \cdots & \acute{\Gamma}_{M-2,0} \\ \acute{\Gamma}_{-2,0} & \acute{\Gamma}_{-1,0} & 1 & \cdots & \acute{\Gamma}_{M-3,0} \\ \vdots & \vdots & \vdots & \ddots & \vdots \\ \acute{\Gamma}_{1-M,0} & \acute{\Gamma}_{2-M,0} & \acute{\Gamma}_{3-M,0} & \cdots & 1 \end{bmatrix}_{M \times M} \tag{4.9}$$

where M is the number of subcarrier. Then, the values of $d_0(\epsilon)$ can be calculated for each single error event ϵ and for each one of the chosen receiver configurations (according to $f_0^{(i)}$, $i = 1, 2, 3$). We remind that the error events are classified according to their spectrum distance $d_0(\epsilon)$. The error events corresponding to the smallest $d_0(\epsilon)$ are called first-order error events, and those corresponding to the second smallest $d_0(\epsilon)$ are called second-order error events. Let us denote by ϵ_1 and ϵ_2 the first and second order error events, respectively.

We also define $w(\epsilon)$ as the number of error positions in the error event ϵ. Table 4.3 and Table 4.4 give the different values of $d_0(\epsilon)$ of the first and second order error events for each receiver configuration, respectively for PHYDYAS and IOTA filter. We also show in the tables the corresponding power of the residual interference (σ^2_{RISI}) and the number of error positions ($w(\epsilon)$) within the first and second error events.

Table 4.3: Spectrum distances and RISI power using PHYDYAS filter

	First Configuration ($f_0^{(1)}$)	Second Configuration ($f_0^{(2)}$)	Third Configuration ($f_0^{(3)}$)
First-order distance	2	1.9534	1.9231
Second-order distance	2.5407	2.6974	2.3526
$w(\epsilon_1)$	1	1	1
$w(\epsilon_2)$	2	2	2
Power of the RISI	0.1771	0.1198	0.0626

Table 4.4: Spectrum distances and RISI power using IOTA filter

	First Configuration ($f_0^{(1)}$)	Second Configuration ($f_0^{(2)}$)	Third Configuration ($f_0^{(3)}$)
First-order distance	2	1.8985	1.7833
Second-order distance	2.3561	2.5395	1.7892
$w(\epsilon_1)$	1	1	3
$w(\epsilon_2)$	2	2	4
Power of the RISI	0.3956	0.2010	0.0065

First, we notice that, in the third configuration using IOTA filter, the values of the two smallest distances are practically the same. Moreover, the first and second order error events contain respectively 3 and 4 error positions ($w(\epsilon_1) = 3$ and $w(\epsilon_2) = 4$), whereas in the other cases they only contain 1 and 2 errors respectively. Consequently, even if the residual interference is perfectly removed, the BER performance would be poor because the most likely error events are those that contain 3 or 4 errors. We can observe in Fig. 4.8 that PaIC/Viterbi-3 receiver with IOTA filter suffers from an SNR loss of about 1.2 dB with respect to OFDM-ML. This SNR loss is due to the errors caused by the Viterbi algorithm it-self. The effect of erroneous tentative decisions are practically negligible because the variance of the residual interference is very small ($\sigma^2_{RISI} \approx 0.007$). This is why the BER performance of PaIC/Viterbi-3 converges almost from the first iteration. In fact, in this situation the tentative detector (MMSE equalizer) is not useful and can be withdrawn.

In the case where PHYDYAS filter is used, we notice, in Fig. 4.9, that the PaIC/Viterbi-3 performance rapidly converges to the OFDM performance. Only two iterations are needed to reach acceptable BER-performance. This is true because the conditions of effective interference cancellation are fulfilled, namely the RISI power is sufficiently small, and the first-order error events are separated enough from the other error events by their spectrum distance.

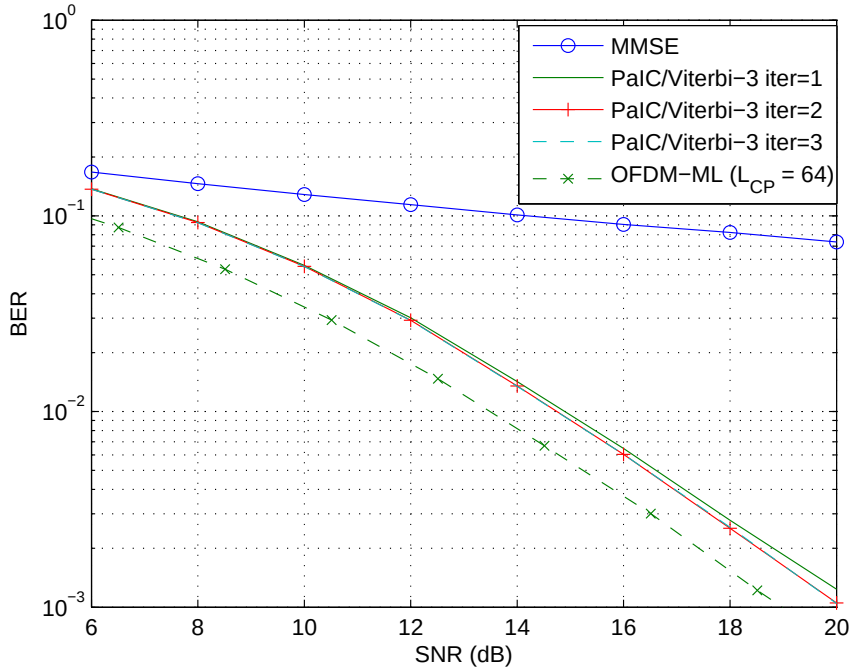

Figure 4.8: BER performance of the PaIC/Viterbi-3 receiver using FBMC/QAM modulation and IOTA filter.

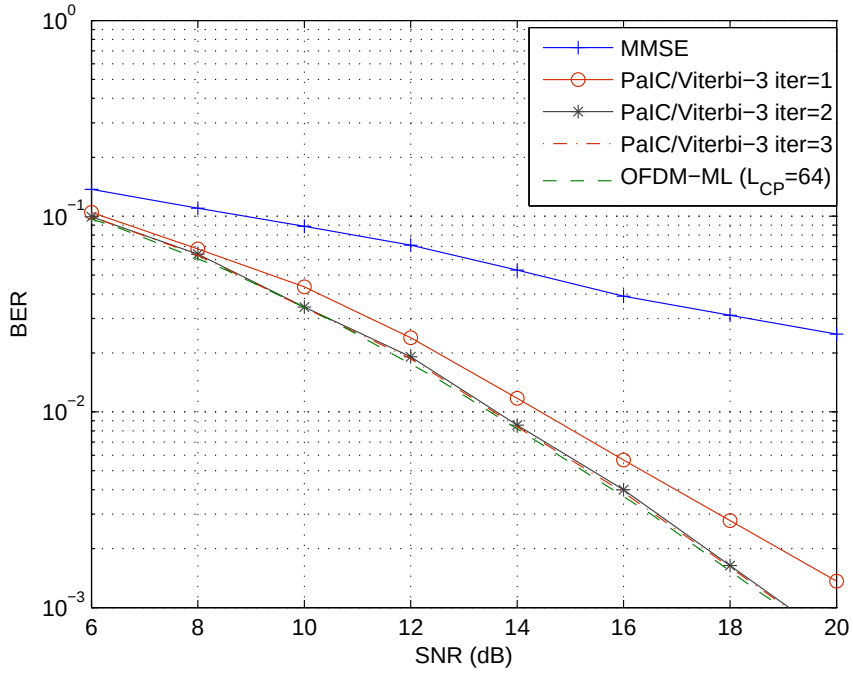

Figure 4.9: BER performance of the PaIC/Viterbi-3 receiver using FBMC/QAM modulation and PHYDYAS filter.

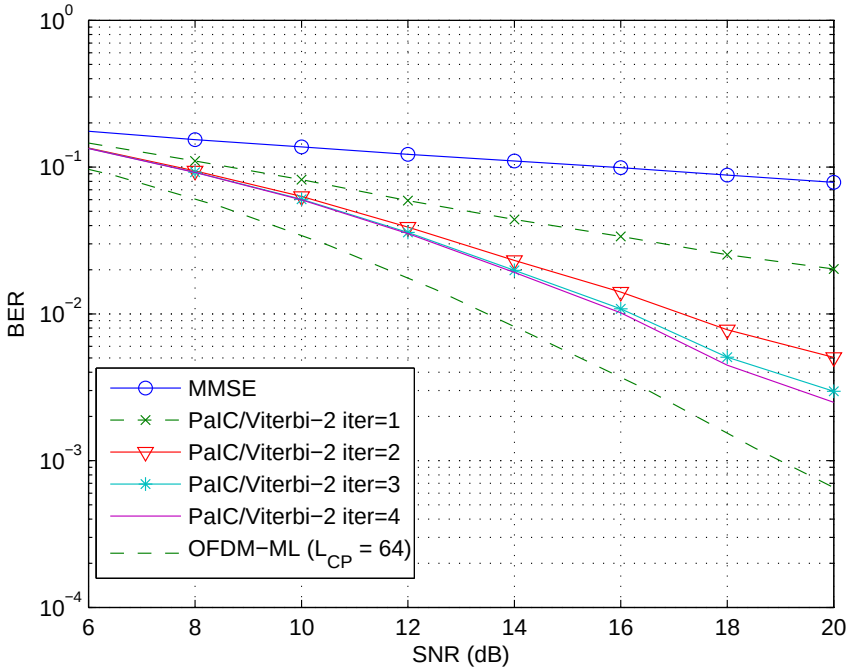

Figure 4.10: BER performance of the PaIC/Viterbi-2 receiver using FBMC/QAM modulation and IOTA filter.

As for the PaIC/Viterbi-2 receiver, we can notice in Fig. 4.10 that with IOTA filter the BER performance does not reach the OFDM one. After 4 iterations we obtain an SNR loss with respect to OFDM of about 2.25 dB at $BER = 10^{-2}$. Hence, PaIC/Viterbi-2 with IOTA filter suffers from error propagation and the interference cancellation is not effective. This performance limitation is explained by the fact that the residual interference variance is not sufficiently small; according to Table 4.4 we have $\sigma^2_{RISI} \approx 0.2$. While in the case where PHYDYAS filter is used, the variance of the residual interference is smaller as shown in Table 4.3; we have $\sigma^2_{RISI} \approx 0.12$. According to the simulation results presented in Fig. 4.11 where PaIC/Viterbi-2 with PHYDYAS filter is considered, the RISI power is small enough that the interference is almost completely removed. We can consider that with 3 iterations, we obtain acceptable BER-performance. We can also observe the effect of the RISI by comparing the BER-performance of the MMSE equalizer in both cases where PHYDYAS or IOTA filter is used. We notice in Fig. 4.10 that the MMSE equalizer reaches the BER value of 10^{-1} at $SNR = 15.5\ dB$, whereas in Fig. 4.11 we have $BER = 10^{-1}$ at $SNR = 9.5\ dB$. This is due to the fact that the BER floor in the IOTA case is much higher than the BER floor in the case where PHYDYAS filter is used.

4.4 Conclusion

In this chapter, we have proposed a modification in the FBMC modulator/demodulator in order to reduce the variance of the intrinsic interference. Indeed, we opted to transmit QAM (complex-valued) symbols on each single period (FBMC/QAM) instead of transmit-

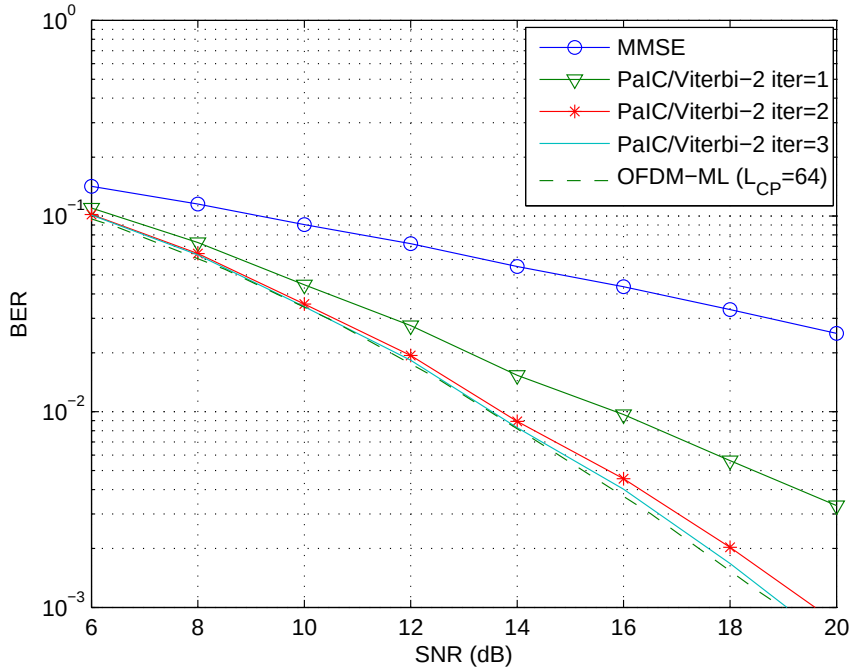

Figure 4.11: BER performance of the PaIC/Viterbi-2 receiver using FBMC/QAM modulation and PHYDYAS filter.

ting OQAM (real-valued) symbols on each half period. Thus, the inherent interference is reduced, but the real orthogonality condition is no longer satisfied. Therefore, an interference cancellation procedure is still required. we have seen that the ISI cancellation is effective only under some strict conditions. One of them is that the ISI power must be sufficiently small and less than a certain threshold. Thanks to the proposed FBMC/QAM, the intrinsic interference power is reduced to 18% when PHYDYAS filter is used, and to 40% when IOTA filter is considered. We have shown by simulations that the performance of the IIC-ML receiver using PHYDYAS filter converges to within $0.5dB$ to the "Genie-Aided" performance after 5 iterations. However, when using IOTA filter, the interference cancellation is not effective due to the relatively high interference variance ($\sigma^2_{ISI} = 0.3956$), and IIC-ML performance is far from the optimum. We obtain an SNR loss of about 7 dB at $BER = 10^{-2}$ in a 2×2 SM system. We have also analyzed and tested PaIC/Viterbi receivers in FBMC/QAM. We pointed out the advantage of performing the PaIC/Viterbi in FBMC/QAM compared to its application in FBMC/OQAM. Indeed, from an implementation complexity point of view, performing the Viterbi algorithm over the frequency axis is less complicated than over the time axis. As for the BER performance, simulation results showed that poor performance is obtained when IOTA filter is used, whereas with PHYDYAS filter the interference cancellation is effective and the BER-performance practically reaches the same OFDM performance.

Chapter 5

A novel filter-bank multicarrier proposal

We have seen that when combining FBMC with MIMO techniques such as STBC or SM-MLD, the presence of the interference term $u_{k,n}$ (which can be seen as a 2D-ISI) causes problems and makes the detection process from $r_{k,n}$ very hard if not impossible. In this chapter, we shall propose a new FBMC scheme and transmission strategy in order to get rid of the inherent interference term. This proposed scheme (called FFT-FBMC [110, 111]) transforms the FBMC system into an equivalent system formulated as OFDM regardless of some residual interference. Thus, any OFDM transmission technique can straightforwardly be performed to the proposed FBMC scheme with a corresponding complexity growth compared to the classical FBMC. First, we will develop the FFT-FBMC in the case of single-input single-output (SISO) configuration. Then, we extend its application to SM-MIMO configuration with MLD and Alamouti coding scheme. Simulation results show that FFT-FBMC can almost reach the OFDM performance, but it remains slightly outperformed by OFDM.

5.1 The proposed FFT-FBMC scheme

5.1.1 System model

The transmultiplexer impulse response is derived from the received signal assuming null data except at one time-frequency position (k_0, n_0) where a unit impulse is applied. Then,

we have:

$$r_{k',n'} = \sum_{m=-\infty}^{+\infty} g_{k_0,n_0}[m] g^*_{k',n'}[m]$$
$$= \sum_{m=-\infty}^{+\infty} g[m] g[m - \Delta n M/2] e^{j\frac{2\pi}{M}\Delta k(\frac{D}{2}-m)} \times e^{j\pi(\Delta k + k_0)\Delta n} e^{-j\frac{\pi}{2}(\Delta k + \Delta n)}, \quad (5.1)$$

where $\Delta n = n' - n_0$ and $\Delta k = k' - k_0$. We notice that the impulse response of the transmultiplexer depends on k_0. Indeed, the sign of some impulse response coefficients depends on the parity of k_0. In this chapter, we essentially exploit this property.

Let us denote the transmultiplexer impulse response obtained in equation (5.1) by $f^{(k_0)}_{\Delta k}(\Delta n)$. The prototype filters are designed in a way that they provide a well-localized spectrum and spread over only a few adjacent subcarriers. The most important interference comes form the same considered subcarrier and immediate neighboring ones. Without loss of generality and for the sake of simplicity, we consider only the interference coming from adjacent subcarriers. Hence, we can split (5.1) into three terms and write

$$r_{k,n} \cong \underbrace{\sum_{i=-\Delta}^{\Delta} f_0^{(k)}(i) a_{k,n-i}}_{t_k} + \underbrace{\sum_{i=-\Delta}^{\Delta} f_1^{(k-1)}(i) a_{k-1,n-i}}_{t_{k-1}}$$
$$+ \underbrace{\sum_{i=-\Delta}^{\Delta} f_{-1}^{(k+1)}(i) a_{k+1,n-i}}_{t_{k+1}}, \quad (5.2)$$

where $a_{k,n}$ are the inputs of the FBMC modulator on the kth subcarrier and the nth time instant, $f_j^{(k)}(i)$ are the coefficients of the transmultiplexer impulse response when the impulse is applied on the kth subcarrier, $\Delta = 2K - 1$ is the one side maximum response spread in time domain. Hence, $i \notin [-\Delta, \Delta] \Rightarrow f_j^{(k)}(i) = 0$.

Now, we consider each term t_i in (5.2) as a point-to-point multipath channel. So, as in conventional OFDM, we can overcome ISI by performing an IDFT on blocks of length $N \geq 2\Delta$ at the transmitter side, and inserting a CP of sufficient length $L \geq 2\Delta$. That is, $a_{k,n'}$ is now considered as the IDFT outputs. The data symbols applied to IDFT input are denoted by $d_{k,n}$. Therefore, unlike in the conventional FBMC, the symbols $a_{k,n'}$, which are the FBMC inputs, are no longer real since they are the IDFT output samples. At the receiver side, the first L samples of each symbol block are discarded. Taking the DFT of the remaining block, one can write

$$Y_{k,n} \cong \underbrace{F_{0,n}^{(k)} d_{k,n}}_{T_k} + \underbrace{F_{1,n}^{(k-1)} d_{k-1,n}}_{T_{k-1}} + \underbrace{F_{-1,n}^{(k+1)} d_{k+1,n}}_{T_{k+1}}. \quad (5.3)$$

where

$$Y_{k,n} = \frac{1}{\sqrt{N}} \sum_{n'=0}^{N-1} r_{k,n'} e^{\frac{-j2\pi n n'}{N}},$$
$$d_{k,n} = \frac{1}{\sqrt{N}} \sum_{n'=0}^{N-1} a_{k,n'} e^{\frac{-j2\pi n n'}{N}},$$

and

$$F_{j,n}^{(k)} = \sum_{n'=-\frac{N}{2}}^{\frac{N}{2}-1} f_j^{(k)}(n') e^{\frac{-j2\pi nn'}{N}}.$$

The sum for F is going from $-N/2$ to $N/2-1$ because, according to (5.2), the function $f_j^{(k)}(i)$ is considered as an acausal FIR filter. Indeed, if we consider, for example, only the first term t_k of (5.2), we have $Y_{k,n} = \frac{1}{\sqrt{N}} \sum_{n'=0}^{N-1} r_{k,n'} e^{-j\frac{2\pi nn'}{N}}$, where $r_{k,n'} = \sum_{i=-\Delta}^{\Delta} f_0^{(k)}(i) a_{k,n'-i}$. Hence,

$$Y_{k,n} = \frac{1}{\sqrt{N}} \sum_{i=-\Delta}^{\Delta} f_0^{(k)}(i) \sum_{n'=0}^{N-1} a_{k,n'-i} e^{-j\frac{2\pi nn'}{N}}. \tag{5.4}$$

Since $a_{k,n}$ are the IDFT outputs of $d_{k,n}$, we have $a_{k,n} = \frac{1}{\sqrt{N}} \sum_{n''=0}^{N-1} d_{k,n''} e^{j\frac{2\pi nn''}{N}}$. Therefore, we can write

$$\begin{aligned} Y_{k,n} &= \frac{1}{N} \sum_{i=-\Delta}^{\Delta} f_0^{(k)}(i) \sum_{n'=0}^{N-1} \sum_{n''=0}^{N-1} d_{k,n''} e^{j\frac{2\pi(n'-i)n''}{N}} e^{-j\frac{2\pi nn'}{N}} \\ &= \frac{1}{N} \sum_{i=-\Delta}^{\Delta} f_0^{(k)}(i) \sum_{n''=0}^{N-1} d_{k,n''} e^{-j\frac{2\pi in''}{N}} \sum_{n'=0}^{N-1} e^{j\frac{2\pi(n''-n)n'}{N}}. \end{aligned} \tag{5.5}$$

We have $\sum_{n'=0}^{N-1} e^{j\frac{2\pi(n''-n)n'}{N}} = N\delta_{n,n''}$. Then,

$$Y_{k,n} = \underbrace{\sum_{i=-\Delta}^{\Delta} f_0^{(k)}(i) e^{-j\frac{2\pi in}{N}}}_{=F_{0,n}^{(k)}} d_{k,n}. \tag{5.6}$$

Since $\frac{N}{2} > \Delta$ and $f_0^{(k)}(i) = 0$ for $i \notin [-\Delta, \Delta]$, then we can finally write:

$$F_{0,n}^{(k)} = \sum_{i=-\frac{N}{2}}^{\frac{N}{2}-1} f_0^{(k)}(i) e^{-j\frac{2\pi in}{N}}. \tag{5.7}$$

Fig. 5.1 depicts the proposed FFT-FBMC scheme. After applying the IDFT and DFT on each subcarrier, respectively, at the transmitter and receiver sides, the interference coming from the same considered subcarrier is transformed (assuming that the CP length L is sufficiently large) into a single coefficient $F_{0,n}^{(k)}$ which is multiplied by the data symbol $d_{k,n}$. Also, the interference coming from both adjacent subcarriers is transformed into two coefficients $F_{1,n}^{(k-1)}$ and $F_{-1,n}^{(k+1)}$ which are, respectively, multiplied by $d_{k-1,n}$ and $d_{k+1,n}$. Hence, the 2-D intersymbol interference in the time-frequency domain is transformed into a 1-D intercarrier interference. That is, the data symbol $d_{k,n}$ interferes only with $d_{k-1,n}$ and $d_{k+1,n}$ (see equation (5.3)).

5.1.2 Transmission strategy

Nevertheless, there is still intercarrier interference. Further, each received data symbol $d_{k,n}$ is multiplied by a coefficient $F_{0,n}^{(k)}$ which deserves to be analyzed. According to (5.1), we

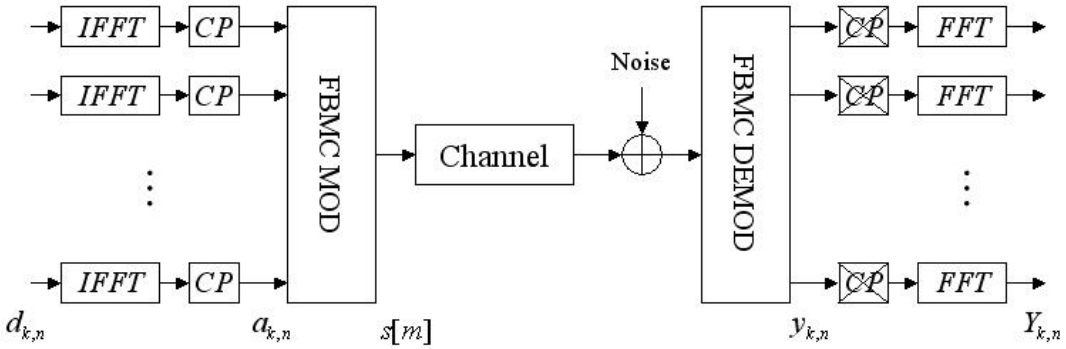

Figure 5.1: The proposed FFT-FBMC scheme.

have

$$f_0^{(k)}(\Delta n) = \sum_{m=-\infty}^{+\infty} g[m]g[m - \Delta nM/2]e^{-j\frac{\pi}{2}\Delta n}e^{j\pi k\Delta n}. \tag{5.8}$$

As a consequence of the orthogonality condition (equation (2.103)), the coefficients $f_0^{(k)}(\Delta n)$ are zeros when Δn is a nonzero even integer. Moreover, one can notice from (5.8) that $f_0^{(k)}(-\Delta n) = f_0^{(k)}(\Delta n)^*$. Hence, we can easily show that $F_{0,n}^{(k)}$ can be written, for $n = 0, ..., N-1$, as

$$F_{0,n}^{(k)} = 1 - 2j \sum_{n'=0}^{\frac{N}{4}-1} f_0^{(k)}(2n'+1) \sin\left(\frac{2\pi n}{N}(2n'+1)\right). \tag{5.9}$$

Therefore, we can derive that

$$F_{0,n}^{(k)} - 1 = 1 - F_{0,|n+N/2|_N}^{(k)}, \quad n = 0, ..., N-1, \tag{5.10}$$

where $|.|_N$ stands for modulo operation by N. That is, one half of the symbols in each subcarrier are amplified (when $|F_{0,n}^{(k)}| > 1$), but the rest are deeply faded (when $|F_{0,n}^{(k)}| < 1$); and this yields a severe performance degradation. The solution that we propose is to transmit no data on the faded positions and double the modulation order, by transmitting complex symbols instead of real ones, on the remaining positions to keep the same throughput.

As aforementioned, $f_0^{(k)}(\Delta n)$ depends on the parity of the subcarrier index k. Let us consider two adjacent subcarriers k and $k+1$, we have

$$\begin{aligned} f_0^{(k+1)}(\Delta n) &= \sum_m g[m]g[m - \Delta nM/2]e^{-j\frac{\pi}{2}\Delta n}e^{j\pi k\Delta n}e^{j\pi\Delta n} \\ &= f_0^{(k)}(\Delta n)e^{j\pi\Delta n}. \end{aligned} \tag{5.11}$$

Taking the DFT of both members of this equation, we find that

$$F_{0,n}^{(k+1)} = F_{0,|n+N/2|_N}^{(k)}.$$

Therefore, $F_{0,n}^{(k+1)}$ is the circularly shifted version of $F_{0,n}^{(k)}$ by $\frac{N}{2}$ samples. Substituting the latter into (5.10), we obtain

$$F_{0,n}^{(k)} - 1 = 1 - F_{0,n}^{(k+1)}.$$

Hence, $F_{0,n}^{(k+1)}$ is also the reflection of $F_{0,n}^{(k)}$ in the horizontal axis $F_{0,n}^{(k)} = 1$. This means that when $|F_{0,n}^{(k)}| > 1$, we have $|F_{0,n}^{(k+1)}| < 1$ and $|F_{0,n}^{(k-1)}| < 1$. Fig. 5.2 depicts the curve of $F_{0,n}^{(k)}$ in both cases of even and odd values of k, where the block length is set to $N = 32$, and the used prototype filter is the PHYDYAS filter.

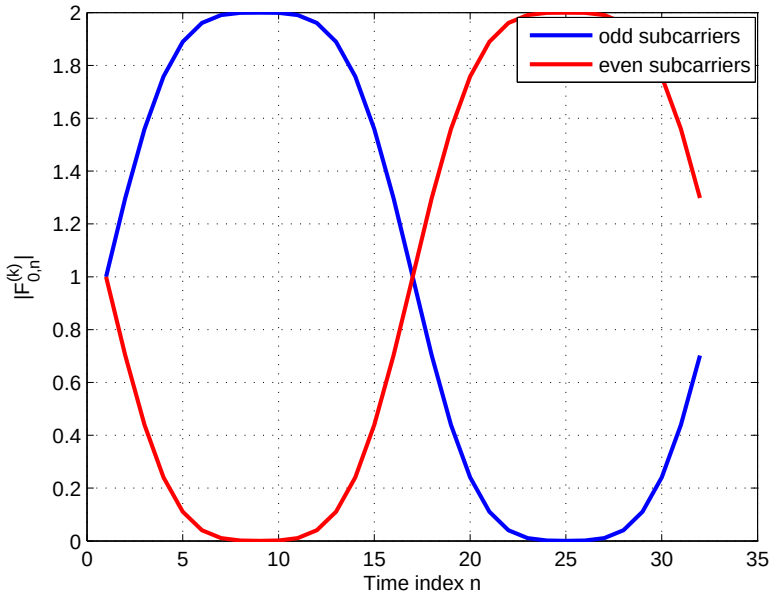

Figure 5.2: The magnitude of $F_{0,n}^{(k)}$ as a function of the time index n within a data block, for even and odd values of k, using PHYDYAS filter.

Hence, when $|F_{0,n}^{(k)}| > 1$, we transmit a complex data symbol $d_{k,n}$ in position (k, n) and we set the positions $(k \pm 1, n)$ to zero because $|F_{0,n}^{(k\pm1)}| < 1$, and vice versa. Thus, thanks to this transmission strategy, illustrated in Fig. 5.3, we also remove the interference terms T_{k-1} and T_{k+1} in (5.3) since $d_{k\pm1,n} = 0$ when $d_{k,n}$ is nonzero. Then, we can write

$$Y_{k,n} \cong \begin{cases} F_{0,n}^{(k)} d_{k,n} & n \in \Omega^{(k)} \\ F_{1,n}^{(k-1)} d_{k-1,n} + F_{-1,n}^{(k+1)} d_{k+1,n} & n \notin \Omega^{(k)} \end{cases} \tag{5.12}$$

where $\Omega^{(k)}$ denotes the set of time indices where we transmit useful data. Hence, $\Omega^{(k)} = \{0, 1, ...\frac{N}{2} - 1\}$ when k is odd, and $\Omega^{(k)} = \{\frac{N}{2}, ...N - 1\}$ when k is even.

Therefore, at the receiver side, we consider only the positions where $n \in \Omega^{(k)}$ to recover the transmitted symbol $d_{k,n}$. Thus, the equalization becomes easier since the received symbols are now free of ISI.

In the presence of the radio channel, we assume that the channel is invariant during N multicarrier symbols, and we can rewrite (5.12), for $n \in \Omega^{(k)}$, as

$$Y_{k,n} \cong h_{k,n} F_{0,n}^{(k)} d_{k,n} + \Gamma_{k,n} \tag{5.13}$$

where $\Gamma_{k,n}$ is the noise term at the output of the demodulator, and $h_{k,n}$ is the channel coefficient.

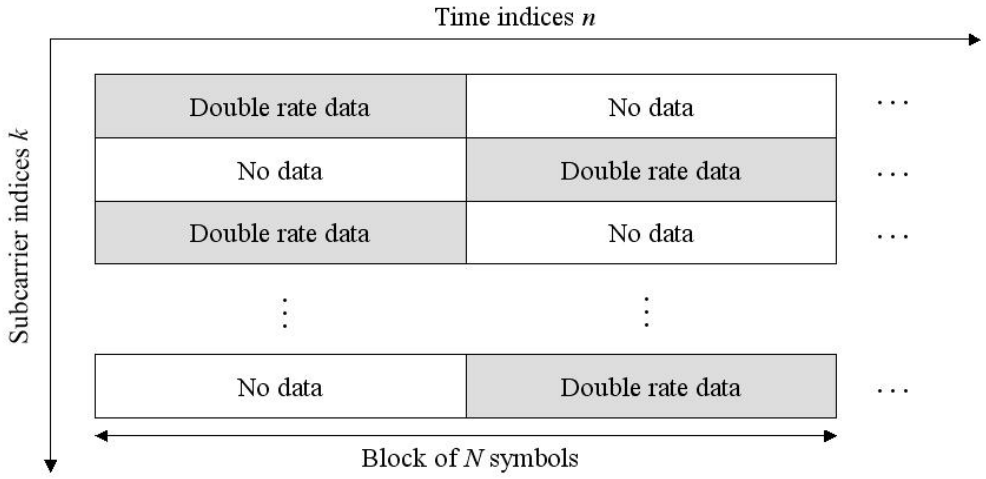

Figure 5.3: Data transmission strategy within a data block

In fact, the block-length N can be adapted to the channel variation. When the channel is fast fading, we have to choose N small enough to respect the assumption. We can define $N_c = T_c/(\frac{M}{2}T_s)$ as the coherence number of multicarrier symbols -by analogy with the coherence time T_c- where T_s is the sampling period. When $N \ll N_c$, we can consider that the channel is invariant during N FBMC symbols. For example, if $M = 512$, the velocity $v = 60$ km/h, the carrier frequency $f_c = 2.5$ GHz, and $T_s = 100$ ns, then $T_c \approx c/(2f_cv) \approx 3.6$ ms *i.e.* $N_c \approx 140$. Hence, it is clear that the channel cannot be invariant during $N = 128$ FBMC symbols, but we can consider it invariant if $N = 16$. For pedestrian channels ($v \approx 3$ km/h), N can be large up to 128 since $N_c \approx 2800$.

5.2 SNR analysis at the demodulator output

According to (5.13), the average SNR at the output of the demodulator can be written as

$$SNR_{k,n} = \frac{\mathbb{E}\{|h_{k,n}|^2\}|F_{0,n}^{(k)}|^2\sigma_d^2}{\sigma_s^2\mathbb{E}\{|\Gamma_{k,n}|^2\}}. \tag{5.14}$$

where σ_d^2 denotes the data power, $\mathbb{E}\{.\}$ is the expected value, $h_{k,n}$ is the channel gain and is assumed to be a complex Gaussian random variable with zero mean and unit variance. σ_s^2 is the average signal power at the modulator output used to normalize the transmitted power to unity. Indeed, the FFT-FBMC modulator affects the transmitted power and $\sigma_s^2 \neq \sigma_d^2$. First of all, let us evaluate σ_s^2.

5.2.1 Evaluation of the average transmitted power (σ_s^2)

From the expression of the transmitted FBMC signal (2.97), we have

$$\begin{aligned}\sigma_s^2[m] &= \mathbb{E}\{s[m]s^*[m]\} \\ &= \sum_{n,n'}\sum_{k,k'=0}^{M-1} \mathbb{E}\{a_{k,n}a^*_{k',n'}\}g[m-n\frac{M}{2}]g[m-n'\frac{M}{2}]e^{j\Phi}\end{aligned} \tag{5.15}$$

with Φ is a phase term given by

$$\Phi = \frac{2\pi\delta k}{M}(m-\frac{D}{2}) + \frac{\pi}{2}(\delta k+\delta n) - \pi(kn-k'n'),$$

where $\delta k = k-k'$ and $\delta n = n-n'$. It is obvious that if $k' \neq k$, then $a_{k,n}$ and $a_{k',n'}$ are statically independent. That is, $\mathbb{E}\{a_{k,n}a^*_{k',n'}\} = 0$ for $k' \neq k$. Hence, we can simplify (5.15) as

$$\sigma_s^2[m] = \sum_{k=0}^{M-1}\sum_{n,n'} \mathbb{E}\{a_{k,n}a^*_{k,n'}\}g[m-n\frac{M}{2}]g[m-n'\frac{M}{2}]e^{j\pi(\frac{1}{2}-k)\delta n}. \tag{5.16}$$

Now, let us determine the analytic expression of $\mathbb{E}\{a_{k,n}a^*_{k,n'}\}$. According to the aforementioned transmission strategy, we have

$$a_{k,n} = \begin{cases} \frac{1}{\sqrt{N}}\sum_{l=0}^{\frac{N}{2}-1} d_{k,l,p}e^{j2\pi\frac{nl}{N}} & \text{for k odd} \\ \frac{1}{\sqrt{N}}\sum_{l=\frac{N}{2}}^{N-1} d_{k,l,p}e^{j2\pi\frac{nl}{N}} & \text{for k even} \end{cases} \qquad \forall n \in B_p,$$

where $d_{k,l,p}$ denotes the data $d_{k,l}$ transmitted in the pth block of length N, and B_p is the indices set of symbols $a_{k,n}$ belonging to the pth block of length $N+L$, that is, $B_p = \{(p-1)(N+L), ..., p(N+L)-1\}$. In a closed form and without loss of generality, we rewrite the latter expression as

$$a_{k,n} = \frac{1}{\sqrt{N}}\sum_{l=0}^{\frac{N}{2}-1} d_{k,l,p}e^{j2\pi\frac{nl}{N}}e^{j\pi n(k+1)}, \quad \forall n \in B_p.$$

Hence, we obtain

$$\mathbb{E}\{a_{k,n}a^*_{k,n'}\} = \frac{1}{N}\sum_{l=0}^{\frac{N}{2}-1}\sum_{l'=0}^{\frac{N}{2}-1} \mathbb{E}\{d_{k,l,p}d^*_{k,l',p'}\}e^{j\frac{2\pi(nl-n'l')}{N}}e^{j\pi(k+1)\delta n}, \quad (n,n') \in B_p \times B_{p'}.$$

Since the data symbols $d_{k,l,p}$ are assumed to be statically independent, we have

$$\mathbb{E}\{d_{k,l,p}d^*_{k,l',p'}\} = \sigma_d^2\delta_{l,l'}\delta_{p,p'}.$$

Therefore,

$$\mathbb{E}\{a_{k,n}a^*_{k,n'}\} = \begin{cases} \frac{\sigma_d^2}{N}\sum_{l=0}^{\frac{N}{2}-1} e^{j\frac{2\pi l\delta n}{N}}e^{j\pi(k+1)\delta n}, & (n,n') \in B_p^2 \\ 0, & \text{elsewhere} \end{cases} \tag{5.17}$$

Substituting this last expression into (5.16), one can obtain the following equation:

$$\sigma_s^2[m] = \sigma_d^2\underbrace{\frac{M}{N}\sum_p \sum_{(n,n')\in B_p^2} e^{j\frac{3\pi}{2}\delta n}g[m-n\frac{M}{2}]g[m-n'\frac{M}{2}]\sum_{l=0}^{\frac{N}{2}-1} e^{j\frac{2\pi l\delta n}{N}}}_{A(m,N,L)}. \tag{5.18}$$

We notice that $\sigma_s^2[m]$ depends on m, *i.e.* the variance $\sigma_s^2[m]$ of the transmitted signal is time varying. Hence, one may wonder if the advantage of an efficient PSD of the conventional FBMC/OQAM system is still preserved with this new modulation scheme. Indeed, we will study the spectrum of the transmitted signal in Section 5.3.

We show in the following that $\sigma_s^2[m]$ is a periodic function with a period of $\frac{M}{2}(N+L)$. Therefore, let $m' = m + \frac{M}{2}(N+L)$. According to (5.18), we have the following expression:

$$\sigma_s^2[m'] = \sigma_d^2 \frac{M}{N} \sum_p \sum_{(n,n')\in B_p^2} e^{j\frac{3\pi}{2}\delta n} g[m-(n-N-L)\frac{M}{2}] g[m-(n'-N-L)\frac{M}{2}] \sum_{l=0}^{\frac{N}{2}-1} e^{j\frac{2\pi l \delta n}{N}} \tag{5.19}$$

Let $n_1 = n-N-L$, and $n_1' = n'-N-L$. When $n \in B_p = \{(p-1)(N+L), ..., p(N+L)-1\}$, then $n_1 \in B_{p-1}$. Since the difference $n_1' - n_1$ also equals δn, then substituting p by $p+1$, $\sigma_s^2[m']$ can be written as:

$$\sigma_s^2[m'] = \sigma_d^2 \frac{M}{N} \sum_p \sum_{(n_1,n_1')\in B_p^2} e^{j\frac{3\pi}{2}\delta n} g[m-n_1\frac{M}{2}] g[m-n_1'\frac{M}{2}] \sum_{l=0}^{\frac{N}{2}-1} e^{j\frac{2\pi l \delta n}{N}} \tag{5.20}$$

Hence,

$$\forall m, \quad \sigma_s^2[m + \frac{M}{2}(N+L)] = \sigma_s^2[m].$$

That is, $\sigma_s^2[m]$ is periodic with a period of $\frac{M}{2}(N+L)$. Fig. 5.4 depicts the curves of $\sigma_s^2[m]$ obtained analytically using (5.18), and the curves of the signal variance obtained by simulations for some different values of N and L. We remark that the theoretical curves match well with the numerical ones, which validates the resulting expression (5.18).

Since the signal variance $\sigma_s^2[m]$ is periodic, then we consider the average output signal power σ_s^2 as the mean of $\sigma_s^2[m]$ over one period and write

$$\sigma_s^2 = \overline{A}(N,L)\sigma_d^2, \tag{5.21}$$

where $\overline{A}(N,L)$ is the mean of $A(m,N,L)$ over one period. In Appendix B.1, we show that σ_s^2 does not depend on the subcarrier number M. Table 5.1 depicts the values of σ_s^2 as a function of N and L for both prototype filters IOTA and PHYDYAS, where $\sigma_d^2 = 1$.

5.2.2 Evaluation of the SNR at the receiver output

We remind the reader that the goal in this section is to evaluate the SNR at the FFT-FBMC demodulator given by (5.14). Now, let us evaluate $|F_{0,n}^{(k)}|^2$ and $\mathbb{E}\{|\Gamma_{k,n}|^2\}$. According to (5.8), we have

$$\begin{aligned} F_{0,n}^{(k)} &= \sum_{m=-\infty}^{+\infty} g[m] \underbrace{\sum_{n'=-\frac{N}{2}}^{\frac{N}{2}-1} g[m-n'\frac{M}{2}] e^{j\pi n'(k-\frac{1}{2})} e^{-j\frac{2\pi}{N}nn'}}_{G_{m,n}^{(k)}} \\ &= \sum_{m=-\infty}^{+\infty} g[m] G_{m,n}^{(k)}. \end{aligned} \tag{5.22}$$

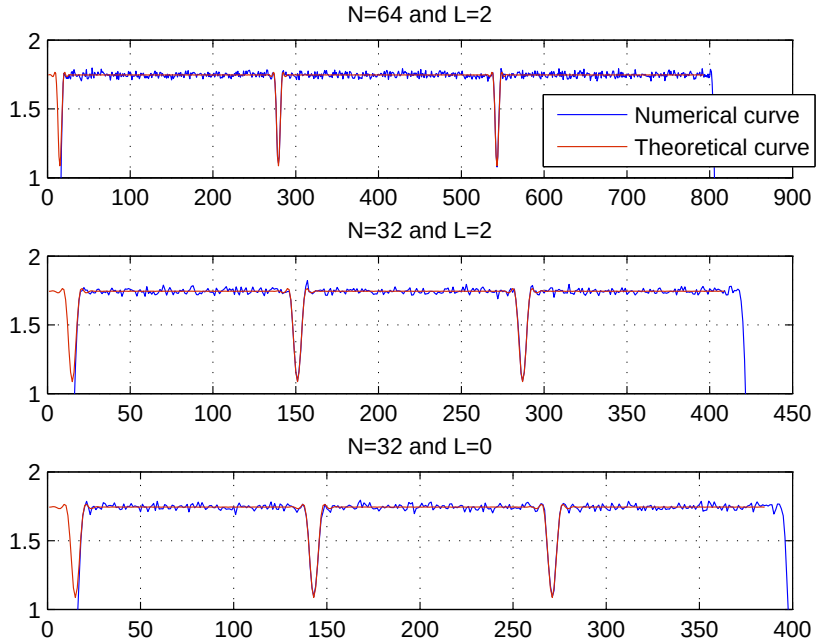

Figure 5.4: Theoretical and numerical variance curves of the modulator output signal using PHYDYAS filter

Now, let $b[m]$ be the noise term at the receiver input. Hence, according to (2.111) we have

$$\gamma_{k,n} = \sum_{m=-\infty}^{+\infty} b[m]g[m - nM/2]e^{j\frac{2\pi}{M}k(\frac{D}{2}-m)}e^{-j\phi_{k,n}}.$$

The noise term $\Gamma_{k,n}$ obtained after performing the FFT operation at the receiver is given by

$$\Gamma_{k,n} = \frac{1}{\sqrt{N}} \sum_{n'=0}^{N-1} \gamma_{k,n'} e^{-j\frac{2\pi}{N}nn'},$$

which yields

$$\Gamma_{k,n} = \frac{e^{j\frac{\pi kD}{M}}}{\sqrt{N}} \sum_{m=-\infty}^{+\infty} b[m]e^{-j\frac{2\pi}{M}km}\acute{G}^{(k)}_{m,n},$$

where

$$\acute{G}^{(k)}_{m,n} = \sum_{n'=0}^{N-1} g[m - n'\frac{M}{2}]e^{-j\phi_{k,n'}}e^{-j\frac{2\pi}{N}nn'}.$$

After processing, we can easily find that

$$\acute{G}^{(k)}_{m,n} = G^{(k)}_{m,n}e^{j\frac{\pi}{2}(Nk-2n-k-\frac{N}{2})}.$$

where $G^{(k)}_{m,n}$ is defined in Equation (5.22).

Table 5.1: The values of the average output signal power σ_s^2 depending on the block length N and the guard interval L for both used prototype filters IOTA and PHYDYAS.

	PHYDYAS			IOTA		
Values of N \ Values of L	0	2	4	0	2	4
16	1.6856	1.6911	1.6955	1.5253	1.5293	1.5325
32	1.7194	1.7208	1.7221	1.5492	1.5503	1.5512
64	1.7342	1.7346	1.7350	1.5598	1.5601	1.5603
128	1.7411	1.7412	1.7413	1.5647	1.5648	1.5649

Now, let us evaluate the variance of the noise term $\Gamma_{k,n}$, one can write

$$\begin{aligned}\mathbb{E}\{|\Gamma_{k,n}|^2\} &= \frac{1}{N} E\left\{\left|\sum_{m=-\infty}^{+\infty} b[m]\acute{G}_{m,n}^{(k)} e^{-j\frac{2\pi}{M}km}\right|^2\right\} \\ &= \frac{1}{N}\sum_{m=-\infty}^{+\infty} |\acute{G}_{m,n}^{(k)}|^2 \mathbb{E}\{|b[m]|^2\} \\ &= \frac{\sigma_0^2}{N}\sum_{m=-\infty}^{+\infty} |G_{m,n}^{(k)}|^2, \end{aligned} \tag{5.23}$$

where σ_0^2 denotes the noise power at the demodulator input. Finally, according to (5.21), (5.22) and (5.23), one can rewrite (5.14) as

$$SNR_{k,n} = \frac{N}{\overline{A}(N,L)} \times \frac{\left|\sum_{m=-\infty}^{+\infty} g[m]G_{m,n}^{(k)}\right|^2}{\sum_{m=-\infty}^{+\infty} |G_{m,n}^{(k)}|^2} SNR_0, \tag{5.24}$$

with $SNR_0 = \sigma_d^2/\sigma_0^2$ is the average SNR at the receiver input before the power normalization.

5.2.3 Equivalent average SNR

Since the SNR depends on the time index n, then the symbol-error rate (SER) also depends on the time index n. Let us denote by P_n, the SER at time index n, with $n \in \Omega^{(k)}$. Hence, the overall symbol-error rate P_e is

$$P_e = \frac{2}{N}\sum_{n\in\Omega^{(k)}} P_n. \tag{5.25}$$

In Rayleigh fading channel, the relationship between P_n and $SNR_{k,n}$ depends on the symbol modulation type and is approximated in the limit of high SNR by [13]

$$P_n \approx \frac{\alpha}{2\beta \times SNR_{k,n}}, \tag{5.26}$$

where α and β are constants that depend on the modulation type. Then, we define an equivalent SNR SNR_{eq} that provides, according to (5.26), the same SER as the overall P_e.

Therefore, from equations (5.26) and (5.25), one can write

$$\frac{\alpha}{2\beta \times SNR_{eq}} \approx \frac{2}{N} \sum_{n \in \Omega^{(k)}} \frac{\alpha}{2\beta \times SNR_{k,n}},$$

which yields

$$SNR_{eq} \approx \frac{N}{2} \Bigg(\sum_{n \in \Omega^{(k)}} \frac{1}{SNR_{k,n}} \Bigg)^{-1}. \tag{5.27}$$

Substituting $SNR_{k,n}$ by its expression given in (5.24), the equation above becomes

$$SNR_{eq} \approx \frac{N^2}{2\overline{A}(N,L)} \Bigg(\sum_{n \in \Omega^{(k)}} \frac{\sum_{m=-\infty}^{+\infty} |G_{m,n}^{(k)}|^2}{\left| \sum_{m=-\infty}^{+\infty} g[m] G_{m,n}^{(k)} \right|^2} \Bigg)^{-1} SNR_0. \tag{5.28}$$

Numerical calculations lead us to draw up Table 5.2, where the values of $\frac{SNR_{eq}}{SNR_0}$ are depicted as a function of N and L for both IOTA and PHYDYAS prototype filters. According to this table, we notice that there is practically no SNR loss (at worst 0.13 dB). Then, we can expect that FFT-FBMC exhibits the same performance as OFDM.

Table 5.2: The values of the average SNR gains $\frac{SNR_{eq}}{SNR_0}$ for various block lengths N and guard interval lengths L for both used prototype filters IOTA and PHYDYAS.

	PHYDYAS			IOTA		
Values of N \ Values of L	0	2	4	0	2	4
16	1.0040	1.0008	0.9982	1.0051	1.0024	1.0003
32	0.9880	0.9871	0.9864	0.9891	0.9884	0.9878
64	0.9770	0.9768	0.9766	0.9796	0.9794	0.9793
128	0.9709	0.9708	0.9708	0.9745	0.9745	0.9745

5.3 Power spectral density of the transmitted FFT-FBMC signal

The main advantage of the filter bank techniques is the well-localization of the spectrum of the transmitted signal. Since and as we have seen, the transmitted signal variance in FFT-FBMC is not stationary, one may wonder if the spectrum well-localization property is still preserved. In this section, we will analyze the spectrum of the transmitted signal and compare it to the conventional FBMC.

Let us consider that only one subcarrier k is activated, then the transmitted signal is:

$$\begin{aligned} s_k[m] &= \sum_n a_{k,n} g_{k,n}[m] \\ &= e^{j\frac{2\pi k}{M}(m-D/2)} \sum_n \underbrace{a_{k,n} e^{j\phi_{k,n}}}_{b_{k,n}} g[m - nM/2] \end{aligned} \tag{5.29}$$

The Power Spectral Density (PSD) of the signal $s[m]$, disregarding the frequency shift term $e^{j\frac{2\pi k}{M}(m-D/2)}$, is given by [112]:

$$S(f) \sim |G(f)|^2 A\left(\frac{M}{2}f\right), \tag{5.30}$$

where $A\left(\nu = \frac{M}{2}f\right)$ is the PSD of $b_{k,n}$, $G(f)$ is the Fourier transform of the prototype filter $g[m]$, and f is the normalized frequency with respect to the sampling frequency f_s. Since $b_{k,n}$ is a discrete random process, its PSD is derived by calculating the Fourier transform of its autocorrelation function. Making use of (5.17), the autocorrelation of $b_{k,n}$ is:

$$\begin{aligned}\mathbb{E}\{b_{k,n}b^*_{k,n-\delta n}\} &= \mathbb{E}\{a_{k,n}a^*_{k,n-\delta n}\}e^{j\phi_{k,n}-j\phi_{k,n-\delta n}} \\ &= \begin{cases} \frac{\sigma_d^2}{N}\sum_{l=0}^{\frac{N}{2}-1} e^{j\frac{2\pi l\delta n}{N}} e^{j\frac{3\pi}{2}\delta n} & (n, n-\delta n) \in B_p^2 \\ 0 & \text{otherwise} \end{cases}\end{aligned} \tag{5.31}$$

We recall that $B_p = \{(p-1)(N+L), ..., p(N+L)-1\}$, with $p \in \mathbb{Z}$. Therefore, $b_{k,n}$ is a non-stationary process as it depends on the time index "n". Then, we define the time-varying spectrum of $b_{k,n}$ as [113]:

$$A_n(\nu) = \sum_{\delta n=-\infty}^{+\infty} \mathbb{E}\{b_{k,n}b^*_{k,n-\delta n}\}e^{-j2\pi\nu\delta n}. \tag{5.32}$$

According to the expression of $\mathbb{E}\{b_{k,n}b^*_{k,n-\delta n}\}$ in (5.31), we can write:

$$\begin{aligned}A_n(\nu) &= \sum_{\delta n=n+1-p(N+L)}^{n-(p-1)(N+L)} \frac{\sigma_d^2}{N}\sum_{l=0}^{\frac{N}{2}-1} e^{j\frac{2\pi l\delta n}{N}} e^{j\frac{3\pi}{2}\delta n} e^{-j2\pi\nu\delta n}, \qquad n \in B_p \\ &= \frac{\sigma_d^2}{N}\sum_{l=0}^{\frac{N}{2}-1} \sum_{\delta n=n+1-p(N+L)}^{n-(p-1)(N+L)} e^{j(\frac{2\pi l}{N}+\frac{3\pi}{2}-2\pi\nu)\delta n}\end{aligned} \tag{5.33}$$

We can easily show that $A_n(\nu)$ is periodic with respect to n with a period of $N+L$. Then, the PSD $A(\nu)$ is calculated by averaging $A_n(\nu)$ with respect to n over one single period [113]:

$$A(\nu) = \frac{1}{N+L}\sum_{n\in B_1} A_n(\nu) = \frac{1}{N+L}\sum_{n=0}^{N+L-1} A_n(\nu). \tag{5.34}$$

For the sake of writing simplicity, let us denote by $X_l(\nu) = \frac{2\pi l}{N} + \frac{3\pi}{2} - 2\pi\nu$. We have:

$$\sum_{\delta n=n+1-p(N+L)}^{n-(p-1)(N+L)} e^{jX_l(\nu)\delta n} = \begin{cases} \frac{1-e^{jX_l(\nu)(N+L)}}{1-e^{jX_l(\nu)}} e^{jX_l(\nu)(n+1-p(N+L))} & \frac{X_l(\nu)}{2\pi} \notin \mathbb{Z} \\ N+L & \frac{X_l(\nu)}{2\pi} \in \mathbb{Z} \end{cases} \tag{5.35}$$

Therefore, we can distinguish two cases for the expressions of $A_n(\nu)$ and $A(\nu)$ according to the frequency values ν:

- $\frac{X_l(\nu)}{2\pi} \notin \mathbb{Z}$, $\forall l \in \{0, ..., \frac{N}{2}-1\}$: in this case, we have:

$$A_n(\nu) = \frac{\sigma_d^2}{N}\sum_{l=0}^{\frac{N}{2}-1} \frac{1-e^{jX_l(\nu)(N+L)}}{1-e^{jX_l(\nu)}} e^{jX_l(\nu)(n+1-p(N+L))}. \tag{5.36}$$

Then,

$$A(\nu) = \frac{\sigma_d^2}{N(N+L)} \sum_{l=0}^{\frac{N}{2}-1} \frac{1-e^{jX_l(\nu)(N+L)}}{1-e^{jX_l(\nu)}} \sum_{n=0}^{N+L-1} e^{jX_l(\nu)(n+1-N-L)}$$
$$= \frac{\sigma_d^2}{N(N+L)} \sum_{l=0}^{\frac{N}{2}-1} \left(\frac{1-e^{jX_l(\nu)(N+L)}}{1-e^{jX_l(\nu)}} \right)^2 e^{jX_l(\nu)(1-N-L)}$$
$$= \frac{\sigma_d^2}{N(N+L)} \sum_{l=0}^{\frac{N}{2}-1} \frac{\sin\left(\frac{X_l(\nu)(N+L)}{2}\right)^2}{\sin\left(\frac{X_l(\nu)}{2}\right)^2}. \tag{5.37}$$

- $\exists l' \in \{0, ..., \frac{N}{2}-1\}$, $\frac{X_{l'}(\nu)}{2\pi} \in \mathbb{Z}$: this second case yields that $\nu = \frac{l'}{N} + \frac{3}{4} + q$ with $q \in \mathbb{Z}$. As $l' \in \{0, ..., \frac{N}{2}-1\}$, then there is at most one single pair (l', q) that satisfies this condition for a given value of ν. Therefore, in this case, we can write:

$$A_n(\nu) = \frac{(N+L)\sigma_d^2}{N} + \frac{\sigma_d^2}{N} \sum_{\substack{l=0 \\ l \neq l'}}^{\frac{N}{2}-1} \frac{1-e^{jX_l(\nu)(N+L)}}{1-e^{jX_l(\nu)}} e^{jX_l(\nu)(n+1-p(N+L))}. \tag{5.38}$$

Then, we obtain:

$$A(\nu) = \frac{(N+L)\sigma_d^2}{N} + \frac{\sigma_d^2}{N(N+L)} \sum_{\substack{l=0 \\ l \neq l'}}^{\frac{N}{2}-1} \frac{\sin\left(\frac{X_l(\nu)(N+L)}{2}\right)^2}{\sin\left(\frac{X_l(\nu)}{2}\right)^2}. \tag{5.39}$$

Therefore, according to the values of ν, the PSD of $b_{k,n}$ is given by either (5.37) or (5.39). From these both expressions, we can conclude that $A(\nu)$ is periodic with a period of 1, which fits well with the sampling theory. Fig. 5.5 depicts the curve of $A(\nu)$.

As for the PSD of the FFT-FBMC transmitted data, we show in Fig. 5.6 the spectrum -given by (5.30)- occupied by one subcarrier, and compare it to the spectrum of the conventional FBMC given by $|G(f)|^2$. In this figure, we have considered the PHYDYAS prototype filter. We observe that the FFT-FBMC spectrum is more selective than the FBMC one, especially in the adjacent subbands. Indeed, the spectrum of FBMC and FFT-FBMC signals have almost the same curves in the even subbands because of the periodicity of $A(\nu)$. In FBMC, we consider that a given subcarrier interfere only the two direct adjacent ones. Whereas in FFT-FBMC the interference in adjacent subbands is considerably reduced. In Fig. 5.7 we depict the FFT-FBMC spectrum for two adjacent subcarriers. We have about 98.83% of the FFT-FBMC transmitted energy in the considered subband, whereas, in conventional FBMC, we have 87.38% of the signal energy in the considered subband. We give in Table 5.3 the interference power in the first three adjacent subcarriers for FBMC and FFT-FBMC signals. The values of the interference power for the FFT-FBMC system in this table are obtained with $N = 64$ and $L = 4$.

5.4 Guard interval reduction

The main drawback of the proposed scheme is the insertion of the CP in each subcarrier. Despite that the FBMC impulse response is spread over $2\Delta = 4K - 2$ time periods, we

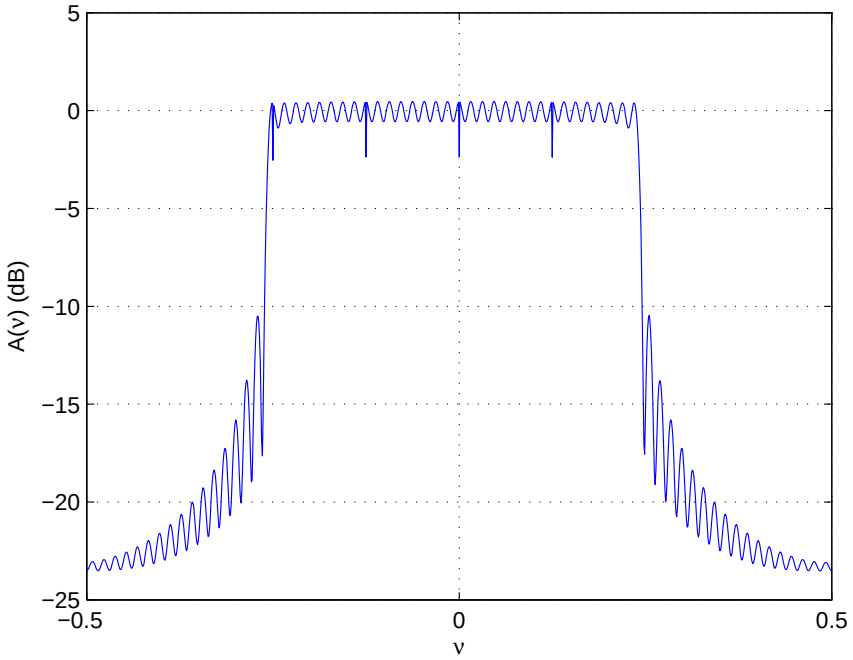

Figure 5.5: PSD curve $A(\nu)$ with $N = 64$ and $L = 4$.

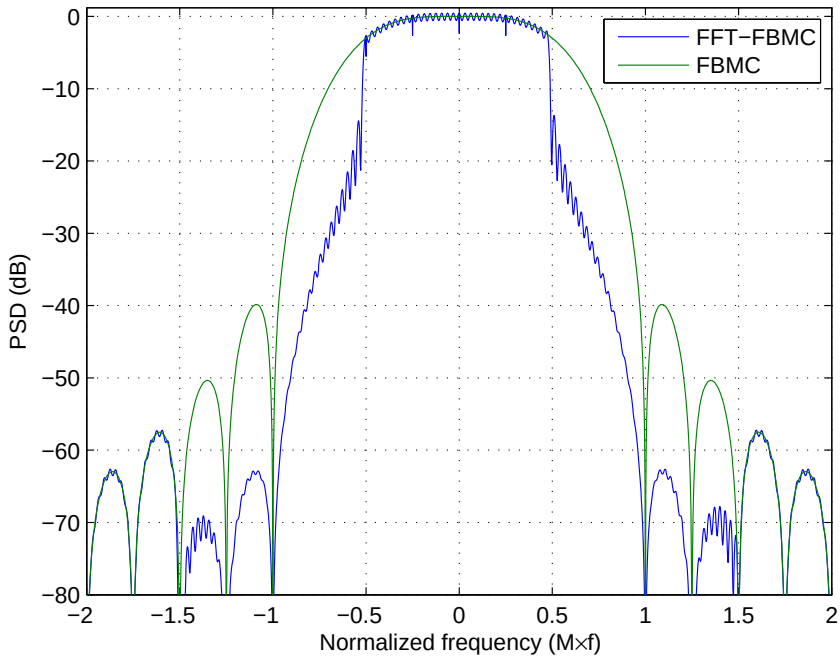

Figure 5.6: PSD comparision between FBMC and FFT-FBMC ($N = 64$,$L = 4$) signals using PHYDYAS filter.

Table 5.3: Values of the interference power

	FFT-FBMC		FBMC	
$k = 1$	1%	-20 dB	6.31%	-12 dB
$k = 2$	3.56e-5%	-64.48 dB	3.14e-5%	-65 dB
$k = 3$	1.46e-8%	-98.37 dB	9.33e-7%	-80.30 dB

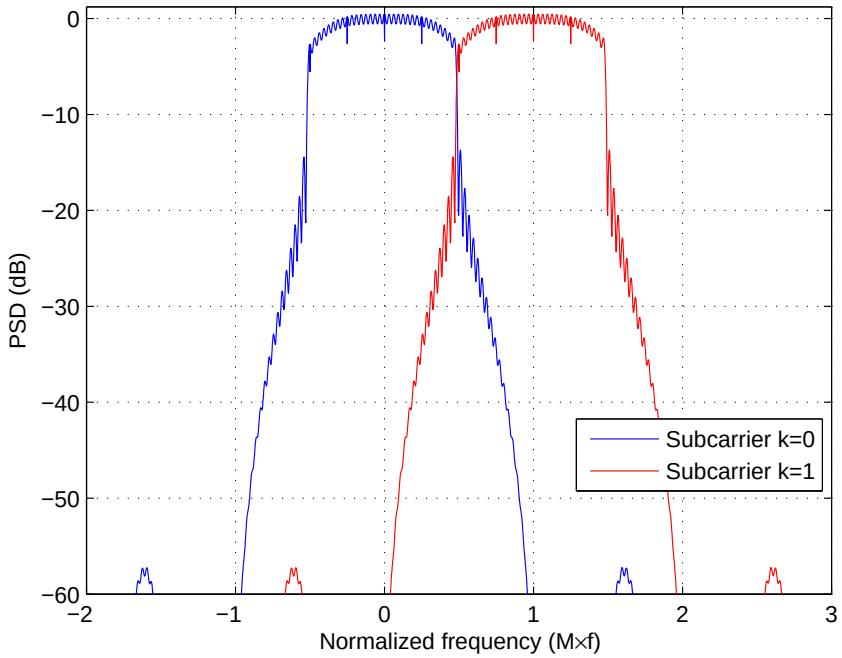

Figure 5.7: FFT-FBMC PSD curves for two adjacent subcarriers.

can reduce the CP in order to decrease the spectral efficiency loss but at the expense of performance degradation. In fact, reducing the CP causes ISI and interblock interference. The performance clearly depends on the ratio between the signal and the interference power (SIR).

Since the values of $f_0^{(k)}(\Delta n)$ are known (they depend only on the prototype filter), we can evaluate the SIR for each value of $n \in \Omega^{(k)}$ and for the different values of L. Equation (5.3) shows that the received signal can be considered as the sum of three terms. First, let us consider only the first term T_k. The same developments can be applied to the other terms.

Let us denote by $\mathbf{a}_k = [a_{k,0}, ..., a_{k,N-1}]^T$ the N-point IFFT output at the kth subcarrier which is expressed by

$$\mathbf{a}_k = \mathbf{W}^H \mathbf{d}_k,$$

where $\mathbf{d}_k = [d_{k,0}, ..., d_{k,N-1}]^T$, and $\mathbf{W}^H$ is the N-point IFFT matrix. According to the transmission strategy, the data vector $\mathbf{d}_k$ contains zero elements in either its first or second half depending on the parity of k. When the CP length is shorter than the maximum spread (2Δ), interference terms are added to the term T_k. Let us consider a received block, after CP removal, at the kth subcarrier $\mathbf{y}_k = [y_{k,0}, ..., y_{k,N-1}]^T$, we can write [114]

$$\mathbf{y}_k = \mathbf{F}_{0,k}\mathbf{a}_k + \mathbf{r}_1 + \mathbf{r}_2 + \mathbf{r}_3, \tag{5.40}$$

where $\mathbf{r}_1 = -\mathbf{A}\mathbf{a}_k$, $\mathbf{r}_2 = \mathbf{B}_1\mathbf{a}_k^+$ and $\mathbf{r}_3 = \mathbf{B}_2\mathbf{a}_k^-$, where $\mathbf{a}_k^+$ and $\mathbf{a}_k^-$ are respectively the blocks transmitted previously and subsequently at the same kth subcarrier. $\mathbf{F}_{0,k}$ is an $N \times N$ circulant matrix with entries given by

$$\mathbf{F}_{0,k}(p,q) = f_0^{(k)}\left(\left|p - q + \frac{N}{2}\right|_N - \frac{N}{2}\right),$$

for $(p,q) \in \{0, ..., N-1\}^2$.

$\mathbf{B}_1 = \mathbf{T_u}\mathbf{P}_L$ and $\mathbf{B}_2 = \mathbf{T_l}\mathbf{P}_{-L}$, where the upper triangular matrix $\mathbf{T_u}$ is given by

$$\mathbf{T_u}(p,q) = f_0^{(k)}(p - q + N + L),$$

with $0 \leq p \leq N-1$, $p \leq q \leq N-1$, and the lower triangular matrix $\mathbf{T_l}$ is given by

$$\mathbf{T_l}(p,q) = f_0^{(k)}(p - q - N - L),$$

with $0 \leq q \leq N-1$, $q \leq p \leq N-1$. Matrix $\mathbf{A}$ is given by

$$\mathbf{A} = \mathbf{T_u}\mathbf{P}_{-L} + \mathbf{T_l}\mathbf{P}_L,$$

where $\mathbf{P}_L$ is a permutation matrix that circularly shifts the columns to the left by L positions. All of $\mathbf{B}_1$, $\mathbf{B}_2$ and $\mathbf{A}$ are sparse matrices, and when $L \geq 2\Delta$, these matrices are zero.

Demodulating $\mathbf{y}_k$ by taking the N-point FFT, we obtain the output vector

$$\mathbf{Y}_k = \mathbf{W}\mathbf{y}_k.$$

Replacing $\mathbf{B}_1$, $\mathbf{B}_2$ and $\mathbf{A}$ by their expressions, we obtain

$$\begin{aligned}\mathbf{Y}_k =& \mathbf{W}\mathbf{F}_{0,k}\mathbf{W}^H\mathbf{d}_k - \mathbf{W}\mathbf{T_u}\mathbf{P}_{-L}\mathbf{W}^H\mathbf{d}_k - \mathbf{W}\mathbf{T_l}\mathbf{P}_L\mathbf{W}^H\mathbf{d}_k \\ &+ \mathbf{W}\mathbf{T_u}\mathbf{P}_L\mathbf{W}^H\mathbf{d}_k^+ + \mathbf{W}\mathbf{T_l}\mathbf{P}_{-L}\mathbf{W}^H\mathbf{d}_k^-.\end{aligned}$$

Since the matrix $\mathbf{F}_{0,k}$ and the permutation matrices $\mathbf{P}_L$ and $\mathbf{P}_{-L}$ are circulant matrices, we can write

$$\mathbf{F}_{0,k} = \mathbf{W}^H \overline{\mathbf{F}}_{0,k} \mathbf{W}$$

and

$$\mathbf{P}_L = \mathbf{W}^H \mathbf{E}_L \mathbf{W},$$

such that $\mathbf{E}_L$ and $\overline{\mathbf{F}}_{0,k}$ are diagonal matrices. Hence, the last equation becomes

$$\begin{aligned}\mathbf{Y}_k =& \overline{\mathbf{F}}_{0,k}\mathbf{d}_k - \left(\overline{\mathbf{T}}_{\mathbf{u}}\mathbf{E}_{-L} + \overline{\mathbf{T}}_{\mathbf{l}}\mathbf{E}_L\right)\mathbf{d}_k \\ &+ \overline{\mathbf{T}}_{\mathbf{u}}\mathbf{E}_L\mathbf{d}_k^+ + \overline{\mathbf{T}}_{\mathbf{l}}\mathbf{E}_{-L}\mathbf{d}_k^-,\end{aligned} \tag{5.41}$$

where $\overline{\mathbf{T}}_{\mathbf{u}} = \mathbf{W}\mathbf{T}_{\mathbf{u}}\mathbf{W}^H$ and $\overline{\mathbf{T}}_{\mathbf{l}} = \mathbf{W}\mathbf{T}_{\mathbf{l}}\mathbf{W}^H$. The diagonal elements of $\overline{\mathbf{F}}_{0,k}$ are given by

$$\overline{\mathbf{F}}_{0,k}(n,n) = \sum_{p=-\frac{N}{2}}^{\frac{N}{2}-1} f_0^{(k)}(p) e^{-j2\pi\frac{np}{N}},$$

and those of $\mathbf{E}_L$ are given by

$$\mathbf{E}_L(n,n) = e^{j2\pi\frac{nL}{N}}.$$

Let us denote by $\mathbf{D}$ the diagonal matrix which contains the diagonal elements of the term $\overline{\mathbf{T}}_{\mathbf{u}}\mathbf{E}_{-L} + \overline{\mathbf{T}}_{\mathbf{l}}\mathbf{E}_L$ in (5.41), and let $\mathbf{T} = \overline{\mathbf{T}}_{\mathbf{u}}\mathbf{E}_{-L} + \overline{\mathbf{T}}_{\mathbf{l}}\mathbf{E}_L - \mathbf{D}$. This last matrix represents the ISI in the same data vector $\mathbf{d}_k$. Thus, we can rewrite (5.41) as

$$\mathbf{Y}_k = (\overline{\mathbf{F}}_{0,k} - \mathbf{D})\mathbf{d}_k - \mathbf{T}\mathbf{d}_k + \overline{\mathbf{T}}_{\mathbf{u}}\mathbf{E}_L\mathbf{d}_k^+ + \overline{\mathbf{T}}_{\mathbf{l}}\mathbf{E}_{-L}\mathbf{d}_k^-. \tag{5.42}$$

The elements of the matrices $\overline{\mathbf{T}}_{\mathbf{l}} = \mathbf{W}\mathbf{T}_{\mathbf{l}}\mathbf{W}^H$ and $\overline{\mathbf{T}}_{\mathbf{u}} = \mathbf{W}\mathbf{T}_{\mathbf{u}}\mathbf{W}^H$ are respectively given by

$$\overline{\mathbf{T}}_{\mathbf{l}}(m,n) = \frac{1}{N}\sum_{q=0}^{N-1}\sum_{p=0}^{N-1-q} f_0^{(k)}(p - L_0) e^{-j2\pi\frac{mp}{N}} e^{j2\pi\frac{(n-m)q}{N}}, \tag{5.43}$$

$$\overline{\mathbf{T}}_{\mathbf{u}}(m,n) = \frac{1}{N}\sum_{q=0}^{N-1}\sum_{p=0}^{q} f_0^{(k)}(L_0 - p) e^{j2\pi\frac{mp}{N}} e^{j2\pi\frac{(n-m)q}{N}}, \tag{5.44}$$

where $L_0 = N + L$. According to (5.8), we have $f_0^{(k)}(p) = \left(f_0^{(k)}(-p)\right)^*$, $\forall p \in \mathbb{Z}$. Hence, we can easily show that the entries of matrix $\mathbf{T}$ can be expressed as

$$\mathbf{T}(m,n) = \begin{cases} 2e^{-j\pi\frac{n-m}{N}}\mathfrak{Re}\left\{\mathbf{G}(m,n)e^{j\pi\frac{n-m}{N}}\right\}, & n \neq m \\ 0, & n = m \end{cases} \tag{5.45}$$

where

$$\mathbf{G}(m,n) = \frac{1}{N}\sum_{q=0}^{N-1}\sum_{p=0}^{q} f_0^{(k)}(L_0 - p) e^{j2\pi\frac{mp}{N}} e^{j2\pi\frac{(n-m)q}{N}} e^{-j2\pi\frac{nL}{N}}.$$

Also, we can show that the diagonal matrix $\mathbf{D}$ has as elements

$$\begin{aligned}\mathbf{D}(n,n) &= 2\mathfrak{Re}\left\{\mathbf{G}(n,n)\right\} \\ &= \frac{2}{N}\mathfrak{Re}\left\{\sum_{p=L+1}^{L+N}(p-L)f_0^{(k)}(p)e^{-j2\pi\frac{np}{N}}\right\}.\end{aligned} \tag{5.46}$$

Until now, we have only considered the first term T_k in (5.3). Regarding the other terms, we can proceed in the same way. Moreover, let us relax the assumption made in Section 5.1.1 that considerer only the interference coming from the immediate neighboring subcarriers. Therefore, we consider all the possible terms T_{k+l} with $|l| = 0, ..., \Delta'$, where Δ' is the maximum spectrum spread over the subcarriers. Hence, we can finally write $\mathbf{Y_k}$ as

$$\mathbf{Y_k} = (\overline{\mathbf{F}}_{0,k} - \mathbf{D})\mathbf{d}_k + \sum_{l=-\Delta'}^{\Delta'}\mathbf{Q}_{l,k}, \tag{5.47}$$

where $\mathbf{Q}_{l,k} = -\mathbf{T}^{(l)}\mathbf{d}_{k+l} + \overline{\mathbf{T}}_{\mathbf{u}}{}^{(l)}\mathbf{E}_L\mathbf{d}^+_{k+l} + \overline{\mathbf{T}}_{\mathbf{l}}{}^{(l)}\mathbf{E}_{-L}\mathbf{d}^-_{k+l}$, with

$$\overline{\mathbf{T}}_{\mathbf{l}}{}^{(l)}(m,n) = \frac{1}{N}\sum_{q=0}^{N-1}\sum_{p=0}^{N-1-q} f_l^{(k+l)}(p-L_0)e^{-j2\pi\frac{mp}{N}}e^{j2\pi\frac{(n-m)q}{N}},$$

$$\overline{\mathbf{T}}_{\mathbf{u}}{}^{(l)}(m,n) = \frac{1}{N}\sum_{q=0}^{N-1}\sum_{p=0}^{q} f_l^{(k+l)}(L_0-p)e^{j2\pi\frac{mp}{N}}e^{j2\pi\frac{(n-m)q}{N}},$$

and

$$\mathbf{T}^{(l)} = \begin{cases}\overline{\mathbf{T}}_{\mathbf{u}}{}^{(0)}\mathbf{E}_{-L} + \overline{\mathbf{T}}_{\mathbf{l}}{}^{(0)}\mathbf{E}_L - \mathbf{D}, & l = 0 \\ \overline{\mathbf{T}}_{\mathbf{u}}{}^{(l)}\mathbf{E}_{-L} + \overline{\mathbf{T}}_{\mathbf{l}}{}^{(l)}\mathbf{E}_L - \overline{\mathbf{F}}_{l,k}, & l \neq 0,\end{cases} \tag{5.48}$$

$\overline{\mathbf{F}}_{l,k}$ is a diagonal matrix with entries given by

$$\overline{\mathbf{F}}_{l,k}(n,n) = \sum_{p=-\frac{N}{2}}^{\frac{N}{2}-1} f_l^{(k+l)}(p)e^{-j2\pi\frac{np}{N}}.$$

Finally, for uncorrelated zero-mean modulation symbols with equal variance, the $SIR_{k,n}$ at the kth subcarrier and at time index n is given by

$$SIR_{k,n} = \frac{\left|\overline{\mathbf{F}}_{0,k}(n,n) - \mathbf{D}(n,n)\right|^2}{\sigma_I^2(k,n)}, \quad \text{for } n \in \Omega^{(k)}, \tag{5.49}$$

where

$$\sigma_I^2(k,n) = \sum_{l=-\Delta'}^{\Delta'}\sum_{r\in\Omega^{(k+l)}} |\mathbf{T}^{(l)}(n,r)|^2 + |\overline{\mathbf{T}}_{\mathbf{u}}{}^{(l)}(n,r)|^2 + |\overline{\mathbf{T}}_{\mathbf{l}}{}^{(l)}(n,r)|^2.$$

By the analogy with the definition of SNR_{eq} in (5.27), we consider the equivalent SIR (SIR_{eq}) that provides the same SER floor as the one caused by all the considered $SIR_{k,n}$. That is, we have:

$$SIR_{eq} \approx \frac{N}{2}\left(\sum_{n\in\Omega^{(k)}}\frac{1}{SIR_{k,n}}\right)^{-1}. \tag{5.50}$$

Table 5.4: Values of the equivalent SIR (dB) depending on N and L

	PHYDYAS			IOTA		
Values of N \ Values of L	0	2	4	0	2	4
16	15.57	26.11	34	16.41	26.52	26.96
32	18.68	29.18	37.05	19.09	26.76	27
64	21.73	32.30	40	21.47	26.89	27
128	24.76	35.22	43.06	23.42	26.96	27

The values of SIR_{eq} for some combinations of L and N are depicted in Table 5.4 for PHYDYAS and IOTA filters.

We remark in Table 5.4 for the IOTA filter that the SIR does not exceed the value of 27 dB. Indeed, since the IOTA filter provides a spectrum spread beyond the immediate adjacent subcarriers, the proposed transmission strategy does not completely eliminate the inherent interference even when $L > 2\Delta = 16$. In fact, there is still interference between subcarriers $k \pm 2$ and k, because $\Omega^{(k\pm1)} = \Omega^{(k)}$. Whereas for PHYDYAS filter, the SIR increases with the increase of L, and $SIR_{eq} = +\infty$ when $L > 2\Delta = 16$. This is because the PHYDYAS filter spectrum is confined only in the immediate adjacent subcarriers.

We also notice, in Table 5.4 for PHYDYAS filter, that for each L, the SIR is incremented by about $+3$ dB when N is doubled. This is explained by the fact that the power of the interference within a block caused by an insufficient CP remains almost the same whatever the value of $N > 2\Delta$. However, after applying the FFT at the receiver, this interference is scattered over the whole block of length of N. Hence, when we double N, the distribution of the interference power is halved, and thus, the SIR is also doubled ($+3$ dB). However, for IOTA filter, the situation is different because the SIR is limited by the ICI caused by the subcarriers $k \pm 2$ as we have explained previously.

5.5 Computational complexity issue

Clearly, the added complexity compared to FBMC lies in the extra M IFFTs and FFTs of size N in the transmitter and the receiver, respectively. Since $N/2$ samples in each subcarrier are zeros at the transmitter, and also only $N/2$ samples are needed in each subcarrier at the receiver, we can use the pruned IFFT/FFT algorithms to reduce the added complexity. According to Skinner's algorithm [115], a pruning input sample with length $N/2$ of an N-point IFFT requires $2N\log_2(\frac{N}{2})$ real multiplications and $3N\log_2(\frac{N}{2}) + N$ real additions. While Markel's algorithm [116] shows that a pruning output samples with length $N/2$ of an N-point FFT requires $2N\log_2(\frac{N}{4})$ real multiplications and $3N\log_2(\frac{N}{2})$ real additions. Therefore, the added complexity in FFT-FBMC compared to FBMC system, in terms of number of elementary operations per block of N FBMC symbols, is $5NM\log_2(\frac{N}{2}) + NM$ for the transmitter, and $5NM\log_2(\frac{M}{2}) - 2NM$ for the receiver.

5.6 Application to MIMO systems

The motivation of this work is to propose an FBMC system which can easily be combined with MIMO techniques such as SM-MLD and STBC. In this section, we will show how the proposed scheme is straightforwardly applied to SM-MLD and STBC.

5.6.1 Spatial multiplexing with ML detection

In the case of $(N_r \times N_t)$ spatial multiplexing, we transmit complex symbols $d_{k,n}^{(i)}$ at the ith transmit antenna and at a given time-frequency position (k,n) such that $n \in \Omega^{(k)}$. The signal at the jth receive antenna, after demodulation, is given by

$$Y_{k,n}^{(j)} = F_{0,n}^{(k)} \sum_{i=1}^{N_t} h_{k,n}^{(ji)} d_{k,n}^{(i)} + \Gamma_{k,n}^{(j)},$$

where $h_{k,n}^{(ji)}$ is the channel coefficient between transmit antenna "i" and receive antenna "j". The MIMO channels can be spatially correlated or uncorrelated. Finally, the matrix formulation of the system can be expressed as

$$\mathbf{Y}_{k,n} = F_{0,n}^{(k)} \mathbf{H}_{k,n} \mathbf{d}_{k,n} + \mathbf{\Gamma}_{k,n},$$

where $\mathbf{Y}_{k,n} = [Y_{k,n}^{(1)}, ..., Y_{k,n}^{(N_r)}]^T$, $\mathbf{d}_{k,n} = [d_{k,n}^{(1)}, ..., d_{k,n}^{(N_t)}]^T$, $\mathbf{\Gamma}_{k,n} = [\Gamma_{k,n}^{(1)}, ..., \Gamma_{k,n}^{(N_r)}]^T$, and $\mathbf{H}_{k,n}$ is an $(N_r \times N_t)$ matrix with entries $\mathbf{H}_{k,n}(j,i) = h_{k,n}^{(ji)}$.

Now since we got rid of the interference terms caused by the FBMC modulation, we can apply the MLD in a straightforward manner. This consists just in searching the data vector $\hat{\mathbf{d}}_{k,n}$ that minimizes the Euclidean distance

$$\hat{\mathbf{d}}_{k,n} = \arg\min_{\mathbf{d}_{k,n}} \left\{ \left\| F_{0,n}^{(k)} \mathbf{H}_{k,n} \mathbf{d}_{k,n} - \mathbf{Y}_{k,n} \right\|^2 \right\}.$$

The sphere decoding can also be applied instead of the basic MLD in order to reduce the complexity especially when large number of antennas or high modulations are used.

5.6.2 Alamouti space time code

As for Alamouti coding [34], we consider the basic scheme with two transmit antennas and one receive antenna. On each subcarrier k, a complex symbol $d_{k,n}^{(1)}$ is transmitted at time instant $n \in \Omega^{(k)}$ from the first antenna whereas the second antenna transmits a second symbol $d_{k,n}^{(2)}$. Then, at time instant $n+1 \in \Omega^{(k)}$, the first antenna transmits $(-d_{k,n}^{(2)})^*$ whereas the second one transmits $(d_{k,n}^{(1)})^*$. We note by $h_{k,1}$ and $h_{k,2}$ the complex and gaussian channel gains at the kth subcarrier from, respectively, the first and the second antenna to the receive one. According to (5.13) and since the coefficient $F_{0,n}^{(k)}$ depends on the time instant n, we can write in a matrix form:

$$\begin{bmatrix} \frac{Y_{k,n}}{F_{0,n}^{(k)}} \\ \left(\frac{Y_{k,n+1}}{F_{0,n+1}^{(k)}}\right)^* \end{bmatrix} = \underbrace{\begin{bmatrix} h_{k,1} & h_{k,2} \\ h_{k,2}^* & -h_{k,1}^* \end{bmatrix}}_{\mathbf{H}_k} \begin{bmatrix} d_{k,n}^{(1)} \\ d_{k,n}^{(2)} \end{bmatrix} + \begin{bmatrix} \frac{\Gamma_{k,n}}{F_{0,n}^{(k)}} \\ \left(\frac{\Gamma_{k,n+1}}{F_{0,n+1}^{(k)}}\right)^* \end{bmatrix}, \quad (n, n+1) \in \Omega^{(k)} \times \Omega^{(k)}. \tag{5.51}$$

Note that $\mathbf{H}_k$ is an orthogonal matrix and

$$\mathbf{H}_k^H \mathbf{H}_k = (|h_{k,1}|^2 + |h_{k,2}|^2)\mathbf{I}_2,$$

where $\mathbf{I}_2$ is the identity matrix of size 2. Hence, Alamouti coding could be performed, and the data estimates $\hat{d}_{k,n}^{(1)}$ and $\hat{d}_{k,n}^{(2)}$ are obtained by using the maximum ratio combining (MRC) equalization [34].

5.7 Simulation results

The performance analysis is based on the bit-error rate (BER) assessment as a function of the SNR. For all the simulations, we assume a perfect channel state information (CSI) at the receiver. The sampling period is $T_s = 100\ ns$, and the carrier frequency is $f_c = 2.5\ GHz$. The number of subcarriers is $M = 512$.

For the FFT-FBMC, we consider different configurations corresponding to $(N, L) \in \{16, 32, 64\} \times \{0, 2\}$. As for OFDM, the CP size (L_{cp}) is adapted to the channel spread length. We define the spectral efficiency loss by $\mu = \frac{L}{N+L}$ for the FFT-FBMC system, whereas for OFDM $\mu = \frac{L_{cp}}{M+L_{cp}}$. We assume pedestrian scenario where the velocity is $v \approx 3\ km/h$. For this application target, the coherence time is $T_c \approx c/(2f_c v) \approx 72\ ms$. We define $N_c = T_c/(\frac{M}{2}T_s)$ as the coherence number of multicarrier symbols, thus, $N_c \approx 2800$. Since $N \ll N_c$, we can pretend that the channel is invariant within an N-block. We test the FFT-FBMC and compare it to OFDM in both MIMO contexts presented in Section 5.6, namely: Spatial Multiplexing with ML detection and Alamouti coding scheme.

Regarding SM-MLD, we considered a basic configuration with two spatially uncorrelated antennas at both transmitter and receiver. First, we consider the Pedestrian-A channel [97] where the parameters are given by:

- Delays = [0 110 190 410] ns,
- Powers = [0 -9.7 -19.2 -22.8] dB.

Hence, for OFDM, we set $L_{cp} = 5$ ($\mu \approx 0.97\%$). The data are QPSK modulated. Fig. 5.8 and Fig. 5.9 show the performance of the FFT-FBMC, respectively, for PHYDYAS and IOTA filters and give a comparison with OFDM and the conventional FBMC using the Rec-ML receiver [117] based on interference estimation and cancelation.

For both IOTA and PHYDYAS filters, we clearly observe that the BER degradation strongly depends on L due to the BER floor effect caused by the insufficiency of the CP. We notice that the BER floor is much higher when there is no CP inserted ($L = 0$). We also notice that the BER floors lower by increasing N. This is explained by the fact that the power of the interference within a block caused by an insufficient CP remains almost the same whatever the value of $N > 2\Delta$. However, after applying the FFT at the receiver, this interference is scattered over the whole block. Hence, when we double N, the distribution of the interference power is halved, and thus, the SIR is also doubled ($+3\ dB$). This matches well with the values in Table 5.4; we notice, for PHYDYAS filter, that for each L, the SIR is incremented by about $+3\ dB$ when N is doubled. As for IOTA filter, the situation is different because the SIR is limited by the ICI caused by the subcarriers $k \pm 2$. The SIR values corresponding to the BER limits match well with Table 5.4. One can check this by

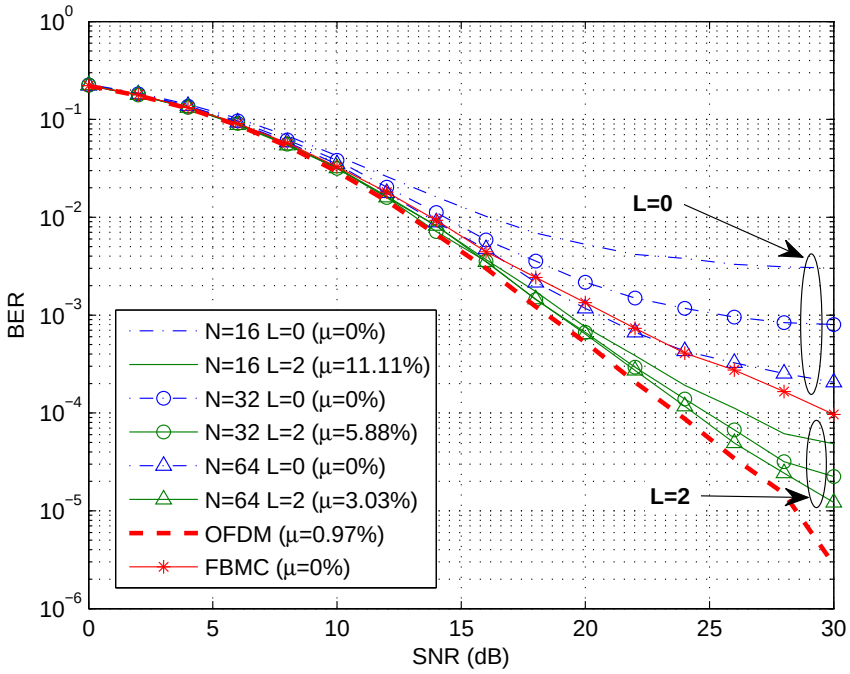

Figure 5.8: Performance of FFT-FBMC using PHYDYAS prototype filter with MIMO (2×2) spatial multiplexing and QPSK modulation in Ped-A channel.

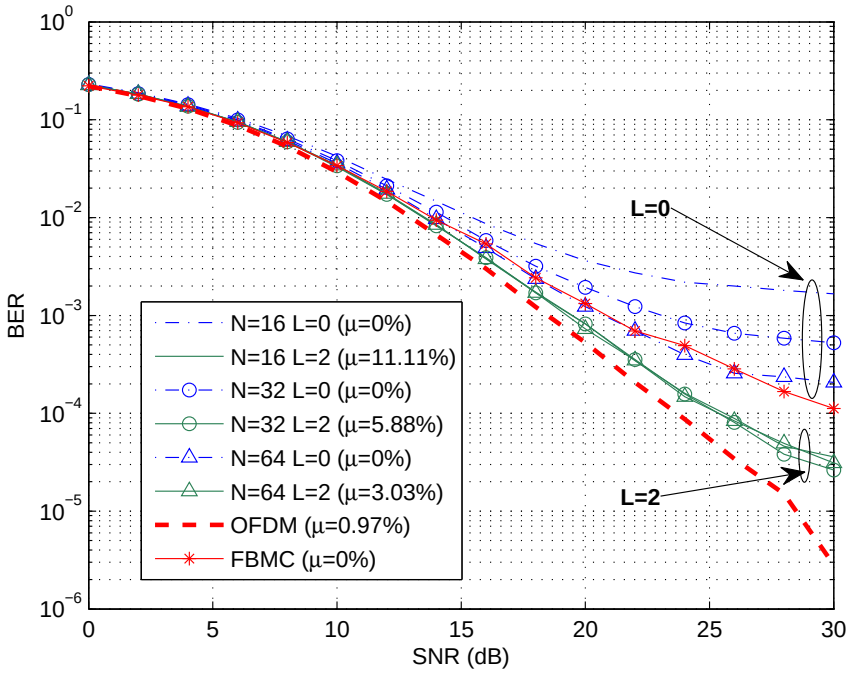

Figure 5.9: Performance of FFT-FBMC using IOTA prototype filter with MIMO (2×2) spatial multiplexing and QPSK modulation in Ped-A channel.

projecting the BER floor values on the OFDM curve and taking the corresponding SNR values.

Since the SIR values are relatively high when $L = 2$, the BER floor would be observed beyond 30 dB. Hence, as long as the SNR is less than 30 dB, we can consider that the FFT-FBMC with $L = 2$ exhibits almost no degradation compared to OFDM and outperforms the FBMC system. We notice that the curves of the FFT-FBMC/IOTA with $L = 2$ are almost independent of N. This matches well with Table 5.4 which shows that FFT-FBMC/IOTA has a SIR limit at 27 dB.

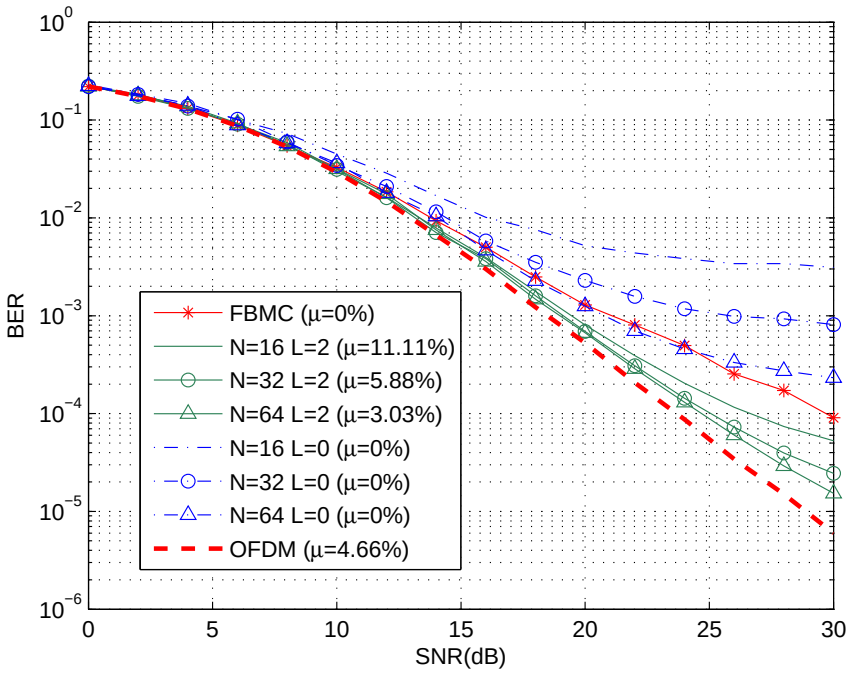

Figure 5.10: Performance of FFT-FBMC using PHYDYAS prototype filter with MIMO (2×2) spatial multiplexing and QPSK modulation in Veh-A channel without mobility.

Now, we test the FFT-FBMC/PHYDYAS with a more frequency selective channel and QPSK modulation, we chose the same channel parameters as the Vehicular-A model (without considering the velocity), that is:

- Delays = [0 300 700 1100 1700 2500] ns,
- Powers = [0 -1 -9 -10 -15 -20] dB.

Then, $L_{cp} = 25$ ($\mu \approx 4.66\%$). Fig. 5.10 shows that we obtain, for all the configurations, almost the same BER performance as in the case of the Pedestrian-A channel model.

Fig. 5.11 and Fig. 5.12 depict the BER performance of FFT-FBMC/PHYDYAS scheme with 16-QAM modulated data, respectively, in the Ped-A and Veh-A channel model. Clearly, the BER floor effects are more significant. Indeed, FFT-FBMC with $L = 0$ has a very high BER limits. However, we can obtain acceptable performance with $L = 2$.

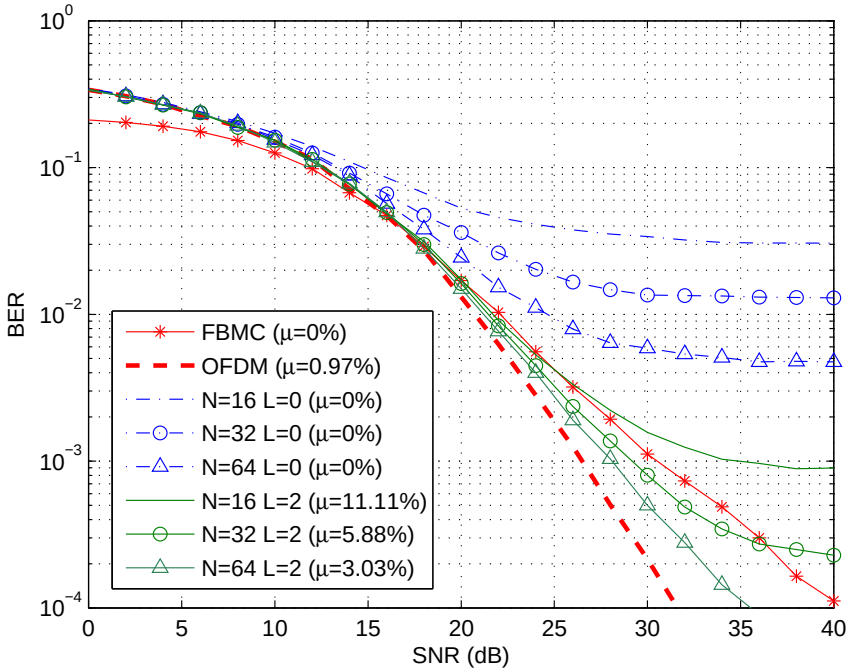

Figure 5.11: Performance of FFT-FBMC using PHYDYAS prototype filter with MIMO (2×2) spatial multiplexing and 16-QAM modulation in Ped-A channel.

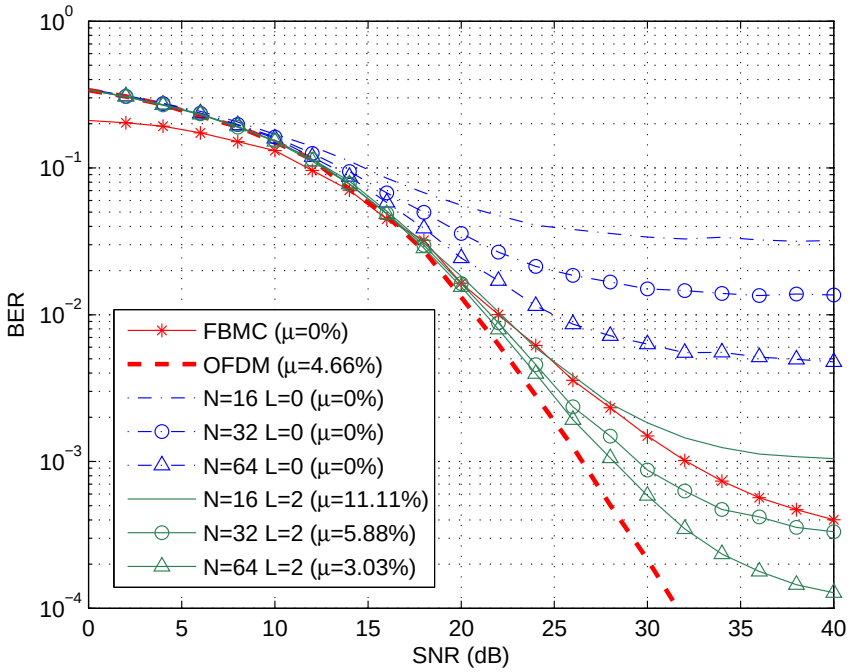

Figure 5.12: Performance of FFT-FBMC using PHYDYAS prototype filter with MIMO (2×2) spatial multiplexing and 16-QAM modulation in Veh-A channel without mobility.

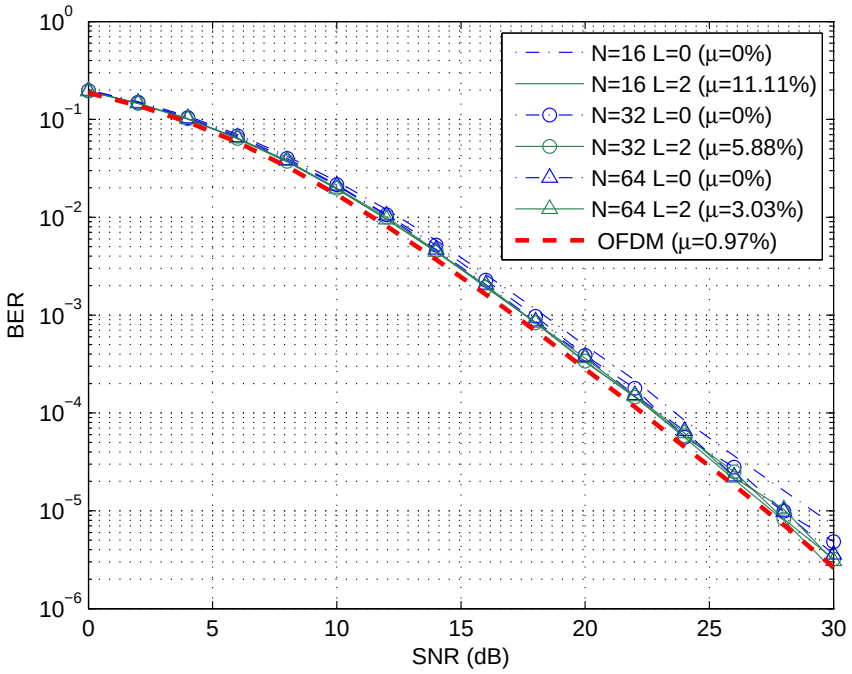

Figure 5.13: Performance of FFT-FBMC using IOTA prototype filter with (2×1) Alamouti coding scheme and QPSK modulation in Ped-A channel.

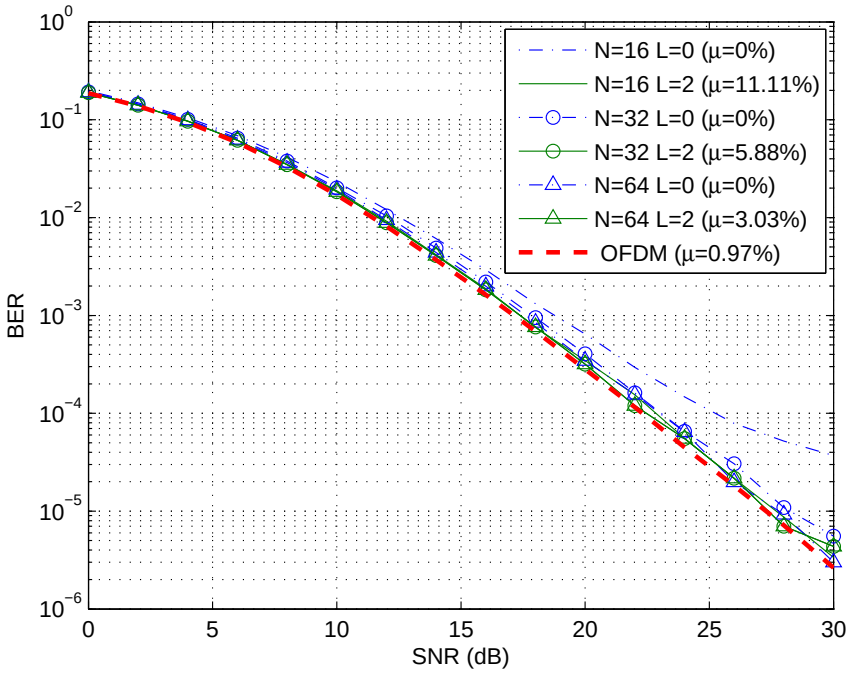

Figure 5.14: Performance of FFT-FBMC using PHYDYAS prototype filter with (2×1) Alamouti coding scheme and QPSK modulation in Ped-A channel.

As for the Alamouti scheme, we provide the performance results for PHYDYAS and IOTA filters, respectively, in Fig. 5.13 and Fig. 5.14. We notice that with IOTA filter, we obtain almost the same performance as OFDM for both values of $L = 0$ and $L = 2$. A very slight degradation with respect to OFDM can be pointed out in the high SNR regime. Unlike the SM case, the non-use of the CP has not resulted in considerable degradations. One can notice, at worst, about 1 dB of SNR loss at $BER = 10^{-4}$.

Regarding PHYDYAS filter, we obtain also almost no degradation compared to OFDM, except the case when $N = 16$ and $L = 0$ where we have about a 2.75 dB SNR loss with respect to OFDM at $BER = 10^{-4}$, and less than 1 dB at $BER = 10^{-2}$. In all BER figures, one can notice that OFDM outperforms the FFT-FBMC system in the whole considered SNR region. This is due to the ISI caused by the insufficient CP considered in the system and the neglected ISI in (5.2). Further, the values of the SNR_{eq}/SNR_0 depicted in table 5.2 show (except when $N = 16$) that SNR_{eq} is slightly smaller than SNR_0.

5.8 Conclusion

In this chapter, we have proposed a new FBMC scheme (called FFT-FBMC) in order to get rid of the intrinsic interference which is an issue when we combine the FBMC with some MIMO techniques such as SM-MLD and Alamouti coding. The FFT-FBMC scheme consists in performing an IDFT and DFT on each subcarrier, respectively, at the transmitter and receiver sides inserting also a CP as in the conventional OFDM. This makes FFT-FBMC more computationally complex than FBMC. The transmission strategy depicted in Fig. 5.3 is applied in order to isolate the adjacent subcarriers. In this way, the equivalent system became formulated as OFDM, and all MIMO techniques can be applied in a straightforward manner. We have proposed to reduce the CP and evaluate the corresponding performance degradation. We tested the proposed scheme with two MIMO techniques: (2×2) SM-MLD and (2×1) Alamouti coding, and also with two values of the CP $L = 2$ and $L = 0$. Simulation results showed that we can almost obtain the same performance as OFDM in some configurations. However, FFT-FBMC remains slightly outperformed by OFDM because of the residual interference.

Chapter 6

Conclusions and Perspectives

6.1 Conclusions

This thesis has mainly considered the study of the association of filter-bank multicarrier (FBMC) systems to the spatial multiplexing (SM) scheme. The issue of applying a maximum likelihood (ML) detection in SM-FBMC system, caused by the presence of the inherent FBMC interference, was the essence and the main motivation of this dissertation.

After reviewing the state of the art, presented in chapter 2, about MIMO, OFDM and FBMC, we have addressed in chapter 3 the interference cancellation technique. We have mainly proposed three receiver structures dealing with the presence of interference. Those three schemes are: MMSE-ML where the interference is directly estimated via the MMSE equalizer, IC-ML and Rec-ML receivers where the whole interference is estimated via the previous tentative decisions, and the third one is PaIC/Viterbi receiver where only a part of the interference is estimated and canceled out. The remaining interference part is treated by a Viterbi detector. The difference between IC-ML and Rec-ML receivers lies in the manner how the tentative decisions are obtained; IC-ML makes use of the MMSE equalizer to get tentative decisions, whereas Rec-ML uses MMSE-ML as tentative detector. The proposed MMSE-ML receiver is the least complicated one among the receivers that we have proposed. However, it turned out that its BER performance is still far from the desired performance curve even though it outperforms MMSE equalizer. Regarding IC-ML performance, we have shown that it is slightly better than MMSE-ML performance but at the price of introducing some processing delay. Rec-ML receiver, which is in fact a combination of IC-ML with MMSE-ML, considerably improves the BER-performance. Nevertheless, Rec-ML performance does not yet reach the OFDM-ML one. However, we have shown that the performance gap between Rec-ML and OFDM-ML is removed when a simple convolutional coding is introduced. Finally, the third proposed scheme in chapter 3 is PaIC/Viterbi. The idea behind this proposal is to reduce the variance of the interference concerned by the cancellation. We have shown that to be able to remove the interference and

obtain the required performance, Viterbi detector has to match at least to the three largest coefficients of the transmultiplexer impulse response. Thus, it turned out that the Viterbi algorithm has to be performed over the frequency axis, *i.e.* on each subcarrier separately.

It followed from chapter 3 that one of the conditions to make the interference cancellation effective is that the interference variance must be small. In chapter 4, we have then proposed to modify the FBMC modulator by transmitting complex QAM symbols instead of OQAM ones. We have shown that in this manner we reduce the interference variance down to 18% when PHYDYAS filter is used, and to 40% when IOTA filter is used. Since this approach drops the orthogonality condition, we have first proposed an iterative interference cancellation (IIC) receiver for the SISO system. We have shown that when PHYDYAS filter is used, IIC performance converges to the optimum one with only 2 iterations. Whereas when IOTA filter is used, IIC suffers from the error propagation effect. This is due to the difference of the interference variance values of each filter. Regarding MIMO configuration, we have seen that the situation is the same as in SISO; IIC-ML receiver suffers from error propagation when IOTA filter is used, and converges to the optimum performance when PHYDYAS filter is used. As for PaIC/Viterbi receivers, we have pointed out the advantage of performing the Viterbi Algorithm over the frequency axis, which means that the Viterbi algorithm is performed once for each one multicarrier symbol. Further, we observed again that PaIC/Viterbi performs well with PHYDYAS filter, but it is not the case with IOTA filter even though the interference variance is very small in the case of PaIC/Viterbi-3. Indeed, in this specific case, the poor BER performance is due to the minimum spectrum distance that corresponds to error events with 3 or 4 error positions. Hence, in summary, the proposed receivers in FBMC/QAM do not perform well with IOTA filter, whereas they exhibit satisfactory performance with PHYDYAS filter. Therefore, the choice of the prototype filter is primordial for the proposed receivers in FBMC/QAM.

Finally, in chapter 5, we have introduced a novel FBMC scheme and a transmission strategy in order to avoid the inherent interference terms. At the transmitter, an IFFT is applied on the data of each subcarrier before being fed to the FBMC modulator. Then, at the receiver side, FFTs are applied at the FBMC demodulator output on each subcarrier. This proposed scheme, that we have called FFT-FBMC, transforms the FBMC system into an equivalent system formulated as OFDM regardless of some residual interference. These extra FFTs/IFFTs operations make the proposed FFT-FBMC more computationally complex than FBMC. But on the other hand, we have shown that any OFDM transmission technique can be straightforwardly performed to FFT-FBMC. Hence, we have tested this scheme with SM-ML system and Alamouti coding. We have seen that we can obtain almost the same performance as OFDM in some configurations. Finally, we have also pointed out the interesting spectral property of the FFT-FBMC signal, which is the fact that the out-of-band radiation is considerably limited compared to the classical FBMC.

6.2 Perspectives and future works

This thesis has addressed the issue of the association of FBMC modulation to spatial multiplexing systems. A number of interesting topics, based on the research issues studied in this thesis, could also be addressed. We hereunder provide perspectives and some possible

extensions to the work that have not been addressed in the thesis, and that could be studied as future works:

- Throughout this thesis, we have tried to cancel and get rid of the FBMC inherent interference. However, a full 2D-Viterbi algorithm in FBMC/OQAM and FBMC/QAM deserves to be investigated despite its high computational complexity. The works carried out in [88–91] can be considered as a starting point. However, besides the considered MIMO context, the receiver has to take into account the fact that the noise at the FBMC demodulator output is colored.

- All the proposed methods and receiver schemes make the simplifying assumption that CSI is fully known at the receiver. It would be of interest to study the influence of channel estimation errors on the performance of the proposed receivers, and adapt them to more realistic conditions.

- Moreover, throughout this dissertation, we have assumed that the channel is not highly frequency selective and invariant over some multicarrier symbols such that the FBMC channel equalization can be done with only one coefficient tap per subcarrier and almost preserve the real orthogonality condition. In case where the channel is highly frequency selective, more complex equalization methods, as the multi-tap per subcarrier equalization [118], have to be performed. Hence, it is wise to extend the developpement of the proposed receivers to the case of high frequency selective channel.

- We have shown in chapter 3 that there is a potential SNR gain for the FBMC/OQAM compared to OFDM in spatial multiplexing with ML detection. However, this performance is achievable only if the interference is perfectly removed. We have seen that when we introduce convolutional coding in the proposed receiver, we can obtain the same BER performance as OFDM. However, we have still a performance gap with respect to the Genie-Aided receiver. Hence, one can expect some BER performance improvements if more sophisticated coding techniques such as turbo-codes are introduced in the system.

- Although some works have been carried out on the combination of Alamouti coding with FBMC, this topic still remains an open issue. In this thesis, we have tested Alamouti scheme only in the proposed FFT-FBMC system. Since the issue is the presence of the inherent interference, Alamouti decoders based on interference estimation and cancellation techniques deserve to be studied and investigated.

Appendices

Appendix A

Relative Appendices in Chapter 3

A.1 Autocovariance expression of the noise in FBMC

According to (3.17), we have

$$\mathbb{E}\{\gamma^*(k',n')\gamma(k,n)\} = \mathbb{E}\left\{\sum_{m,m'} b^*[m]b[m]g[m-n'\frac{M}{2}]g[m'-n\frac{M}{2}]e^{j\frac{2\pi}{M}\left(k(\frac{D}{2}-m')-k'(\frac{D}{2}-m)\right)}e^{j(\phi_{k',n'}-\phi_{k,n})}\right\}. \tag{A.1}$$

Since the noise $b[m]$ is uncorrelated, then we can write

$$\mathbb{E}\{\gamma^*(k',n')\gamma(k,n)\} = \sigma^2\sum_m g[m-n'\frac{M}{2}]g[m-n\frac{M}{2}]e^{j\frac{2\pi}{M}(k-k')(\frac{D}{2}-m)}e^{j(\phi_{k',n'}-\phi_{k,n})}. \tag{A.2}$$

Substituting m by $m+n'\frac{M}{2}$, we obtain

$$\mathbb{E}\{\gamma^*(k',n')\gamma(k,n)\} = \sigma^2\sum_m g[m]g[m-(n-n')\frac{M}{2}]e^{j\frac{2\pi}{M}(k-k')(\frac{D}{2}-m)}e^{-j\pi n'(k-k')}e^{j(\phi_{k',n'}-\phi_{k,n})}.$$

Now using (2.98), we have $\phi_{k',n'}-\phi_{k,n} = \frac{\pi}{2}(k'-k+n'-n)+\pi(kn-k'n')$. Hence

$$\mathbb{E}\{\gamma^*(k',n')\gamma(k,n)\} = \underbrace{\sigma^2\sum_m g[m]g[m-(n-n')\frac{M}{2}]e^{j\frac{2\pi}{M}(k-k')(\frac{D}{2}-m)}e^{-j\frac{\pi}{2}(k-k'+n-n')}}_{=f(k-k',n-n')e^{-j\pi(n-n')(k-k')}}e^{j\pi(n-n')k}.$$

Finally, according to (3.16) we can write

$$\mathbb{E}\{\gamma^*(k',n')\gamma(k,n)\} = \sigma^2 f(k-k',n-n')e^{j\pi(n-n')k'}.$$

A.2 Derivation of the expressions of the filters W and C

In this appendix, we derive the expressions of the filters $\underline{W}$ and $\underline{C}$ satisfying both conditions (3.27) and (3.28).

Let us first develop the condition (3.27). Replacing $\epsilon(k,n)$ by its expression, we obtain for $(u,v) \neq (0,0)$

$$\mathbb{E}\{\mathfrak{U}^*(k,n)a(k-u,n-v) - \mathfrak{V}^*(k,n)a(k-u,n-v) - a^*(k,n)a(k-u,n-v)\} = 0. \quad \text{(A.3)}$$

The samples $a(k,n)$ are assumed to be independent. Hence, when $(u,v) \neq (0,0)$ we have $\mathbb{E}\{a^*(k,n)a(k-u,n-v)\} = 0$. Therefore, we can simplify the latter as:

$$\mathbb{E}\{\mathfrak{U}^*(k,n)a(k-u,n-v)\} = \mathbb{E}\{\mathfrak{V}^*(k,n)a(k-u,n-v)\}. \quad \forall (u,v) \neq (0,0) \quad \text{(A.4)}$$

According to (3.22) and (3.15), the left hand side term of (A.4) becomes

$$\begin{aligned}\mathbb{E}\{\mathfrak{U}^*(k,n)a(k-u,n-v)\} &= \mathbb{E}\left\{\sum_{y=-Y}^{Y}\sum_{z=-Z}^{Z} W^*(y,z)r^*(k-y,n-z)a(k-u,n-v)\right\} \\ &= \mathbb{E}\left\{\sum_{y=-Y}^{Y}\sum_{z=-Z}^{Z} W^*(y,z)\sum_{p=-P}^{P}\sum_{q=-Q}^{Q} a^*(k-y-p,n-z-q)a(k-u,n-v)f^*(p,q)(-1)^{q(k-y-p)}\right\}.\end{aligned} \quad \text{(A.5)}$$

Since $a(k,n)$ are statically independent, hence $\mathbb{E}\{a^*(k-y-p,n-z-q)a(k-u,n-v)\} = 0$ when $(p,q) \neq (u-y,v-z)$. Then,

$$\mathbb{E}\{\mathfrak{U}^*(k,n)a(k-u,n-v)\} = \sigma_a^2 \sum_{y=-Y}^{Y}\sum_{z=-Z}^{Z} W^*(y,z)f^*(u-y,v-z)(-1)^{(v-z)(k-u)}, \quad \text{(A.6)}$$

where $\sigma_a^2 = \mathbb{E}\{|a(k,n)|^2\}$ is the variance of the transmitted symbols.

Similarly, according to (3.23), the right hand side term of (A.4) is written

$$\begin{aligned}\mathbb{E}\{\mathfrak{V}^*(k,n)a(k-u,n-v)\} &= \mathbb{E}\left\{\sum_{u'=-U}^{U}\sum_{v'=-V}^{V} C^*(u',v')a^*(k-u',n-v')a(k-u,n-v)\right\} \\ &= \sigma_a^2 C^*(u,v).\end{aligned} \quad \text{(A.7)}$$

Therefore, from (A.6) and (A.7), we can express the first condition (A.4) as

$$C^*(u,v) = \sum_{y=-Y}^{Y}\sum_{z=-Z}^{Z} W^*(y,z)f^*(u-y,v-z)(-1)^{(v-z)(k-u)}, \quad \forall (u,v) \neq (0,0). \quad \text{(A.8)}$$

Regarding the second condition (3.28), we also replace $\epsilon(k,n)$ by its expression and we obtain

$$\mathbb{E}\{\mathfrak{U}^*(k,n)r(k-y,n-z) - \mathfrak{V}^*(k,n)r(k-y,n-z) - a^*(k,n)r(k-y,n-z)\} = 0. \quad \text{(A.9)}$$

Using (3.22), the first term is written

$$\mathbb{E}\{\mathfrak{U}^*(k,n)r(k-y,n-z)\} = \sum_{z'=-Z}^{Z}\sum_{y'=-Y}^{Y} W^*(y',z')\mathbb{E}\left\{r^*(k-y',n-z')r(k-y,n-z)\right\}. \quad \text{(A.10)}$$

According to (3.15), we have

$$\mathbb{E}\{r^*(k-y',n-z')r(k-y,n-z)\} = \mathbb{E}\{\gamma^*(k-y',n-z')\gamma(k-y,n-z)\} + \sum_{p=-P}^{P}\sum_{q=-Q}^{Q}\sum_{p'=-P}^{P}\sum_{q'=-Q}^{Q}\mathbb{E}\{a^*(k-y'-p,n-z'-q)a(k-y-p',n-z-q')\} \times f^*(p,q)f(p',q')(-1)^{q(k-y'-p)}(-1)^{q'(k-y-p')}. \quad (A.11)$$

Since $a(k,n)$ are statically independent, we can write

$$\mathbb{E}\{r^*(k-y',n-z')r(k-y,n-z)\} = \sigma_a^2\sum_{p=-P}^{P}\sum_{q=-Q}^{Q} f^*(p,q)f(p+y'-y,q+z'-z)(-1)^{(z-z')(k-y'-p)} + \mathbb{E}\{\gamma^*(k-y',n-z')\gamma(k-y,n-z)\}. \quad (A.12)$$

Then, we replace this expression in (A.10) and it yields

$$\mathbb{E}\{\mathfrak{U}^*(k,n)r(k-y,n-z)\} = \sum_{z'=-Z}^{Z}\sum_{y'=-Y}^{Y} W^*(y',z')\mathbb{E}\{\gamma^*(k-y',n-z')\gamma(k-y,n-z)\} + \sigma_a^2\sum_{z'=-Z}^{Z}\sum_{y'=-Y}^{Y} W^*(y',z')\sum_{p=-P}^{P}\sum_{q=-Q}^{Q} f^*(p,q)f(p+y'-y,q+z-z')(-1)^{(z'-z)(k-y'-p)} \quad (A.13)$$

Regarding the second term of (A.9), we have

$$\mathbb{E}\{\mathfrak{V}^*(k,n)r(k-y,n-z)\} = \sum_{u=-U}^{U}\sum_{v=-V}^{V} C^*(u,v)\mathbb{E}\{a^*(k-u,n-v)r(k-y,n-z)\}. \quad (A.14)$$

According to (3.15) we have

$$\mathbb{E}\{a^*(k-u,n-v)r(k-y,n-z)\} = \mathbb{E}\{a^*(k-u,n-v)\gamma(k,n)\} + \sum_{p=-P}^{P}\sum_{q=-Q}^{Q}\mathbb{E}\{a^*(k-u,n-v)a(k-y-p,n-z-q)\}f(p,q)(-1)^{q(k-y-p)}. \quad (A.15)$$

Since $a(k,n)$ and $\gamma(k,n)$ are statically independent and $a(k,n)$ samples are uncorrelated, we can write

$$\mathbb{E}\{a^*(k-u,n-v)r(k-y,n-z)\} = \sigma_a^2 f(u-y,v-z)(-1)^{(v-z)(k-u)}. \quad (A.16)$$

Then, equation (A.14) becomes

$$\mathbb{E}\{\mathfrak{V}^*(k,n)r(k-y,n-z)\} = \sigma_a^2\sum_{u=-U}^{U}\sum_{v=-V}^{V} C^*(u,v)f(u-y,v-z)(-1)^{(v-z)(k-u)}. \quad (A.17)$$

The third term of (A.9) can be obtained from (A.16) and setting $(u,v)=(0,0)$, hence

$$\mathbb{E}\{a^*(k,n)r(k-y,n-z)\} = \sigma_a^2 f(-y,-z)(-1)^{-zk}. \quad (A.18)$$

Therefore, according to (A.13), (A.17) and (A.18), we can rewrite (A.9) as

$$\begin{aligned}
&\sigma_a^2 \sum_{z'=-Z}^{Z} \sum_{y'=-Y}^{Y} W^*(y',z') \sum_{p=-P}^{P} \sum_{q=-Q}^{Q} f^*(p,q) f(p+y'-y, q+z-z')(-1)^{(z'-z)(k-y'-p)} \\
&+ \sum_{z'=-Z}^{Z} \sum_{y'=-Y}^{Y} W^*(y',z') \mathbb{E}\{\gamma^*(k-y', n-z')\gamma(k-y, n-z)\} = \sigma_a^2 f(-y,-z)(-1)^{-zk} \\
&+ \sigma_a^2 \sum_{u=-U}^{U} \sum_{v=-V}^{V} C^*(u,v) f(u-y, v-z)(-1)^{(v-z)(k-u)}. \qquad \text{(A.19)}
\end{aligned}$$

Appendix B

Relative Appendices in Chapter 5

B.1 Independence of σ_s^2 on M

Let us calculate the mean of $A(m, N, L)$ over one period, thus we obtain:

$$\overline{A}(N,L) = \frac{2}{N(N+L)} \sum_{p} \sum_{(n,n')\in B_p^2} e^{j\frac{3\pi}{2}\delta n} \sum_{l=0}^{\frac{N}{2}-1} e^{j\frac{2\pi l \delta n}{N}} \underbrace{\sum_{m=0}^{\frac{M}{2}(N+L)-1} g[m - n\frac{M}{2}]g[m - n'\frac{M}{2}]}_{I_{n,n'}} \tag{B.1}$$

The term $I_{n,n'}$ is certainly zero when

$$g[m - n\frac{M}{2}]g[m - n'\frac{M}{2}] = 0$$

between $m = 0$ and $m = \frac{M}{2}(N + L) - 1$.

Since $g[m] = 0$ for $m \notin \{1, ..., KM - 1\}$, then $I_{n,n'} = 0$ when $(n, n') \notin \Psi = \{1 - 2K, ..., N + L - 1\}^2$.

Ψ overlaps only with B_0 and B_1, and the intersection is $C_1 \cup B_1^2$, where $C_1 = \{1 - 2K, ..., -1\}^2$. Let $C_3 = \{N + L - 2K + 1, ..., N + L - 1\}^2$ be a subset of B_1^2, and C_2 be the relative complement of C_3 in B_1^2, that is, $C_2 = B_1^2 \backslash C_3 = (\{1, ..., N + L - 2K\} \times B_1) \cup (B_1 \times \{1, ..., N + L - 2K\})$.

When $(n, n') \in C_2$, it means that $n \in \{1, ..., N + L - 2K\}$ or $n' \in \{1, ..., N + L - 2K\}$. As a consequence, the term $g[m - n\frac{M}{2}]g[m - n'\frac{M}{2}]$ is zero beyond the summation set $\{0, ..., \frac{M}{2}(N + L) - 1\}$. Hence, $I_{n,n}$ equals the FBMC coefficient $f_0^{(k)}(\Delta n)$ to within a phase rotation. Then, $I_{n,n}$ is a constant independent from M when $(n, n') \in C_2$.

When $(n, n') \in C_1$, we can show that the term

$$c_1 = \sum_{(n,n')\in C_1} e^{j\frac{3\pi}{2}\delta n} \sum_{l=0}^{\frac{N}{2}-1} e^{j\frac{2\pi l \delta n}{N}} I_{n,n'}$$

is independent from M. Let $n_1 = -2K - n'$ and $n_1' = -2K - n$. We have $(n, n') \in C_1 \Longleftrightarrow (n_1, n_1') \in C_1$. Because of the prototype filter symmetry ($g[m] = g[KM - m - 1]$), $I_{n_1,n_1'}$ is written as

$$\begin{aligned} I_{n_1,n_1'} &= \sum_{m=0}^{\frac{M}{2}(N+L)-1} g[m + n\frac{M}{2} + KM]g[m + n'\frac{M}{2} + KM] \\ &= \sum_{m=0}^{\frac{M}{2}(N+L)-1} g[-m - n\frac{M}{2} - 1]g[-m - n'\frac{M}{2} - 1] \\ &= \sum_{m=-\frac{M}{2}(N+L)}^{-1} g[m - n\frac{M}{2}]g[m - n'\frac{M}{2}]. \end{aligned}$$

Hence,

$$I_{n,n'} + I_{n_1,n_1'} = \sum_{m=-\frac{M}{2}(N+L)}^{\frac{M}{2}(N+L)-1} g[m - n\frac{M}{2}]g[m - n'\frac{M}{2}],$$

and it is independent from M because $g[m - n\frac{M}{2}]g[m - n'\frac{M}{2}] = 0$ for all $|m| \geq \frac{M}{2}(N + L)$ when $(n, n') \in C_1$.

Now, since $\delta n_1 = n_1' - n_1 = n' - n = \delta n$, we can write

$$\begin{aligned} c_1 &= \sum_{(n,n')\in C_1} e^{j\frac{3\pi}{2}\delta n} \sum_{l=0}^{\frac{N}{2}-1} e^{j\frac{2\pi l\delta n}{N}} I_{n,n'} \\ &= \frac{1}{2} \sum_{(n,n')\in C_1} e^{j\frac{3\pi}{2}\delta n} \sum_{l=0}^{\frac{N}{2}-1} e^{j\frac{2\pi l\delta n}{N}} (I_{n,n'} + I_{n_1,n_1'}). \end{aligned}$$

Therefore, c_1 is independent from M.

As for the last term

$$c_3 = \sum_{(n,n')\in C_3} e^{j\frac{3\pi}{2}\delta n} \sum_{l=0}^{\frac{N}{2}-1} e^{j\frac{2\pi l\delta n}{N}} I_{n,n'},$$

we proceed in the same manner by considering $n_2 = 2(N + L - K) - n'$ and $n_2' = 2(N + L - K) - n$. We will also find that $I_{n,n'} + I_{n_2,n_2'}$ is independent from M when $(n, n') \in C_3$.

Finally, we have shown that all the three terms corresponding to the summation sets C_1, C_2, and C_3 are independent from M. Then, $\overline{A}(N, L)$ is also independent from M.

Bibliography

[1] H. Atarashi, N. Maeda, S. Abeta, and M. Sawahashi, "Broadband packet wireless access based on VSF-OFCDM and MC/DS-CDMA," in *Personal, Indoor and Mobile Radio Communications, 2002. The 13th IEEE International Symposium on*, sept. 2002, vol. 3, pp. 992 – 997 vol.3.

[2] K. Fazel and S. Kaiser, *Multi-Carrier and Spread Spectrum Systems: From OFDM and MC-CDMA to LTE and WiMax*, John Wiley & Sons, 2009.

[3] K. Etemad and M.-Y. Lai, *WiMAX Technology and Network Evolution*, John Wiley, 2011.

[4] WiMax Forum, *Mobile System Profile*, release 1.0 approved specification, Revision 1.5.0, Nov. 2007.

[5] 3GPP TS 36.211, *Evolved Universal Terrestrial Radio Access (E-UTRA); Physical Channels and Modulation (Release 8)*.

[6] T. Hidalgo Stitz, *Filter Bank Techniques for the Physical Layer in Wireless Communications*, Ph.D. thesis, Tampere University of Technology, 2010.

[7] Y. Medjahdi, M. Terre, D. Le Ruyet, D. Roviras, and A. Dziri, "Performance Analysis in the Downlink of Asynchronous OFDM/FBMC Based Multi-Cellular Networks," *Wireless Communications, IEEE Transactions on*, vol. 10, no. 8, pp. 2630 –2639, august 2011.

[8] Y. Medjahdi, M. Terre, D. Le Ruyet, D. Roviras, J.A. Nossek, and L. Baltar, "Inter-cell interference analysis for OFDM/FBMC systems," in *Signal Processing Advances in Wireless Communications, 2009. SPAWC '09. IEEE 10th Workshop on*, june 2009, pp. 598 –602.

[9] B. Saltzberg, "Performance of an Efficient Parallel Data Transmission System," *Communication Technology, IEEE Transactions on*, vol. 15, no. 6, pp. 805 –811, december 1967.

[10] P. Siohan, C. Siclet, and N. Lacaille, "Analysis and design of OFDM/OQAM systems based on filterbank theory ," *Signal Processing, IEEE Transactions on*, vol. 50, no. 5, pp. 1170 –1183, may 2002.

[11] M. El Tabach, J.-P. Javaudin, and M. Helard, "Spatial Data Multiplexing Over OFDM/OQAM Modulations," in *Communications, 2007. ICC '07. IEEE International Conference on*, june 2007, pp. 4201 –4206.

[12] M. Renfors, T. Ihalainen, and T.H. Stitz, "A block-Alamouti scheme for filter bank based multicarrier transmission," in *Wireless Conference (EW), 2010 European*, april 2010, pp. 1031 –1037.

[13] Andrea Goldsmith, *Wireless Communications*, Cambridge University Press, New York, NY, USA, 2005.

[14] A. Peled and A. Ruiz, "Frequency domain data transmission using reduced computational complexity algorithms," in *Acoustics, Speech, and Signal Processing, IEEE International Conference on ICASSP '80.*, apr 1980, vol. 5, pp. 964 – 967.

[15] H. Schulze and C. Lüders, *Theory and Applications of OFDM and CDMA: Wideband Wireless Communications*, John Wiley, 2005.

[16] C.R. Rao and S.K. Mitra, *Generalized inverse of matrices and its applications*, Wiley series in probability and mathematical statistics: Applied probability and statistics. Wiley, 1971.

[17] Crislin Lélé, *OFDM/OQAM : Méthodes d'Estimation de Canal, et Combinaison avec l'Accès Multiple CDMA ou les Systèmes Multi-Antennes*, Ph.D. thesis, Conservatoire National des Arts et Métiers, Paris, France, 2008.

[18] Xu Zhu and R.D. Murch, "Performance analysis of maximum likelihood detection in a MIMO antenna system," *Communications, IEEE Transactions on*, vol. 50, no. 2, pp. 187 –191, feb 2002.

[19] R. Zakaria, D. Le Ruyet, and Y. Medjahdi, "On ISI cancellation in MIMO-ML detection using FBMC/QAM modulation," in *Wireless Communication Systems (ISWCS), 2012 International Symposium on*, aug. 2012, pp. 949 –953.

[20] Y. Zhao and S.-G. Haggman, "Sensitivity to Doppler shift and carrier frequency errors in OFDM systems-the consequences and solutions," in *Vehicular Technology Conference, 1996. 'Mobile Technology for the Human Race'., IEEE 46th*, apr-1 may 1996, vol. 3, pp. 1564 –1568 vol.3.

[21] J. Armstrong, "Analysis of new and existing methods of reducing intercarrier interference due to carrier frequency offset in OFDM," *Communications, IEEE Transactions on*, vol. 47, no. 3, pp. 365 –369, mar 1999.

[22] Y. Medjahdi, M. Terre, D. Le Ruyet, D. Roviras, and A. Dziri, "The Impact of Timing Synchronization Errors on the Performance of OFDM/FBMC Systems," in *Communications (ICC), 2011 IEEE International Conference on*, june 2011, pp. 1 –5.

[23] G. Cherubini, E. Eleftheriou, and S. Olcer, "Filtered multitone modulation for VDSL," in *Global Telecommunications Conference, 1999. GLOBECOM '99*, 1999, vol. 2, pp. 1139 –1144 vol.2.

[24] G. Cherubini, E. Eleftheriou, S. Oker, and J.M. Cioffi, "Filter bank modulation techniques for very high speed digital subscriber lines," *Communications Magazine, IEEE*, vol. 38, no. 5, pp. 98 –104, may 2000.

[25] G. Cherubini, E. Eleftheriou, and S. Olcer, "Filtered multitone modulation for very high-speed digital subscriber lines," *Selected Areas in Communications, IEEE Journal on*, vol. 20, no. 5, pp. 1016 –1028, jun 2002.

[26] Behrouz Farhang-Boroujeny and Chung Him Yuen, "Cosine modulated and offset QAM filter bank multicarrier techniques: a continuous-time prospect," *EURASIP J. Adv. Signal Process*, vol. 2010, pp. 6:1–6:11, Jan. 2010.

[27] R. W. Chang, "High-speed multichannel data transmission with bandlimited orthogonal signals," *Bell Syst. Tech. J.*, vol. 45, pp. 1775 –1796, Dec. 1966.

[28] Lekun Lin and Behrouz Farhang-Boroujeny, "Cosine-modulated multitone for very-high-speed digital subscriber lines," *EURASIP J. Appl. Signal Process.*, vol. 2006, pp. 79–79, Jan. 2006.

[29] M.G. Bellanger, "Specification and design of a prototype filter for filter bank based multicarrier transmission," in *Acoustics, Speech, and Signal Processing, 2001. Proceedings. (ICASSP '01). 2001 IEEE International Conference on*, 2001, vol. 4, pp. 2417 –2420 vol.4.

[30] B. Hirosaki, "An Orthogonally Multiplexed QAM System Using the Discrete Fourier Transform," *Communications, IEEE Transactions on*, vol. 29, no. 7, pp. 982 – 989, jul 1981.

[31] Y. Medjahdi, M. Terre, D. Le Ruyet, and D. Roviras, "Asynchronous OFDM/FBMC interference analysis in selective channels," in *Personal Indoor and Mobile Radio Communications (PIMRC), 2010 IEEE 21st International Symposium on*, sept. 2010, pp. 538 –542.

[32] Y. Medjahdi, M. Terre, D. Le Ruyet, and D. Roviras, "On spectral efficiency of asynchronous OFDM/FBMC based cellular networks," in *Personal Indoor and Mobile Radio Communications (PIMRC), 2011 IEEE 22nd International Symposium on*, sept. 2011, pp. 1381 –1385.

[33] D. Gesbert, M. Shafi, Da shan Shiu, P.J. Smith, and A. Naguib, "From theory to practice: an overview of MIMO space-time coded wireless systems," *Selected Areas in Communications, IEEE Journal on*, vol. 21, no. 3, pp. 281 – 302, apr 2003.

[34] S.M. Alamouti, "A simple transmit diversity technique for wireless communications," *Selected Areas in Communications, IEEE Journal on*, vol. 16, no. 8, pp. 1451 –1458, oct 1998.

[35] Chrislin Lélé, Pierre Siohan, and Rodolphe Legouable, "The Alamouti Scheme with CDMA-OFDM/OQAM.," *EURASIP J. Adv. Sig. Proc.*, vol. 2010, 2010.

[36] Hao Lin, C. Lele, and P. Siohan, "A pseudo alamouti transceiver design for OFDM/OQAM modulation with cyclic prefix," in *Signal Processing Advances in Wireless Communications, 2009. SPAWC '09. IEEE 10th Workshop on*, june 2009, pp. 300 –304.

[37] John G. Proakis, *Digital Communications*, McGraw-Hill, 1995.

[38] J. Winters, "On the Capacity of Radio Communication Systems with Diversity in a Rayleigh Fading Environment," *Selected Areas in Communications, IEEE Journal on*, vol. 5, no. 5, pp. 871 – 878, jun 1987.

[39] Gerard J. Foschini, "Layered space-time architecture for wireless communication in a fading environment when using multi-element antennas," *Bell Labs Technical Journal*, vol. 1, no. 2, pp. 41–59, 1996.

[40] G. J. Foschini and M. J. Gans, "On limits of wireless communications in a fading environment when using multiple antennas," *Wireless Personal Communications*, vol. 6, pp. 311–335, 1998.

[41] Emre Telatar, "Capacity of Multi-antenna Gaussian Channels," *European Transactions on Telecommunications*, vol. 10, no. 6, pp. 585–595, 1999.

[42] David Tse and Pramod Viswanath, *Fundamentals of Wireless Communication*, Cambridge University Press, New York, NY, USA, 2005.

[43] ETSI, "Frame structure channel coding and modulation for a second generation digital terrestrial television broadcasting system (DVB-T2)," *European standard, DVB document A122*, June 2008.

[44] V. Tarokh, H. Jafarkhani, and A.R. Calderbank, "Space-time block codes from orthogonal designs," *Information Theory, IEEE Transactions on*, vol. 45, no. 5, pp. 1456 –1467, jul 1999.

[45] G. Ganesan and P. Stoica, "Space-time block codes: a maximum SNR approach," *Information Theory, IEEE Transactions on*, vol. 47, no. 4, pp. 1650 –1656, may 2001.

[46] Xue-Bin Liang, "Orthogonal designs with maximal rates," *Information Theory, IEEE Transactions on*, vol. 49, no. 10, pp. 2468 – 2503, oct. 2003.

[47] M.O. Damen, K. Abed-Meraim, and J.-C. Belfiore, "Diagonal algebraic space-time block codes," *Information Theory, IEEE Transactions on*, vol. 48, no. 3, pp. 628 –636, mar 2002.

[48] M.O. Damen and N.C. Beaulieu, "On diagonal algebraic space-time block codes," *Communications, IEEE Transactions on*, vol. 51, no. 6, pp. 911 – 919, june 2003.

[49] J. Boutros and E. Viterbo, "Signal space diversity: a power- and bandwidth-efficient diversity technique for the Rayleigh fading channel," *Information Theory, IEEE Transactions on*, vol. 44, no. 4, pp. 1453 –1467, jul 1998.

[50] H. Jafarkhani, "A quasi-orthogonal space-time block code," *Communications, IEEE Transactions on*, vol. 49, no. 1, pp. 1 –4, jan 2001.

[51] O. Tirkkonen, A. Boariu, and A. Hottinen, "Minimal non-orthogonality rate 1 space-time block code for 3+ Tx antennas," in *Spread Spectrum Techniques and Applications, 2000 IEEE Sixth International Symposium on*, 2000, vol. 2, pp. 429 –432 vol.2.

[52] C.B. Papadias and G.J. Foschini, "Capacity-approaching space-time codes for systems employing four transmitter antennas," *Information Theory, IEEE Transactions on*, vol. 49, no. 3, pp. 726 – 732, mar 2003.

[53] N. Sharma and C.B. Papadias, "Improved quasi-orthogonal codes through constellation rotation," *Communications, IEEE Transactions on*, vol. 51, no. 3, pp. 332 – 335, march 2003.

[54] Weifeng Su and Xiang-Gen Xia, "Signal constellations for quasi-orthogonal space-time block codes with full diversity," *Information Theory, IEEE Transactions on*, vol. 50, no. 10, pp. 2331 – 2347, oct. 2004.

[55] Dung Ngoc Dao, Chau Yuen, C. Tellambura, Yong Liang Guan, Tjeng Thiang Tjhung, Chau Yuen, Yong Liang Guan, and Tjeng Thiang Tjhung, "Four-Group Decodable Space-Time Block Codes," *Signal Processing, IEEE Transactions on*, vol. 56, no. 1, pp. 424 –430, jan. 2008.

[56] Yi Jiang, M.K. Varanasi, and Jian Li, "Performance Analysis of ZF and MMSE Equalizers for MIMO Systems: An In-Depth Study of the High SNR Regime," *Information Theory, IEEE Transactions on*, vol. 57, no. 4, pp. 2008 –2026, april 2011.

[57] R. van Nee, A. van Zelst, and G. Awater, "Maximum likelihood decoding in a space division multiplexing system," in *Vehicular Technology Conference Proceedings, 2000. VTC 2000-Spring Tokyo. 2000 IEEE 51st*, 2000, vol. 1, pp. 6 –10 vol.1.

[58] B. Hassibi and H. Vikalo, "On the sphere-decoding algorithm I. Expected complexity," *Signal Processing, IEEE Transactions on*, vol. 53, no. 8, pp. 2806 – 2818, aug. 2005.

[59] E. Viterbo and J. Boutros, "A universal lattice code decoder for fading channels," *Information Theory, IEEE Transactions on*, vol. 45, no. 5, pp. 1639 –1642, jul 1999.

[60] Xu Zhu and R.D. Murch, "Performance analysis of maximum likelihood detection in a MIMO antenna system," *Communications, IEEE Transactions on*, vol. 50, no. 2, pp. 187 –191, feb 2002.

[61] M. Kiessling, J. Speidel, N. Geng, and M. Reinhardt, "Performance analysis of MIMO maximum likelihood receivers with channel correlation, colored Gaussian noise, and linear prefiltering," in *Communications, 2003. ICC '03. IEEE International Conference on*, may 2003, vol. 5, pp. 3026 – 3030 vol.5.

[62] Wei Peng, Shaodan Ma, Tung-Sang Ng, and Jiangzhou Wang, "A novel analytical method for maximum likelihood detection in MIMO multiplexing systems," *Communications, IEEE Transactions on*, vol. 57, no. 8, pp. 2264 –2268, aug. 2009.

[63] V. Tarokh, N. Seshadri, and A.R. Calderbank, "Space-time codes for high data rate wireless communication: performance criterion and code construction," *Information Theory, IEEE Transactions on*, vol. 44, no. 2, pp. 744 –765, mar 1998.

[64] Lizhong Zheng and D.N.C. Tse, "Diversity and multiplexing: a fundamental tradeoff in multiple-antenna channels," *Information Theory, IEEE Transactions on*, vol. 49, no. 5, pp. 1073 – 1096, may 2003.

[65] H. El Gamal, G. Caire, and M.O. Damen, "Lattice coding and decoding achieve the optimal diversity-multiplexing tradeoff of MIMO channels," *Information Theory, IEEE Transactions on*, vol. 50, no. 6, pp. 968 –985, june 2004.

[66] H. Yao and G.W. Wornell, "Structured space-time block codes with optimal diversity-multiplexing tradeoff and minimum delay," in *Global Telecommunications Conference, 2003. GLOBECOM '03. IEEE*, dec. 2003, vol. 4, pp. 1941 – 1945 vol.4.

[67] Jr. Cimini, L., "Analysis and simulation of a digital mobile channel using orthogonal frequency division multiplexing," *Communications, IEEE Transactions on*, vol. 33, no. 7, pp. 665 – 675, jul 1985.

[68] S. Weinstein and P. Ebert, "Data transmission by frequency-division multiplexing using the discrete fourier transform," *Communication Technology, IEEE Transactions on*, vol. 19, no. 5, pp. 628 –634, october 1971.

[69] Alan V. Oppenheim, Ronald W. Schafer, and John R. Buck, *Discrete-time signal processing (2nd ed.)*, Prentice-Hall, Inc., Upper Saddle River, NJ, USA, 1999.

[70] James Cooley and John Tukey, "An algorithm for the machine calculation of complex fourier series," *Mathematics of Computation*, vol. 19, no. 90, pp. 297–301, 1965.

[71] B. Muquet, Zhengdao Wang, G.B. Giannakis, M. de Courville, and P. Duhamel, "Cyclic prefixing or zero padding for wireless multicarrier transmissions?," *Communications, IEEE Transactions on*, vol. 50, no. 12, pp. 2136 – 2148, dec 2002.

[72] B. Farhang-Boroujeny, "OFDM Versus Filter Bank Multicarrier," *Signal Processing Magazine, IEEE*, vol. 28, no. 3, pp. 92 –112, may 2011.

[73] T.A. Weiss and F.K. Jondral, "Spectrum pooling: an innovative strategy for the enhancement of spectrum efficiency," *Communications Magazine, IEEE*, vol. 42, no. 3, pp. S8 – 14, mar 2004.

[74] H.G. Feichtinger and T. Strohmer, *Gabor analysis and algorithms: theory and applications*, Applied and numerical harmonic analysis. Birkhäuser, 1998.

[75] M. Bellanger and J. Daguet, "TDM-FDM Transmultiplexer: Digital Polyphase and FFT," *Communications, IEEE Transactions on*, vol. 22, no. 9, pp. 1199 – 1205, sep 1974.

[76] M. Bellanger and PHYDYAS team, "FBMC physical layer: a primer," *website: www.ict-phydyas.org*, 2010 June.

[77] P. Chevillat and G. Ungerboeck, "Optimum FIR Transmitter and Receiver Filters for Data Transmission Over Band-Limited Channels," *Communications, IEEE Transactions on*, vol. 30, no. 8, pp. 1909 – 1915, aug 1982.

[78] B. Boashash, *Time frequency signal analysis and processing: a comprehensive reference*, Elsevier, 2003.

[79] M. Alard, "Construction of a multicarrier signal," *Patent WO 96/35278*, 1996.

[80] B. Le Floch, M. Alard, and C. Berrou, "Coded orthogonal frequency division multiplex," *Proceedings of the IEEE*, vol. 83, no. 6, pp. 982 –996, jun 1995.

[81] P. Siohan and C. Roche, "Cosine-modulated filterbanks based on extended Gaussian functions ," *Signal Processing, IEEE Transactions on*, vol. 48, no. 11, pp. 3052 –3061, nov 2000.

[82] Ari Viholainen, Maurice Bellanger, and Mathieu Huchard, "Prototype filter and structure optimization," *website: www.ict-phydyas.org: Document D5.1 deliverable*, 2009 January.

[83] T. W. Parks and C. S. Burrus, *Digital filter design*, Wiley-Interscience, New York, NY, USA, 1987.

[84] Ari Viholainen, Tero Ihalainen, Tobias Hidalgo Stitz, Markku Renfors, and Maurice Bellanger, "Prototype filter design for filter bank based multicarrier transmission," in *17th European Signal Processing Conference (EUSIPCO 2009)*, August 2009, pp. 1359–1363.

[85] L.L. Hanzo and T. Keller, *OFDM and MC-CDMA: A Primer*, John Wiley & Sons, 2007.

[86] Hao Lin and P. Siohan, "A new transceiver system for the OFDM/OQAM modulation with Cyclic Prefix," in *Personal, Indoor and Mobile Radio Communications, 2008. PIMRC 2008. IEEE 19th International Symposium on*, sept. 2008, pp. 1 –5.

[87] PHYDYAS team, "MIMO Techniques and Beamforming," *website: www.ict-phydyas.org: Document D4.2 deliverable*, 2010 Feb.

[88] W.M.J. Coene, D.M. Bruls, A.H.J. Immink, A.M. van der Lee, A.P. Hekstra, J. Riani, S. van Beneden, M. Ciacci, J.W.M. Bergmans, and M. Furuki, "Two-dimensional optical storage," in *Acoustics, Speech, and Signal Processing, 2005. Proceedings. (ICASSP '05). IEEE International Conference on*, march 2005, vol. 5, pp. v/749 – v/752 Vol. 5.

[89] A.H.J. Immink, W.M.J. Coene, A.M. van der Lee, C. Busch, A.P. Hekstra, J.W.M. Bergmans, J. Riani, S.J.L.V. Beneden, and T. Conway, "Signal processing and coding for two-dimensional optical storage," in *Global Telecommunications Conference, 2003. GLOBECOM '03. IEEE*, dec. 2003, vol. 7, pp. 3904 – 3908 vol.7.

[90] S. Van Beneden, J. Riani, and J.W.M. Bergmans, "Cancellation of Linear Intersymbol Interference for Two-Dimensional Storage Systems," in *Communications, 2006. ICC '06. IEEE International Conference on*, june 2006, vol. 7, pp. 3173 –3178.

[91] Brian M. Kurkoski, "Towards Efficient Detection of Two-Dimensional Intersymbol Interference Channels," *IEICE Trans. Fundam. Electron. Commun. Comput. Sci.*, vol. E91-A, no. 10, pp. 2696–2703, Oct. 2008.

[92] A. P. Hekstra, W. M. J. Coene, and C. Baggen, "Iterative stripewise trellis-base symbol detection method and device," *Patent Application EPO02292937.6, IB2003/005208*, Nov. 2003.

[93] J.F. Heanue, K. Gürkan, and L. Hesselink, "Decision feedback Viterbi detector for page-access optical memories," 1998.

[94] Li Huang, G. Mathew, and Tow Chong Chong, "Reduced complexity Viterbi detection for two-dimensional optical recording," *Consumer Electronics, IEEE Transactions on*, vol. 51, no. 1, pp. 123 – 129, feb. 2005.

[95] G. D. Forney, "The Viterbi algorithm," *Proceedings of the IEEE*, vol. 61, no. 3, pp. 268–278, Mar. 1973.

[96] B.A. Bjerke and J.G. Proakis, "Multiple-antenna diversity techniques for transmission over fading channels," in *Wireless Communications and Networking Conference, 1999. WCNC. 1999 IEEE*, 1999, pp. 1038 –1042 vol.3.

[97] ITU-R M.1225, "Guidelines for evaluations of radio transmission technologies for IMT-2000," 1997.

[98] J.G. Proakis, "Adaptive nonlinear filtering techniques for data transmission," in *Adaptive Processes (9th) Decision and Control, 1970. 1970 IEEE Symposium on*, dec. 1970, vol. 9, p. 152.

[99] A Gersho and T. L Lim, "Adaptive cancellation of intersymbol interference for data transmission," *Bell System Technical Journal*, vol. 60, pp. 1997–2021, Nov 1981.

[100] Namshik Kim, Yusung Lee, and H. Park, "Performance Analysis of MIMO System with Linear MMSE Receiver," *Wireless Communications, IEEE Transactions on*, vol. 7, no. 11, pp. 4474 –4478, november 2008.

[101] Xiaodong Wang and H.V. Poor, "Iterative (turbo) soft interference cancellation and decoding for coded CDMA," *Communications, IEEE Transactions on*, vol. 47, no. 7, pp. 1046 –1061, jul 1999.

[102] B. Steingrimsson, Zhi-Quan Luo, and Kon Max Wong, "Soft quasi-maximum-likelihood detection for multiple-antenna wireless channels," *Signal Processing, IEEE Transactions on*, vol. 51, no. 11, pp. 2710 – 2719, nov 2003.

[103] B.M. Hochwald and S. ten Brink, "Achieving near-capacity on a multiple-antenna channel," *Communications, IEEE Transactions on*, vol. 51, no. 3, pp. 389 – 399, march 2003.

[104] IEEE 802.16e 2005, "IEEE Standard for Local and Metropolitan Area Networks Part 16," *3GPP*, 2006.

[105] R. Zakaria and D. Le Ruyet, "On spatial data multiplexing over coded filter-bank multicarrier with ML detection," in *Personal Indoor and Mobile Radio Communications (PIMRC), 2011 IEEE 22nd International Symposium on*, sept. 2011, pp. 1391 –1395.

[106] O.E. Agazzi and N. Seshadri, "On the use of tentative decisions to cancel intersymbol interference and nonlinear distortion (with application to magnetic recording channels)," *Information Theory, IEEE Transactions on*, vol. 43, no. 2, pp. 394 –408, mar 1997.

[107] R. Zakaria and D. Le Ruyet, "Partial ISI cancellation with viterbi detection in MIMO filter-bank multicarrier modulation," in *Wireless Communication Systems (ISWCS), 2011 8th International Symposium on*, nov. 2011, pp. 322 –326.

[108] C. Lele, P. Siohan, R. Legouable, and J.-P. Javaudin, "Preamble-based channel estimation techniques for ofdm/oqam over the powerline," in *Power Line Communications and Its Applications, 2007. ISPLC '07. IEEE International Symposium on*, march 2007, pp. 59 –64.

[109] J. Anderson and S. Mohan, "Sequential Coding Algorithms: A Survey and Cost Analysis," *Communications, IEEE Transactions on*, vol. 32, no. 2, pp. 169 – 176, feb 1984.

[110] R. Zakaria and D. Le Ruyet, "A novel FBMC scheme for Spatial Multiplexing with Maximum Likelihood detection," in *Wireless Communication Systems (ISWCS), 2010 7th International Symposium on*, sept. 2010, pp. 461 –465.

[111] R. Zakaria and D. Le Ruyet, "A Novel Filter-Bank Multicarrier Scheme to Mitigate the Intrinsic Interference: Application to MIMO Systems," *Wireless Communications, IEEE Transactions on*, vol. 11, no. 3, pp. 1112 –1123, march 2012.

[112] L.W. Couch, *Digital & Analog Communication Systems*, Prentice Hall, 2012.

[113] William A. Gardner, "The spectral correlation theory of cyclostationary time-series," *Signal Processing*, vol. 11, no. 1, pp. 13–36, July 1986.

[114] Shaoping Chen and Cuitao Zhu, "ICI and ISI analysis and mitigation for OFDM systems with insufficient cyclic prefix in time-varying channels," *Consumer Electronics, IEEE Transactions on*, vol. 50, no. 1, pp. 78 – 83, feb. 2004.

[115] D. Skinner, "Pruning the decimation in-time FFT algorithm," *Acoustics, Speech and Signal Processing, IEEE Transactions on*, vol. 24, no. 2, pp. 193 – 194, apr 1976.

[116] J. Markel, "FFT pruning," *Audio and Electroacoustics, IEEE Transactions on*, vol. 19, no. 4, pp. 305 – 311, dec 1971.

[117] R. Zakaria, D. Le Ruyet, and M. Bellanger, "Maximum likelihood detection in spatial multiplexing with FBMC," in *Wireless Conference (EW), 2010 European*, april 2010, pp. 1038 –1041.

[118] Tero Ihalainen, Tobias Hidalgo Stitz, Mika Rinne, and Markku Renfors, "Channel equalization in filter bank based multicarrier modulation for wireless communications," *EURASIP J. Appl. Signal Process.*, vol. 2007, no. 1, pp. 140–140, Jan. 2007.